Herausgeber
Tom Lahmer Timon Rabczuk Carsten Könke

ISM-Bericht 1/2017 ISSN: 1610-7381
Institut für Strukturmechanik
Fakultät Bauingenieurwesen
Bauhaus-Universität Weimar
Marienstraße 15
D-99423 Weimar
Germany

Tel. +49 (0)3643/584504
Fax. +49(0)3643/584514

http://www.uni-weimar.de/Bauing/ism

Identification and separation of physical effects of coupled systems by using defined model abstractions

(Identifikation und Separation physikalischer Effekte von gekoppelten Systemen mittels definierter Modellabstraktionen)

DISSERTATION

Zur Erlangung des akademischen Grades
Doktor-Ingenieur (Dr.-Ing.)
an der Fakultät Bauingenieurwesen
der Bauhaus-Universität Weimar

vorgelegt von
Dipl.- Wirtschaftsing. (FH) Rainer Martin Jakob Abeltshauser M.Eng.
geboren am 15.11.1987 in Schrobenhausen

Weimar, 3. November 2015

Mentor:
Prof. Dr.-Ing. habil. Carsten Könke, Bauhaus-Universität Weimar

Gutachter:
Prof. dr.ir. Daniel J. Rixen, Technische Universität München
Prof. Dr. rer. nat. Tom Lahmer, Bauhaus-Universität Weimar
Dr.-Ing. Christian Guist, BMW Group

Tag der Disputation: 13. September 2016

Für meine Familie

Vorwort

Die vorliegende Arbeit entstand während meiner Tätigkeit in der Antriebsentwicklung der BMW Group und als externer Doktorand der Bauhaus-Universität Weimar.

Mein besonderer Dank gilt Herrn Prof. Dr.-Ing. habil. Carsten Könke für die hervorragende wissenschaftliche Betreuung und bereitwillige Unterstützung während der Entstehung dieser Arbeit. Die zahlreichen fachlichen Diskussionen, sowie die vertrauensvollen Gespräche waren von sehr großem Wert.

Ebenso bedanke ich mich bei Herrn Dr.-Ing. Christian Guist für die ausgezeichnete fachliche Betreuung seitens der BMW Group. Die vielen anregenden Gespräche bildeten einen idealen Rahmen und waren maßgeblich für den erfolgreichen Abschluss dieser Arbeit. Ebenso möchte ich mich bei allen Mitarbeitern der BMW Group, des Instituts für Strukturmechanik und des Graduiertenkollegs 1462 der Bauhaus-Universität Weimar bedanken, die mir stets mit Rat und Tat zur Seite standen.

Weiter bedanke ich mich bei Herrn Prof. Dr.-Ing. Rixen der Technischen Universität München für die fachlichen Gespräche im Rahmen von weiteren Forschungstätigkeiten und die Übernahme des Korreferates.

Abschließend danke ich meinen Eltern und Großeltern für die jahrelange Unterstützung und Förderung meiner Interessen, was die Grundlagen für das Gelingen dieser Arbeit darstellen.

Abstract

The thesis investigates at the computer aided simulation process for operational vibration analysis of complex coupled systems. As part of the internal methods project “Absolute Values” of the BMW Group, the thesis deals with the analysis of the structural dynamic interactions and excitation interactions. The overarching aim of the methods project is to predict the operational vibrations of engines.

Simulations are usually used to analyze technical aspects (e. g. operational vibrations, strength, ...) of single components in the industrial development. The boundary conditions of submodels are mostly based on experiences. So the interactions with neighboring components and systems are neglected. To get physically more realistic results but still efficient simulations, this work wants to support the engineer during the preprocessing phase by useful criteria.

At first suitable abstraction levels based on the existing literature are defined to identify structural dynamic interactions and excitation interactions of coupled systems. So it is possible to separate different effects of the coupled subsystems. On this basis, criteria are derived to assess the influence of interactions between the considered systems. These criteria can be used during the preprocessing phase and help the engineer to build up efficient models with respect to the interactions with neighboring systems. The method was developed by using several models with different complexity levels. Furthermore, the method is proved for the application in the industrial environment by using the example of a current combustion engine.

Kurzfassung

Die Arbeit beschäftigt sich mit rechnergestützten Simulationsprozessen zur Betriebsschwingungsanalyse von komplexen gekoppelten Systemen. Im Rahmen des internen Methodenprojekts „Absolutaussagen“ der BMW Group, mit dem Ziel der Prognose von Betriebsschwingungen von Antrieben, beschäftigt sich diese Arbeit mit der Untersuchung von strukturdynamischen Wechselwirkungen und Anregungswechselwirkungen.

Im industriellen Entwicklungsumfeld werden Simulationen typischerweise zur Analyse eines technischen Aspekts (z. B. Betriebsschwingung, Festigkeit, …) hinsichtlich einer Komponente verwendet. Hierzu sind Teilmodelle mit meist erfahrungsbasierten Randbedingungen im Einsatz. Somit werden Wechselwirkungen mit angrenzenden Komponenten und Systemen oft vernachlässigt. Um die Simulationen weiterhin effizient zu halten und dennoch physikalisch realitätsnähere Ergebnisse zu erzielen, soll diese Arbeit den Berechnungsingenieur bereits während des Modellaufbaus mittels geeigneter Kriterien unterstützen.

Folglich wurden auf Basis der bereits vorhandenen Literatur geeignete Modellabstraktionsgrade ermittelt, um die strukturdynamischen Wechselwirkungen sowie Anregungswechselwirkungen von gekoppelten Systemen zu identifizieren. So gelingt es verschiedene Effekte der Kopplung von Teilsystemen zu separieren. Darauf aufbauend sind Kriterien abgeleitet, die es ermöglichen, den Einfluss der Wechselwirkungen bereits während des Modellaufbaus einzuschätzen. Das in der Dissertation erarbeitete allgemeine Verfahren wurde mittels mehrerer Modelle unterschiedlicher Komplexität entwickelt und auf die industrielle Anwendbarkeit am Beispiel eines aktuellen Verbrennungsmotors geprüft.

Contents

Symbols and abbreviations v

1 Introduction 1

1.1 Motivation 1

1.2 Aim of the dissertation 3

1.3 Restrictions of the dissertation 4

1.4 Outline 4

2 Mechanical foundations 7

2.1 Introduction to mechanical oscillations 7

2.2 Introduction to structural dynamics 9

2.2.1 Types of load 10

2.2.2 Mechanical loads and vibrations in time and frequency domain 14

2.3 Discrete systems 17

2.3.1 Single-mass oscillator 17

2.3.2 Multi-mass oscillator 24

2.4 Definition of Terms 25

2.4.1 Coupled system 25

2.4.2 Structural coupling 28

2.4.3 Excitation interaction 30

2.4.4 Efficient abstraction level 34

2.5 Different solution processes 36

2.5.1 Overview 36

2.5.2 Continuum systems 37

2.5.3 Finite Element Method 45

3 State of research 61

3.1 What is reality? 61

3.2 Kinds of models 62

3.3 Classification of mathematical models 63

3.4 Complexity of mathematical models 65

3.5 Abstraction levels of models 68

3.5.1 Submodels 68

3.5.2 Abstraction levels to calculate operational vibrations 70

3.5.3 Blocked Force Method 75

3.5.4 Cutting Force Principle 81

3.5.5 Structural coupling of mass dampers 83

4 Definition and application of wise abstraction levels 87

4.1 Methodic procedure 87

4.2 Explanation of the abstraction levels for a simple multi-mass system 92

4.2.1 Description of the total system 92

4.2.2 Abstraction level A1 94

4.2.3 Abstraction level A2 97

4.2.4 Abstraction level A3 98

4.2.5 Abstraction level A4 103

4.2.6 Decision method of considering structural coupling effects 105

4.2.7 Application of the developed assessment method 127

4.3 Explanation of the abstraction levels for a flexible-body system 132

4.3.1 Description of the total system 132

4.3.2 Abstraction level A1 134

4.3.3 Abstraction level A2 143

4.3.4 Abstraction level A3 153

4.3.5 Abstraction level A4 156

4.4 Explanation of the abstraction levels for a complex reference system..... 160
4.4.1 Description of the total system 160
4.4.2 Abstraction level A1 162
4.4.3 Abstraction level A2 163
4.4.4 Abstraction level A3 164
4.4.5 Abstraction level A4 168
5 Conclusion 171
References 175

Symbols and abbreviations

General notations

$\delta(\cdot)$	Variation of ·
$\hat{\cdot}$	Maximum value of ·
$\phi(\cdot)$	General function of ·
x, y, z	Global coordinates
x', y', z'	Local coordinates
x', φ	Polar coordinates
$\mathbf{x}$	Position vector $\mathbf{x} = [x, y, z]^T$
$\mathbf{u}$	Displacement vector $\mathbf{u} = [u, v, w]^T$
t	Time
T	Period of time
f	Frequency
Ω	Rotational frequency
ω_d	Damped eigen angular frequency
ω	Undamped eigen angular frequency
δ	Damping degree
D	Lehr's damping measure
$\boldsymbol{f}$	Frequency vector
$\boldsymbol{D}$	Lehr's damping measure vector
m	Mass parameter
k	Stiffness parameter
d	Viscous damping parameter
f	Force value
$\mathbf{M}$	Mass matrix
$\mathbf{D}$	Damping matrix
$\mathbf{K}$	Stiffness matrix
$\mathbf{f}$	Force vector $\mathbf{f} = [\mathrm{f}_x, \mathrm{f}_y, \mathrm{f}_z]^T$

N	Number of ·
n	Number of ·
k	Number of·
E	Young's modulus
ν	Poisson ratio
ρ	Density
λ_i	Real-valued weight
λ_s	Rod ratio
r	Length of crank
$s(\cdot)$	Approximated function of (·)

Structural dynamics

J_1, J_2, J_n	Stochastic events
$P(\cdot)$	Statistic probability of (·)
X	Random variable
a_0, a_n , b_n	Constant values
c	Offset of an interval
F_n	Complex value to describe the amplitude of the sinus and cosines parts
i	Complex number $i = \sqrt{-1}$
f_k	Spring force
f_d	Damping force
f_I	Inertia force
Λ, λ	Constants
x_p	Particular part of the solution
Γ	Amplification factor
$\mathbf{\Gamma}$	Amplification matrix
x_{stat}	Static displacement at a constant force
x_{dyn}	Dynamic displacement at an oscillating force
η	Frequency ratio
l	Distance between two points
f_{exc}	Excitation frequency
$H_{efficient}$	Coefficient of efficient
$p_{accuracy}$	Accuracy of results

Continuum systems

$\mathbf{X}$	Position vector in the reference configuration
$\mathbf{x}$	Position vector in the deformed configuration
B_0	Kinematic relationship of the reference configuration
B_t	Kinematic relationship of the deformed configuration
$\mathbf{F}$	Deformation gradient
$\mathbf{R}$	Orthogonal rotation tensor
$\mathbf{U}$	Right stretch tensor
$\mathbf{V}$	Left stretch tensor
$\mathbf{G}$	Green-Lagrangian strain tensor
$\mathbf{C}$	Cauchy-Green tensor
$\mathbf{t}$	Stress vector
s	Surface
$\mathbf{f}_t$	Force on a surface
$\mathbf{T}$	Cauchy stress tensor
$\mathbf{n}$	Normal vector
$\mathbf{P}$	First Piola-Kirchhoff stress tensor
$\mathbf{S}$	Second Piola-Kirchhoff stress tensor
$\mathbb{C}$	Elasticity tensor
$\boldsymbol{\epsilon}$	Linearized strain tensor
$\boldsymbol{\sigma}$	Linearized stress tensor
$\mathbf{E}$	Elastic constitutive matrix
A	Cross section

Finite Element Method

$\mathbf{D}_e$	Differential operator
σ	Internal forces / stresses
$\mathbf{D}_k$	Differential operator
ϵ	Internal displacement / strains
$\mathbf{u}_S$	Prescribed displacement on the Dirichlet boundary surface
S^u	Dirichlet boundary surface
$\mathbf{t}_S$	Prescribed traction on the Neumann boundary surface
S^t	Neumann boundary surface

B	Linear elastic continuum
$\mathbf{B}_e$	Strain-displacement matrix of element
W	Total work
W_{ext}	External work
W_{int}	Internal work
$\mathbf{N}_e$	Shape function
$\mathbf{q}_e$	Local element load vector
$\mathbf{T}_e$	Element transformation matrix
$\mathbf{T}_{GM}$	Transformation matrix of Guyan Method
$\mathbf{T}_{CBM}$	Transformation matrix of Craig Bampton Method
$\mathbf{q}_{gl}$	Global load vector
α, δ	Parameter
$\mathbf{Q}$	Orthogonal matrix
$\mathbf{R}$	Triangular matrix
$\mathbf{L}$	Lower triangular matrix of the LU factorization
$\mathbf{U}$	Upper triangular matrix of the LU factorization
$\mathbf{\Phi}$	Eigenvector
$\mathbf{\Phi_c}$	Vector of forced deformation
$\mathbf{\Phi_n}$	Natural modes
$\mathbf{q_n}$	Modal coordinates

State of research

z	Impedance
y	Admittance
Z	Dynamic impedance
Y	Dynamic admittance
$\mathbf{Z}(\cdot)$	Dynamic impedance matrix of (·)
$\mathbf{Y}(\cdot)$	Dynamic admittance matrix of (·)
μ	Mass ratio
κ_{opt}	Optimal frequency ratio
ζ_{opt}	Optimal Lehr's damping measure

Abbreviations

BEM	Boundary Element Method
DFT	Discrete Fourier Transform
DOE	Design of Experiment
DOF	Degree of freedom
EHD	Elastohydrodynamic
FDM	Finite Difference Method
FEM	Finite Element Method
FFT	Fast Fourier Transform
FVM	Finite Volume Method
GRK	Graduiertenkolleg
MBS	Multi Body System
NVH	Noise Vibration Harshness
RBF	Radial basis function
rpm	Rounds per minute
RSM	Response Surface Modeling
SQM	System, Questions, Mathematical statements

1 Introduction

1.1 Motivation

The presented thesis investigates at the computer aided simulation process for operational vibration analysis. In this context, the modeling of complex coupled systems with periodic force excitations is focused. New products get more complex in the industrial environment. The costs and the time to market should decrease, but the product quality should increase. That is a conflict of aims and a big challenge for the engineers in the industrial development. The focus is on improving the development process and cutting costs by increasing the use of simulations and decreasing the use of experiments. (Keßler and Träbing 2001), (Dresig 2001)

Therefore, an internal BMW project called “Absolute Values” was started in 2011. Several scientific and industrial partners are involved in this project until today. The aim is to calculate operational vibrations of complex systems in automotive industry (e. g. engine, gearbox, chassis, door systems and so on) on an absolute scale. It means that the frequencies and amplitudes of operational vibrations are predictable and assessable without additional experiments. So the project partners conduct scientific investigations on four scientific fields:

- Calculation Method
- Excitation Calculation
- Modeling Structure
- Damping Effects

Referring to the project leader Dr. Christian Guist (BMW Group) a calculation model can be generated and a prediction of operational vibrations should be possible, if all relevant effects of the scientific fields are understood and implemented in the simulation.

But there are many challenges to generate such high-quality models. (Dresig 2001) says that a calculation model cannot represent a real drive system, so it is always an abstraction of the reality which is usable for a special purpose. Generally, a calculation model has the function to represent the qualitative structural dynamic behavior and the quantitative calculation of variables (e. g. forces and motion quantities), so that the influence of the significant parameter to the structural dynamic behavior of the structure under investigation is observable and interpretable, (Dresig 2001, S. 5).

Furthermore, the data volume of such models for a complex industrial system is very difficult to handle due to the currently limited technical resources. The calculation leads to a very time-consuming and memory-consuming procedure, so high-performance computers are necessary. With the development of new high performance computers and the use of efficient numerical methods, the complexity of models raises immediately. (Duddeck 1993) Nevertheless, the use of complex coupled models is still a challenge for the engineers. (Most 2011) adduced that the lack of knowledge about input parameters is also an essential factor for the accuracy of a calculation model. Here it should be mentioned that there is few knowledge about local damping factors of bolted joints, which (Theiler and Könke 2013) analyzed and discussed. Moreover to reduce the model complexity, the interactions between subsystems are often neglected. (Rombach 2008) mentioned some problems with regard to realistic modeling of physical reality:

- The modeling of such complex models is fault-prone.
- Afterthought modifications are difficult to consider.
- And the plausibility check of the results is difficult, too.

So there are a lot of challenges to use such high-quality models in industrial environment. Due to the mentioned problems, the engineers still have to use models of subsystems for the next few years. As a result of the described necessary assumptions, calculation models are only able to calculate results on a relative scale. Therefore, each calculation model has been validated by experiments and the engineers can only assess changes of the validated calculation model. There are several submodels for different kind of tasks in the field of engineering. Typically, the models look at one aspect of development (e. g. operational vibrations) and one component. So the model includes the component of interest and experience-based

boundary conditions, but the structural dynamic behavior of the system housing and the coupling to other subsystems is often neglected, (Reuter 2012).

In summary, it is not possible to predict the operational vibrations at this time due to the mentioned necessary assumptions and simplifications. Accordingly, the engineers need helpful criteria to estimate the influences of interactions between subsystems during the modeling process to improve the simulation results. This represents one step to achieve the aim of calculating operational vibrations on an absolute scale.

1.2 Aim of the dissertation

The aim of the dissertation is the development of a general procedure to help the engineers to model complex coupled systems for operational vibration analysis. So the dissertation identifies several abstraction levels based on scientific literature review. By comparing the results of the different abstraction levels, the effects of structural coupling and excitation interaction can be identified. Based on the identified effects, criteria are developed to estimate the influence of the coupling of subsystems to the operational vibrations. Furthermore, the engineers get a recommendation as to which abstraction level should be used for the calculation of operational vibrations.

On the basis of this assignment of tasks, two essential research questions are defined:

- Which criteria can be used to identify a high coupling effect?
- Which criteria can be used to choose an efficient abstraction level[1]?

The questions should be answered by using simple general models to transfer the knowledge in many specialist areas. The models consist of mass points, stiffness and damping factors as well as modal-reduced FE-Models also called substructures. The validation of the methods is represented on a complex engine model to show the applicability. In chapter 1.4, the outline and the structure of the dissertation is explained in detail.

[1] The term “efficient abstraction level“ is defined as the best relation between complexity and effort. A detailed explanation of efficient abstraction level is shown in Chapter 2.4.4.

1.3 Restrictions of the dissertation

This thesis deals with the calculation of operational vibrations of complex coupled systems. The identification, definition and comparison of abstraction levels is part of the dissertation to develop a general procedure that help the engineers to choose an efficient abstraction level. The focus is on the assessment of structural coupling and excitation interaction effects. So the engineers should be able to estimate the influence of coupling effects before modeling by using simple criteria. With the developed criteria in this work, the engineers should be able to choose the most efficient abstraction level for the system of interest. So the engineers are able to save modeling time and calculation capacity by knowing negligence of effects.

Furthermore, the thesis only deals with harmonic and periodic excitation forces. Other excitation forces are not reviewed in this dissertation and should be analyzed in following thesis. All analyses are based on models with linear behavior. So the nonlinear stiffness and damping of bearings are linearized in this dissertation.

1.4 Outline

This work is divided into five chapters. After the introduction, the second chapter explains the mechanical foundations that are necessary for understanding the following chapters. So there is an introduction to the specialist field of structural dynamics and the Finite Element Method. Additionally, the most important terms that are used in this work are explained in detail.

The third chapter starts with a short discussion about the term “reality” and shows the current state of research about the classification of models. Furthermore, the common used abstraction levels are explained as well as the mathematical background of the Blocked Force Method and the Cutting Force Principle.

The fourth chapter represents the core work. So the developed abstraction levels are explained and three systems with different complexity levels are analyzed to identify coupling effects. The analyses start with a simple multi-mass system. The system is modeled for each abstraction level. The comparison of the results identifies

interactions between subsystems. The effects are analyzed and a method is developed to forecast the identified effects. The developed method is used and validated by using a three-dimensional flexible-body system. Here it is possible to identify additional effects by using the abstraction levels. These effects are analyzed and a method to forecast the effects is developed, too. The last analyzed system is the most complex system in this work. It represents a combustion engine which is used in the automotive industry. So it can be shown that the developed abstraction levels are applicable in the industrial environment to separate the different kinds of structural coupling and excitation interaction effects.

The fifth chapter summarizes the presented results of the work and gives a suggestion for future researches.

2 Mechanical foundations

This chapter explains the theoretical foundations that are used in this work. Furthermore, the chapter defines the most important terms of the dissertation, which are necessary to understand the explained effects in the following chapters.

2.1 Introduction to mechanical oscillations

Let's have a short introduction to the theory of oscillations based on (Stelzmann et al. 2008), (Dubbel et al. 2001), (Waller and Schmidt 1989), and (Vöth 2006).

General oscillations are defined as time-dependent events. They are observable in different areas like finance market, electrical engineering, or mechanical engineering. (Waller and Schmidt 1989) This dissertation focuses on mechanical oscillations that can be loads or structural vibrations. A load oscillation can result from a movement of a body in the mechanical engineering. A structural vibration is a time-dependent displacement of a structural element about a position of rest. (Stelzmann et al. 2008)

Referring to (Vöth 2006) a system with one state parameter is regarded to give a mathematical description about mechanical oscillations. So let's assume a plane pendulum with the state parameter φ "deflection angle". The state parameter of the dynamic system is time-variant, as shown in Eq. (2.1).

$$\varphi = \varphi(t) \qquad (2.1)$$

A periodic oscillation is defined as a recurring process, so each state will be reached again after a time T

$$\varphi(t + T) = \varphi(t). \qquad (2.2)$$

T is also called period of a periodic oscillation. The reciprocal of the period defines the frequency f of the oscillation

$$f = \frac{1}{T}. \qquad (2.3)$$

To describe an harmonic oscillation, the sine- or cosine-functions are typically used, as shown in Eq. (2.4).

$$\varphi(t) = \hat{\varphi} cos(\Omega t - \varphi_0) \qquad (2.4)$$

$\hat{\varphi}$ describes the maximum amplitude of φ and φ_0 represents the phase angle. By using Eq. (2.5), the time offset to the original cosine function can be calculated.

$$t_{offset} = \frac{\varphi_0}{\Omega} \qquad (2.5)$$

The angular frequency Ω can be followed by the argument of the cosine function, because the argument of the cosine function has to be increased about 2π in the time interval of $t = 0$ and $t = T$. So the angular frequency Ω is defined in Eq. (2.6).

$$\Omega = 2\pi f = \frac{2\pi}{T} \qquad (2.6)$$

Figure 2.1 shows a harmonic oscillation by using a cosine function with a phase angle $\varphi_0 = -\frac{\pi}{2}$. So it can be described as well as a sine function without a phase angle, referred to Eq. (2.7).

$$\hat{\varphi} \cos\left(\Omega t - \frac{\pi}{2}\right) = \hat{\varphi} sin(\Omega t) \qquad (2.7)$$

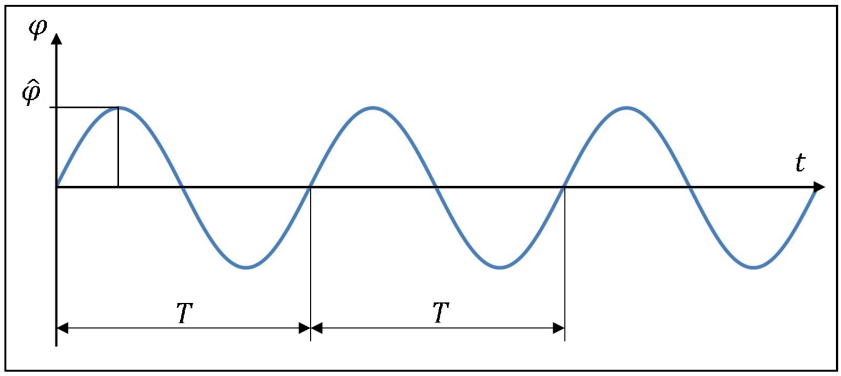

Figure 2.1: Harmonic oscillation

Real dynamic systems do not consist of only one state parameter. Most properties of real systems are distributed continuously. This can be modeled by using a continuum system model or the discretization of a continuum model. The discrete formulation

can be used to calculate the system behavior by using numerical methods. (Vöth 2006) Figure 2.2 shows different degrees of discretization.

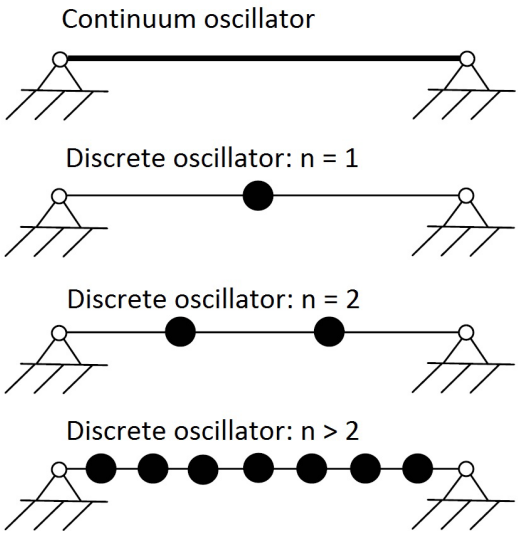

Figure 2.2: Oscillators with a different degree of discretization (Vöth 2006)

With a higher number of discrete oscillators, more physical effects can usually be represented, because the results converge to the solution of the continuum oscillator.

2.2 Introduction to structural dynamics

The specialist area “structural dynamics” analyzes the behavior of constructions during a time-dependent load. Generally, loads are always time-dependent. But many loads are applied very slowly, so the time-dependency can be neglected and a static calculation is possible. Due to the rising focus on light-weight constructions and NVH (= Noise Vibrations Harshness), the analysis of dynamic problems is getting more important for many industrial sectors, e. g. bridges, tower buildings, airplanes, vehicles, and so on. (Stelzmann et al. 2008)

2.2.1 Types of load

The dissertation is focused on the calculation of operational vibrations of complex coupled systems. The operational vibration of each structure or rather technical component is a combination of time-dependent and position-dependent loads $\mathbf{f}(t,x,y,z)$ and the structural dynamic behavior of the mechanical system. Eq. (2.8) shows the general equation of motion. The left side represents the structural dynamic behavior of the vibrational mechanical system and the right side shows the external load.

$$\mathbf{M\ddot{u}} + \mathbf{D\dot{u}} + \mathbf{Ku} = \mathbf{f}(t,x,y,z) \qquad (2.8)$$

A load in the field of mechanical engineering results from a movement of a body or from the environment of the construction, e. g. earthquake, wind, or explosion. The following classification of load types is inspired by the work of (Dubbel et al. 2001), (Stelzmann et al. 2008), and (Magnus et al. 2013).

One classification of loads is the load characteristic over time. The loads can be divided into five types:

- Free oscillation
- Static load
- Periodic load
- Non-periodic load
- Stochastic load

Some types can be divided into sub-categories. Figure 2.3 shows an overview of load types. It also shows example curves for each category. The list of category is not complete, but it display the most important load types.

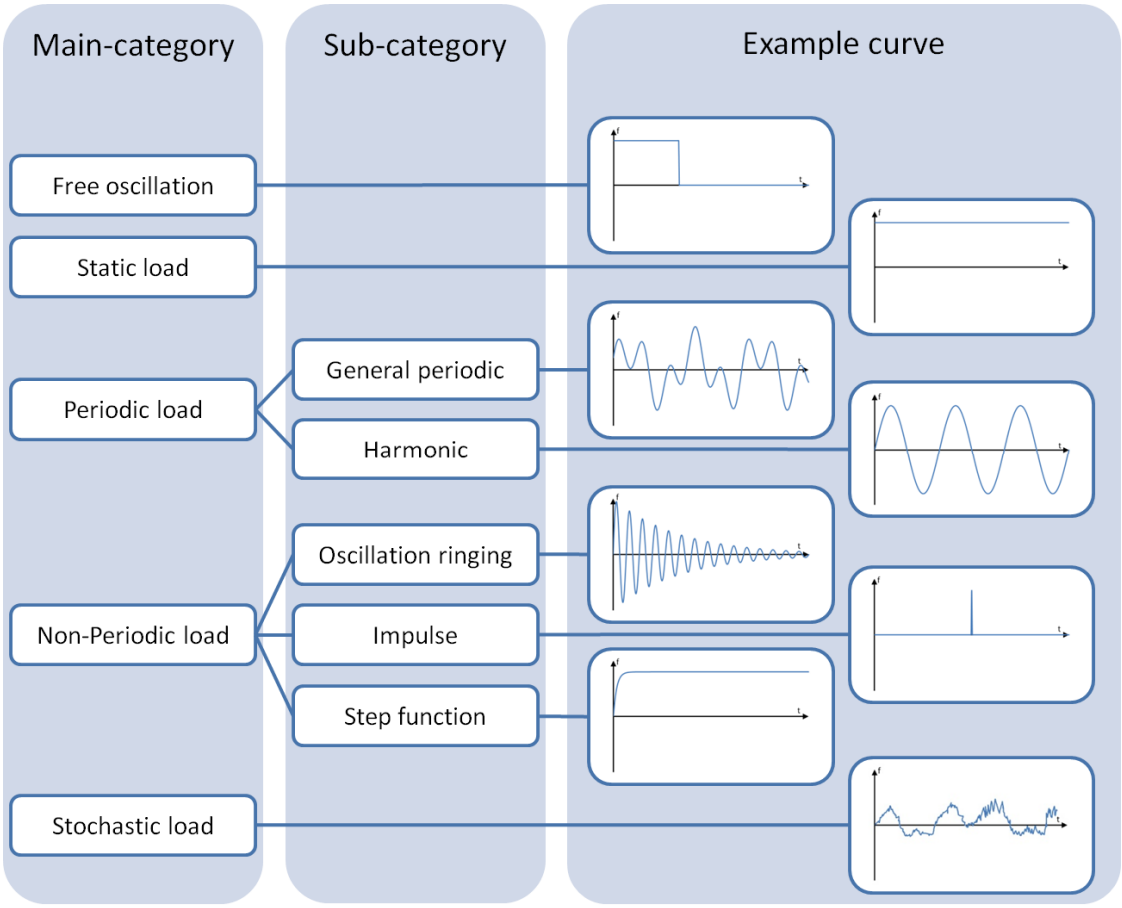

Figure 2.3: Overview of load types based on (Stelzmann et al. 2008) and (Dubbel et al. 2001)

A **free oscillation** load means that the structure is preloaded at the beginning and then the load goes to zero abruptly. So the structure will oscillate in its eigenfrequency without external loads. An example could be a roof which is preloaded by snow. If the snow slips off, the roof gets unloaded abruptly and the roof/building oscillates in its eigenfrequency, (Stelzmann et al. 2008). Eq. (2.9) represents the function of the displayed free oscillation load in Figure 2.3.

$$\mathrm{f}(t) = \begin{cases} \mathrm{f}_0 \; f\ddot{u}r \; t < t_0 \\ 0 \; f\ddot{u}r \; t \geq t_0 \end{cases} \qquad (2.9)$$

A **static load** does not generate oscillations, but it leads to deformations of the structure. A static load is a preload of a bolt or the gravity load, for example. Eq. (2.10) represents the function of the displayed static load in Figure 2.3.

$$\mathrm{f}(t) = \mathrm{f}_0 \qquad (2.10)$$

The **general periodic load** considers more than one frequency. Every general periodic load can be divided in a Fourier-series of harmonic oscillations. General periodic loads can be produced by transversal oscillating masses, e. g. a crank drive of an engine or stamping tool. The **harmonic load** is a special case of a periodic load. It only considers one frequency and can be generated by a rotating mass like a balance shaft of an engine. In the next chapter, the equation of the general periodic oscillation is explained in detail.

The sub-categories of the **non-periodic load** is not complete. The **oscillation ringing** represents a load so that the amplitude decreases and the frequency stays constant. Also it can be a swinging up oscillation so that the amplitude increases and the frequency stays constant. The displayed oscillation in Figure 2.3 is described in Eq. (2.11).

$$\mathrm{f}(t) = \sin(\Omega t) e^{-t} \qquad (2.11)$$

The next sub-category is called **impulse load**. Here an ideal Dirac impulse on the condition $\int_{-\infty}^{+\infty} \mathrm{f}(t) = 1$ is shown. An ideal Dirac impulse is theoretically possible, but it is impossible to generate an ideal Dirac impulse in reality. Eq. (2.12) describes the ideal Dirac impulse which is shown in Figure 2.3.

$$\mathrm{f}(t) = \begin{cases} 0 \; für \; t < t_0 \\ \mathrm{f}_0 \; für \; t = t_0 \\ 0 \; für \; t > t_0 \end{cases} \qquad (2.12)$$

So there are a lot of characteristics of impulse loads that are not described in this thesis, e. g. square, triangular, sinusoidal impulse loads, and so on. Important is that an impulse is defined as a load that duration is short compared to the total time of the movement of the system. Real-life examples are explosions, impact of birds, and so on. A **step function load** is defined as a load that moves to a load value and load the structure for a longer period of time.

$$\mathrm{f}(t) = \begin{cases} 0 \; für \; t < t_0 \\ \mathrm{f}_0 \; für \; t \geq t_0 \end{cases} \qquad (2.13)$$

Till now, all loads can be called deterministic loads. The term “determinism” is defined as the conception that all past, present and future events are clearly determined by

preconditions, (Jordan and Nimtz 2009). A further type of load is the **stochastic load** whose time response is irregular. For example vehicle loads of the road, a wind load to a building, or an earthquake are called stochastic loads. It is difficult to describe a stochastic load in a calculation. So the engineers often use measured loads or a random signal to load the vibrational structure. A random signal contains stochastic events $J_1, J_2, \dots, J_n$ with an allocated statistic probability $P(J_1), P(J_2), \dots, P(J_n)$.

$$0 \leq P(J_1) \leq 1 \qquad (2.14)$$

Eq. (2.14) defines the statistic probability of J_1. If $P(J_1) = 0$, the event J_1 does not occur. If $P(J_1) = 1$, the event J_1 does occur. Now each event should assign a numerical value to get the random variable X. The empirical distribution function $\phi(x)$ in Eq. (2.15) shows the probability that the value of X is less than x. (Waller and Schmidt 1989)

$$\phi(x) = P(X \leq x) \qquad (2.15)$$

More detailed information about stochastic modeling methods and their use in numerical calculations can be found in (Most 2005).

Furthermore, the loads can be classified by position variance. There are two types of loads, the deterministic-position load and the stochastic-position load. The **deterministic-position load** can be defined as forces which load the structure on exactly defined positions over the time. Generally, each load is subject to a position-variance. If the variance is small, a deterministic-position load can be assumed. In the civil engineering, a percussion hammer is called a deterministic-position load. In the mechanical engineering, a deterministic-position load is an injector, a bolt preload, and so on.

The **stochastic-position load** can be defined as forces which load the structure on different positions over the time. Some examples for such loads are wind loads, earthquake loads, and so on. In the mechanical engineering, the cross wind load is interesting for the aerodynamic development of vehicles. Also the wind load is interesting for the development of bridges and wind power plants. In many cases the stochastic-position loads are impressed on the structure by using a statistic probability like the stochastic load over the time. Another widely-used option is to neglect the

effect of stochastic-position loads and the engineers use deterministic loads with the frequency of interest.

This dissertation only focuses on deterministic-position loads with a periodic time response and the mechanical loads result from the movement of bodies (e. g. technical components).

2.2.2 Mechanical loads and vibrations in time and frequency domain

Up to now, the oscillations were only described in time domain. But many analyses of mechanical loads and vibrations are based on frequency domain. So this chapter gives a short explanation as the oscillations in time domain can be transformed into frequency domain. Figure 2.4 shows a periodic function in time domain. The transformed function in frequency domain is shown in Figure 2.5.

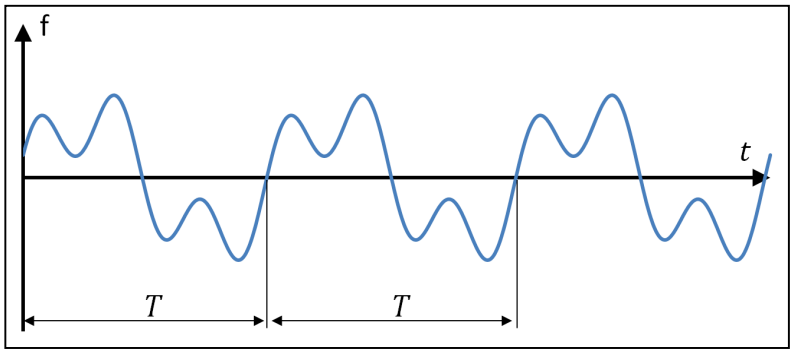

Figure 2.4: Periodic oscillation in time domain

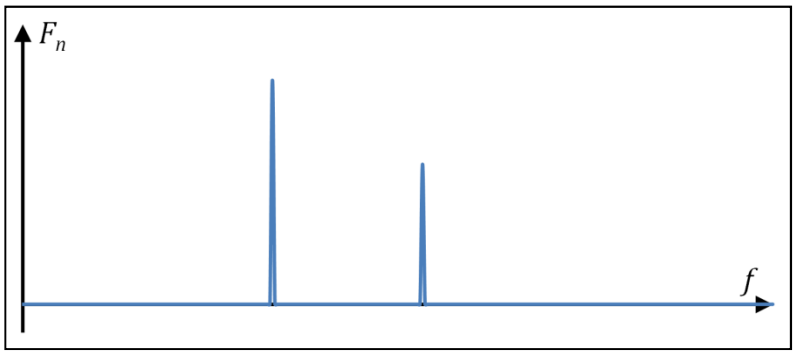

Figure 2.5: Periodic oscillation in frequency domain

(Waller and Schmidt 1989) gives a good introduction that is used in the following explanation.

Fourier Series:

A piecewise continuous and periodic function (Figure 2.4) can be described by Fourier Series

$$\mathrm{f}(t) = \frac{1}{T}\left[\frac{a_0}{2} + \sum_{n=1}^{\infty}(a_n\, cos(n\Omega t) + b_n\, sin(n\Omega t))\right]. \qquad (2.16)$$

The Fourier Series consists of a constant part $\frac{a_0}{2}$ and the sum of trigonometric functions $\sum_{n=1}^{\infty}(a_n\, cos(n\Omega t) + b_n\, sin(n\Omega t))$ with the constant values a_n and b_n. The constants can be calculated by using the following equations with $n = 0,1,2,3, \ldots$

$$\frac{a_0}{2} = \frac{1}{T}\int_{c}^{c+T} \mathrm{f}(t)dt, \qquad (2.17)$$

$$a_n = 2\int_{-\frac{T}{2}}^{\frac{T}{2}} \mathrm{f}(t)\, cos(n\Omega t)\, dt, \qquad (2.18)$$

$$b_n = 2\int_{-\frac{T}{2}}^{\frac{T}{2}} \mathrm{f}(t)\, sin(n\Omega t)\, dt, \qquad (2.19)$$

c is an offset of the interval and Ω is called the basis oscillation which is defined by using the period T in Eq. (2.20).

$$\Omega = \frac{2\pi}{T} \qquad (2.20)$$

Often the Fourier Series is described by complex numbers

$$\mathrm{f}(t) = \sum_{n=-\infty}^{\infty} F_n e^{in\Omega t} \qquad (2.21)$$

with

$$F_n = \frac{1}{2T}(a_n - ib_n) \qquad (2.22)$$

or rather

$$F_n = \frac{1}{T}\int_{-\frac{T}{2}}^{\frac{T}{2}} \mathrm{f}(t)e^{-in\Omega t}dt \qquad (2.23)$$

The complex value F_n shows the amplitude of the sine and cosine parts.

Fourier Transform:

The Fourier Series is only usable for periodic functions. To transform a non-periodic function from time domain into frequency domain, the so called Fourier Transform has to be used. It is defined as

$$F(\Omega) = \int_{-\infty}^{\infty} \mathrm{f}(t)e^{-i\Omega t}dt \qquad (2.24)$$

and

$$\mathrm{f(t)} = \frac{1}{2\pi}\int_{-\infty}^{\infty} F(\Omega)e^{i\Omega t}d\Omega \qquad (2.25)$$

The Fourier Transform can be derived from using the Fourier Series and the following conditions:

- $T \to \infty$
- $\Omega \to d\Omega$
- $n\Omega \to \Omega$
- $F_n \to F(\Omega)$
- $T = \frac{2\pi}{\Omega} \to \frac{2\pi}{d\Omega}$

For many functions $\mathrm{f}(t)$ it is very time-consuming to apply the Fourier Transform by using analytical methods, so it is necessary to consider some calculation rules that are listed in (Waller and Schmidt 1989). In most cases the numerical method so called discrete Fourier Transform is used to transform the functions from time domain into

frequency domain. Here a finite time interval T is discretized in N sampling points. So the Eq. (2.26) and Eq. (2.27) define the Discrete Fourier Transform.

$$F_n = \frac{T}{N} \sum_{\mathrm{k}=0}^{N-1} \mathrm{f_k} e^{-i2\pi n \mathrm{k} \frac{1}{N}} \qquad (2.26)$$

$$\mathrm{f_k} = \frac{1}{T} \sum_{n=0}^{N-1} F_n e^{i2\pi n \mathrm{k} \frac{1}{N}} \qquad (2.27)$$

A detailed explanation of the Discrete Fourier Transform can be found in (Waller and Schmidt 1989), (Randall 1987), and (Neubauer 2012). To reduce the number of arithmetic operations, the Fast Fourier Transform algorithm is often used. The common used algorithm was published in 1965 (Cooley and Tukey 1965) and revolutionized the signal analysis. This thesis resigns from a detailed explanation of the Fast Fourier Transform. In (Randall 1987) and (Brigham 1995) a detailed explanation of the Fast Fourier Transform can be found. In the following analysis of the dissertation, the Fast Fourier Transform is used to transform the function from time domain into frequency domain.

2.3 Discrete systems

All analyses in this dissertation are based on discrete models and many effects can be explained by using a simple single-mass or a multi-mass oscillator. In this chapter, the single-mass and the multi-mass oscillator are explained in detail, which is also necessary to understand the definition of terms in the next chapter.

2.3.1 Single-mass oscillator

The single-mass oscillator is the simplest discrete dynamic system that can be imagined. The derivation of the single-mass oscillator can be found in many publications. In this chapter, the publications (Waller and Schmidt 1989) and (Vöth 2006) are used. For modeling the damped single-mass oscillator in Figure 2.6, it is necessary to define three system parameters:

- the mass m
- the stiffness k
- and the viscous damping d

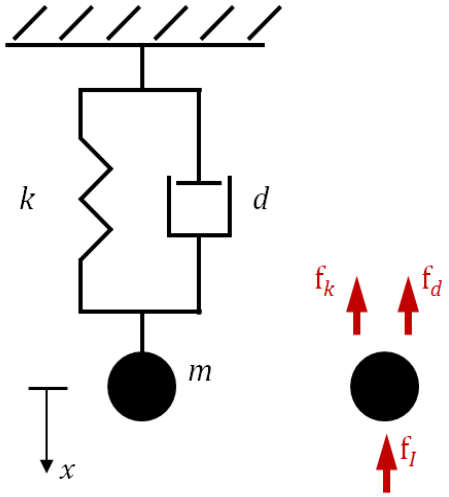

Figure 2.6: Single-mass oscillator with damping

Three forces are working on the mass, as shown in Figure 2.6. f_k represents the spring force

$$\mathrm{f}_k = kx \tag{2.28}$$

which depends on the position x. The viscous damping force is defined as

$$\mathrm{f}_d = d\dot{x} \tag{2.29}$$

and depends on the velocity $\dot{x}$. The inertia force

$$\mathrm{f}_I = m\ddot{x} \tag{2.30}$$

depends on the acceleration $\ddot{x}$. The equilibrium equation of forces is given in Eq. (2.31).

$$m\ddot{x} + d\dot{x} + kx = 0 \tag{2.31}$$

By using the damping degree

$$\delta = \frac{1}{2}\frac{d}{m} \tag{2.32}$$

and the undamped eigen angular frequency

$$\omega = \sqrt{\frac{k}{m}}, \qquad (2.33)$$

the equilibrium equation can be written as

$$\ddot{x} + 2\delta\dot{x} + \omega^2 x = 0\,. \qquad (2.34)$$

Now the linear homogenous differential equation of second order in Eq. (2.34) can be solved by using the trial function (2.35) and their derivatives with respect to time (2.36), (2.37) with the constants Λ and λ:

$$x(t) = \Lambda e^{\lambda t} \qquad (2.35)$$

$$\dot{x}(t) = \Lambda\lambda e^{\lambda t} \qquad (2.36)$$

$$\ddot{x}(t) = \Lambda\lambda^2 e^{\lambda t} \qquad (2.37)$$

By inserting Eq. (2.35) - (2.37) into Eq. (2.34) we obtain Eq. (2.38).

$$(\lambda^2 + 2\delta\lambda + \omega^2)\Lambda e^{\lambda t} = 0 \qquad (2.38)$$

This equation can only become zero if the term in brackets is zero

$$\lambda^2 + 2\delta\lambda + \omega^2 = 0\,. \qquad (2.39)$$

So Eq. (2.39) have two solutions for λ

$$\lambda_{1/2} = -\delta \pm \sqrt{\delta^2 - \omega^2}\,. \qquad (2.40)$$

With the use of the Lehr's damping measure

$$D = \frac{\delta}{\omega}, \qquad (2.41)$$

the Eq. (2.40) can be written as

$$\lambda_{1/2} = -\delta \pm \sqrt{D^2 - 1}\,. \qquad (2.42)$$

Now three cases can be distinguished:

- supercritical damping: $D > 1$
- critical damping: $D = 1$
- subcritical damping: $D < 1$

Let's start with the supercritical damping case. A supercritical damped oscillator does not oscillate. If the system is deformed or excited, the system goes back to the position of rest by a creeping velocity, because the damping force is already high at small velocities and work against the spring force. Inserting the substitution

$$\mu = \omega\sqrt{D^2 - 1}\,, \tag{2.43}$$

in the trial function (2.44)

$$x(t) = \Lambda_1 e^{\lambda_1 t} + \Lambda_2 e^{\lambda_2 t}\,, \tag{2.44}$$

the solution for the position is obtained by

$$x(t) = e^{-\delta t}(\Lambda_1 e^{\mu t} + \Lambda_2 e^{-\mu t})\,. \tag{2.45}$$

The second case is the critical damping case also called aperiodic borderline case. The system is not able to oscillate and the mass returns to the initial undeformed position. The difference to the strong damping case is that the position of rest is reached as quickly as possible, because the damping factor is the lowest damping factor for a non-oscillating system. Inserting $D = 1$ in Eq. (2.42) shows that one solution for λ fulfills the differential equation

$$\lambda_1 = \lambda_2 = -\delta\,. \tag{2.46}$$

So the solution of the position has a double zero point.

$$x(t) = \Lambda_1 e^{-\delta t} + \Lambda_2 t e^{-\delta t}\,, \tag{2.47}$$

The subcritical damping case is defined as $D < 1$. So the solution λ is a complex value.

$$\lambda_{1/2} = -\delta \pm i\omega_d \tag{2.48}$$

Thus the solution for the position $x(t)$ is:

$$x(t) = e^{-\delta t}(\Lambda_1 e^{i\omega_d t} + \Lambda_2 e^{-i\omega_d t}) \tag{2.49}$$

Eq. (2.49) can be transformed into Eq. (2.51) by using the substitution

$$e^{\pm i\omega t} = cos(\omega t) \pm isin(\omega t)\,. \tag{2.50}$$

$$x(t) = e^{-\delta t}((\Lambda_1 + \Lambda_2)\, cos(\omega_d t) + i(\Lambda_1 - \Lambda_2)\, sin(\omega_d t)) \quad (2.51)$$

In Eq. (2.51) it can be seen that the system oscillates with a damped eigen angular frequency ω_d which is lower than the undamped eigen angular frequency in Eq. (2.33). The damped eigen angular frequency is defined in Eq. (2.52).

$$\omega_d = \omega\sqrt{1 - D^2} \quad (2.52)$$

Now the single-mass oscillator is loaded by a harmonic excitation force

$$\mathrm{f}(t) = \mathrm{f}_0\, cos(\Omega t). \quad (2.53)$$

Therewith the equilibrium equation changes to

$$m\ddot{x} + d\dot{x} + kx = \mathrm{f}(t). \quad (2.54)$$

By inserting the damping degree in Eq. (2.32), the undamped eigen angular frequency in Eq. (2.33) and the substitution in Eq. (2.55), the inhomogeneous differential equation (2.56) can be generated.

$$\mathrm{f}_0 = kx_0 \quad (2.55)$$

$$\ddot{x} + 2\delta\dot{x} + \omega^2 x = \omega^2 x_0 cos\,(\Omega t) \quad (2.56)$$

So it is possible to calculate the amplification function of the single-mass oscillator by the particular part of the solution. The trial function (2.57) can be chosen for the steady state condition of the system.

$$x_p = x_0 \Gamma\, cos\,(\Omega t - \varphi) \quad (2.57)$$

Γ represents the amplification function, which is defined in Eq. (2.58).

$$\Gamma = \frac{x_{dyn}}{x_{stat}} \quad (2.58)$$

φ is the phase between the force excitation and the displacement of the mass. By inserting the trial function and their derivatives in Eq. (2.56), the Eq. (2.59) can be written.

$$\begin{aligned}(\eta^2 cos\varphi + 2D\eta sin\varphi + cos\varphi - 1)\Gamma\, cos(\Omega t) \\ + (-\eta^2 sin\varphi - 2D\eta cos\varphi + sin\varphi)\Gamma\, sin(\Omega t) = 0\end{aligned} \quad (2.59)$$

η is defined as frequency ratio defined by Eq. (2.60).

$$\eta = \frac{\Omega}{\omega} \tag{2.60}$$

In case that the equation is true, both terms in the brackets of Eq. (2.59) have to be zero. By using the second term, the phase frequency response is defined in Eq. (2.61). It represents the phase dependent on the frequency ratio.

$$tan\varphi = \frac{2D\eta}{1-\eta^2} \tag{2.61}$$

The amplification function $\Gamma(\eta)$ in Eq. (2.64) can be defined by using the substitution in Eq. (2.62) and Eq. (2.63).

$$sin\varphi = \frac{tan\varphi}{\sqrt{1+tan^2\varphi}} \tag{2.62}$$

$$cos\varphi = \frac{1}{\sqrt{1+tan^2\varphi}} \tag{2.63}$$

$$\Gamma(\eta) = \frac{1}{\sqrt{(1-\eta^2)^2+(2D\eta)^2}} \tag{2.64}$$

Figure 2.7 shows the amplification function and Figure 2.8 shows the phase frequency response with different Lehr's damping measure. Three cases can be distinguished:

- $\Gamma(\eta = 0) = 1$ and $\varphi(\eta = 0) = 0$: The force is applied very slowly, so it is a quasi-static load. Thus very low inertia forces occur.
- $\Gamma(\eta = 1) = \frac{1}{2D}$ and $\varphi(\eta = 1) = \frac{\pi}{2}$: The excitation force frequency is equal to the eigenfrequency of the system and the amplitude is only limited by the damping.
- $\Gamma(\eta \to \infty) \to 0$ and $\varphi(\eta \to \infty) \to \pi$: The mass is accelerated very fast and the inertia forces get very high. So the excitation force does not cause large deformation.

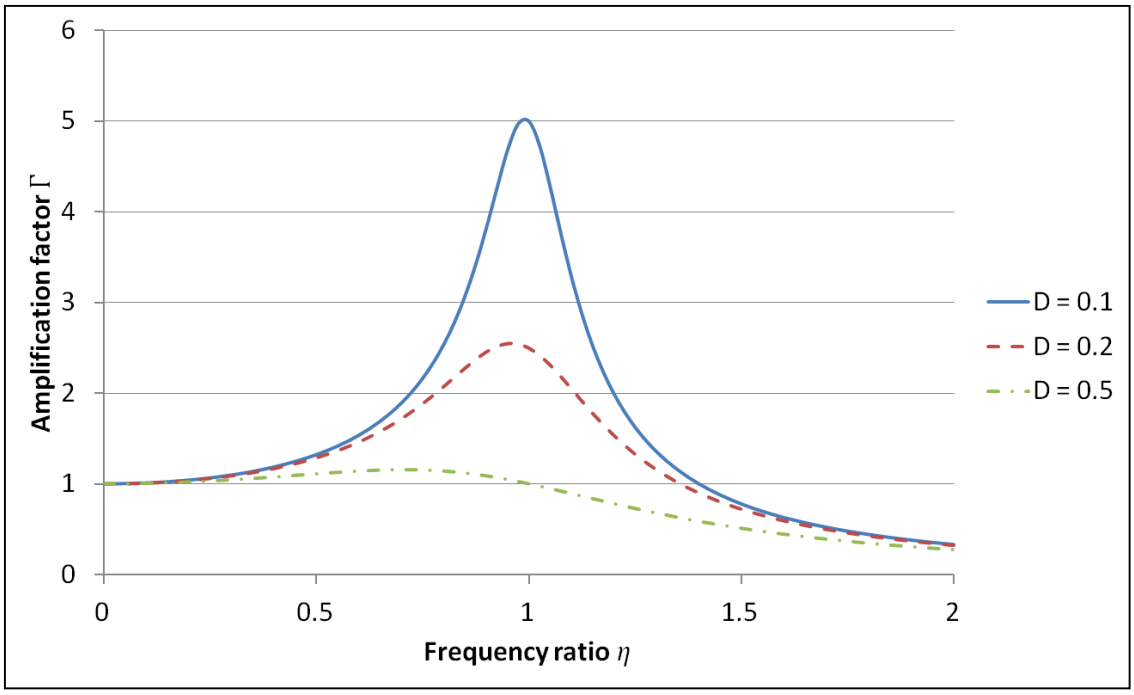

Figure 2.7: Amplification function with different Lehr's damping measure

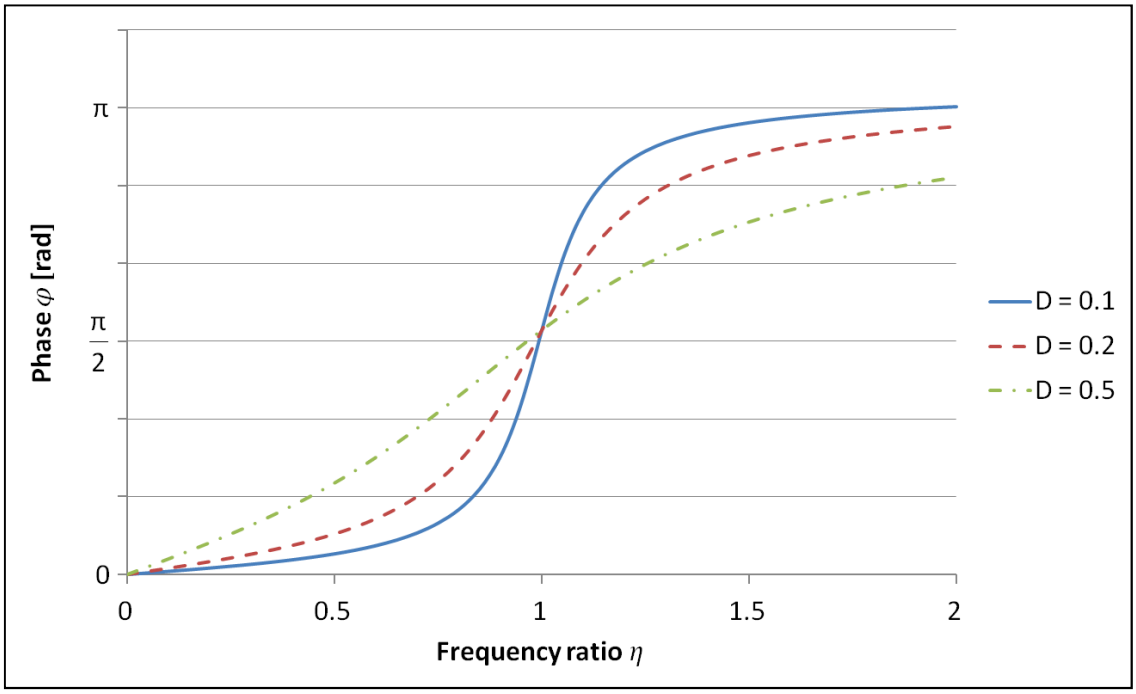

Figure 2.8: Phase frequency response with different Lehr's damping measure

2.3.2 Multi-mass oscillator

Most systems cannot be modeled by a single-mass oscillator, so the multi-mass oscillator has to be used. Analogous to the single-mass oscillator, the multi-mass oscillator can be described by a differential equation. Figure 2.9 shows a multi-mass oscillator with two masses and the respective internal forces. The equilibrium equation of forces is shown in Eq. (2.65).

$$\begin{aligned} \mathrm{f}_{k1} - \mathrm{f}_{k2} + \mathrm{f}_{d1} - \mathrm{f}_{d2} + \mathrm{f}_{I1} - \mathrm{f}_1 = 0 \\ \mathrm{f}_{k2} + \mathrm{f}_{d2} + \mathrm{f}_{I2} - \mathrm{f}_2 = 0 \end{aligned} \qquad (2.65)$$

By using the mass, stiffness, damping, displacement/position, velocity and acceleration, the equilibrium equation of forces can be written as shown in Eq. (2.66).

$$\begin{aligned} k_1 x_1 - k_2(x_2 - x_1) + d_1 \dot{x}_1 - d_2(\dot{x}_2 - \dot{x}_1) + m_1 \ddot{x}_1 - \mathrm{f}_1 = 0 \\ k_2(x_2 - x_1) + d_2(\dot{x}_2 - \dot{x}_1) + m_2 \ddot{x}_2 - \mathrm{f}_2 = 0 \end{aligned} \qquad (2.66)$$

Also it is possible to write the equilibrium of forces in the matrix form:

$$\begin{bmatrix} m_1 & 0 \\ 0 & m_2 \end{bmatrix} \begin{bmatrix} \ddot{x}_1 \\ \ddot{x}_2 \end{bmatrix} + \begin{bmatrix} d_1 + d_2 & -d_2 \\ -d_2 & d_2 \end{bmatrix} \begin{bmatrix} \dot{x}_1 \\ \dot{x}_2 \end{bmatrix} + \begin{bmatrix} k_1 + k_2 & -k_2 \\ -k_2 & k_2 \end{bmatrix} \begin{bmatrix} x_1 \\ x_2 \end{bmatrix} = \begin{bmatrix} \mathrm{f}_1 \\ \mathrm{f}_2 \end{bmatrix} \qquad (2.67)$$

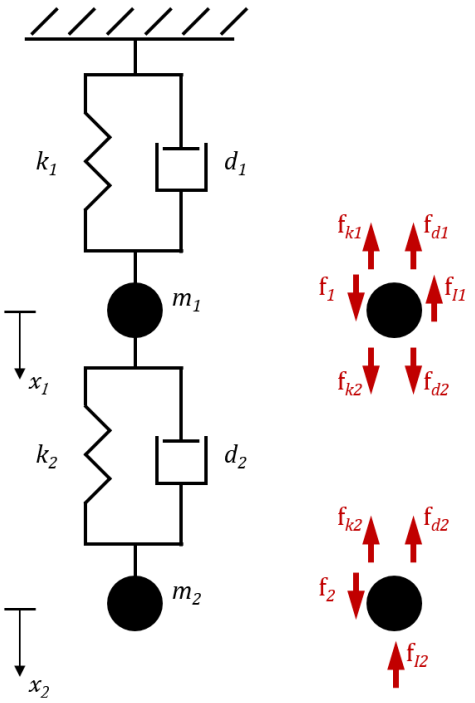

Figure 2.9: Multi-mass oscillator with damping and excitation

The analytical solution of the undamped eigenfrequencies is shown in Eq. (2.68), a detailed derivation can be found in (Gelbert 2007).

$$f_{1,2} = \frac{1}{2\pi} \cdot \sqrt{\frac{\frac{k_1 + k_2}{m_1} + \frac{k_2}{m_2}}{2} \pm \sqrt{\left(\frac{\frac{k_1 + k_2}{m_1} + \frac{k_2}{m_2}}{2}\right)^2 - \frac{k_1 + k_2}{m_1} \cdot \frac{k_2}{m_2} + \frac{k_2^2}{m_1 \cdot m_2}}} \qquad (2.68)$$

Sometimes it is difficult to find an analytical solution for multi-mass systems, so the numerical integration is a further possibility to solve the problem. A detailed explanation of numerical methods is offered in chapter 2.5. (Vöth 2006)

2.4 Definition of Terms

2.4.1 Coupled system

The dissertation looks at coupled systems. (Zienkiewicz et al. 2005) defined a coupled system as an interaction between physical systems. Here the meaning and theoretical foundation of coupled subsystems is explained on basis of a multi-mass oscillator. The multi-mass oscillator with two masses is the simplest coupled system that can be imagined. Furthermore, the multi-mass oscillator can be seen analogous to a complex coupled system with two subsystems. In the following explanations, the effect of damping is neglected, because the regard of damping effects is not necessary to understand the mechanical problem. Let's start with the description of the first subsystem. The subsystem consists of a single-mass oscillator with the mass m_1 and the stiffness k_1. An additional mass m_{U1} is pivot-mounted to the mass m_1 and rotate with the constant rotational frequency Ω_1. The distance between mass m_{U1} and m_1 is l_1. In Eq. (2.69) the differential equation of the subsystem 1 is shown.

$$m_1 \ddot{x}_1 + k_1 x_1 = m_{U1} \cdot l_1 \cdot \Omega_1^2 \cdot sin(\Omega_1 t) \qquad (2.69)$$

The second subsystem consists of the same components as the first subsystem, but the values of the parameters are different. The Eq. (2.70) shows the differential equation of the subsystem 2.

$$m_2\ddot{x}_2 + k_2 x_2 = m_{U2} \cdot l_2 \cdot \Omega_2^2 \cdot sin(\Omega_2 t) \qquad (2.70)$$

Both subsystems are shown in Figure 2.10.

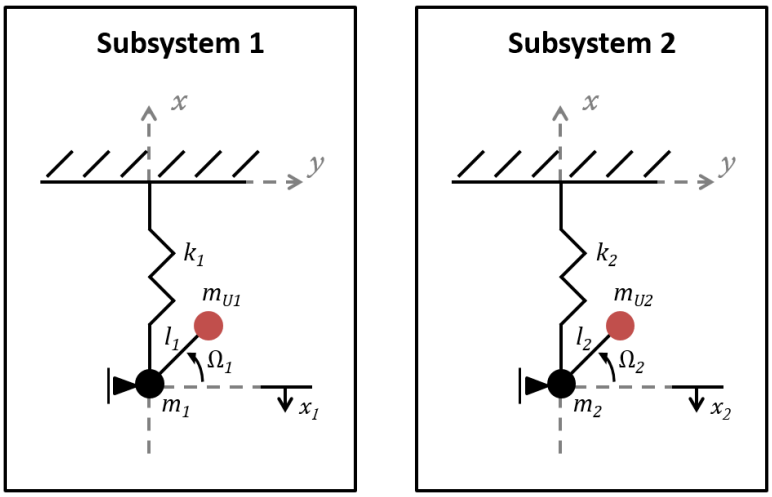

Figure 2.10: Graphical representation of subsystem 1 and 2

On the left side of Figure 2.11 the coupled system is shown, which consists of the two described subsystems. The interaction forces of the coupled system are shown on the right side to derive the differential equation of the coupled system.

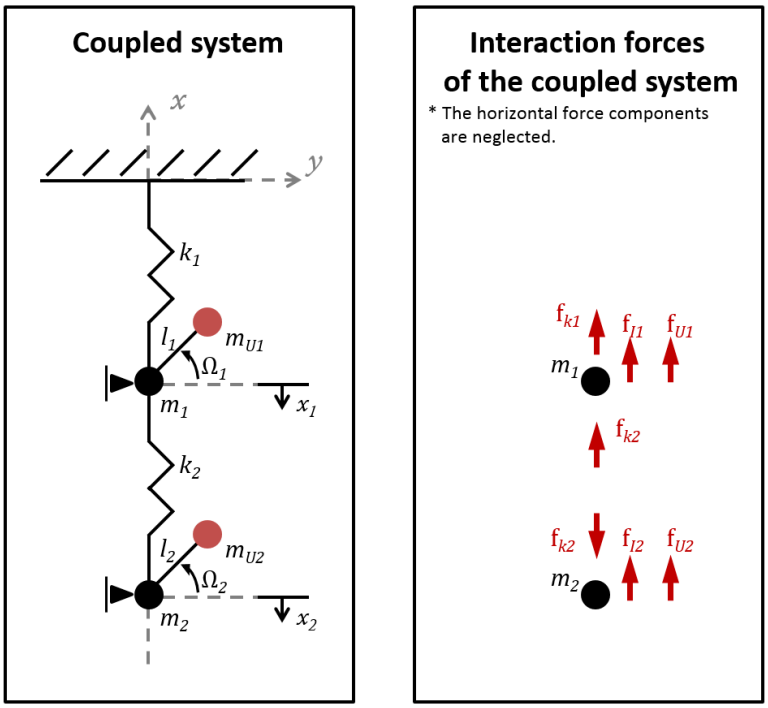

Figure 2.11: Graphical representation of the coupled system

f_{U1} and f_{U2} are the external loads due to the rotating masses m_{U1} and m_{U2}. f_{I1} and f_{I2} describe the inertia forces of the masses m_1 and m_2. f_{k1} and f_{k2} represent the spring forces. Now the equilibrium equations of forces can be build up in Eq. (2.71) and Eq. (2.72).

$$\mathrm{f}_{I1} + \mathrm{f}_{k1} + \mathrm{f}_{k2} = \mathrm{f}_{U1} \qquad (2.71)$$

$$\mathrm{f}_{I2} - \mathrm{f}_{k2} = \mathrm{f}_{U2} \qquad (2.72)$$

The equilibrium equations of forces (Eq. (2.71) and Eq. (2.72)) can also be written by using the masses, stiffness, displacements, accelerations and the parameters for the excitation force.

$$m_1\ddot{x}_1 + k_1x_1 + k_2(x_1 - x_2) = m_{U1} \cdot l_1 \cdot \Omega_1^2 \cdot sin(\Omega_1 t) \qquad (2.73)$$

$$m_2\ddot{x}_2 - k_2(x_1 - x_2) = m_{U2} \cdot l_2 \cdot \Omega_2^2 \cdot sin(\Omega_2 t) \qquad (2.74)$$

Also the equations can be written in matrix form (Eq. (2.75)).

$$\begin{bmatrix} m_1 & 0 \\ 0 & m_2 \end{bmatrix}\begin{bmatrix} \ddot{x}_1 \\ \ddot{x}_2 \end{bmatrix} + \begin{bmatrix} k_1 + k_2 & -k_2 \\ -k_2 & k_2 \end{bmatrix}\begin{bmatrix} x_1 \\ x_2 \end{bmatrix} = \begin{bmatrix} m_{U1} \cdot l_1 \cdot \Omega_1^2 \cdot sin(\Omega_1 t) \\ m_{U2} \cdot l_2 \cdot \Omega_2^2 \cdot sin(\Omega_2 t) \end{bmatrix} \qquad (2.75)$$

Eq. (2.75) shows the structural coupling of two subsystems which is represented by the stiffness matrix with the parameter k_2. A similar coupling situation could be seen in the damping matrix, if damping would have been considered. (Zienkiewicz et al. 2005) distinguishes between a strong coupling and a weak coupling dependent on the degree of interaction, but (Zienkiewicz et al. 2005) does not explain the differentiation in detail.

This thesis differs between the “structural coupling” and the “excitation interaction”. In chapter 4.2.6, there is further differentiation between a strong and weak structural coupling for structural dynamic systems. So there is a strong structural coupling, if the eigenfrequency of the subsystem 1 (which is coupled to the environment) is lower than the eigenfrequency of the subsystem 2 (which is coupled to the subsystem 1). And there is a weak structural coupling, if the eigenfrequency of the subsystem 1 (which is coupled to the environment) is higher than the eigenfrequency of the subsystem 2 (which is coupled to the subsystem 1).

2.4.2 Structural coupling

2.4.2.1 Structural coupling of subsystems

A coupled system can be split up in several subsystems similar to the multi-mass oscillator. Each subsystem has its own structural dynamic behavior. A complex coupled system consists of many subsystems that are coupled to each other with a stiffness factor and damping factor. Many models of complex systems are not fully coupled to save modeling and calculation time. The structural dynamic behavior of a few subsystems can be neglected, because the influence on the total system behavior is very small. But it is not easy to decide, if a subsystem has a significant influence on the total system. In chapter 4.2.6 and 4.2.7, a method for the modeling engineer is described to decide quickly, if a subsystem has a significant influence on the structural dynamic behavior of the total system.

2.4.2.2 Structural coupling of excitation components

Another point is the “structural coupling of excitation components”. This means that the excitation force can be calculated with and without structural coupling to the ambient flexible structure. In Figure 2.12 an example of the two calculations is shown.

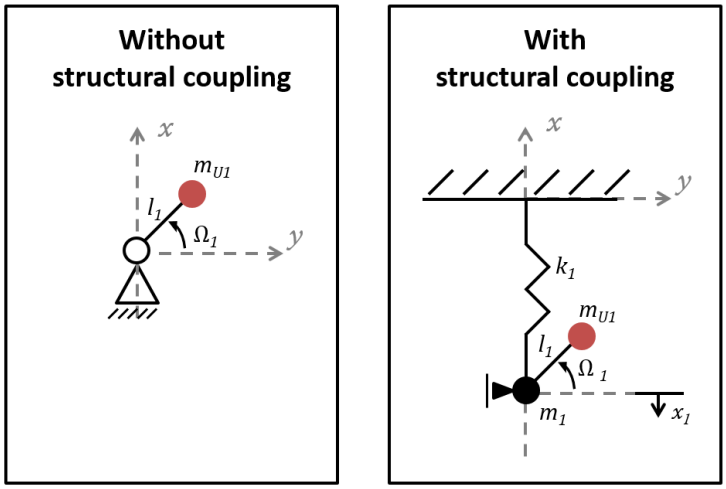

Figure 2.12: Example of structural coupling of excitation components

The difference can be explained by a single-mass oscillator with an additional rotating mass. The left model in Figure 2.12 shows the calculation without structural coupling. The excitation component (rotating mass m_{U1}) is pivot-mounted to the rigid environment. The boundary conditions for the translation x and y are zero and the rotation φ is dependent on the rotational frequency Ω_1. Eq. (2.76) shows the calculation of the force $\mathrm{f}_{U1}(t)$ in x-direction.

$$\mathrm{f}_{U1}(t) = m_{U1} \cdot l_1 \cdot \Omega_1^2 \cdot sin(\Omega_1 t) \qquad (2.76)$$

The model on the right side of Figure 2.12 shows the calculation with structural coupling. The excitation component is pivot-mounted to the single-mass oscillator. So the force calculation regards the structural dynamic behavior of the ambient flexible structure. The boundary condition for the translation x is free and for y is zero. The rotation position φ is dependent on the rotational frequency Ω_1. Eq. (2.77) shows the balance of forces.

$$m_1 \ddot{x}_1 + k_1 x_1 = m_{U1} \cdot l_1 \cdot \Omega_1^2 \cdot sin(\Omega_1 t) \qquad (2.77)$$

After clearance cutting the system, it can be shown that the force $\mathrm{f}_{U1}(t)$ in x-direction for the pivot-mount is

$$\mathrm{f}_{U1}(t) = m_{U1} \cdot l_1 \cdot \Omega_1^2 \cdot sin(\Omega_1 t) - (m_1 + m_{U2})\ddot{x}_1 \,. \qquad (2.78)$$

The force $\mathrm{f}_{U1}(t)$ can also be calculated in frequency domain by using the amplification function of the system. The amplitude of the rotating mass can be calculated by Eq. (2.79) without structural coupling.

$$\mathrm{f}_{U1}(\Omega_1) = m_{U1} \cdot l_1 \cdot \Omega_1^2 \qquad (2.79)$$

The excitation frequency is defined as

$$f_{exc} = \frac{\Omega_1}{2\pi}. \qquad (2.80)$$

The amplification function shows an amplification factor for every excitation frequency. To calculate the force amplitude with regarding the structural coupling, the force amplitude $\mathrm{f}_{U1}(\Omega_1)$ in Eq. (2.79) has to be multiplied by the amplification factor $\Gamma(f_{exc})$ of the excitation frequency.

The force calculation without structural coupling neglects the structural dynamic behavior of the ambient flexible structure and the force $f_{U1}(t)$ only contains the structural dynamic behavior of the excitation component. The calculation with structural coupling considers the structural dynamic behavior of the ambient flexible structure with the excitation component. So the force $f_{U1}(t)$ contains the force multiplied by the amplification factor of the amplification function. Therefore, the calculated forces of both methods show the same frequency but different amplitudes. So the engineer has to decide, if the ambient flexible structure influences the excitation force and the operational vibration of the system significantly.

2.4.3 Excitation interaction

"Excitation interaction" means the influence of one excitation to another excitation. The example in Figure 2.13 shows both force calculations.

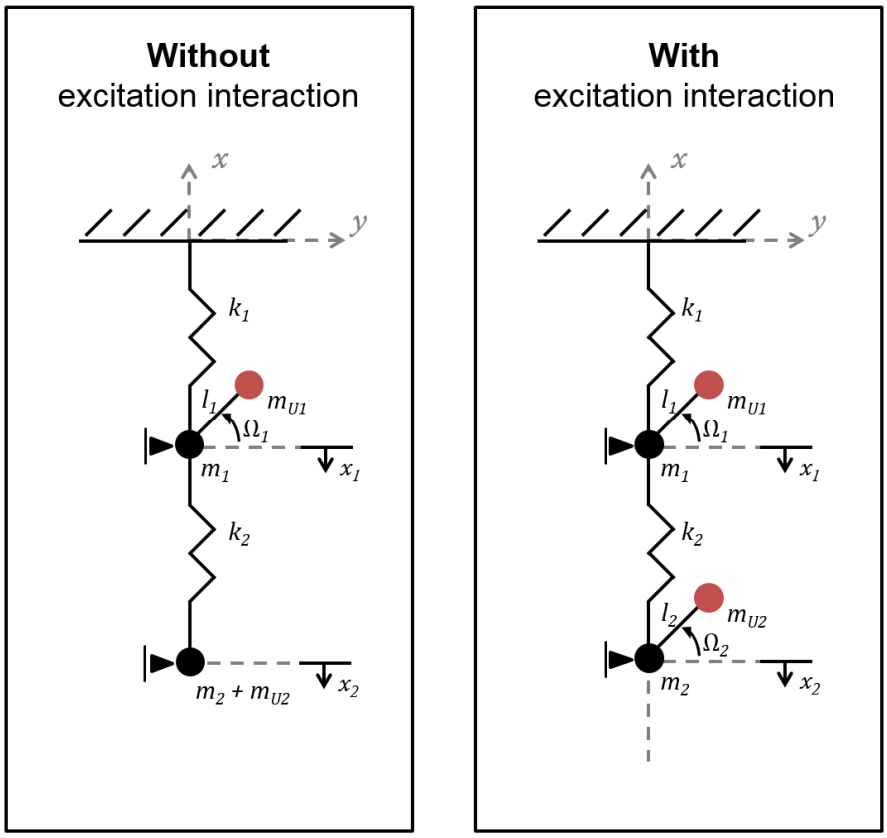

Figure 2.13: Comparison of calculation method with and without excitation interaction

The left model in Figure 2.13 shows the force calculation without excitation interaction. So the force $\mathrm{f}_1(t)$ in the pivot-mounting of mass m_1 can be seen in the first row of the right side in Eq. (2.81).

$$\begin{bmatrix} m_1 & 0 \\ 0 & m_2 + m_{U2} \end{bmatrix} \begin{bmatrix} \ddot{x}_1 \\ \ddot{x}_2 \end{bmatrix} + \begin{bmatrix} k_1 + k_2 & -k_2 \\ -k_2 & k_2 \end{bmatrix} \begin{bmatrix} x_1 \\ x_2 \end{bmatrix} = \begin{bmatrix} m_{U1} \cdot \Omega_1^2 \cdot l_1 \cdot sin(\Omega_1 t) - m_{U1} \ddot{x}_1 \\ 0 \end{bmatrix} \quad (2.81)$$

The right model in Figure 2.13 shows the calculation with excitation interaction. So the force $\mathrm{f}_1(t)$ in the pivot-mounting of mass m_1 can be seen in the first row of the right side in Eq. (2.82). The second row of the right side represents the force $\mathrm{f}_2(t)$ in the pivot-mounting of mass m_2.

$$\begin{bmatrix} m_1 & 0 \\ 0 & m_2 \end{bmatrix} \begin{bmatrix} \ddot{x}_1 \\ \ddot{x}_2 \end{bmatrix} + \begin{bmatrix} k_1 + k_2 & -k_2 \\ -k_2 & k_2 \end{bmatrix} \begin{bmatrix} x_1 \\ x_2 \end{bmatrix} = \begin{bmatrix} m_{U1} \cdot \Omega_1^2 \cdot l_1 \cdot sin(\Omega_1 t) - m_{U1} \ddot{x}_1 \\ m_{U2} \cdot \Omega_2^2 \cdot l_2 \cdot sin(\Omega_2 t) - m_{U2} \ddot{x}_2 \end{bmatrix} \quad (2.82)$$

At the first view the equation of the pivot-mounting force $\mathrm{f}_1(t)$ seems the same as in Eq. (2.81).

$$\mathrm{f}_1(t) = m_{U1} \cdot l_1 \cdot \Omega_1^2 \cdot sin(\Omega_1 t) - m_1 \ddot{x}_1 \quad (2.83)$$

The difference of the calculated forces is the value of acceleration $\ddot{x}_1$, because the acceleration is the second differentiation of the displacement and the displacements of the masses are coupled by the stiffness k_2. The influence of the excitation interaction can also be explained in frequency domain. The matrix $\boldsymbol{\Gamma}$ in Eq. (2.84) describes the structural dynamic behavior of the system in frequency domain. The amplification factors have to be multiplied by the force amplitudes without structural coupling.

$$\begin{bmatrix} \mathrm{f}_1(f) \\ \mathrm{f}_2(f) \end{bmatrix} = \begin{bmatrix} \Gamma_{11}(f) & \Gamma_{12}(f) \\ \Gamma_{21}(f) & \Gamma_{22}(f) \end{bmatrix} \begin{bmatrix} \mathrm{f}_{U1}(f_{exc,U1}) \\ \mathrm{f}_{U2}(f_{exc,U2}) \end{bmatrix} \quad (2.84)$$

Let's compare the force $\mathrm{f}_1(f)$ calculated without excitation interaction and with excitation interaction. Eq. (2.85) shows the calculation with excitation interaction.

$$\mathrm{f}_1(f) = \Gamma_{11}(f_{exc,U1})\mathrm{f}_{U1}(f_{exc,U1}) + \Gamma_{12}(f_{exc,U2})\mathrm{f}_{U2}(f_{exc,U2}) \quad (2.85)$$

And Eq. (2.86) shows the calculation without excitation interaction. Without excitation interaction the second excitation force $\mathrm{f}_{U2}(f_{exc,U2})$ is zero and the pivot-mounting force $\mathrm{f}_1(f)$ only consists of the amplitude and frequency of the first excitation force $\mathrm{f}_{U1}(f_{exc,U1})$.

$$\mathrm{f}_1(f) = \Gamma_{11}(f_{exc,U1})\mathrm{f}_{U1}(f_{exc,U1}) + \Gamma_{12}(f_{exc,U2}) \cdot 0 \quad (2.86)$$

This effect is represented in Figure 2.14. The black curve displays the force $\mathrm{f}_1(f)$ without excitation interaction and the blue dashed curve displays the force $\mathrm{f}_1(f)$ with excitation interaction. So there can be seen that the black line consists of one harmonic excitation force ($\mathrm{f}_{U1}(t)$) and the blue dashed line consists of two harmonic (periodic) excitation forces ($\mathrm{f}_{U1}(t)$ and $\mathrm{f}_{U2}(t)$).

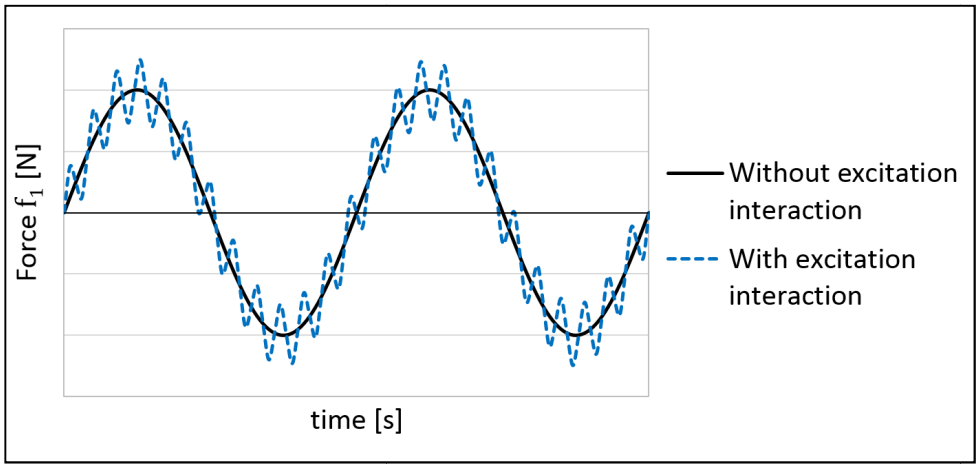

Figure 2.14: Comparison of calculated forces with and without excitation interaction

If both excitation forces contain the same frequency, the amplitudes of the forces are influenced by the excitation interaction. The direction and the height of the effect are dependent on the phase shift between the excitation forces. Figure 2.15 shows the amplitude effect of excitation interaction at a phase shift of $\frac{\pi}{2}$. So the black curve shows the first excitation force with structural coupling. The blue dashed curve represents the force in the pivot-mounting of mass m_1 that referring to the second excitation. The total force f_1 in the pivot-mounting of mass m_1 is the addition of both force components which is represented by the green dotted curve. The diagram shows that the total force amplitude rise and the frequency content stays the same.

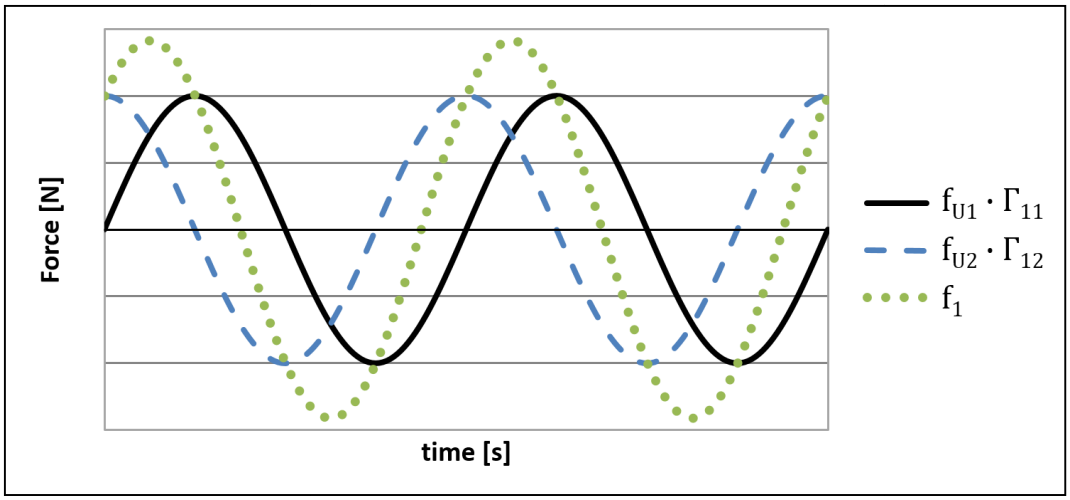

Figure 2.15: Example of the amplitude effect of excitation interaction at a phase shift of $\frac{\pi}{2}$

The maximum of the total amplitude exists at a phase shift of zero. In Figure 2.16 an example is shown of a phase shift of zero between the two force components.

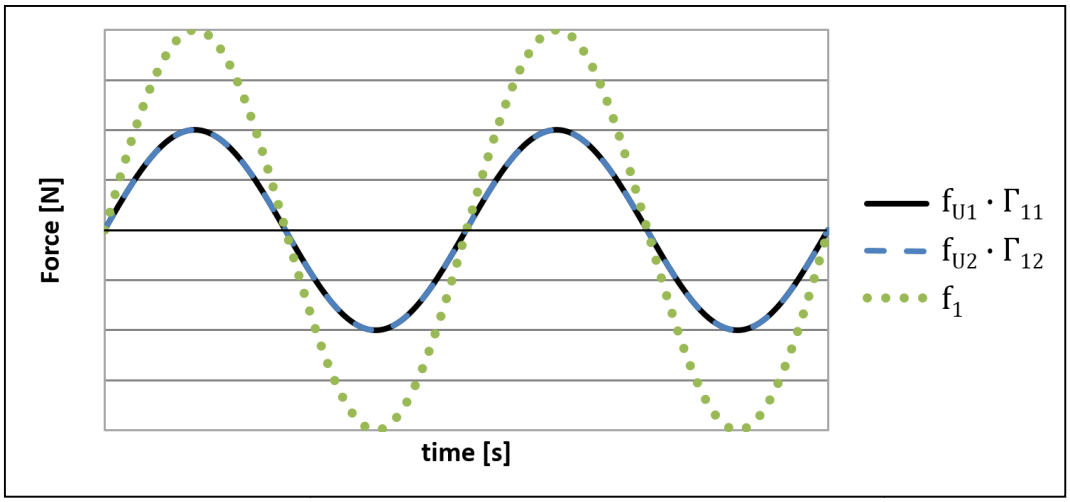

Figure 2.16: Example of the amplitude effect of excitation interaction at a phase shift of 0

But the effect can also be used to minimize the total force in the mounting. In Figure 2.17 the amplitude effect is shown at a phase shift of π. If the amplitudes of the force components are equal, the total force f_1 is eliminated.

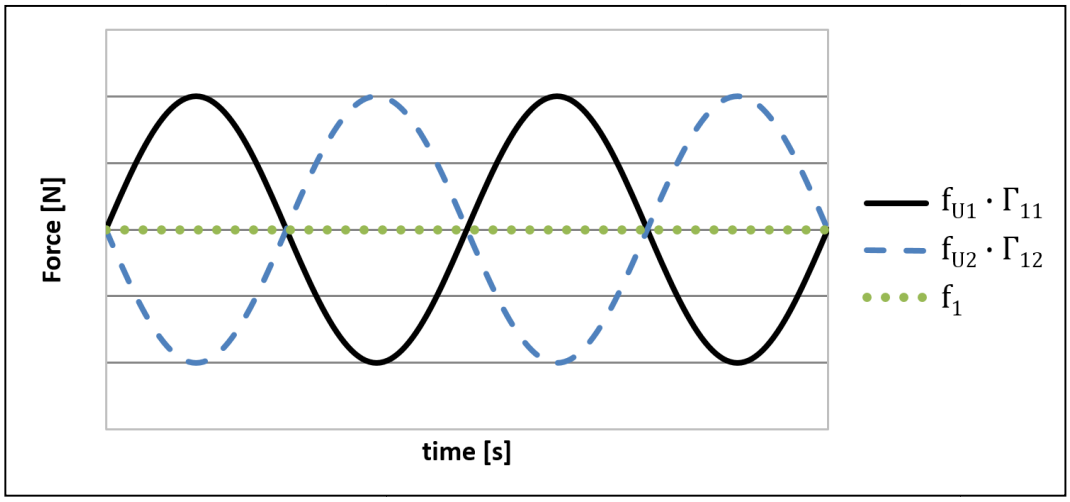

Figure 2.17: Example of the amplitude effect of excitation interaction at a phase shift of π

2.4.4 Efficient abstraction level

The term “efficient” is defined as “effectively and economically”. It is a very important factor for the usability of methods in the industrial environment. An efficient abstraction level is a compromise between **accuracy of results**, **processing time** and **computer memory space** which is necessary to calculate and analyze the results.

The **accuracy of results** represents the deviation to a reference model. The measurement of the accuracy depends on the task formulation. This dissertation is focused on operational vibrations, so the deviation criteria for the accuracy are defined as the amplitude and frequency of selected measurement points. The reference model is defined as the model with the lowest abstraction level, because this model contains the most physical effects of the regarded models in this thesis. Results of a physical experiment are also able to use as reference, but the experimental measurements are often very expensive.

The **processing time** is not only the calculation time of a calculation model. It is important to look at the whole working process to get a result. A typical flowchart of a calculation is shown in Figure 2.18, following (Klein 2010). In the first step “Idealization”, it is important to analyze the problem and to define the aim of the calculation. The second step “Preprocessing” is one of the time-consuming steps for

the engineer. He or she has to build up the model with all boundaries and load conditions. Now the model can be calculated by the computer, whose time duration is dependent on the computer performance. In the next step “Postprocessing”, the calculated results have to be worked up and shown. The last step is for checking the plausibility of the results. Here the numerical results can be compared with an analytical calculation, measurements, or experience.

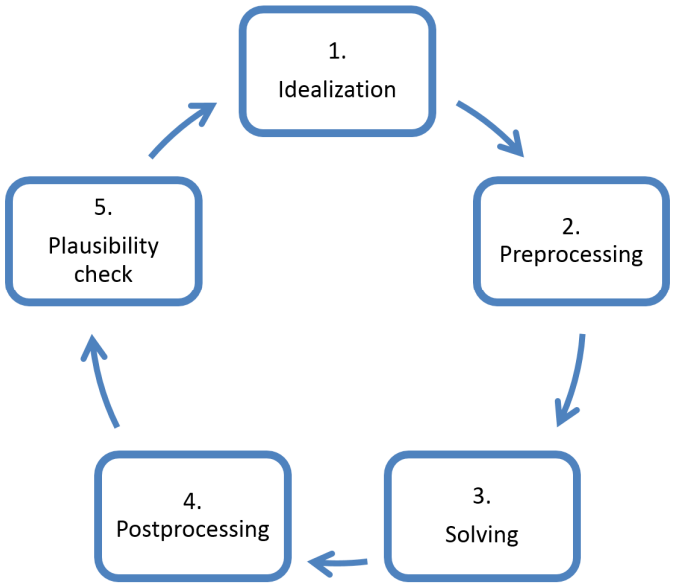

Figure 2.18: Flowchart of a simulation based on (Klein 2010)

The necessary **computer memory space** is dependent on the amount of output values. This criterion was very important in the past, because of the high costs of memory space. Of course, there are limits of memory space till today, but it should not be a hard criterion. So the costs of memory space are substantially lower today.

This dissertation focuses on the time of preprocessing $t_{preprocessing}$ and solving the equations $t_{solving}$ as well as the accuracy of results $p_{accuracy}$. So the term “efficient” is defined as the relation between the processing time and accuracy of results in this thesis

$$H_{efficient} = \frac{p_{accuracy}}{t_{preprocessing} + t_{solving}}. \qquad (2.87)$$

An efficient abstraction level saves calculation time and offers simultaneous engineering to build up calculation models. The results of the calculation should be

accurate enough to achieve the defined aim at the same time. This dissertation shows criteria to create an abstraction level for different stages of the development process. The method can be used for every technical product development process. An automotive engine is the preferred example in this work.

2.5 Different solution processes

2.5.1 Overview

Different solution processes are used in different development areas like structural mechanics, acoustics, fluid mechanics, and many other engineering fields. Also there are different solution processes in the different development stages like concept phase, design phase and series development phase.

The solution processes can be split up in two main groups, the analytical and the numerical solution processes. The analytical solution processes calculate the exact solution by solving the differential equation. Analytical methods are fast methods to calculate forces, displacements, stresses and so on in the practical use of the product development. There are two analytical methods to differ, the static definite and the static indefinite calculation. In this dissertation, the analytical methods are not described in more detail, because it is not the core of the work. But there are a lot of literatures for both analytical methods. For example, the methods are explained in (Mayr 2002), (Krätzig et al. 2010), and (Krätzig et al. 2014). In the concept phase of a product design process, the analytical methods are very useful, because the models can be build up very quickly and the calculation is very fast. So it is possible to have a look at the principal character of a system. Another application is to check the plausibility of numerical simulations. This is necessary, because the numerical simulations are very complex and the modeling process is error-prone.

For complex problems it is very difficult to build up the differential equation and solve it with analytical methods. So the numerical methods can be used to approximate the exact solution of the differential equation. In the industrial environment, the analytical

methods are used for simple problems like movements of rigid bodies or deformations of two-dimensional beams. For such simple problems the analytical methods are very fast. The numerical methods are used to calculate complex problems like movement of flexible bodies or deformations of three-dimensional bodies. The use of numerical methods is more complex than the use of analytical methods. A numerical model needs more time to build up and to calculate. At first it is important to choose a suitable numerical method for the observed result. To do this, we have to know a good overview about different numerical methods. There are a lot of different numerical methods, so we will only describe the well-known methods like the Finite Element Method (FEM), Multi Body System (MBS), Boundary Element Method (BEM), Finite Difference Method (FDM), and Finite Volume Method (FVM).

The FEM is used in a lot of engineering tasks and is established in mechanical engineering. In the following chapter, the FEM is explained in more detail.

In some tasks the BEM can be used instead of FEM. So it is possible to simulate the noise emission with a minimum number of Degree Of Freedom (DOF). In (Gaul and Fiedler 2013) the BEM is described.

The Multi Body System method (MBS) is specialized to calculate motions of bodies and is often used to get excitation forces. The MBS is explained in (Woernle 2011), (Rill and Schaeffer 2014), (Schiehlen 1990), and (Schwertassek and Wallrapp 1999).

The Finite Difference Method (FDM) can be used for problems in the process technology, for example. In (Smith 1985) the FDM is illuminated in detail.

The Finite Volume Method (FVM) is based on the balance equations and is usually used in the field of fluid mechanics. In (Versteeg and Malalasekera 2007) the FVM is explained in detail.

2.5.2 Continuum systems

Although the dissertation focuses on discrete models, the results can be also used by application of continuum systems. Furthermore, the most discrete models are derived

from continuum systems, so this chapter explains the basics for the derivation of modeling discrete models.

2.5.2.1 Continuum formulation

The basic knowledge about the fundamentals of continuum mechanics is necessary to understand the numerical methods in the following chapters. The geometrical definitions are referred to a Cartesian coordinate system.

The continuum mechanics is a part of structural mechanics. It focuses on the movement of deformable bodies due to external loads. In (Altenbach 2012), (Jog 2002), and (Ottosen and Ristinmaa 2005) the fundamentals of continuum mechanics and the constitutive modeling is explained in detail. A technical structure exists of material points. Each point is defined by their position vector in the reference configuration

$$\mathbf{X} = X_i \mathbf{e}_i \tag{2.88}$$

or by their position vector in the deformed configuration

$$\mathbf{x} = x_i \mathbf{e}_i \, . \tag{2.89}$$

The subtraction of the two position vectors shows the displacement vector for each material point.

$$\mathbf{u} = \mathbf{x} - \mathbf{X} \tag{2.90}$$

Figure 2.19 shows the kinematic relationship of the reference configuration B_0 and the deformed configuration B_t. B_0 shows the material point at the time $t = 0$. B_t shows the same material point of the body at the time $t = t$. The Lagrangian description of the motion describes the material points as a function of the reference coordinates.

$$\mathbf{x} = \phi(\mathbf{X}, t) \tag{2.91}$$

The Lagrangian description is mostly used in solid mechanics.

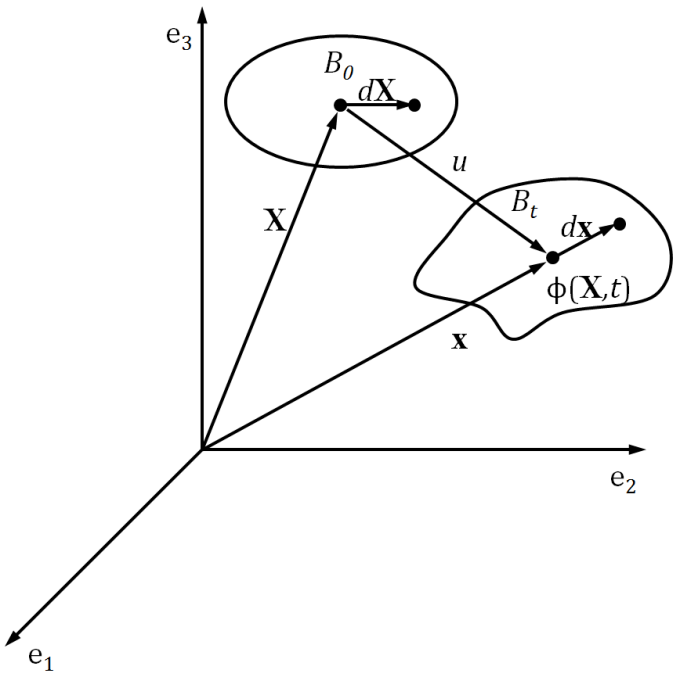

Figure 2.19: Kinematic relationship between reference configuration B_0 and deformed configuration B_t

The deformation gradient

$$\operatorname{grad}\mathbf{x} = \mathbf{F} = \frac{\partial \mathbf{x}}{\partial \mathbf{X}} \qquad (2.92)$$

is an asymmetric tensor of second order and describes the deformation of a differential line element. So the deformation gradient $\mathbf{F}$ considers the rigid body motions and the deformation. By using the orthogonal rotation tensor $\mathbf{R}$ and the symmetric material right stretch tensor $\mathbf{U}$, the deformation gradient $\mathbf{F}$ can be decomposed.

$$\mathbf{F} = \mathbf{R}\,\mathbf{U} \qquad (2.93)$$

This decomposition is called a right polar decomposition. The left polar decomposition is possible by using the symmetric spatial left stretch tensor $\mathbf{V}$ and the orthogonal rotation tensor $\mathbf{R}$.

$$\mathbf{F} = \mathbf{V}\,\mathbf{R} \qquad (2.94)$$

To show exclusively the deformation, the Green-Lagrangian strain tensor $\mathbf{G}$ in Eq. (2.95) can be used.

$$\mathbf{G} = \frac{1}{2}(\mathbf{C} - \mathbf{1}) \qquad (2.95)$$

The Cauchy-Green tensor $\mathbf{C}$ is defined as

$$\mathbf{C} = \mathbf{F}^T\mathbf{F}\,. \qquad (2.96)$$

By using the Eq. (2.97) and Eq. (2.98) the absolute elongation can be calculated in Eq. (2.99).

$$ds^2 = d\boldsymbol{x}^T d\mathbf{x} \qquad (2.97)$$

$$dS^2 = d\mathbf{X}^T d\mathbf{X} \qquad (2.98)$$

$$\begin{aligned} ds^2 - dS^2 &= d\mathbf{x}^T d\mathbf{x} - d\mathbf{X}^T d\mathbf{X} \\ &= d\mathbf{X}^T \mathbf{C}\, d\mathbf{X} - d\mathbf{X}^T d\mathbf{X} \\ &= d\mathbf{X}^T (\mathbf{C} - \mathbf{1}) d\mathbf{X} \\ &= d\mathbf{X}^T 2\mathbf{G}\, d\mathbf{X} \end{aligned} \qquad (2.99)$$

Following the first Piola-Kirchhoff stress tensor is explained based on the Cauchy stress formula. The Eq. (2.100) shows the integral of the stress $\mathbf{t}$ over the surface s to calculate the force $\mathbf{f}_t$ on the surface s.

$$\begin{aligned} \mathbf{f}_t &= \int_s \mathbf{t}(\mathbf{x}, t, \mathbf{n}) ds \\ &= \int_s \mathbf{T}\mathbf{n} ds \\ &= \int_s \mathbf{T} ds \end{aligned} \qquad (2.100)$$

Figure 2.20 helps to understand the notation of Eq. (2.100) and shows the deformed configuration with the surface s and the stress $\mathbf{t}$. The multiplication of the symmetric Cauchy stress tensor $\mathbf{T}$ and the normal vector $\mathbf{n}$ to the surface s_t ensure the resulting force $\mathbf{f}_t$.

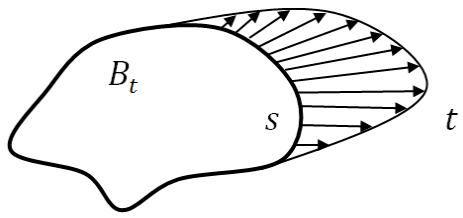

Figure 2.20: Stress at the surface of the deformed configuration

By using the transformation of the infinitesimal surface element

$$ds = \det(\mathbf{F})\,(\mathbf{F}^T)^{-1} dS \qquad (2.101)$$

the Eq. (2.100) can be written as

$$\mathbf{f}_t = \int_s \det(\mathbf{F})\ \mathbf{T}\,(\mathbf{F}^T)^{-1}\, dS. \qquad (2.102)$$

So the first Piola-Kirchhoff stress tensor is defined in Eq. (2.103).

$$\mathbf{P} = \det(\mathbf{F})\ \mathbf{T}\,(\mathbf{F}^T)^{-1} \qquad (2.103)$$

The second Piola-Kirchhoff stress tensor or energy conjugate stress tensor $\mathbf{S}$ is defined as

$$\mathbf{S} = \mathbf{F}^{-1}\,\mathbf{P}\,. \qquad (2.104)$$

The Hooke's law of linear elastic materials in Eq. (2.105) shows the relationship between the Green-Lagrangian strain tensor $\mathbf{G}$ and the energy conjugate stress tensor $\mathbf{S}$ by using the elasticity tensor $\mathbb{C}$.

$$\mathbf{S} = \mathbb{C}\,\mathbf{G} \qquad (2.105)$$

For small strain the linearized strain tensor $\boldsymbol{\epsilon}$ can be used. The linearized strain tensor $\boldsymbol{\epsilon}$ in Eq. (2.106) results from the linearization of the Green-Lagrangian strain tensor $\mathbf{G}$.

$$\epsilon_{ij} = \frac{1}{2}\left(\frac{\partial u_i}{\partial X_j} + \frac{\partial u_j}{\partial X_i}\right) \qquad (2.106)$$

The linearized stress tensor $\boldsymbol{\sigma}$ results from the multiplication of the elastic constitutive matrix $\mathbf{E}$ and the linearized strain tensor $\boldsymbol{\epsilon}$.

$$\boldsymbol{\sigma} = \mathbf{E}\,\boldsymbol{\epsilon} \qquad (2.107)$$

In this thesis are only used isotropic material definitions. So the constitutive matrix $\mathbf{E}$ of an isotropic material with the Young's modulus E and the Poisson ratio ν is shown in Eq. (2.108).

$$\mathbf{E} = \frac{E}{(1+\nu)(1-2\nu)} \begin{bmatrix} 1-\nu & \nu & \nu & & & \\ \nu & 1-\nu & \nu & & \mathbf{0} & \\ \nu & \nu & 1-\nu & & & \\ & & & \frac{1-2\nu}{2} & 0 & 0 \\ & \mathbf{0} & & 0 & \frac{1-2\nu}{2} & 0 \\ & & & 0 & 0 & \frac{1-2\nu}{2} \end{bmatrix} \quad (2.108)$$

By using the constitutive matrix and the assumption of small strains, the theory of continuum oscillations is explained in the following section.

2.5.2.2 Continuum oscillations

The following descriptions and derivations are based on (Waller and Schmidt 1989). Further introductions into continuum oscillations can be found in (Wauer 2008) and (Magnus et al. 2013).

Continuum oscillators can be described by partial differential equations in contrast to discrete oscillators which can be described by ordinary differential equations. There are two widely-used procedures to generate ordinary differential equations from a partial differential equation, so it can be solved. The first opportunity is to find solution approaches to solve the equation with an analytical method. The second opportunity is to model the continuum system by using a physical analogous model, difference equations or finite elements. Here we will describe the continuum formulation for a dynamic/compression tension rod by neglecting damping effects. The differential equation of a continuum oscillator can be derived by using the basic equations of mechanics. Figure 2.21 shows the tension rod excited by a time-depending load.

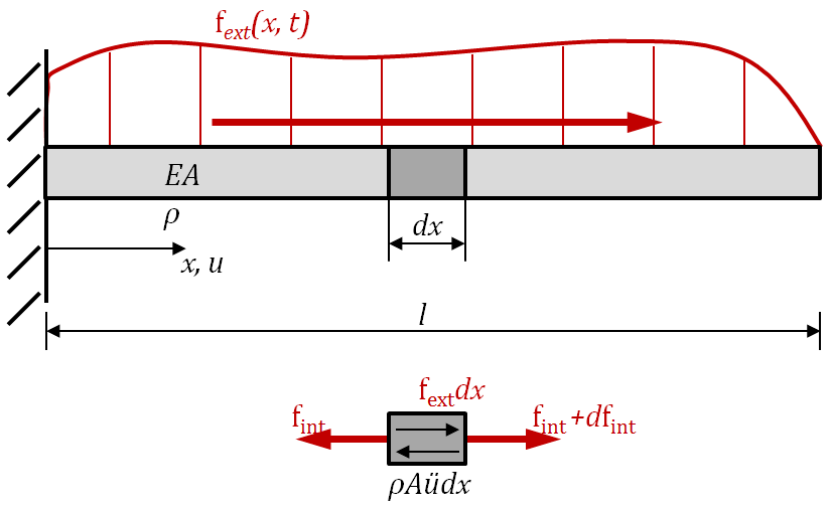

Figure 2.21: Tension rod excited by a time depending load based on (Waller and Schmidt 1989)

Mathematical derivations over the time t are marked by a point and derivations of change in position x are marked by a dash. The equation of forces is shown in Eq. (2.109).

$$\mathrm{f}_{int} + d\mathrm{f}_{int} - \mathrm{f}_{int} - \rho A dx\ddot{u} + \mathrm{f}_{ext}(x,t)dx = 0 \qquad (2.109)$$

ρ represents the material density, A is the cross section of the rod, f_{int} is the internal axial force and u is used for the displacement.

To generate the differential equation, it is necessary to define some additional conditions:

- Hooke's material law:

$$\sigma = E\,\epsilon \qquad (2.110)$$

- Compatibility condition:

$$\epsilon = u' = \frac{du}{dx} \qquad (2.111)$$

So the differential equation (2.112) can be expressed for $EA = constant$.

$$\rho\ddot{u} - Eu'' = \frac{\mathrm{f}_{ext}(x,t)}{A} \qquad (2.112)$$

The differential equation (2.112) for the tension rod has the form of the general wave equation. (Also a torsion rod can be described by the general wave equation.) The partial differential equation

$$\rho\ddot{u} - Eu'' = 0 \qquad (2.113)$$

can be solved by the approach (2.114).

$$u = \phi(x + \omega t) = \phi(w) \qquad (2.114)$$

With the second derivative with respect to time t in Eq. (2.115)

$$\ddot{u} = \frac{\mathrm{d}^2\phi}{\mathrm{dw}^2}\omega^2 \qquad (2.115)$$

and the second derivative with respect to space x in Eq. (2.116)

$$u'' = \frac{\mathrm{d}^2\phi}{\mathrm{dw}^2} \qquad (2.116)$$

the differential equation can be written as

$$\rho\omega^2\frac{\mathrm{d}^2\phi}{\mathrm{dw}^2} - E\frac{\mathrm{d}^2\phi}{\mathrm{dw}^2} = 0. \qquad (2.117)$$

Multiplied by $\frac{\mathrm{dw}^2}{\mathrm{d}^2\phi}$, the Eq. (2.118)

$$\rho\omega^2 - E = 0 \qquad (2.118)$$

lead to the eigen angular frequency ω in Eq. (2.119).

$$\omega = \pm\sqrt{\frac{E}{\rho}} \qquad (2.119)$$

Therefore, the solution of the general wave equation for the displacement u is

$$u = \phi_1(x + \omega t) + \phi_2(x - \omega t). \qquad (2.120)$$

By using the initial conditions $u(x,0) = u_0$ and $\dot{u}(x,0) = \dot{u}_0$,

$$u_0 = \phi_1(x) + \phi_2(x) \qquad (2.121)$$

$$\dot{u}_0 = \omega\left(\frac{\mathrm{d}\phi_1}{dw} - \frac{\mathrm{d}\phi_2}{dw}\right) \qquad (2.122)$$

the form function ϕ_1 and ϕ_2 can be assigned:

$$\phi_1(x) = \frac{1}{2}u_0 + \frac{1}{2\omega}\int_{x_1}^{x_2} \dot{u}_0 dx \qquad (2.123)$$

$$\phi_2(x) = \frac{1}{2}u_0 - \frac{1}{2\omega}\int_{x_1}^{x_2} \dot{u}_0 dx\,. \qquad (2.124)$$

2.5.3 Finite Element Method

In many situations the engineer wants to solve a physical problem by using the Finite Element Method (FEM). But the FEM cannot solve the physical problem. The FEM is a numerical approximation procedure to solve a mathematical model by element-wise discretization. So the engineer's task is to idealize the physical problem to get a mathematical model. A detailed explanation of the FEM and examples to engineering problems are also published in (Bathe 1996), (Klein 2010), and (Hughes 2000).

2.5.3.1 Fundamentals of the Finite Element Method

By using the following equations the structural dynamic behavior of a mechanical system can be described for linear elastic continuums $B \in R^3$.

Let's start with the equilibrium equation (2.125), which uses the differential operator $\mathbf{D}_e$ in B to describe the relationship between the internal forces $\boldsymbol{\sigma}$ and external forces $\mathbf{f}_{ext}$.

$$\mathbf{D}_e\boldsymbol{\sigma} + \mathbf{f}_{ext} = \mathbf{0} \qquad (2.125)$$

The kinematic equation (2.126), which uses the differential operator $\mathbf{D}_k$ in B to describe the relationship between internal displacements $\boldsymbol{\epsilon}$ and external displacements $\mathbf{u}$.

$$\boldsymbol{\epsilon} = \mathbf{D}_k \, \mathbf{u} \tag{2.126}$$

The constitutive law (2.127), which uses the constitutive matrix $\mathbf{E}$ in B to describe the relationship between the internal forces $\boldsymbol{\sigma}$ and internal displacements $\boldsymbol{\epsilon}$.

$$\boldsymbol{\sigma} = \mathbf{E} \, \boldsymbol{\epsilon} \tag{2.127}$$

The kinematic boundary conditions (2.128) describe the prescribed displacements $\mathbf{u}_S$ on the Dirichlet boundary surface S^u.

$$\mathbf{u} = \mathbf{u}_S \tag{2.128}$$

The static boundary conditions (2.129) describe the prescribed traction $\mathbf{t}_S$ on the Neumann boundary surface S^t.

$$\mathbf{t} = \mathbf{t}_S \tag{2.129}$$

It is necessary that the boundary surface is conform to the conditions in (2.130) and (2.131).

$$S^u \cap S^t = \emptyset \tag{2.130}$$

$$S = S^u \cup S^t \tag{2.131}$$

Now let's have a look at the energy law of mechanics shown in Eq. (2.132).

$$W = \int_B \mathbf{u}^T \mathbf{f}_{ext} dB + \int_{S^t} \mathbf{u}^T \mathbf{t}_s dS^t - \int_B \boldsymbol{\epsilon}^T \boldsymbol{\sigma} dB = 0 \tag{2.132}$$

It describes the equilibrium of the internal energy, external energy and boundary surface energy. Generally, an external loaded elastic body is at equilibrium, if the external work (2.133) is equal to the internal work (2.134).

$$W_{ext} = \int_B \mathbf{u}^T \mathbf{f}_{ext} dB + \int_{S^t} \mathbf{u}^T \mathbf{t}_s dS^t \tag{2.133}$$

$$W_{int} = \int_B \boldsymbol{\epsilon}^T \boldsymbol{\sigma} dB \tag{2.134}$$

To get the weak form of the equilibrium (2.137), the virtual displacements $\partial\mathbf{u}$ can be used. So the Eq. (2.135) and Eq. (2.136) show the varied displacements and strains.

$$\mathbf{u} = \bar{\mathbf{u}} + \partial\mathbf{u} \tag{2.135}$$

$$\boldsymbol{\epsilon} = \mathbf{D}_k\,(\bar{\mathbf{u}} + \partial\mathbf{u}) = \bar{\boldsymbol{\epsilon}} + \partial\boldsymbol{\epsilon} \tag{2.136}$$

$$\partial W = \int_B \partial\mathbf{u}^T \mathbf{f}_{ext} dB + \int_{S^t} \partial\mathbf{u}^T \mathbf{t}_s dS^t - \int_B \partial\boldsymbol{\epsilon}^T \boldsymbol{\sigma} dB = 0 \tag{2.137}$$

So the external displacements are the independent variables. Thereby, the computer can solve the equation of the continuum, the displacements has to be discretizised. So the displacement of a material point is defined as a displacement of a discrete node by the help of a shape function.

$$\mathbf{u}_e = \mathbf{N}_e\,\tilde{\mathbf{u}}_e \tag{2.138}$$

The matrix of shape functions $\mathbf{N}_e$interpolates the displacements $\mathbf{u}_e$ in an element e from the nodal degrees of freedom $\tilde{\mathbf{u}}_e$. Every shape function has the value 1 at the associated node and the shape function value is zero at each other node. To get the element strain, the Eq. (2.138) has introduced into Eq. (2.126). The Eq. (2.140) shows the element strain tensor $\boldsymbol{\epsilon}_e$ with the strain-displacement matrix

$$\mathbf{B}_e = \mathbf{D}_k\mathbf{N}_e. \tag{2.139}$$

$$\boldsymbol{\epsilon}_e = \mathbf{B}_e\,\tilde{\mathbf{u}}_e \tag{2.140}$$

Eq. (2.141) and Eq. (2.142) shows the equations of displacement and strain after applying the variation of displacement.

$$\partial\mathbf{u}_e = \mathbf{N}_e\,\partial\tilde{\mathbf{u}}_e \tag{2.141}$$

$$\partial\boldsymbol{\epsilon}_e = \mathbf{B}_e\,\partial\tilde{\mathbf{u}}_e \tag{2.142}$$

Now the discrete formulation of the principle of virtual displacements can be generated for one element by introducing Eq. (2.141) and Eq. (2.142) into the weak form of the equilibrium (2.137)

$$\int_B \partial\tilde{\mathbf{u}}_e^T\,\mathbf{N}_e^T\,\mathbf{f}_{ext}\,dB_e + \int_{S^t} \partial\tilde{\mathbf{u}}_e^T\,\mathbf{N}_e^T\,\mathbf{t}_s\,dS_e^t - \int_B \partial\tilde{\mathbf{u}}_e^T\,\mathbf{B}_e^T\,\mathbf{E}\,\mathbf{B}_e\,\tilde{\mathbf{u}}_e\,dB_e = 0. \tag{2.143}$$

Given that the virtual nodal displacement $\partial\tilde{\mathbf{u}}_e^T$ is an independent arbitrary displacement, so it is not affected by the integrals and the Eq. (2.143) can be reduced.

$$\int_B \mathbf{N}_e^T \, \mathbf{f}_{ext} dB_e + \int_{S^t} \mathbf{N}_e^T \, \mathbf{t}_s \, dS_e^t - \int_B \mathbf{B}_e^T \, \mathbf{E} \, \mathbf{B}_e \, dB_e \cdot \tilde{\mathbf{u}}_e = 0 \qquad (2.144)$$

The integrals of the external work of Eq. (2.144) can be defined as the local element load vector

$$\mathbf{f}_e = \int_B \mathbf{N}_e^T \, \mathbf{f}_{ext} \, dB_e + \int_{S^t} \mathbf{N}_e^T \, \mathbf{t}_s \, dS_e^t. \qquad (2.145)$$

And the integral of the internal work of Eq. (2.144) can be defined as the local element stiffness matrix

$$\mathbf{k}_e = \int_B \mathbf{B}_e^T \, \mathbf{E} \, \mathbf{B}_e \, dB_e. \qquad (2.146)$$

Now the discrete equilibrium formulation can be generated by a simple element-stiffness relationship, as shown in Eq. (2.147).

$$\mathbf{k}_e \, \tilde{\mathbf{u}}_e = \int_B \mathbf{N}_e^T \, \mathbf{f}_{\boldsymbol{ext}} \, dB_e + \int_{S^t} \mathbf{N}_e^T \, \mathbf{t}_s \, dS_e^t \qquad (2.147)$$

The next step is to generate a global stiffness relationship of the total structure. So the nodal degrees of freedom $\tilde{\mathbf{u}}_e$ of each element has to be transformed element-wise to the global coordinate system by using the transformation matrix $\mathbf{T}_e$ and the vector of the global degrees of freedom $\tilde{\mathbf{u}}_{gl}$.

$$\tilde{\mathbf{u}}_e = \mathbf{T}_e \, \tilde{\mathbf{u}}_{gl} \qquad (2.148)$$

The global stiffness matrix is defined as

$$\mathbf{K} = \sum_e \mathbf{T}_e^T \mathbf{k}_e \mathbf{T}_e \qquad (2.149)$$

and the global load vector as

$$\mathbf{q}_{gl} = \sum_e \mathbf{T}_e \, \mathbf{q}_e. \qquad (2.150)$$

So the global stiffness relationship can be written as

$$\mathbf{K}\,\tilde{\mathbf{u}}_{gl} = \mathbf{q}_{gl}. \tag{2.151}$$

The load vector $\mathbf{q}_e$ contains the volume forces and the d'Alembert inertial forces by the integral $\int_B \mathbf{N}_e^T\,\mathbf{f}_{ext}\,dB_e$. For dynamic problems can be written:

$$\mathbf{f}_{ext} = -\boldsymbol{\rho}(\mathbf{x},\mathbf{y},\mathbf{z})\ddot{\mathbf{u}} - \mathbf{d}(\mathbf{x},\mathbf{y},\mathbf{z})\dot{\mathbf{u}} \tag{2.152}$$

By using Eq. (2.153) and Eq. (2.154)

$$\frac{\mathrm{d}\mathbf{u}_e}{\mathrm{d}t} = \mathbf{N}_e\,\frac{\mathrm{d}\tilde{\mathbf{u}}_e}{\mathrm{d}t} \tag{2.153}$$

$$\frac{\mathrm{d}^2\mathbf{u}_e}{\mathrm{d}t^2} = \mathbf{N}_e\,\frac{\mathrm{d}^2\tilde{\mathbf{u}}_e}{\mathrm{d}t^2} \tag{2.154}$$

the load vector is defined as

$$\mathbf{q}_e = -\left[\int_B \mathbf{N}_e^T\,\rho\,\mathbf{N}_e\,dB_e\right]\frac{\mathrm{d}^2\mathbf{u}_e}{\mathrm{d}t^2} - \left[\int_B \mathbf{N}_e^T\,d\,\mathbf{N}_e\,dB_e\right]\frac{\mathrm{d}\mathbf{u}_e}{\mathrm{d}t} + \int_{S^t} \mathbf{N}_e^T\,\mathbf{t}_s\,dS_e^t. \tag{2.155}$$

Now the element mass matrix $\mathbf{m}_e$, element damping matrix $\mathbf{d}_e$ and the external force vector $\mathbf{f}_e$ can be described by Eq. (2.156), Eq. (2.157), and Eq. (2.158).

$$\mathbf{m}_e = \int_B \mathbf{N}_e^T\,\rho\,\mathbf{N}_e\,dB_e \tag{2.156}$$

$$\mathbf{d}_e = \int_B \mathbf{N}_e^T\,d\,\mathbf{N}_e\,dB_e \tag{2.157}$$

$$\mathbf{f}_e = \int_{S^t} \mathbf{N}_e^T\,\mathbf{t}_s\,dS_e^t \tag{2.158}$$

After transforming into the global coordinate system, the general equation of motion for a finite element model can be written:

$$\mathbf{M}\frac{\mathrm{d}^2\tilde{\mathbf{u}}_{gl}}{\mathrm{d}t^2} + \mathbf{D}\frac{\mathrm{d}\tilde{\mathbf{u}}_{gl}}{\mathrm{d}t} + \mathbf{K}\,\tilde{\mathbf{u}}_{gl} = \mathbf{f} \tag{2.159}$$

Now the Eq. (2.159) can be solved by computer. So it is possible to calculate the unknown global displacements for a loaded structure.

2.5.3.2 Transient Analysis

The time iteration method (transient analysis) is a general method to solve the equation of motion. It is applicable for linear, nonlinear, damped and undamped systems, but the method is very time consuming so it is usually used for short durations. The method abstains from transforming the normal coordinates and solves stepwise the equation of motion. Referring to (Stelzmann et al. 2008) the common used time integration methods are listed:

- Generalized-alpha Method
    - Hilber-Hughes-Taylor-Method
        - Newmark-Method
            - Central Differences Method
            - Houbolt-Method
            - Wilson-Θ-Method
                - Linear acceleration Method

The following explanations of selected time iteration methods are based on (Leibbrandt 2002) and (Stelzmann et al. 2008).

Central Differences Method:

The Central Differences Method is a special case of the Newmark-Method and if the mass and damping matrix are diagonal, the solving of the equation is very simple. Additionally, if the time step and the damping matrix are constant at the same time, so the stiffness matrix has not been factorized to solve the equation, which is an advantage of the method. The first disadvantage of the method is the first calculation step to define the start conditions. So the equation of the velocity and the acceleration at the time t has to be transformed to eliminate the displacement $u_{t-\Delta t}$ and to get the displacement $u_{-\Delta t}$ of the first time interval.

$$u_{-\Delta t} = u_0 - \Delta t \cdot \dot{u}_0 + \frac{\Delta t^2}{2} \cdot \ddot{u}_0 \qquad (2.160)$$

The start values are u_0, $\dot{u}_0$ and $\ddot{u}_0$ and two of them have to be known at the beginning of the calculation. The third start value can be calculated by solving the equation of motion. By using the value of $u_{-\Delta t}$, the calculation can be started at the time $t = 0$.

A further disadvantage of the method is the necessary small time steps Δt. The Eq. (2.161) shows the calculation of the maximal applicable time step Δt_{max}.

$$\Delta t \leq \Delta t_{max} = \frac{T_n}{\pi} \qquad (2.161)$$

T_n is the oscillation period of the highest eigenfrequency. By using bigger time steps then Δt_{max} , the method can be numerical instable.

Let's explain the procedure of the Central Differences Method. For the calculation it is necessary to know the values of several time steps. So the equilibrium of the time t has to be constructed by using the values of the time step before $(t - \Delta t)$ and after $(t + \Delta t)$ the time t. Figure 2.22 shows the displacements at the time steps by using the Central Differences Method.

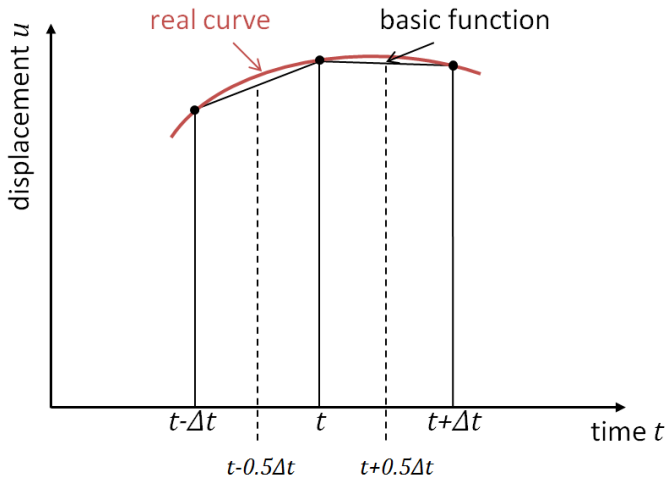

Figure 2.22: Displacement-time-curve by using the Central Differences Method based on (Stelzmann et al. 2008)

So it is possible to calculate the velocities at the time $\left(t + \frac{\Delta t}{2}\right)$ and $\left(t - \frac{\Delta t}{2}\right)$.

$$\dot{u}_{t+\frac{\Delta t}{2}} = \frac{u_{t+\Delta t} - u_t}{\Delta t} \qquad (2.162)$$

$$\dot{u}_{t-\frac{\Delta t}{2}} = \frac{u_t - u_{t-\Delta t}}{\Delta t} \qquad (2.163)$$

The velocity of the time t is due to the arithmetic average of Eq. (2.162) and Eq. (2.163).

$$\dot{u}_t = \frac{\dot{u}_{t+\frac{\Delta t}{2}} + \dot{u}_{t-\frac{\Delta t}{2}}}{\Delta t} \qquad (2.164)$$

The acceleration at the time t can be calculated by the differences of the velocities.

$$\ddot{u}_t = \frac{u_{t-\Delta t} - 2u_t + u_{t+\Delta t}}{\Delta t} \qquad (2.165)$$

Now the equations of the displacement, velocity and acceleration at the time t can be used in the general equation of motion. Furthermore, the equation of motion has to be transformed, so that the unknown displacement $u_{t+\Delta t}$ is on the left side of the equation and the right side of the equation only consists of known values. So the method is also called an explicit calculation method.

$$\left(\frac{1}{\Delta t^2}\mathbf{M} + \frac{1}{2\Delta t}\mathbf{D}\right)\mathbf{u}_{t+\Delta t} = \mathbf{f_t} - \left(\mathbf{K_t} - \frac{2}{\Delta t^2}\mathbf{M_t}\right)\mathbf{u}_t - \left(\frac{1}{\Delta t^2}\mathbf{M_t} - \frac{1}{2\Delta t}\mathbf{D_t}\right)\mathbf{u}_{t-\Delta t} \qquad (2.166)$$

Newmark-Method

The Newmark-Method is a one-step and an implicit method. By using the two parameters (α and δ), the stability and the accuracy of the method can be changed. One advantage of the method is that only the values at the time t are necessary to know, which is an attribute of all one-step methods. Another advantage is that the Newmark-Method is unlimited stable, if the parameter $\delta \geq 0.5$ and $\alpha \geq 0.25(0.5 + \delta)^2$. And last but not least the method does not need a specific start procedure in the first time step. A disadvantage of the method is the time consuming calculation, because the stiffness matrix is on the left side of the equation. Especially nonlinear structural dynamic behavior results in a very time consuming calculation.

Let's explain the procedure of the Newmark-Method in detail. Figure 2.23 shows the linear acceleration curve between the time t and $t + \Delta t$.

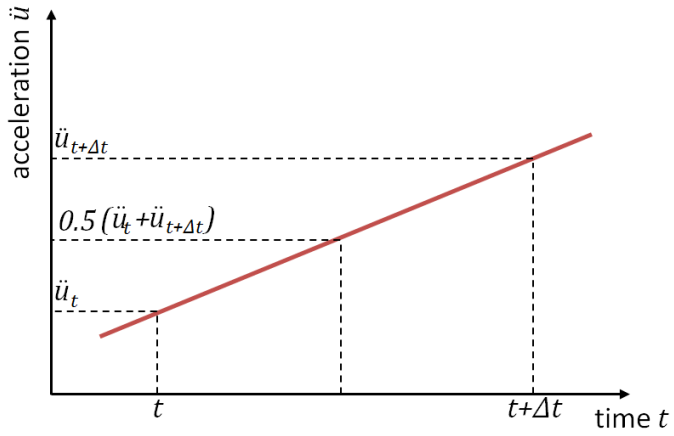

Figure 2.23: Linear acceleration-time-curve with constant mean acceleration based on (Stelzmann et al. 2008)

For the velocity and the displacement, it is necessary to use the assumption in Eq. (2.167) and Eq. (2.168).

$$\dot{u}_{t+\Delta t} = \dot{u}_t + [(1-\delta)\ddot{u}_t + \delta\ddot{u}_{t+\Delta t}]\Delta t \qquad (2.167)$$

$$u_{t+\Delta t} = u_t + \dot{u}_t\Delta t + [(0.5-\alpha)\ddot{u}_t + \alpha\ddot{u}_{t+\Delta t}]\Delta t^2 \qquad (2.168)$$

Now the Eq. (2.167) and Eq. (2.168) can be transformed in order to calculate the velocity and acceleration at the time $t + \Delta t$ by using the known values at the time t. Then the unknown displacement at the time $t + \Delta t$ can be calculated by using the equation of equilibrium.

$$\mathbf{M}\ddot{\mathbf{u}}_{t+\Delta t} + \mathbf{D}\dot{\mathbf{u}}_{t+\Delta t} + \mathbf{K}\mathbf{u}_{t+\Delta t} = \mathbf{f}_{t+\Delta t} \qquad (2.169)$$

Now the displacement at the time $t + \Delta t$ is calculated and can be used in the Eq. (2.167) and Eq. (2.168) to get the velocity and acceleration at the time $t + \Delta t$.

2.5.3.3 Harmonic Frequency Analysis

This chapter describes the Harmonic Frequency Analysis based on (Stelzmann et al. 2008). The Harmonic Frequency Analysis calculates the stationary oscillation answer of a loaded structure. The loads can only be harmonic loads with different amplitudes, frequencies, phase angles, and loading positions. The input and the output of the calculation are defined in frequency domain. So the calculation is in

frequency domain, too. The Harmonic Frequency Analysis is only applicable if the structure is modeled as a linear system and the load function is describable by harmonic oscillations. So the load function $\mathrm{f}(t)$ in time domain has to be described in frequency domain. The Eq. (2.170) shows the load function $\mathrm{f}(t)$ in frequency domain by using the complex numbers. f_r is the real part and f_i describes the imaginary part. Ω represents the angular frequency and φ shows the phase angle.

$$\mathrm{f}(t) = \mathrm{f}_r\, cos(\Omega t) - \mathrm{f}_i\, sin(\Omega t) + i(\mathrm{f}_r\, cos(\Omega t) + \mathrm{f}_i\, sin(\Omega t)) \qquad (2.170)$$

The displacements of the linear structure moves with same angular frequency Ω.

$$u(t) = u_r\, cos(\Omega t) - u_i\, sin(\Omega t) + i(u_r\, cos(\Omega t) + u_i\, sin(\Omega t)) \qquad (2.171)$$

By using the relations of $\mathrm{f}(t)$ and $u(t)$ in the equation of motion, the Eq. (2.172) can be written.

$$\left(-\Omega^2\mathbf{M} + i\Omega\mathbf{D} + \mathbf{K}\right)(\mathbf{u}_r + i\,\mathbf{u}_i) = (\mathbf{f}_r + i\,\mathbf{f}_i) \qquad (2.172)$$

The first bracket can also be called equivalent stiffness matrix

$$\mathbf{K}^{eq} = \left(-\Omega^2\mathbf{M} + i\Omega\mathbf{D} + \mathbf{K}\right). \qquad (2.173)$$

So there is a linear complex equation to calculate the unknown displacements of the structure in frequency domain. The equation is similar to an equation of a static calculation. The difference is that there are not only real parts of the loads and degree of freedoms of the structure, there are imaginary parts, too. Another difference is that the equivalent stiffness matrix $\mathbf{K}^{eq}$ is dependent on the angular frequency Ω. So the equivalent stiffness matrix has to be calculated for each angular frequency Ω. As result of the calculation can be shown the real part u_r and the imaginary part u_i of the displacements. By using the Eq. (2.174) and Eq. (2.175), the results can be transformed into the amplitude u_{max} and phase φ of the displacement oscillation for each frequency.

$$u_{max} = \sqrt{u_r^2 + u_i^2} \qquad (2.174)$$

$$\varphi = \arctan\left(\frac{u_i}{u_r}\right). \qquad (2.175)$$

2.5.3.4 Modal Superposition

The Modal Superposition uncouples the system of equations to get n uncoupled equations. These uncoupled equations are solved to assemble the solution of the total system. The transformation from a coupled system of equations to an uncoupled system of equations can be realized by using the separation approach of the displacements. So the dependency on the position is described by the eigenvectors $\mathbf{\Phi_i}$ and the dependency on the time is described by the function $y_i(t)$.

$$\mathbf{u(t)} = \sum_{i=1}^{n} \mathbf{\Phi_i} \cdot y_i(t) \qquad (2.176)$$

n represents the number of all eigenvectors of the system. To reduce the calculation effort, the higher eigenvectors are often neglected. So the calculation only uses p eigenvectors instead of n eigenvectors.

$$\mathbf{u(t)} = \mathbf{\Phi} \cdot \mathbf{y(t)} \qquad (2.177)$$

So this relation can be used in the equation of equilibrium. After multiplying the equation of equilibrium by $\mathbf{\Phi^T}$, the system of equation is uncoupled

$$\mathbf{\Phi^T M \Phi} \cdot \ddot{\mathbf{y}} + \mathbf{\Phi^T D \Phi} \cdot \dot{y} + \mathbf{\Phi^T K \Phi} \cdot \mathbf{y} = \mathbf{\Phi^T f}\,. \qquad (2.178)$$

Now all matrices only have diagonal values, which are unequal to zero. So the system of equations can be called uncoupled system of equations and each line can be solved like a single-mass oscillator by using a transient method or a harmonic frequency analysis. The total solution can be assembled by the single solutions, as shown in Eq. (2.179).

$$u(t) = \Phi_1 y_1(t) + \Phi_2 y_2(t) + \cdots + \Phi_p y_p(t) \qquad (2.179)$$

One disadvantage of the method is that only linear systems can be solved. So nonlinearity is not allowed. Also it is impossible to use discrete damping elements or material damping. The method only works with modal damping. Furthermore, it is not possible to calculate displacement loads. But the method has some advantages, too. So stiffening as a result of stresses can be considered and the calculation is very fast, if the numbers of eigenvectors is within limits. So before the Modal Superposition

Method can be used, it is necessary to get the eigenvectors of the system. This can be done by using the Modal Analysis, which is explained in the following section.

2.5.3.5 Modal Analysis

The eigenfrequencies and the mode shapes are very important for dynamic analysis of linear systems. A Modal Analysis is defined as a calculation of eigenfrequencies and mode shapes. Mathematically, an eigenvalue problem has to be solved, at which the eigenvectors represent the mode shapes and the squares of the eigen angular frequencies represent the eigenvalues. There are a lot of solution methods, but it is not necessary to know them all. So the dissertation only describes the basics of numerical solution method. (Stelzmann et al. 2008)

Here the QR-algorithm to solve a standard eigenvalue problem is explained.

$$(\mathbf{A} - \lambda \mathbf{1})\mathbf{u} = \mathbf{0} \qquad (2.180)$$

At first the matrix $\mathbf{A}$ has to be split up in an orthogonal Matrix $\mathbf{Q}$ and an upper triangular matrix $\mathbf{R}$. An upper triangular matrix $\mathbf{A_{k+1}}$ is stepwise generated by using the Eq. (2.181) and Eq. (2.182). The values of the main diagonal of matrix $\mathbf{A_{k+1}}$ are the eigen values of the standard eigenvalue problem (2.180).

$$\mathbf{A_k} = \mathbf{Q_k} \cdot \mathbf{R_k} \qquad (2.181)$$

$$\mathbf{A_{k+1}} = \mathbf{R_k} \cdot \mathbf{Q_k} \qquad (2.182)$$

So the matrix $\mathbf{A_{k+1}}$ is generated by a similarity transformation of matrix $\mathbf{A}$, which is defined in Eq. (2.183).

$$\mathbf{A_{k+1}} = \left(\prod_{\mathbf{i=1}}^{\mathbf{k}} \mathbf{Q_k} \right)^{-1} \mathbf{A} \left(\prod_{\mathbf{i=1}}^{\mathbf{k}} \mathbf{Q_k} \right) \qquad (2.183)$$

For a symmetric matrix $\mathbf{A}$, each column of the transformation matrix represents an eigenvector and can be calculated by the Eq. (2.184).

$$\mathbf{\Phi} = \left(\prod_{\mathbf{i=1}}^{\mathbf{k}} \mathbf{Q_k} \right) \qquad (2.184)$$

For a non-symmetric matrix , the eigenvectors has to be calculated by e. g. the inverse power method. Therefore, a LU factorization has to be executed. It is a factorization of the matrix $\mathbf{\Phi}$ as the product of a lower triangular matrix $\mathbf{L}$ and an upper triangular matrix $\mathbf{U}$. Then a start vector has to be chosen to start the iteration process. By using the forward substitution in Eq. (2.185) and backward substitution in Eq. (2.186), the eigenvectors of the standard eigenvalue problems can be calculated.

$$\mathbf{L} \cdot \mathbf{\Phi}' = \mathbf{\Phi_k} \qquad (2.185)$$

$$\mathbf{U} \cdot \widetilde{\mathbf{\Phi}}_{\mathbf{k+1}} = \mathbf{\Phi}' \qquad (2.186)$$

Other well known methods are called the Block-Lanczos-Method and the subspace method. Both methods are used for the Modal Analysis of undamped systems with symmetric matrices. The Block-Lanczos-Method is an efficient and fast method and applicable for big FEM-Models. It was developed by Peter Montgomery and published in 1995. In (Montgomery 1995) the method is explained in detail. The Lanczos algorithm can be read in (Lanczos 1950). The subspace method has to calculate the eigenvalues in rising sequence, beginning with the smallest. So the subspace method is generally slower than the Block-Lanczos-Method, but is often used to calculate a small number of lower eigenvalues.

2.5.3.6 Substructures

Substructures are usually used to reduce the calculation time of big linear FE-Models. Referring to (Clough and Penzien 1975) the number of degree of freedoms can be reduced by 15 % till 50 % without losses of accuracy. But the losses of accuracy are also dependent on the position of master degree of freedom. The following list represents some simple criteria to choose the position of master degree of freedom. (Stelzmann et al. 2008)

- At positions of high mass and/or small stiffness
- At positions of external displacements or loads

- At positions of measurements
- Evenly distributed about the structure
- The mode shapes should be represented by the master degree of freedom

The dissertation explains the method of Guyan and Craig Bampton. Both methods can be used for dynamic analysis, whereupon the Craig Bampton method is more accurate for calculation of higher frequencies.

Guyan Method

Let's start with the explanation of the Guyan method, which is explained in detail by (Guyan 1965). At first a transformation matrix $\mathbf{T}_{GM}$ has to be generated. So the mass matrix and the damping matrix of the equation of equilibrium are neglected and the static equation (2.187) is only used.

$$\mathbf{K} \cdot \mathbf{u} = \mathbf{f} \tag{2.187}$$

Now the displacements $\mathbf{u}$ are separated by the displacement of the master degree of freedoms $\mathbf{u_m}$ and the slave degree of freedoms $\mathbf{u_s}$.

$$\begin{bmatrix} \mathbf{K_{mm}} & \mathbf{K_{ms}} \\ \mathbf{K_{sm}} & \mathbf{K_{ss}} \end{bmatrix} \cdot \begin{Bmatrix} \mathbf{u_m} \\ \mathbf{u_s} \end{Bmatrix} = \begin{Bmatrix} \mathbf{f_{mm}} \\ \mathbf{f_{ss}} \end{Bmatrix} \tag{2.188}$$

The next step is to eliminate the slave degree of freedom $\mathbf{u_s}$ by using the transformation matrix $\mathbf{T}_{GM}$.

$$\mathbf{T}_{GM}^{\mathbf{T}} \cdot \begin{bmatrix} \mathbf{K_{mm}} & \mathbf{K_{ms}} \\ \mathbf{K_{sm}} & \mathbf{K_{ss}} \end{bmatrix} \cdot \mathbf{T}_{GM} \cdot \begin{Bmatrix} \mathbf{u_m} \\ \mathbf{u_s} \end{Bmatrix} = \mathbf{T}_{GM}^{\mathbf{T}} \cdot \begin{Bmatrix} \mathbf{f_{mm}} \\ \mathbf{f_{ss}} \end{Bmatrix} \tag{2.189}$$

$$\mathbf{T}_{GM} = \begin{bmatrix} \mathbf{I} \\ -\mathbf{K_{ss}^{-1}} \cdot \mathbf{K_{sm}} \end{bmatrix} \tag{2.190}$$

By using the generated transformation matrix $\mathbf{T}_{GM}$, the stiffness matrix $\mathbf{K}$ and the mass matrix $\mathbf{M}$ can be reduced, as shown in Eq. (2.191) and Eq. (2.192).

$$\mathbf{K_m} = \mathbf{T}_{GM}^{\mathbf{T}} \cdot \mathbf{K} \cdot \mathbf{T}_{GM} \tag{2.191}$$

$$\mathbf{M_m} = \mathbf{T}_{GM}^{\mathbf{T}} \cdot \mathbf{M} \cdot \mathbf{T}_{GM} \tag{2.192}$$

So the masses of the slave degree of freedom are averaged to the master degree of freedom dependent on the stiffness.

The damping matrix $\mathbf{D}$ will be assembled by the stiffness and mass matrix, which is called Rayleigh-damping. The explanation of the Rayleigh-damping can be found in (Stelzmann et al. 2008). Another option is to use the transformation matrix $\mathbf{T}_{GM}$, also to reduce the damping matrix $\mathbf{D}$.

$$\mathbf{D_m} = \mathbf{T}_{GM}^{\mathbf{T}} \cdot \mathbf{D} \cdot \mathbf{T}_{GM} \quad (2.193)$$

Craig Bampton Method

The Craig Bampton Method is usually used for dynamic calculations with higher frequencies. So the method uses a previous Modal Analysis to represent higher eigenmodes. A detailed explanation can be found in (Craig and Bampton 1968). To consider the dynamic behavior of the structure, the method uses the modal degree of freedoms additionally. There are a lot of special cases of the Craig Bampton Method. The dissertation only uses the Fixed-Interface-Method. At first the displacement $\mathbf{u}$ is separated in master degree of freedoms $\mathbf{u_m}$ and slave degree of freedoms $\mathbf{u_s}$. By using the Ritz-Transformation, the vector can be defined as a linear combination of the forced deformations $\mathbf{\Phi_c}$ and the natural modes $\mathbf{\Phi_n}$. The Ritz-Transformation is also explained in (Stelzmann et al. 2008). The natural modes can be calculated by solving the general eigenvalue problem (2.194) on the condition that all master degrees of freedom are fixed.

$$(\mathbf{K_{ss}} - \boldsymbol{\omega}^2\mathbf{M_{ss}})\mathbf{\Phi_n} = \mathbf{0} \quad (2.194)$$

To calculate the forced deformations, a unit displacement is impressed on one after another master degree of freedom. Meanwhile all other master degrees of freedom are fixed.

$$-\mathbf{K_{ss}^{-1}} \cdot \mathbf{K_{sm}} = \mathbf{\Phi_c} \quad (2.195)$$

By using the modal coordinates $\mathbf{q_n}$, the transformation matrix $\mathbf{T_{CBM}}$ can be defined, as shown in Eq. (2.196).

$$\begin{bmatrix}\mathbf{u_m}\\ \mathbf{u_s}\end{bmatrix} = \begin{bmatrix}\mathbf{I} & \mathbf{0}\\ \mathbf{\Phi_c} & \mathbf{\Phi_m}\end{bmatrix}\begin{bmatrix}\mathbf{u_m}\\ \mathbf{q_n}\end{bmatrix} = \mathbf{T_{CBM}}\begin{bmatrix}\mathbf{u_m}\\ \mathbf{q_n}\end{bmatrix} \quad (2.196)$$

3 State of research

3.1 What is reality?

This dissertation is a part of the project “Absolute Values” which was announced in the introduction. The superior aim of the project is to predict operational vibrations of complex coupled systems. From this it follows that the models should simulate the reality. So the first question is: “What is reality?”

It is a philosophical topic to define the term “reality”. The definition depends on philosophical preconditions. In the widely-used epistemology are defined five different positions of realism: naive realism, critical realism, semantic realism, epistemic realism, weak realism. Detailed information are written in (Keuth 2004) and (Russ 2004). Further interesting philosophical deliberations about the topic “What is reality” can be found in (Vollmer 1985).

In the context of science, reality is everything that can be observed by the use of scientific methods. So reality is measurable in the context of science. The philosophy of science reaches from a strong metaphysical realism to the aspect that all objects are abstractions of reality. In the product development, the engineers work with abstractions of reality to design the components of a product. The vehicle development is a good example. The customer drives the car on the road. This seems to be reality. The first Level of Abstraction in the development process is that an expert drives the car on the road. The next abstraction level is the analysis on test benches which neglects the effects of the natural environment. Furthermore, there are test benches for the single systems like engine, chassis, and so on. Here the single systems are developed by neglecting the coupling of the systems to a total car. So it can be seen that every model is an abstraction of reality. (Stein et al. 2010) The mathematical models and experimental models only represent a part of the physical reality. So the mathematical model of an experiment can only generate results in the quality of the equivalent experimental model.

Further should be mentioned the definition of “reality” from (Werner 2010) at the area of civil engineer. He defined the term “reality” as the natural conditions of a building during its construction and use.

In summary, it is very difficult to determine “reality”. So the different models in the dissertation are compared with one reference model, which considers most physical effects.

3.2 Kinds of models

Models are used in many subject areas, e. g. medicine, geophysics, and so on. More examples are listed in (Bungartz et al. 2009). This dissertation only concentrates on engineering models.

Models help the engineer to predict the system behavior or to understand the behavior of a system, (Informationsverarbeitung in der Produktentwicklung 2003). If a bridge broke down, the engineers try to understand, why the bridge broke down to use this knowledge for future bridges. If a bridge will be built at an earthquake prone area, the engineers try to predict the mechanical strength of the bridge which is loaded by the maximal earthquake level. But it is always important to know that every model is an abstraction of reality.

Generally, there are two main types of models, the experimental model and the mathematical model. So the engineers have to decide which model is convenient to generate results for his physical problem in respect of the technical and economical conditions. (Informationsverarbeitung in der Produktentwicklung 2003) This decision is often based on experiences of the engineers.

An **experimental model** is a real physical model instance of an engine on a test bench. The advantage of the experimental model is that mostly more physical effects can be considered than in a mathematical model, but it is expensive to build up an experimental model (e. g. product prototype). Another disadvantage is that a system optimization through variation of parameters is limited by the required expenditure of time and the high costs. (Informationsverarbeitung in der Produktentwicklung 2003) describes additional advantages and disadvantages of experimental models.

Referring to (Aris 1994) a **mathematical model** is defined as a system of equations that express the laws of the system and the solution shows some aspects of the systems behavior. It offers the possibility to look inside the system. So it is able to have a look at parameters which are not measureable in the experiment. Furthermore, the input parameters can be changed quickly and it is simple to explore the consequences. (Dresig 2001) Further advantages and disadvantages can be found in (Informationsverarbeitung in der Produktentwicklung 2003). To reduce the complexity and the effort of an analysis, the engineers use models of subsystems (also called submodels). Each complex coupled system consists of several subsystems and the subsystems are coupled to each other. Especially for analysis of dynamic problems, the engineers have to look at the coupling of the subsystems. If there is a significant structural coupling between subsystems, it is risky to neglect this effect. So the statements of the analysis can be wrong, because the structural coupling modify the structural dynamic behavior of the interesting subsystem elementary. A big problem is to understand how different models affect each other and the interesting results. (Stein et al. 2010)

The dissertation focuses on mathematical models. The next chapter shows different opportunities to classify mathematical models.

3.3 Classification of mathematical models

The literature shows different ways to classify mathematical models. So it is not able to list all classification opportunities in this dissertation. Some selected classifications of models are explained in the following itemization.

- **Calculation method:** Generally, the solving of mathematical models can be grouped in analytical methods and numerical methods. These two methods can be grouped in many subgroups. Here a more detailed description is omitted. In chapter 2.5, several solution processes of mathematical models are specified.

- **Physical problem:** Also the mathematical models can be classified by the physical problem that should be solved. Examples for physical problems are

acoustics, thermodynamics, fluid mechanics, and many more. A complete list of all physical problems is not provided.

- **Model complexity:** The complexity of a model can be described by different aspects. For example, it is possible to classify the models into linear and nonlinear models. The next chapter goes in detail about complexity of mathematical models.

- **Component function:** The models are classified into functional groups. Each component of a total system has a function that can be assigned to a functional group. In (Schilling 2003) and (Petersen 1993) the components are classified this way.

- **Level of Abstraction:** The classification into Levels of Abstraction can start with component models that use idealized boundary condition, for example. So the models have no couplings to the neighboring components and neglect the resulting effects of structural coupling. The next level considers a subsystem with a defined function. Here more components are coupled to accomplish a defined task. The lowest Level of Abstraction considers the total system with all subsystems. This Level of Abstraction is very time-consuming and non-trivial for the calculation and modeling. Due to the expenditure of time, most development processes of industrial products do not use such detailed models. The explanation of the classification into Levels of Abstraction is drawn on (Schilling 2003).

A further classification method is explained in (Velten 2009). The models are classified by the SQM (**S**ystem, **Q**uestions, **M**athematical statements) space of mathematical models. The SQM space method shows a classification from the black-box to the white-box model. A black-box model simulates the system behavior by using equations which are based on empiric studies. A white-box model uses physical equations to describe the system behavior. So the engineers are able to analyze the system in detail. This thesis does not use this method to classify the models, so the classification method is only mentioned and not explained in detail. The following chapters explain the classification by using the complexity and abstraction levels.

3.4 Complexity of mathematical models

The complexity of mathematical models can be defined by the number of considered physical processes. Generally, the consideration of more physical processes leads to an increasing number of input parameters. (Most 2011) In this thesis, the Level of Complexity is described by the number of input parameters for the total system.

So if the model complexity rises, the calculation time and the result accuracy rise, too. But this statement is not useable for every mathematical model, because the accruing uncertainty has to be considered. Many models consider a lot of physical effects, but contain a high uncertainty. This high uncertainty can result in a high output-deviation to the reference model (e. g. experiment). So a model should only be as complex as necessary. (Most 2011), (Informationsverarbeitung in der Produktentwicklung 2003) The uncertainty can be split up in two kinds of uncertainty, aleatoric and epistemic uncertainty. The increasing complexity of a model results in a decreasing epistemic uncertainty, but also an increasing uncertainty of parameters, following (Knetsch 2003) and (Reuter 2012). The total uncertainty is the sum of the epistemic uncertainty and the aleatoric uncertainty. Figure 3.1 shows the model complexity in relation to the kinds of uncertainty. The diagram only shows curves for the uncertainties exemplarily.

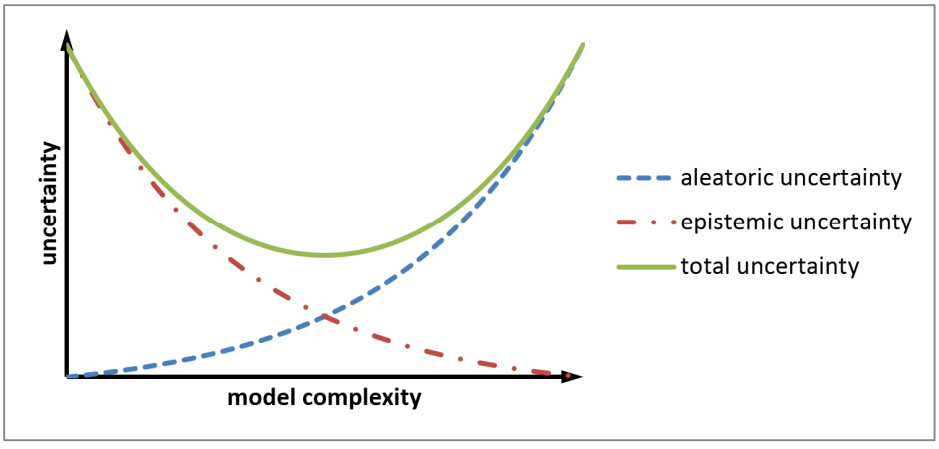

Figure 3.1: Model complexity in relation to the uncertainty based on (Reuter 2012)

Let's define the kinds of uncertainties. The **aleatoric uncertainty** derives from lat. *alea* and is dependent on the statistic accuracy of the input parameter. For example, the material analysis in (Eibner 2010) shows that the young's modulus and the density of high quality aluminum are not constant in a real technical component. (Eibner 2010)

explore real technical components made of steel, aluminium alloy and cast iron. The analysis occurred by using an ultrasonic installation on different measurement points of the technical components. In Figure 3.2 and Figure 3.3 selected diagrams are shown which can be found in (Eibner 2010). Figure 3.2 shows the variance of density and Figure 3.3 shows the variance of young's modulus. Both diagrams show the variance of parameters for a small supporting arm of an engine. Each sampling identification number represents a defined measurement point on the supporting arm.

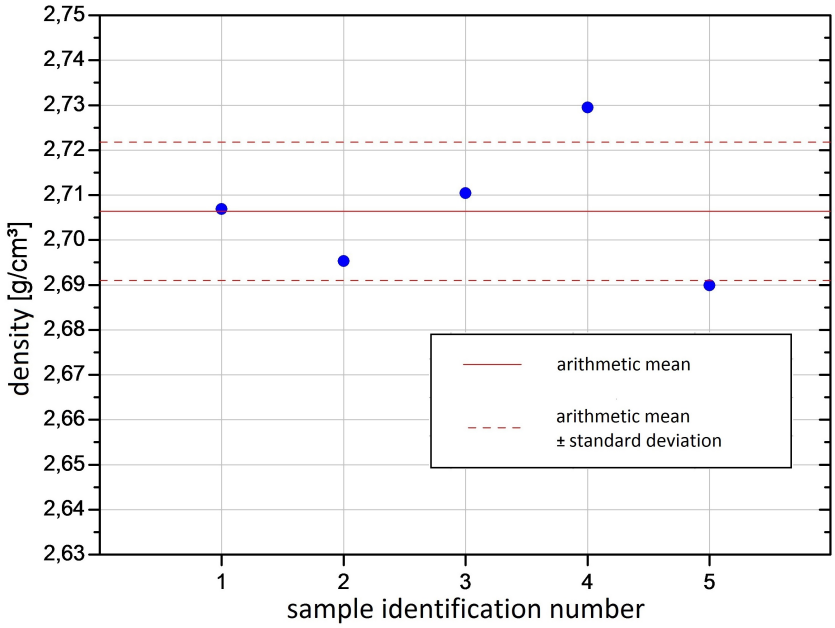

Figure 3.2: Variance of density for a supporting arm made of aluminium alloy (Eibner 2010)

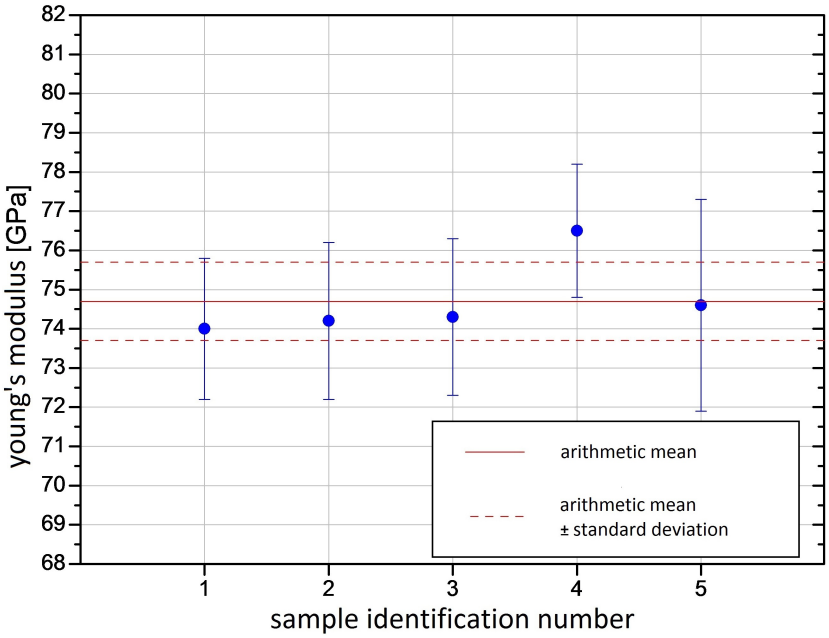

Figure 3.3: Variance of Young's modulus for a supporting arm made of aluminium alloy (Eibner 2010)

The **epistemic uncertainty** derives from the Greek word *episteme* and shows the difference between the experimental measured and the calculated results. So the epistemic uncertainty is based on the unsatisfactory modeling of the significant physical effects. Referring to (Reuter 2012) the quantification of the epistemic uncertainty is only possible by comparing the results of the mathematical model with the measured results of the experimental model.

In (Most 2011) the uncertainties that affect model quality are categorized in three groups (model framework uncertainty, model niche uncertainty and model input uncertainty).

The **model framework uncertainty** results from the uncertainty of the underlying science and algorithm of a model. So it is based on the lack of knowledge about model parameters or the simplifications that are necessary to get a mathematical model.

The **model niche uncertainty** follows from the uncertainty by using a model outside their original system. A further example of a model niche uncertainty is a coupled model which consists of several models with different spatial or temporal scales.

The **model input uncertainty** follows from the uncertainty of model parameter values, measurement errors and the difference between the values that are used in the mathematical model and the measured values due to e. g. averaging or filtering.

Furthermore, (Most 2011) discuses several methods of model assessment in consideration of uncertainties.

3.5 Abstraction levels of models

The abstraction level is an important factor for the efficiency and accuracy of a calculation. Clever selected abstraction levels offer the potential for simultaneous engineering. These represent a big advantage for the development of complex systems. So several engineers are able to work on different subsystems at the same time and reduce the total development time. If a subsystem is not significantly influenced by other subsystems, the engineer is able to design the subsystem and optimize it by using a submodel which neglects the coupling effects to other subsystems.

3.5.1 Submodels

In the product development, engineers often use submodels to design and optimize the components of their responsibility. This approach entails advantages and disadvantages. At first the work with a submodel reduces the complexity and the interpretation of results becomes easier. (Rombach 2008) Furthermore, the calculations with submodels are less time-consuming and save memory capacity. The disadvantages of using submodels can be found in neglecting structural coupling effects and excitation interaction effects. A compromise is to model a simplified interaction between the submodels. So the coupling between the submodels is often approximated by a linear behavior. Therefore, nonlinear effects of the interaction are not considered. (Reuter 2012)

To choose reasonable system boundaries for submodels, it is necessary to use predefined criteria. The GRK 1462 of the Bauhaus-University of Weimar investigates

the applicability of submodels and the influence of the couplings between the submodels. Some important criteria should be mentioned in the following itemization.

- **Physical theory:** To describe a complex coupled system completely, it is not enough to consider one physical specific area. The physical parameters of several physical specific areas are coupled which result in interactions between the physical fields. The most complex systems contain several physical theories like classical mechanics, electro dynamics, thermo dynamics, and so on. If the interaction of the physical fields is negligible, the engineer can only consider the physical theory of their interest.

- **Model scale:** Physical effects occur at appropriate levels also called model scales. Mathematical models work on a scale and put on the more detailed scale. More information about model scales can be read in (Bungartz et al. 2009). For example, in (Iesulauro 2002) the mostly used model scales of simulations in the field of fractural mechanics are described.
    - Macro scale: If the engineer is interested in strains and stresses of the continuum, the behavior of the material is assumed as homogeneously.
    - Meso scale: The meso scale uses different material behavior for the polycrystal and the crystal boundaries.
    - Micro scale: Simulations of the atomic lattice allows analyzing the splitting of atomic bonds.

- **Geometrical arrangement:** The geometrical arrangement of the components is also used as a criterion for generating submodels. For example, a vehicle can be divided in a chassis, engine and the vehicle body.

- **Functional subdivision:** Furthermore, the functional subdivision in material laws or load definitions can be used.

The GRK 1462 of the Bauhaus-University of Weimar analyze the reliability of decoupled submodels and the influence of different coupling opportunities since 2008. For more information and further aspects the publications of (Lahmer et al. 2011), (Fröbel and Stein 2011), (Karplus 1977), and (Stein 2001) are recommended.

3.5.2 Abstraction levels to calculate operational vibrations

This chapter explains the common abstraction levels for complex coupled systems to calculate the operational vibrations in the industrial and scientific environment. Generally, two main methods can be distinguished, the full coupled and the decoupled abstraction level. The following description of the methods extends the description in (Bohn 2006) to include additional excitation subsystems. (Bohn 2006) does not separate between models and the solution process. So this chapter does not separate between models and solution process, too. In the following chapters, the dissertation shows the differences between the abstraction levels independent of the solution process.

3.5.2.1 Full coupled abstraction level

The probably most accurate method is the direct solution of forces, moments and operational vibrations by the full coupled abstraction level. But it only may be the most accurate method, if the statements in chapter 3.4 and (Most 2011) are considered. So the aleatoric uncertainty is often very high in complex calculation models like in the full coupled abstraction level. A simplified flowchart of the full coupled abstraction level for complex systems to calculate the operational vibrations is shown in Figure 3.4.

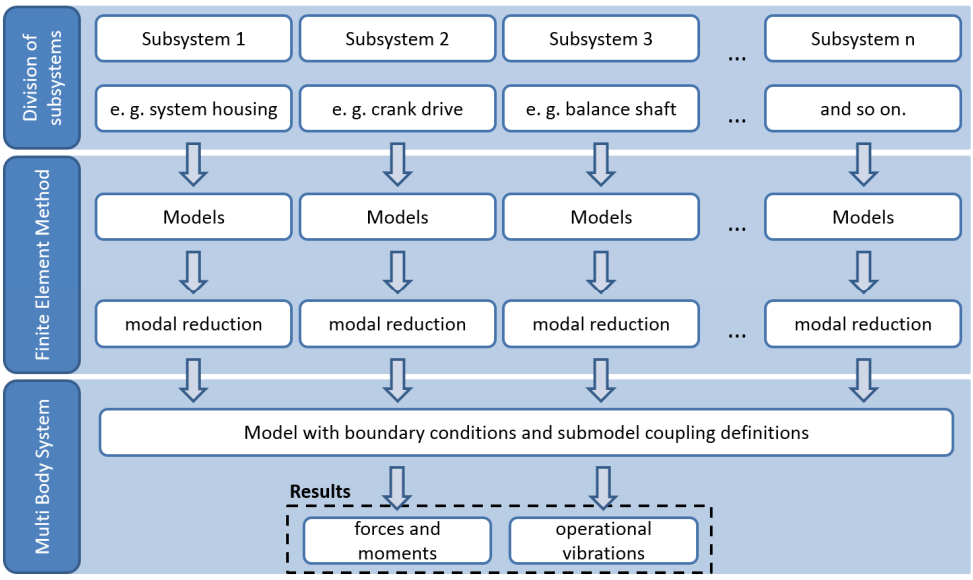

Figure 3.4: Simplified flowchart of the full coupled abstraction level for complex systems

The process starts with the division of subsystems. Here the engineer has to group the total system into subsystems. Chapter 3.5.1 gives helpful criteria to group a total system into several reasonable subsystems. The flowchart shows an example of an engine that is grouped into three subsystems, the system housing, the crank drive and the balance shaft. Further subsystems can be a valve train, gear drive, turbo charger, and so on.

In the second step, the single components of the subsystems have to be discretized. Here the engineer has to decide, if the structural dynamic behavior of the single component has to be considered. In this dissertation some criteria are developed in chapter 4.2.6 to support the engineer's decision. So if the structural dynamic behavior of the single component should be neglected, it can be modeled as a rigid body with mass and inertia. If the structural dynamic behavior should be considered, it has to be discretized in finite elements. It is important to decide which element approach is the most reasonable for the modeled component. (Dassault Systèmes 2013) gives helpful criteria to decide which element approaches are reasonable for the different materials and how the discretization should look like. Now the discretized components have to be modally reduced by using the e. g. Craig Bampton Method that is explained in chapter 2.5.3.6 and (Craig and Bampton 1968).

The last step is to model the total system by including all single components of the subsystems. Also the boundary conditions and the couplings between the reduced component models have to be defined. After calculating the model of the total system, the results can be visualized. So the engineer is able to have a look at the forces, moments and operational vibrations.

Here the abstraction level results in one MBS-Model that includes the movement of the excitation bodies and the structural dynamic behavior of the total system. So the calculation results contain the structural coupling effects and the excitation interactions between the subsystems. The calculation of a full coupled model is very time-consuming and needs a lot of memory space. Another challenge is the modeling of such a big calculation model and their couplings between the subsystems. In the industrial environment, it is unusual to use the full coupled abstraction level, because the effort and complexity to implement the process is very high and the calculation time takes long. The advantage of the abstraction level is that the model provides the

excitation forces and moments as well as the operational vibrations with respect to the interactions between the subsystems.

3.5.2.2 Decoupled abstraction level

The most commonly used abstraction level is the decoupled abstraction level which is shown in Figure 3.5. This abstraction level has some essential advantages for the industrial product development.

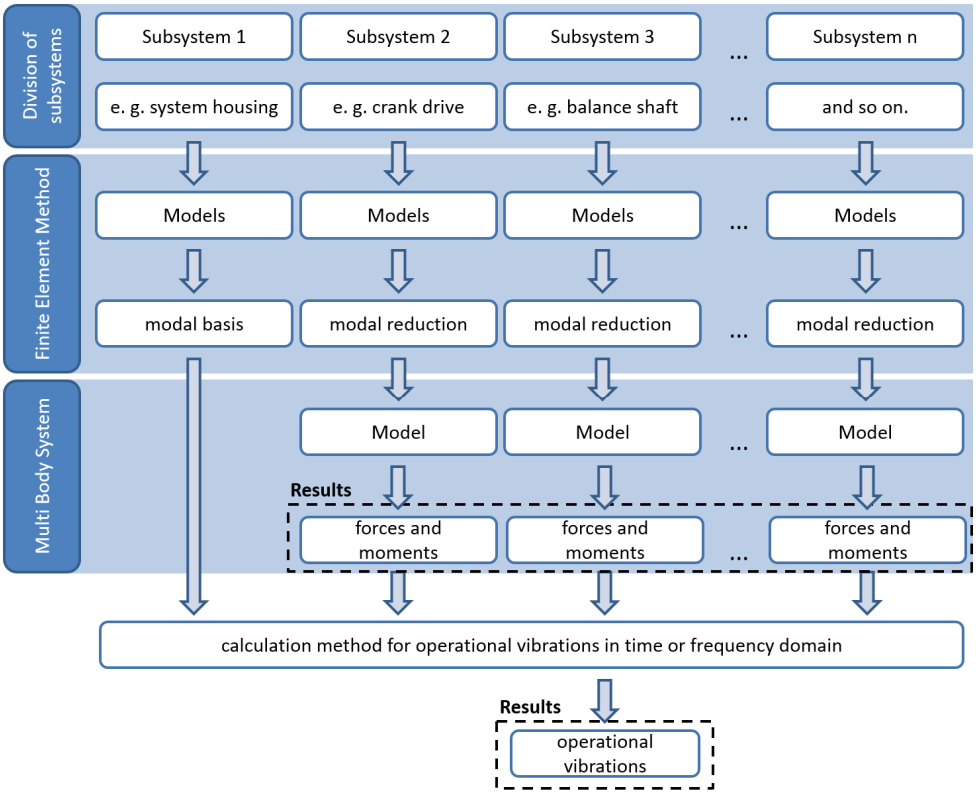

Figure 3.5: Simplified flowchart of the decoupled abstraction level for complex systems

The first and the second step are the same as described in the full coupled abstraction level. So the complex system has to be grouped into subsystems and the single components have to be discretized. Afterwards the FE-Models of the single components can be modally reduced by e. g. the Craig Bampton Method.

The third step differs from the full coupled abstraction level. So there will be modeled one full coupled MBS-Model in the full coupled abstraction level. In the decoupled

abstraction level are modeled one MBS-Model of each subsystem. The advantage is that engineers of different development areas can model a “simple” subsystem for their interests (e. g. mechanical strength of single components). This approach supports the simultaneous engineering concept to reduce product development time. The submodels only contain the structural dynamic behavior of the subsystem without any structural coupling to other subsystems. The boundary conditions of the submodels are mostly dependent on the knowledge of the engineer who modeled the subsystem. The coupling interface forces to the other submodels can be calculated and used in the next step.

After calculating the forces and moments of the single submodels, the output data are used as input data for the model to calculate the operational vibration. Referring to the third Newton’s law (Newton 1687) the forces and moments of the submodels can be used as cutting forces for the calculation of the operational vibrations. The principle of cutting forces is explained in chapter 3.5.4. To calculate the operational vibrations, there are two calculation methods. The first one is the calculation in time domain. This method is mostly very time-consuming dependent on the number of degree of freedoms. Since many FE-Models have more than one million degree of freedom, the solution occurs in frequency domain. For the calculation in frequency domain, it is necessary to do some precalculations. So the forces and moments of the MBS-Submodels have to be split up in their frequency parts by using a Fourier Transform. The Fast Fourier Transform (FFT) (Brigham 1995) is a widely used method, which breaks the Discrete Fourier Transform (DFT) (Neubauer 2012) into smaller DFTs. The most common used FFT algorithm is also called Cooley-Tukey algorithm (Cooley and Tukey 1965). The development of FFT algorithm goes back to Gauss’s unpublished work in 1805. Now the modal basis of the FE-Model of the system housing has to be calculated. The modal basis consists of the eigenfrequencies and the eigenvectors for each element node. A explanation about the calculation of a modal analysis is in chapter 2.5.3.5. Now the imaginary and real part of the forces and moments can be impressed on the modal basis of the system housing to calculate the operational vibrations.

Let’s explain the common used decoupled abstraction level for the calculation of the operational vibration of an engine, following (Bohn 2006). Referring to

(Engler and Katzula 1983) the gas forces and the mass forces of the crank drive are responsible for most of the vibrations. At first the crank drive forces are calculated by using a modal-reduced FE-Model of the crankshaft and a suitable calculation method of the hydrodynamic bearings. (Knoll et al. 1993) explains three possible calculation methods (Impedance, Online-FEM and EHD) for the hydrodynamic bearings into an engine which differ from each other by considering different physical effects. The system housing (engine and gear) is modeled as a rigid body with mass and inertial. It is supported by nonlinear engine mounts and gearbox mounts. Due to the negligence of the structural dynamic behavior of the system housing, the calculation time is within limits. But the MBS-Model is not able to calculate the operational vibrations of higher frequencies. So it is necessary to calculate the operational vibrations in a second calculation step.

Referring to the third Newton's law the cutting forces and moments from the crank drive to the system housing are output data from the MBS-Submodel and are used as input data in the calculation of operational vibrations. This calculation can be done in time domain or in frequency domain. Based on time saving, the common approach is the calculation in frequency domain. So the forces and moments have to be transformed from the time domain into the frequency domain. The second step is to generate the modal basis of the system housing. The modal basis contains the eigenfrequencies and the eigenvectors of the FE-Model. Local damping effects are not considered by using the modal basis and the common used damping method is called modal damping. Therefore, amplitudes of the oscillations cannot be calculated on an absolute scale. In the last step, the cutting forces and moments are impressed on the modal basis of the system housing to get the operational vibrations.

Sometimes the engineers disagree at the question, if the mass inertia of the crank drive has to be considered in the modal basis of the system housing. Referring to (Payer 2001) the negligence of the crank drive mass inertia falsified the operational vibrations, because the eigenfrequencies of the system housing without the crank drive are too high. So the mass of the crank drive is split up and coupled to the crankshaft bearings. But now the third Newton's law is injured and the mass inertia at the crankshaft bearings is too high. So the result tends to lower operational vibrations in comparison to the experimental model. This problem is also explained by

(Payer 2001). The conclusion is that the calculation of operational vibrations by using the common decoupled abstraction level is always tainted with an error. In this dissertation, some decoupled abstraction levels are shown by using the Blocked Forces Method and Cutting Forces Principle that are based on a more substantial mathematical foundation.

3.5.3 Blocked Force Method

The explanation of the Blocked Force Method is mainly based on the publication of (Rixen et al. 2013) in this chapter. (Rixen et al. 2013) uses the method in the field of experimental tests. The dissertation uses the method to derive a useful abstraction level for calculating operational vibrations in the field of mathematical modeling. In (Hixson 2010) the Blocked Force Method is explained by characterizing an excitation component that is done as an application of Thévenin's and Norton's theorems. Primarily the Blocked Force Method derives from the electric circuit analysis and is not often applied in mechanical engineering. The Thévenin's and Norton's theorems in (Norton 1926), (Thévenin 1883), and (Helmholtz 1853) are focused on the electric circuit analysis. Referring to (Rixen et al. 2013) there are two reasons, why this method is not often used in the mechanical engineering.

1. In mechanical engineering, it is more difficult to obtain good measurements than in the electric circuits.
2. The understanding of the mathematical background which permits the method and the verbal interpretation is not trivial.

The Blocked Force Method can be useful in a decoupled abstraction level to calculate operational vibrations. This dissertation defines abstraction levels that use the Blocked Force Method to calculate operational vibrations. Furthermore, the dissertation identifies the limits of the method in chapter 4.4.4. Now the mathematics of the method is explained in detail for a better understanding, following (Rixen et al. 2013).

The explanation occurs by using the example of a five-mass oscillator which consists of two subsystems, as shown in Figure 3.6. The dynamic equilibrium in frequency domain

can be written by using the impedance form or the admittance form. Generally, the impedance z is defined as

$$z = \frac{\mathrm{f}}{u} \qquad (3.1)$$

and the admittance y is defined as

$$y = \frac{u}{\mathrm{f}}. \qquad (3.2)$$

Here the notation f represents the force and u represents the displacement or velocities or accelerations depending on the specific nature of the admittance and impedance.

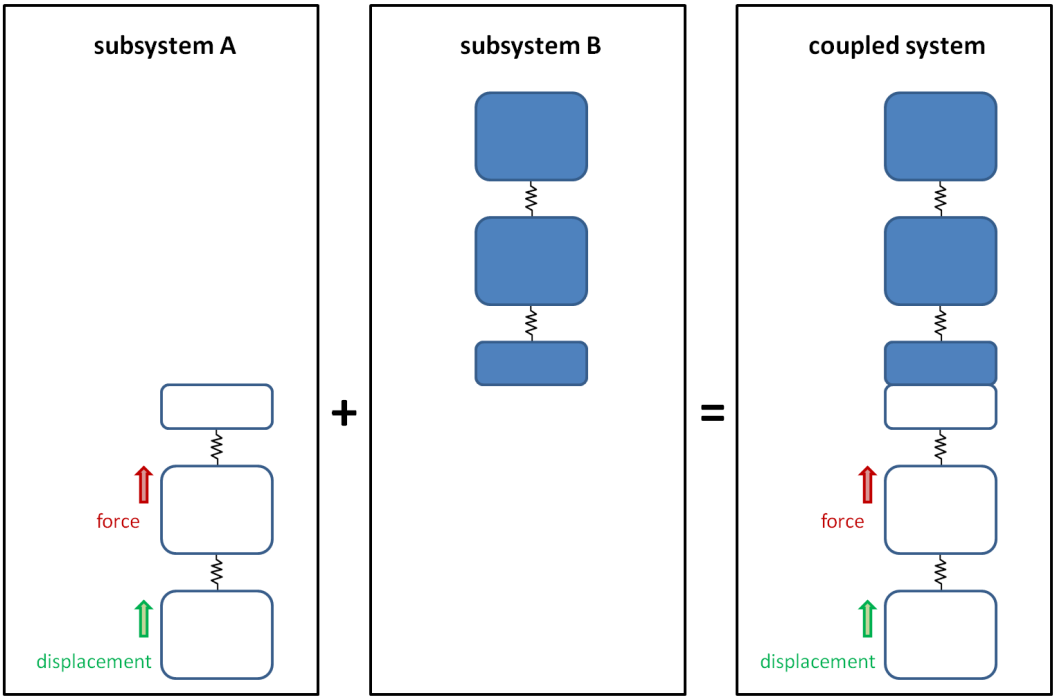

Figure 3.6: Example model for the explanation of the Blocked Force Method based on (Rixen et al. 2013)

The structural dynamic behavior of subsystem A is described by the dynamic impedance matrix $\mathbf{Z}^A(\Omega)$ or the dynamic admittance matrix $\mathbf{Y}^A(\Omega)$ in frequency domain. (3.3) and (3.4) show the partitions of the matrices of subsystem A. The subscript i is used for the internal degree of freedoms (DOFs) inside a subsystem. The subscript c is used for the external degree of freedoms that are connected to another subsystem.

$$\mathbf{Z}^A(\Omega) = \begin{bmatrix} Z_{ii}^A & Z_{ic}^A \\ Z_{ci}^A & Z_{cc}^A \end{bmatrix} \quad (3.3)$$

$$\mathbf{Y}^A(\Omega) = \begin{bmatrix} Y_{ii}^A & Y_{ic}^A \\ Y_{ci}^A & Y_{cc}^A \end{bmatrix} \quad (3.4)$$

Analog to the dynamic impedance and dynamic admittance matrix of the subsystem A, the matrices can be generated for the subsystem B

$$\mathbf{Z}^B(\Omega) = \begin{bmatrix} Z_{ii}^B & Z_{ic}^B \\ Z_{ci}^B & Z_{cc}^B \end{bmatrix}, \quad (3.5)$$

$$\mathbf{Y}^B(\Omega) = \begin{bmatrix} Y_{ii}^B & Y_{ic}^B \\ Y_{ci}^B & Y_{cc}^B \end{bmatrix}. \quad (3.6)$$

For both subsystems the dynamic equilibrium can be described by the admittance form or the impedance form. Eq. (3.7) shows the dynamic equilibrium of subsystem A by using the admittance form. The vector $\mathbf{u}$ represents the displacements or velocities or accelerations of the subsystem depending on the specific nature of the admittance and impedance matrix. The vector $\mathbf{f}$ represents the external and internal forces of a subsystem.

$$\begin{bmatrix} Y_{ii}^A & Y_{ic}^A \\ Y_{ci}^A & Y_{cc}^A \end{bmatrix} \begin{bmatrix} \mathrm{f}_i^A \\ \mathrm{f}_c^A \end{bmatrix} = \begin{bmatrix} u_i^A \\ u_c^A \end{bmatrix} \quad (3.7)$$

Eq. (3.8) shows the dynamic equilibrium of subsystem A by using the impedance form.

$$\begin{bmatrix} Z_{ii}^A & Z_{ic}^A \\ Z_{ci}^A & Z_{cc}^A \end{bmatrix} \begin{bmatrix} u_i^A \\ u_c^A \end{bmatrix} = \begin{bmatrix} \mathrm{f}_i^A \\ \mathrm{f}_c^A \end{bmatrix} \quad (3.8)$$

The dynamic equilibrium of the subsystem B is analog to the Eq. (3.7) and Eq. (3.8) by changing the indices A to B.

If the subsystem A and B are coupled to one coupled system, the structural dynamic behavior will be modified. The dynamic equilibrium of the coupled system is shown in Eq. (3.9) by using the admittance form and in Eq. (3.10) by using the impedance form.

$$\begin{bmatrix} Y_{ii}^A & Y_{ic}^A & \mathbf{0} & \\ Y_{ci}^A & Y_{cc}^A & & \\ & \mathbf{0} & Y_{cc}^B & Y_{ci}^B \\ & & Y_{ic}^B & Y_{ii}^B \end{bmatrix} \begin{bmatrix} \mathrm{f}_i^A \\ \mathrm{f}_c^A \\ \mathrm{f}_c^B \\ \mathrm{f}_i^B \end{bmatrix} = \begin{bmatrix} u_i^A \\ u_c^A \\ u_c^B \\ u_i^B \end{bmatrix} \tag{3.9}$$

$$\begin{bmatrix} Z_{ii}^A & Z_{ic}^A & \mathbf{0} & \\ Z_{ci}^A & Z_{cc}^A & & \\ & \mathbf{0} & Z_{cc}^B & Z_{ci}^B \\ & & Z_{ic}^B & Z_{ii}^B \end{bmatrix} \begin{bmatrix} u_i^A \\ u_c^A \\ u_c^B \\ u_i^B \end{bmatrix} = \begin{bmatrix} \mathrm{f}_i^A \\ \mathrm{f}_c^A \\ \mathrm{f}_c^B \\ \mathrm{f}_i^B \end{bmatrix} \tag{3.10}$$

The following explanation only uses the impedance form. The dynamic equilibrium of the coupled system can also be written in a primal or a dual assembled impedance form. The explanation of the dual assembled impedance form can be read in (Rixen et al. 2013). This dissertation uses the primal assembled impedance form that is explained now.

The primal variables are the displacements u^A and u^B by using the impedance form. At first a unique set u_c of connecting DOFs has to be defined

$$u_c = u_c^A - (u_c^A - u_c^B) = u_c^B. \tag{3.11}$$

Also u_c can be defined as

$$u_c = u_c^B + (u_c^A - u_c^B) = u_c^A. \tag{3.12}$$

For the force of connecting DOFs obtains the Eq. (3.13).

$$\mathrm{f}_c = \mathrm{f}_c^A + \mathrm{f}_c^B \tag{3.13}$$

If the defined u_c in Eq. (3.11) and the Eq. (3.13) is used in the dynamic equation (3.10), the Eq. (3.14) can be constructed.

$$\begin{bmatrix} Z_{ii}^A & Z_{ic}^A & 0 \\ Z_{ci}^A & Z_{cc}^A + Z_{cc}^B & Z_{ci}^B \\ 0 & Z_{ic}^B & Z_{ii}^B \end{bmatrix} \begin{bmatrix} u_i^A \\ u_c \\ u_i^B \end{bmatrix} = \begin{bmatrix} \mathrm{f}_i^A - Z_{ic}^A(u_c^A - u_c^B) \\ \mathrm{f}_c - Z_{cc}^A(u_c^A - u_c^B) \\ \mathrm{f}_i^B \end{bmatrix} \tag{3.14}$$

With the derivation of the primal assembled impedance form, the basis for the explanation of the Blocked Force Method is given. The Eq. (3.15) shows the problem of the coupled system by assuming the difference between u_c^A and u_c^B is zero, the

external force is only impressed on subsystem A and there is no impressed external displacement.

$$\begin{bmatrix} Z_{ii}^{A} & Z_{ic}^{A} & 0 \\ Z_{ci}^{A} & Z_{cc}^{A}+Z_{cc}^{B} & Z_{ci}^{B} \\ 0 & Z_{ic}^{B} & Z_{ii}^{B} \end{bmatrix} \begin{bmatrix} u_i^A \\ u_c \\ u_i^B \end{bmatrix} = \begin{bmatrix} \mathrm{f}_i^A \\ \mathrm{f}_c^A \\ 0 \end{bmatrix} \quad (3.15)$$

For the practical use in hardware experiments, it is advantageous to eliminate the internal forces, because the internal forces cannot be measured in most cases. At first the internal DOFs u_i^A are eliminated in Eq. (3.16).

$$\begin{bmatrix} (Z_{cc}^{A}+Z_{cc}^{B}) - Z_{ci}^{A}{Z_{ii}^{A}}^{-1}Z_{ic}^{A} & Z_{ci}^{B} \\ Z_{ic}^{B} & Z_{ii}^{B} \end{bmatrix} \begin{bmatrix} u_c \\ u_i^B \end{bmatrix} = \begin{bmatrix} f_c^A - Z_{ci}^{A}{Z_{ii}^{A}}^{-1}\mathrm{f}_i^A \\ 0 \end{bmatrix} \quad (3.16)$$

The next step is to measure or calculate the force on the interface of subsystem A by fixing the DOFs u_c. This reaction forces are called blocked forces. The Eq. (3.17) shows the dynamic equilibrium of the subsystem A with fixed interface DOFs.

$$\begin{bmatrix} Z_{ii}^{A} & Z_{ic}^{A} \\ Z_{ci}^{A} & Z_{cc}^{A} \end{bmatrix} \begin{bmatrix} u_i^A \\ 0 \end{bmatrix} = \begin{bmatrix} \mathrm{f}_i^A \\ \mathrm{f}_c^A + \mathrm{f}_{c,blocked\ force}^A \end{bmatrix} \quad (3.17)$$

The equation can be solved for the blocked force $\mathrm{f}_{c,blocked\ force}^A$ that is shown in Eq. (3.18).

$$\mathrm{f}_{c,blocked\ force}^A = -\mathrm{f}_c^A + Z_{ci}^A u_i^A = -\mathrm{f}_c^A + Z_{ci}^A {Z_{ii}^A}^{-1}\mathrm{f}_i^A \quad (3.18)$$

In Eq. (3.18) can be seen that the blocked force multiplied by -1 is equal to the right hand side of Eq. (3.16). So it is possible to use Eq. (3.18) and Eq. (3.17) in Eq. (3.16) to get Eq. (3.19).

$$\begin{bmatrix} (Z_{cc}^{A}+Z_{cc}^{B}) - Z_{ci}^{A}{Z_{ii}^{A}}^{-1}Z_{ic}^{A} & Z_{ci}^{B} \\ Z_{ic}^{B} & Z_{ii}^{B} \end{bmatrix} \begin{bmatrix} u_c \\ u_i^B \end{bmatrix} = \begin{bmatrix} -\mathrm{f}_{c,blocked\ force}^A \\ 0 \end{bmatrix} \quad (3.19)$$

Therefore, a substitutive expression for the coupled system without considering internal forces can be written.

$$\begin{bmatrix} Z_{ii}^A & Z_{ic}^A & 0 \\ Z_{ci}^A & Z_{cc}^A + Z_{cc}^B & Z_{ci}^B \\ 0 & Z_{ic}^B & Z_{ii}^B \end{bmatrix} \begin{bmatrix} u_i^A \\ u_c \\ u_i^B \end{bmatrix} = \begin{bmatrix} 0 \\ -\mathrm{f}_{c,blocked\ force}^A \\ 0 \end{bmatrix} \quad (3.20)$$

The internal DOFs of u_i^A in the solution of the substitutive problem result to a different solution, but usually that is not the focus of the analysis. The important results in most analyses are the displacements of the subsystem B u_i^B.

(Rixen et al. 2013) focuses on the use of the Blocked Force Method for experimental tests. This dissertation uses the Blocked Force Method for numerical calculations, see also (van der Valk and Rixen 2013). The procedure to apply the method is analog. At first the coupling interface of the excitation subsystem has to be fixed to an infinitely stiff support, respectively a boundary condition with zero displacement. Now the blocked force on the interface can be calculated. The force only contains the structural dynamic behavior of the subsystem A. Afterwards the subsystem A and the subsystem B has to be coupled and the blocked force can be impressed on the coupling interface. For a better understanding, the Figure 3.7 shows a graphical representation of the Blocked Force Method by using a three-mass oscillator.

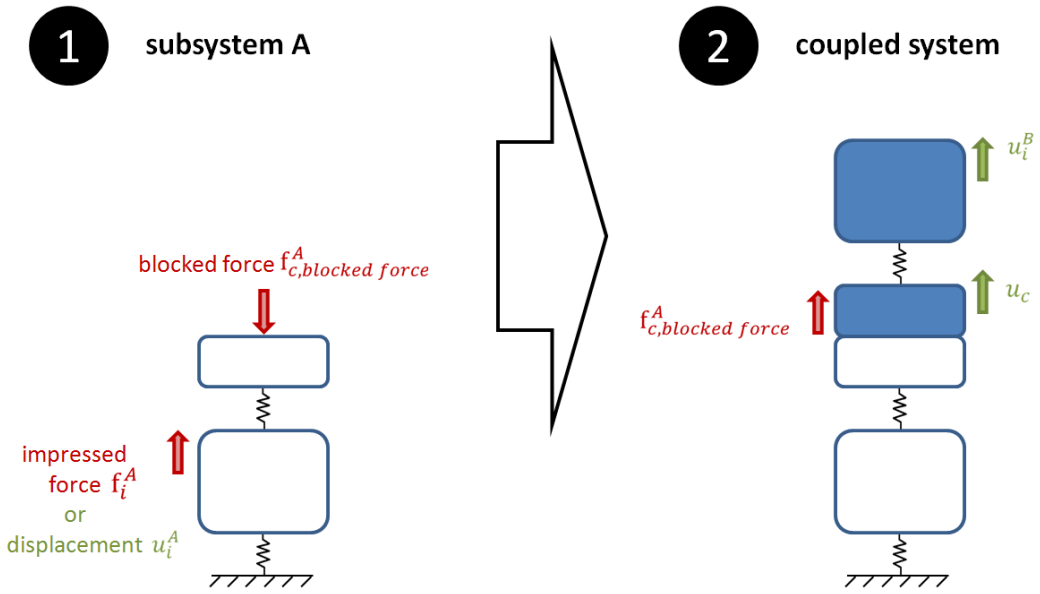

Figure 3.7: Graphical representation of the application of the Blocked Force Method based on (Rixen et al. 2013)

Beside the Blocked Force Method another method should be mentioned. The interface Free Velocity Method is analog to the Blocked Force Method. The main difference is that the coupling interface is not fixed in the first step of the procedure. So the displacement can be calculated on the interface of subsystem A. In the second step the calculated displacement on the coupling interface can be impressed on the coupled system. The Free Velocity Method is often used in the field of acoustics and vibro-acoustics (Cremer et al. 2005, Petersson and Gibbs 2000).

3.5.4 Cutting Force Principle

The Cutting Force Principle is based on the third Newton's law. The third Newton's law is the lex tertia of Sir Isaac Newton and was first published in 1687 (Newton 1687). The law says that forces always occur pairwise. If a body A exerts a force to another body B, so an opposed force of the same amount exerts from body B to body A.

$$\vec{f}_{A\to B} = -\vec{f}_{B\to A} \qquad (3.21)$$

The third law of Isaac Newton can be used for the calculation of operational vibrations. Figure 3.8 shows the process of the application of the Cutting Force Principle.

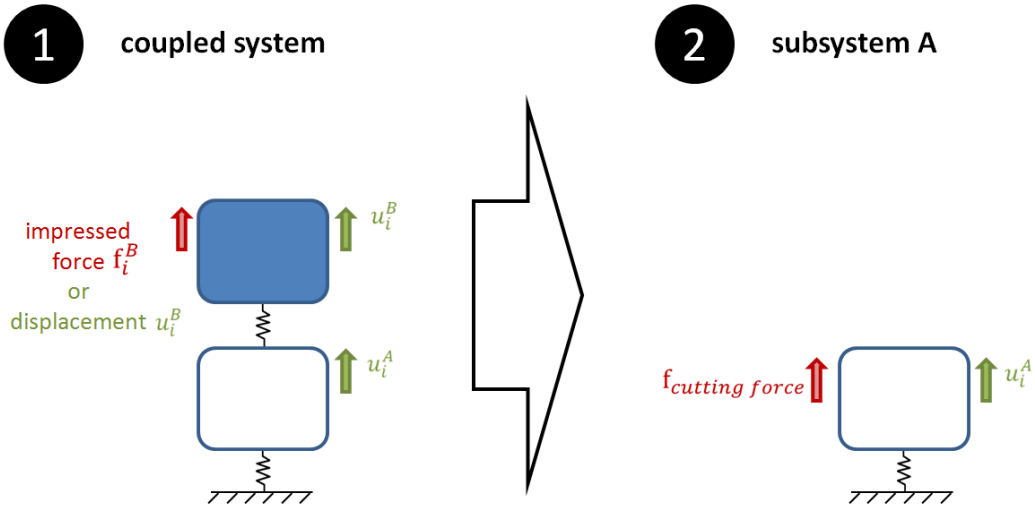

Figure 3.8: Graphical representation of the application of the Cutting Force Principle

Here the Cutting Force Principle is explained by a two-mass oscillator. At first the coupled system has to be modeled. Eq. (3.22) shows the dynamic impedance matrix of the two-mass oscillator.

$$\mathbf{Z}(\Omega) = \begin{bmatrix} Z_{AA} & Z_{AB} \\ Z_{BA} & Z_{BB} \end{bmatrix} \quad (3.22)$$

The matrix elements Z_{AA} and Z_{BB} represent the point impedance of subsystem A (Z_{AA}) and subsystem B (Z_{BB}). A point impedance means the division of the impressed force by the measured displacement, velocity or acceleration at the same position of force-impressing. The matrix elements Z_{AB} and Z_{BA} represent the transfer impedance between the subsystems A and B. A transfer impedance means the relation between the impressed force to the measured displacement, velocity or acceleration at another position of the system. (de Klerk 2004)

Eq. (3.23) shows the dynamic equilibrium of a two-mass oscillator.

$$\begin{bmatrix} Z_{AA} & Z_{AB} \\ Z_{BA} & Z_{BB} \end{bmatrix} \begin{bmatrix} u_i^A \\ u_i^B \end{bmatrix} = \begin{bmatrix} \mathrm{f}_i^A \\ \mathrm{f}_i^B \end{bmatrix} \quad (3.23)$$

The vector $\mathbf{u}$ represents the displacement, velocity or acceleration of the masses depending on the specific nature of the impedance matrix. The vector $\mathbf{f}$ represents the forces on the masses. Let's assume that the force f_i^A is zero and the force f_i^B represents an external force. Now the value of u_i^A should be calculated by using the Cutting Force Principle. The Eq. (3.24) shows the dynamic equilibrium of the coupled system (e. g. two-mass oscillator).

$$\begin{aligned} Z_{AA} u_i^A + Z_{AB} u_i^B &= 0 \\ Z_{BA} u_i^A + Z_{BB} u_i^B &= \mathrm{f}_i^B \end{aligned} \quad (3.24)$$

The multiplication of Z_{AB} and u_i^B is equal to the cutting force $\mathrm{f}_{cutting\ force}$ which can be used for the second step. The second step only uses the subsystem A and the pre-calculated cutting force $\mathrm{f}_{cutting\ force}$. Eq. (3.25) shows the dynamic equilibrium of subsystem A.

$$Z_{AA} u_i^A = 0 \tag{3.25}$$

Referring to the third Newton's law in Eq. (3.21), the negate cutting force can be impressed.

$$Z_{AA} u_i^A = -\mathrm{f}_{cutting\ force} \tag{3.26}$$

So the cutting force is defined as the multiplication of Z_{AB} and u_i^B and can be replaced in Eq. (3.27), whereupon u_i^B is already known.

$$Z_{AA} u_i^A = -Z_{AB} u_i^B \tag{3.27}$$

Now the Eq. (3.27) has one unknown variable u_i^A and can be solved.

$$u_i^A = \frac{-Z_{AB} u_i^B}{Z_{AA}} \tag{3.28}$$

Eq. (3.28) is equal to the first row of the coupled system in Eq. (3.24) with the difference that the variable u_i^B in Eq. (3.28) is already known.

In this simple example, the application of the Cutting Force Principle does not get any advantage, because the variable of interest u_i^A is already calculated in the first step. But for complex coupled systems, the Cutting Force Principle can be useful to reduce calculation time. For example, the subsystem B can be used as a reduced FE-Model in a MBS-Simulation, because a MBS-Simulation with the complete FE-Model can be very time-consuming for complex models with many DOFs and uses a lot of memory capacity. But the nodal displacements of the complete FE-Model can be interesting for the engineer. So at first the forces on the coupling interfaces between the subsystems can be calculated by using the MBS-Simulation. And the second step of calculation uses the complete FE-Model and the calculated cutting forces from the MBS-Simulation. The advantage of this method is that modeled nonlinear behaviors are considered, if both calculation steps are in time domain.

3.5.5 Structural coupling of mass dampers

This chapter deals with the dimensioning of mass dampers to reduce high vibrations of systems in a defined frequency range. The knowledge about dimensioning of mass

dampers is the basis for the described method in chapter 4.2.6. The following explanation is based on (Maurer Söhne 2011), which concentrates on vibration damping of civil engineering constructive works. The eigenfrequencies of civil engineering structures are often low as well as the modal damping. So the use of the civil engineering structures is impossible or only possible in a limited way. Furthermore, the civil engineering structures can be damaged by vibrations. In order to avoid these scenarios, mass dampers can be used. The dimensioning of the mass damper is mainly based on the frequency, mass and direction of the oscillation. To reduce the vibrations, a defined structural coupling between the system (e. g. civil engineering structures) and the mass damper is the desired aim. Simplified a single-mass oscillator can be imagined, whose amplification factor should be reduced by using a mass damper.

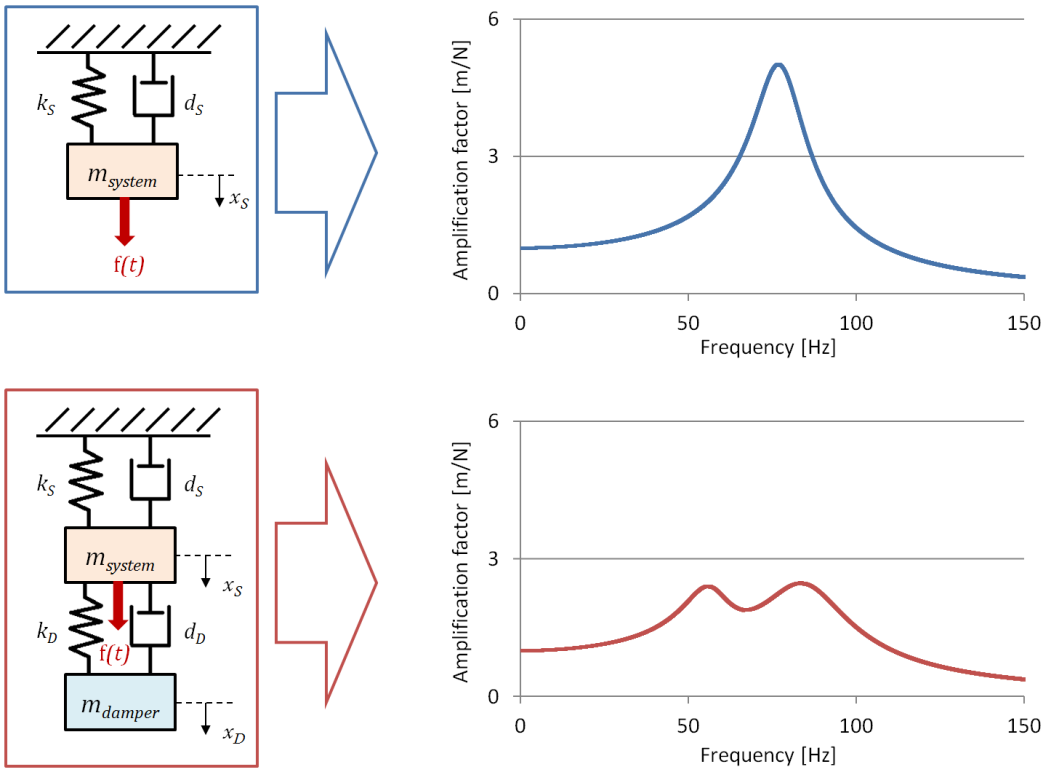

Figure 3.9: Comparison of the amplification functions of a system with and without a mass damper based on (Maurer Söhne 2011)

Figure 3.9 shows the effect of the mass damper to the amplification function of the single-mass oscillator. To reach the optimal vibration reducing, the mass, stiffness and damping of the mass damper has to be dimensioned by using the following criteria.

The mass ratio μ between the mass of the mass damper and the oscillating mass of system is shown in Eq. (3.29).

$$\mu = \frac{m_{damper}}{m_{system}} \qquad (3.29)$$

Referring to (Maurer Söhne 2011) a mass ratio smaller than 0.02 results in high amplitudes of the mass damper relative to the system and a small frequency range of the vibration reducing effect. For mass ratios higher than 0.025, the amplitudes of the mass damper are smaller and the range of vibration reducing is higher, too.

Another criterion to dimensioning a mass damper is the ratio between the eigenfrequency of the mass damper and the system. Referring to (Maurer Söhne 2011) the frequency ratio criterion has the highest influence to the efficiency of the mass damper. For a harmonic force excitation, the optimal frequency ratio according to DEN HARTOG is:

$$\kappa_{opt} = \frac{f_{eigen,damper}}{f_{eigen,system}} = \frac{1}{1+\mu} < 1 \qquad (3.30)$$

Furthermore, the damping factor of the mass damper has to be dimensioned by the used mass ratio. Referring to (Maurer Söhne 2011) the optimal damping has a low influence as against the optimal frequency ratio for the efficiency of the mass damper. The optimal Lehr's damping factor can be calculated by using the Eq. (3.31).

$$\zeta_{opt} = \sqrt{\frac{3\mu}{8(1+\mu)^3}} \qquad (3.31)$$

(Buck 2005) describes the basis challenges of the dimensioning of linear mass dampers in the automotive industry. Here mass dampers are used to reduce nuisance sounds and vibrations. Furthermore, lifetime problems due to vibrations can be solved. Important is the right choice of the elastomer coupling, which determines the stiffness and damping of the mass damper. The advantage of the material is the high damping factor, but the disadvantage is the high nonlinearity of the material. So it is difficult to design the elastomer coupling for several load cases and temperatures. A detailed list of elastomer properties can be found in (Dubbel et al. 2001) and (Hempel 2002).

4 Definition and application of wise abstraction levels

4.1 Methodic procedure

This chapter deals with the methodic procedure of the dissertation. A reminder: The dissertation should help the engineers to model complex coupled systems for calculating operational vibrations. So the engineers have to apply an efficient abstraction level. To decide which abstraction level is the probably best for the analyzing problem, the engineers have to know which effects are considered or neglected by the abstraction levels. The dissertation focuses on structural coupling and excitation interaction effects. (Chapter 1)

Now the different abstraction levels have to be identified. Before the abstraction levels can be described in detail, the aims of the abstraction levels have to be concretized. The following itemization shows the aims for the identification of the abstraction levels.

- Effects of coupled systems should be separated by different abstraction levels.
- The abstraction levels should be generally applicable.
- The abstraction levels should calculate the excitation forces and the operational vibrations of the system housing.

Based on the mentioned literature in chapter 2 and 3 the reasonable abstraction levels in Figure 4.1 can be identified.

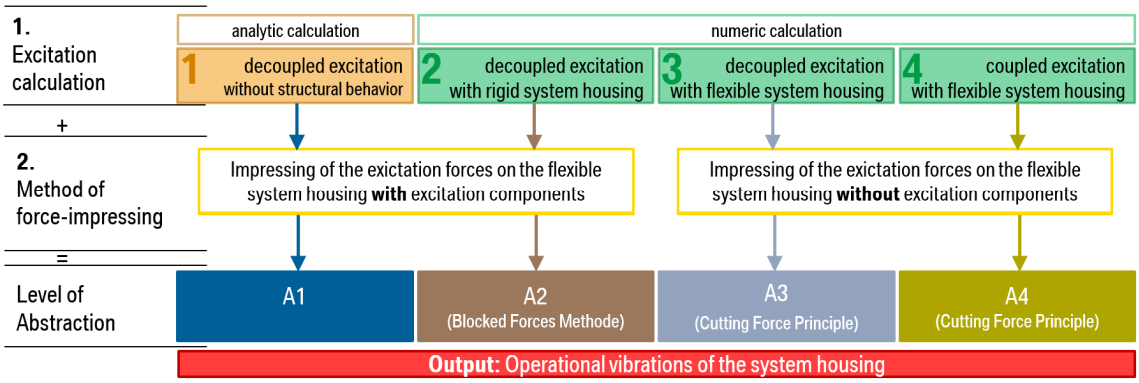

Figure 4.1: Defined abstraction levels

Figure 4.1 shows four abstraction levels from A1 to A4. Each abstraction level can be split up in an excitation calculation and a force-impressing calculation. So there are four different excitation calculations and two different methods of force-impressing.

The excitation calculation calculates the forces and moments which result from moved components of the system. This forces and moments can be impressed on the system housing with or without the excitation components in time or frequency domain to calculate the operational vibrations of the system housing. For the excitation calculation 1 and 2 the force-impressing method with excitation components is reasonable that can be concluded from understanding the explained Blocked Force Method in chapter 3.5.3. Likewise, the calculated forces from the excitation calculation 3 and 4 should only be impressed on the system housing without excitation components, see chapter 3.5.4.

Now each abstraction level should be explained separately.

A1: The abstraction level A1 represents the highest abstraction level. The forces and moments from the movement of the excitation components are calculated by using rigid bodies. So the structural dynamic behavior of the excitation components and the structural dynamic behavior of the system housing are not contained in the forces and moments. The excitation model is quite simple to build up and the calculation time is very short. Finally, the forces and moments can be impressed on the system housing with excitation components in time or frequency domain. At this calculation, the structural dynamic behavior of the

system housing with excitation components and their couplings are considered.

A2: A2 is more complex than A1. The excitation calculation is decoupled from the system housing and other subsystems. Mostly it is recommended to use an MBS-Simulation method with reduced FE-Models to calculate the forces. It contains the structural dynamic behavior of the excitation components that are reduced by e. g. the Craig Bampton Method. The interfaces that are adjacent to other structures (system housing, submodel of a second excitation, and so on) have a fixed boundary condition in displacements. The forces and moments that result at the interfaces can be used as input parameter for the calculation of the operational vibration. So the forces and moments can be impressed on the system housing with excitation components like in abstraction level A1.

A3: The excitation calculation is decoupled from other excitation subsystems. The difference to the excitation calculation in A2 is the considering of the structural dynamic behavior of the system housing at the force calculation. So the excitation calculation considers the correct structural dynamic behavior in each time-step of the simulation and the Cutting Force Principle can be used. The forces and moments can be impressed on the system housing without excitation interaction, referred to the Cutting Force Principle that is explained in chapter 3.5.4.

A4: The abstraction level A4 is a full coupled model. Here the excitation calculation contains the structural dynamic behavior of the system housing and the interaction with other excitation subsystems. This abstraction level represents a very time-consuming calculation and a challenge for the modeling engineer. So it is difficult to handle such complex coupled models. The resulting forces and moments of the excitation calculation can be impressed on the system housing without excitation components, referred to the Cutting Force Principle.

After getting this short overview about the four abstraction levels that are used in this dissertation, the separation of the effects of structural couplings and excitation interaction can be explained.

A1 ↔ A2: The comparison of the results of A1 and A2 shows the influence of the structural dynamic behavior of the excitation components to the operational vibrations. In chapter 4.2.6.1, the dissertation explains a criterion that helps the engineer to decide, if the structural dynamic behavior of an excitation component can be neglected.

A2 ↔ A3: Referred to the theory of the Blocked Force Method in chapter 3.5.3, the comparison of the results of A2 and A3 should not show any difference. This statement is correct for models that comply with some criteria. So the dissertation shows the limits of the Blocked Force Method by using the comparison of A2 and A3 in chapter 4.4.4.

A3 ↔ A4: The comparison of the results of A3 and A4 shows the influence of the excitation interaction. So the abstraction level A3 considers the structural dynamic behavior of the system and the abstraction level A4, too. But additionally to the structural dynamic behavior, the abstraction level A4 considers the excitation interaction with other excitation components of the system.

Now we know how the effects of structural coupling and excitation interaction can be separated by using reasonable abstraction levels. But sometimes it is very difficult to interpret the effects by using complex systems. So it is necessary to use different Level of Complexity. Figure 4.2 shows the calculation matrix that is used to separate the physical effects. The Level of Complexity reaches from a simple multi-mass system and a simple three-dimensional model to a complex three-dimensional reference model. So if a physical effect cannot be identified by comparing two abstraction levels using a simple multi-mass system, the physical effect can be identified and interpreted by using the next Level of Complexity.

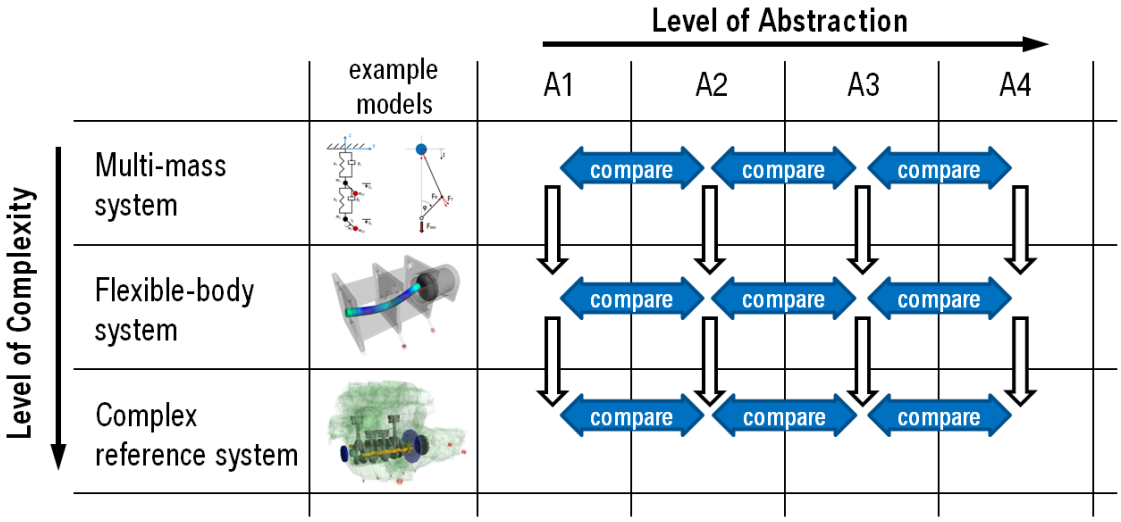

Figure 4.2: Methodical procedure matrix to separate physical effects

The next chapters are structured as shown in the matrix of Figure 4.2. It starts with the first Level of Complexity (multi-mass system) by using all Levels of Abstraction and go on with the next Level of Complexity.

4.2 Explanation of the abstraction levels for a simple multi-mass system

4.2.1 Description of the total system

At first the total system in Figure 4.3 should be described that is used in this chapter.

Set of parameter

m_1 = 100kg
m_2 = 100kg
m_{U1} = 20kg
m_{U2} = 20kg

k_1 = 1579.8N/mm
k_2 = 1579.8N/mm

d_1 = 1.5798Ns/mm
d_2 = 1.5798Ns/mm

l_1 = 500mm
l_2 = 1000mm

Ω_1 = 20Hz
Ω_2 = 10Hz
Ω_{ext} = 5Hz

$\hat{f}_{ext,x'}$ = 100kN

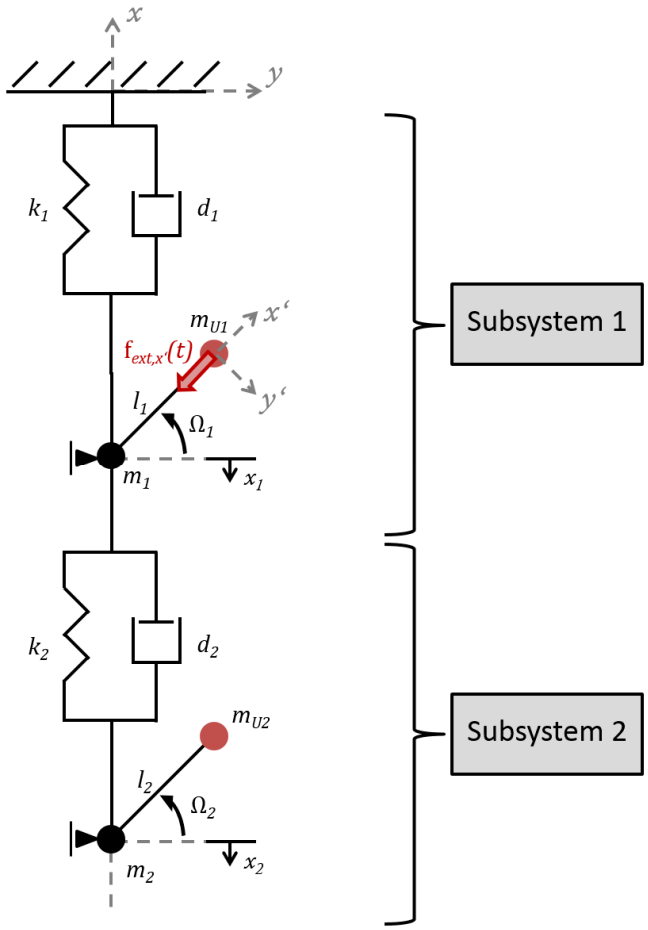

Figure 4.3: Total multi-mass system

It is based on the coupled system in chapter 2.4.1 and is extended by the viscous damping parameters d_1, d_2 and an external force $f_{ext,x'}(t)$, which operates on the mass m_{U1} with an angular frequency Ω_{ext}. Eq. (4.1) shows the differential equation of the two-mass oscillator with rotating masses extended by the damping matrix. The external force is excluded in Eq. (4.1) .

$$\begin{bmatrix} m_1 & 0 \\ 0 & m_2 \end{bmatrix}\begin{bmatrix} \ddot{x}_1 \\ \ddot{x}_2 \end{bmatrix} + \begin{bmatrix} d_1 + d_2 & -d_2 \\ -d_2 & d_2 \end{bmatrix}\begin{bmatrix} \dot{x}_1 \\ \dot{x}_2 \end{bmatrix} + \begin{bmatrix} k_1 + k_2 & -k_2 \\ -k_2 & k_2 \end{bmatrix}\begin{bmatrix} x_1 \\ x_2 \end{bmatrix} = \begin{bmatrix} m_{U1} \cdot \Omega_1^2 \cdot l_1 \cdot sin(\Omega_1 t) - m_{U1}\ddot{x}_1 \\ m_{U2} \cdot \Omega_2^2 \cdot l_2 \cdot sin(\Omega_2 t) - m_{U2}\ddot{x}_2 \end{bmatrix} \quad (4.1)$$

The external force $\mathrm{f}_{ext,x'}(t)$ operates in the local rotating coordinate system x', y' and is defined in Eq. (4.2). $\hat{\mathrm{f}}_{ext,x'}$ represents the maximum value of the force

$$\mathrm{f}_{ext,x'}(t) = \hat{\mathrm{f}}_{ext,x'} \cdot cos\,(\Omega_{ext} t)\,. \quad (4.2)$$

To include the external force in the differential equation of the two-mass oscillator, it is necessary to transform Eq. (4.2) in the global stationary coordinate system x, y. Therefore, a transfer from the rotating coordinate system to the stationary coordinate system occurs, which results in an amplitude modulation. So the force $\mathrm{f}_{ext,x'}(t)$ has to be projected on the axis of the stationary coordinate system (see Figure 4.4).

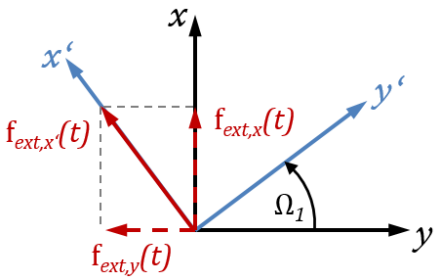

Figure 4.4: Coordinate transform

Due to the overlaying rotation Ω_1, the force $\mathrm{f}_{ext,x}(t)$ can be written as

$$\mathrm{f}_{ext,x}(t) = \mathrm{f}_{ext,x'}(t) \cdot sin(\Omega_1 t) = \hat{\mathrm{f}}_{ext,x'} \cdot cos\,(\Omega_{ext} t) \cdot sin(\Omega_1 t)\,. \quad (4.3)$$

By using the addition theorem in Eq. (4.4).

$$sin(x)\,cos(y) = \frac{1}{2}(sin(x - y) + sin(x + y)) \quad (4.4)$$

It is possible to get a pure sine function for the external force $\mathrm{f}_{ext,x}(t)$ in the stationary coordinate system

$$\mathrm{f}_{ext,x}(t) = \frac{\hat{\mathrm{f}}_{ext,x'}}{2} \cdot \left[sin\big((\Omega_1 - \Omega_{ext})t\big) + sin((\Omega_1 + \Omega_{ext})t)\right]. \quad (4.5)$$

Figure 4.5 shows the external force in time and frequency domain. The upper diagrams show the force $f_{ext,x'}(t)$ in the rotating coordinate system and the lower diagrams show the force $f_{ext,x}(t)$ in the stationary coordinate system. So it can be seen that the two-mass oscillator is excited by the two modulated oscillations $(\Omega_1 - \Omega_{ext})$ and $(\Omega_1 + \Omega_{ext})$.

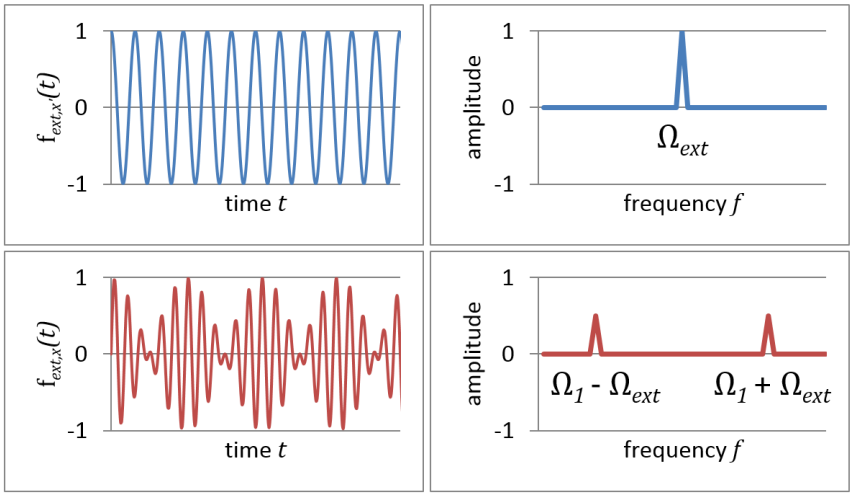

Figure 4.5: Amplitude modulation in time and frequency domain

The differential equation of the total system with the external force can be written as

$$\begin{bmatrix} m_1 & 0 \\ 0 & m_2 \end{bmatrix}\begin{bmatrix} \ddot{x}_1 \\ \ddot{x}_2 \end{bmatrix} + \begin{bmatrix} d_1 + d_2 & -d_2 \\ -d_2 & d_2 \end{bmatrix}\begin{bmatrix} \dot{x}_1 \\ \dot{x}_2 \end{bmatrix} + \begin{bmatrix} k_1 + k_2 & -k_2 \\ -k_2 & k_2 \end{bmatrix}\begin{bmatrix} x_1 \\ x_2 \end{bmatrix} = \begin{bmatrix} m_{U1} \cdot \Omega_1^2 \cdot l_1 \cdot sin(\Omega_1 t) - m_{U1}\ddot{x}_1 + f_{ext,x}(t) \\ m_{U2} \cdot \Omega_2^2 \cdot l_2 \cdot sin(\Omega_2 t) - m_{U2}\ddot{x}_2 \end{bmatrix}. \quad (4.6)$$

4.2.2 Abstraction level A1

The highest Level of Abstraction is represented by the abstraction level A1 in this dissertation. It is a mixture of two calculation methods, the rigid body system and the flexible body system simulation. The rigid body system simulation is used to calculate the excitation forces (right side of the differential equation) without structural dynamic behavior and excitation interaction. Eq. (4.7) shows the right side of the differential equation (4.6) to calculate the excitation forces $f_{x1}(t)$ and $f_{x2}(t)$.

$$\begin{bmatrix} \mathrm{f}_{x1}(t) \\ \mathrm{f}_{x2}(t) \end{bmatrix} = \begin{bmatrix} m_{U1} \cdot \Omega_1^2 \cdot l_1 \cdot sin(\Omega_1 t) - m_{U1}\ddot{x_1} + \mathrm{f}_{ext,x}(t) \\ m_{U2} \cdot \Omega_2^2 \cdot l_2 \cdot sin(\Omega_2 t) - m_{U2}\ddot{x_2} \end{bmatrix} \quad (4.7)$$

Given that the structural coupling of the excitation components to the two-mass oscillator is neglected, the accelerations $\ddot{x_1}$ and $\ddot{x_2}$ can be set to zero and the equation can be written as

$$\begin{bmatrix} \mathrm{f}_{x1}(t) \\ \mathrm{f}_{x2}(t) \end{bmatrix} = \begin{bmatrix} m_{U1} \cdot \Omega_1^2 \cdot l_1 \cdot sin(\Omega_1 t) + \mathrm{f}_{ext,x}(t) \\ m_{U2} \cdot \Omega_2^2 \cdot l_2 \cdot sin(\Omega_2 t) \end{bmatrix}. \quad (4.8)$$

The forces can be calculated, because the equations do not contain an unknown parameter of the two-mass oscillator (displacement, velocity, acceleration).

The next step is to impress the calculated forces on the flexible structure (two-mass oscillator) with excitation components. It is important to add the excitation components to the two-mass oscillator, because the excitation components influence the structural dynamic behavior of the total system. In this example, the excitation components consist of a mass point and a rigid rod, so it is possible to add the components by modifying the mass matrix. Due to the excitation components are rigid coupled to the two-mass oscillator and the impressed forces in one dimension, the abstraction level A1 considers the structural dynamic behavior of the total system and the effects of excitation interaction. If these restrictions are not given, the results do not contain the correct structural dynamic behavior and excitation interaction. The difference in results can be seen in the complexity level of flexible-body systems. The Eq. (4.9) shows the differential equation by impressed force output of the rigid body system simulation, which can typically be solved by a numeric method.

$$\begin{bmatrix} m_1 + m_{U1} & 0 \\ 0 & m_2 + m_{U2} \end{bmatrix} \begin{bmatrix} \ddot{x_1} \\ \ddot{x_2} \end{bmatrix} + \begin{bmatrix} d_1 + d_2 & -d_2 \\ -d_2 & d_2 \end{bmatrix} \begin{bmatrix} \dot{x}_1 \\ \dot{x}_2 \end{bmatrix} + \begin{bmatrix} k_1 + k_2 & -k_2 \\ -k_2 & k_2 \end{bmatrix} \begin{bmatrix} x_1 \\ x_2 \end{bmatrix} = \begin{bmatrix} \mathrm{f}_{x1}(t) \\ \mathrm{f}_{x2}(t) \end{bmatrix} \quad (4.9)$$

In this case, the excitation components can be switched to the right side of the equation, as shown in Eq. (4.10).

$$\begin{bmatrix} m_1 & 0 \\ 0 & m_2 \end{bmatrix}\begin{bmatrix} \ddot{x}_1 \\ \ddot{x}_2 \end{bmatrix} + \begin{bmatrix} d_1 + d_2 & -d_2 \\ -d_2 & d_2 \end{bmatrix}\begin{bmatrix} \dot{x}_1 \\ \dot{x}_2 \end{bmatrix} + \begin{bmatrix} k_1 + k_2 & -k_2 \\ -k_2 & k_2 \end{bmatrix}\begin{bmatrix} x_1 \\ x_2 \end{bmatrix} = \begin{bmatrix} \mathrm{f}_{x1}(t) - m_{U1}\ddot{x}_1 \\ \mathrm{f}_{x2}(t) - m_{U2}\ddot{x}_2 \end{bmatrix} \quad (4.10)$$

If we replace the rigid body forces ($\mathrm{f}_{x1}(t)$ and $\mathrm{f}_{x2}(t)$) by the analytic force equation in Eq. (4.8), the Eq. (4.10) is equal to the Eq. (4.6), which represents the total system with structural coupling and excitation interaction effects.

Additionally, Figure 4.6 displays the abstraction level A1 as a graphical schema to give a better understanding.

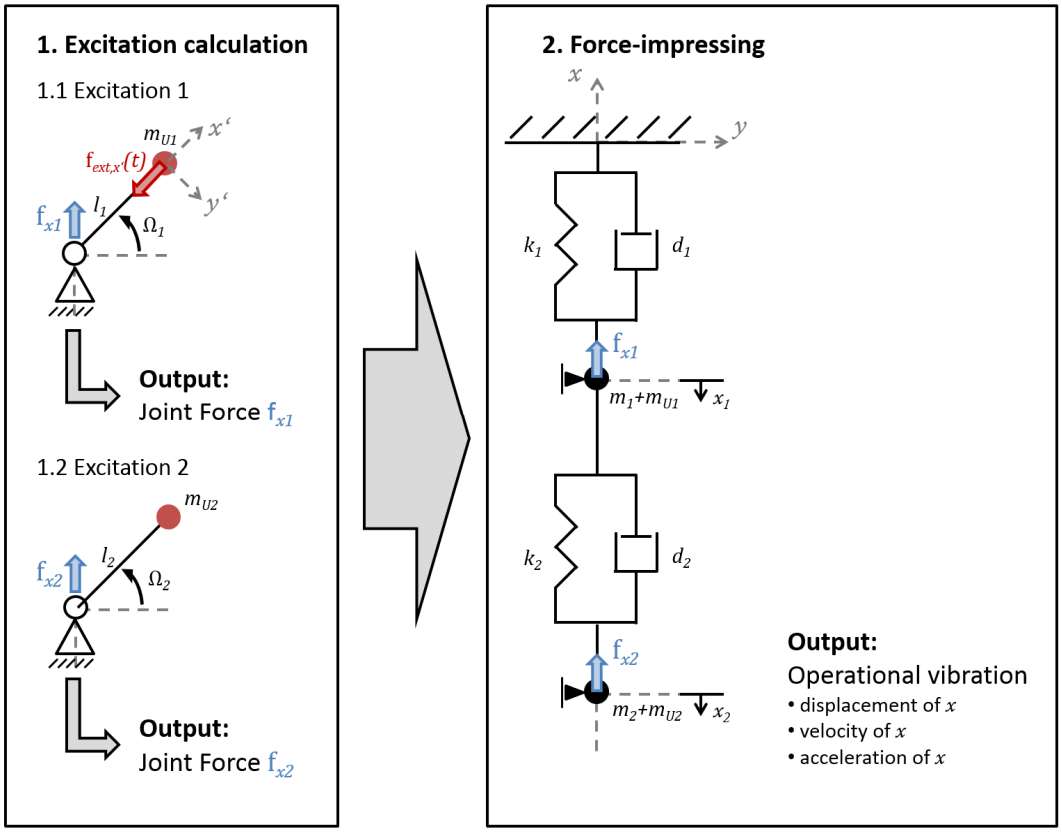

Figure 4.6: Abstraction level A1

Figure 4.7 shows the calculated accelerations $\ddot{x}_1$ and $\ddot{x}_2$ of the masses in time and frequency domain. Although the impressed forces do not contain the structural coupling and excitation interaction effects, the results of displacement, velocity and acceleration are exactly the same (by neglecting numerical errors) as the calculation with the abstraction level A4, which contains all coupling effects. The reason is that the

excitation components in this example can be added to the left side of the differential equation. So the structural dynamic behavior and the excitation interaction of the total system are contained in the numerical solution of the second step of the abstraction level.

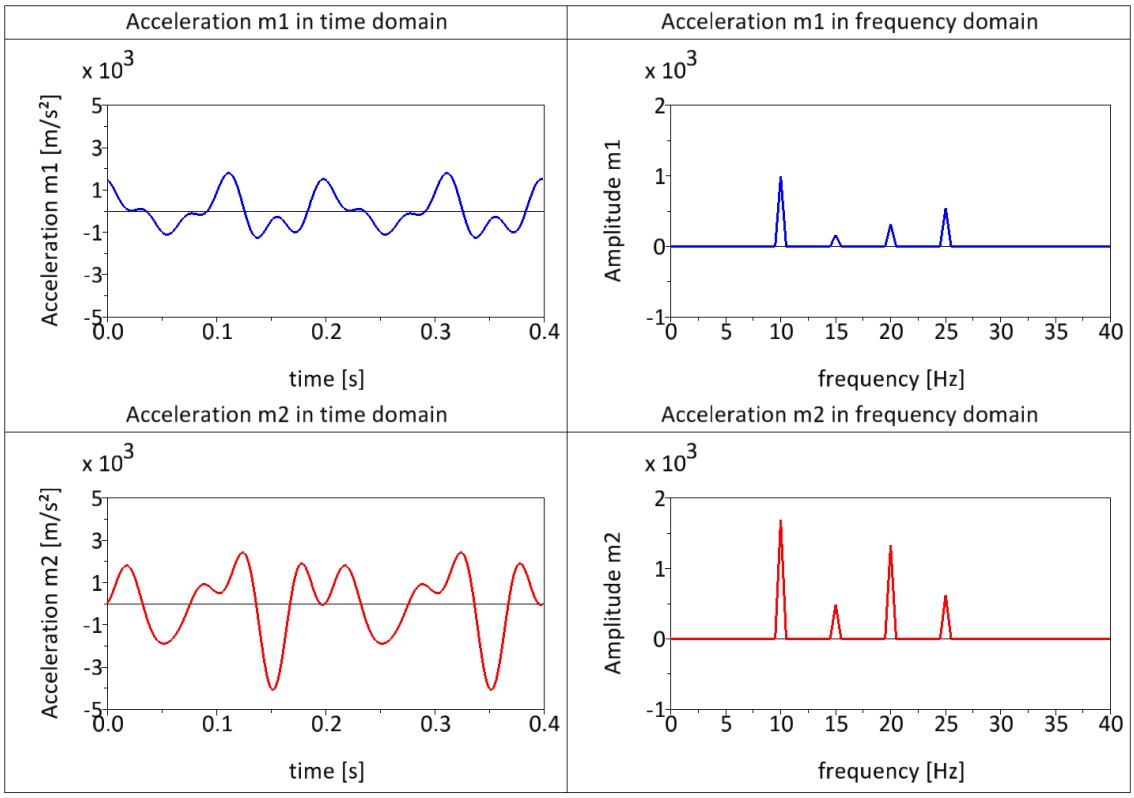

Figure 4.7: Accelerations m_1 and m_2 in time and frequency domain

4.2.3 Abstraction level A2

The difference between the abstraction level A2 and A1 can be found in the calculation of the external forces. So the abstraction level A2 bases on the Blocked Force Method, which is explained in chapter 3.5.3. In this special case, the same force equation will be solved for both abstraction levels. But generally in A1 the equation is solved by using rigid excitation bodies and in A2 the force equation is solved by using flexible excitation bodies. Given that the excitation components are rigid in this example, the difference between the calculated forces and displacements of the multi-mass system results from the numerical error. Figure 4.8 shows two identical output-curves,

because the numerical error is very low. As in A1, the abstraction level A2 also contains the structural coupling and the excitation interaction effects.

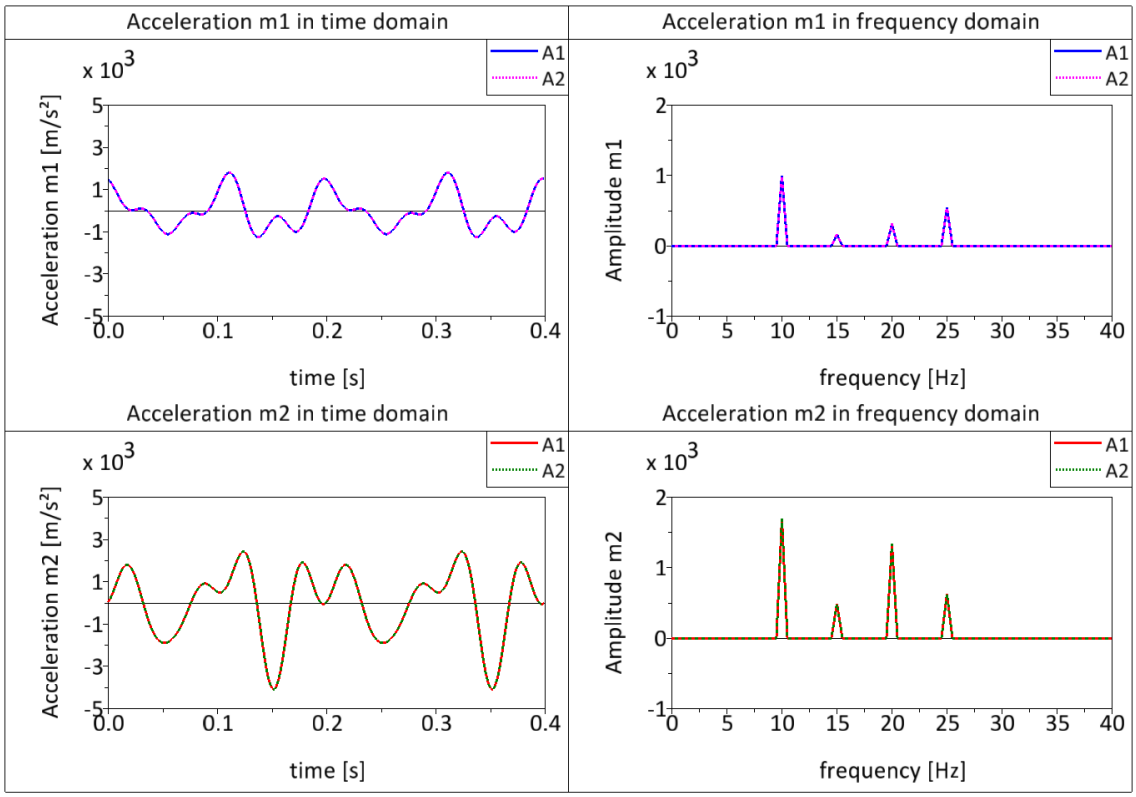

Figure 4.8: Comparison A1 and A2 in time and frequency domain

The next complexity level “flexible-body system” will show some differences in the force results, because the abstraction level A2 considers the structural dynamic behavior of the excitation components.

4.2.4 Abstraction level A3

The abstraction level A3 bases on the principle of cutting forces. Figure 4.9 shows the schematic procedure of the abstraction level A3 for the multi-mass system. Here the forces and the displacements are calculated by using numerical methods.

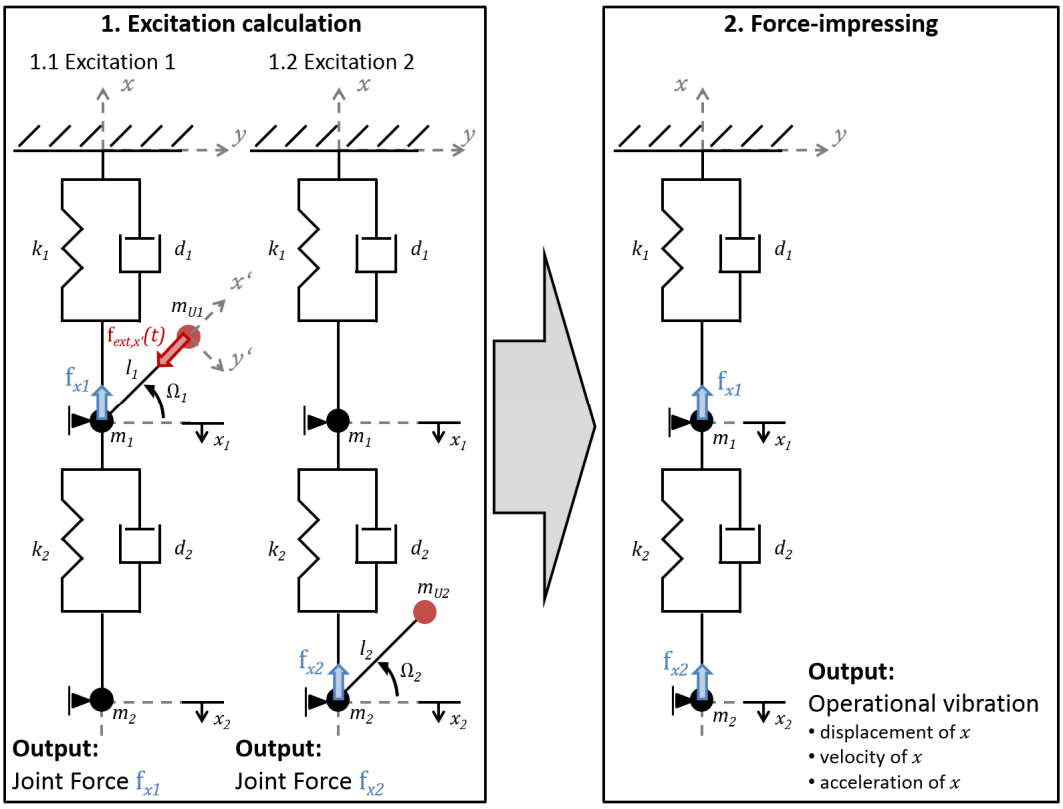

Figure 4.9: Abstraction level A3

The first step is to calculate the resulting forces of the rotating mass m_{U1} and the external force $f_{ext,x'}(t)$. In Eq. (4.11) it can be seen that the structural dynamic behavior of the multi-mass system is regarded, so that the Cutting Force Principle can be used to calculate the operational vibrations.

$$\begin{bmatrix} m_1 & 0 \\ 0 & m_2 + m_{U2} \end{bmatrix} \begin{bmatrix} \ddot{x}_1 \\ \ddot{x}_2 \end{bmatrix} + \begin{bmatrix} d_1 + d_2 & -d_2 \\ -d_2 & d_2 \end{bmatrix} \begin{bmatrix} \dot{x}_1 \\ \dot{x}_2 \end{bmatrix} + \begin{bmatrix} k_1 + k_2 & -k_2 \\ -k_2 & k_2 \end{bmatrix} \begin{bmatrix} x_1 \\ x_2 \end{bmatrix} = \begin{bmatrix} m_{U1} \cdot \Omega_1^2 \cdot l_1 \cdot sin(\Omega_1 t) - m_{U1}\ddot{x}_1 + f_{ext,x}(t) \\ 0 \end{bmatrix} \quad (4.11)$$

The first row of the external force vector represents the excitation force $f_{x1}(t)$ which is calculated and exported to the result file. The term $-m_{U1}\ddot{x}_1$ represents the resulting force out of the structural dynamic behavior of the multi-mass system. The second row is zero, because the second excitation is not modeled in the first step.

Analogically, the second step observes the excitation force $f_{x2}(t)$ which is represented by the second row of the external force vector in Eq. (4.12). The term $-m_{U2}\ddot{x}_2$

describes the resulting force out of the structural dynamic behavior of the multi-mass system.

$$\begin{bmatrix} m_1 + m_{U1} & 0 \\ 0 & m_2 \end{bmatrix} \begin{bmatrix} \ddot{x}_1 \\ \ddot{x}_2 \end{bmatrix} + \begin{bmatrix} d_1 + d_2 & -d_2 \\ -d_2 & d_2 \end{bmatrix} \begin{bmatrix} \dot{x}_1 \\ \dot{x}_2 \end{bmatrix} + \begin{bmatrix} k_1 + k_2 & -k_2 \\ -k_2 & k_2 \end{bmatrix} \begin{bmatrix} x_1 \\ x_2 \end{bmatrix} = \begin{bmatrix} 0 \\ m_{U2} \cdot \Omega_2^2 \cdot l_2 \cdot sin(\Omega_2 t) - m_{U2} \ddot{x}_2 \end{bmatrix} \quad (4.12)$$

From the results of the two calculations, it can be build an external force vector, which contains the structural dynamic behavior of the system and neglect the excitation interaction. To calculate the operational vibrations by using the Cutting Force Principle, the force vector has to be impressed on the two-mass oscillator, as shown in Eq. (4.13).

$$\begin{bmatrix} m_1 & 0 \\ 0 & m_2 \end{bmatrix} \begin{bmatrix} \ddot{x}_1 \\ \ddot{x}_2 \end{bmatrix} + \begin{bmatrix} d_1 + d_2 & -d_2 \\ -d_2 & d_2 \end{bmatrix} \begin{bmatrix} \dot{x}_1 \\ \dot{x}_2 \end{bmatrix} + \begin{bmatrix} k_1 + k_2 & -k_2 \\ -k_2 & k_2 \end{bmatrix} \begin{bmatrix} x_1 \\ x_2 \end{bmatrix} = \begin{bmatrix} \mathrm{f}_{x1}(t) \\ \mathrm{f}_{x2}(t) \end{bmatrix} \quad (4.13)$$

The comparison of the accelerations by using the abstraction level A2 and A3 shows the influence of the excitation interaction. Figure 4.10 shows significant differences in the time and frequency domain. So it can be very important to consider the excitation interaction, if the engineer is interested in the amplitudes of the operational vibrations.

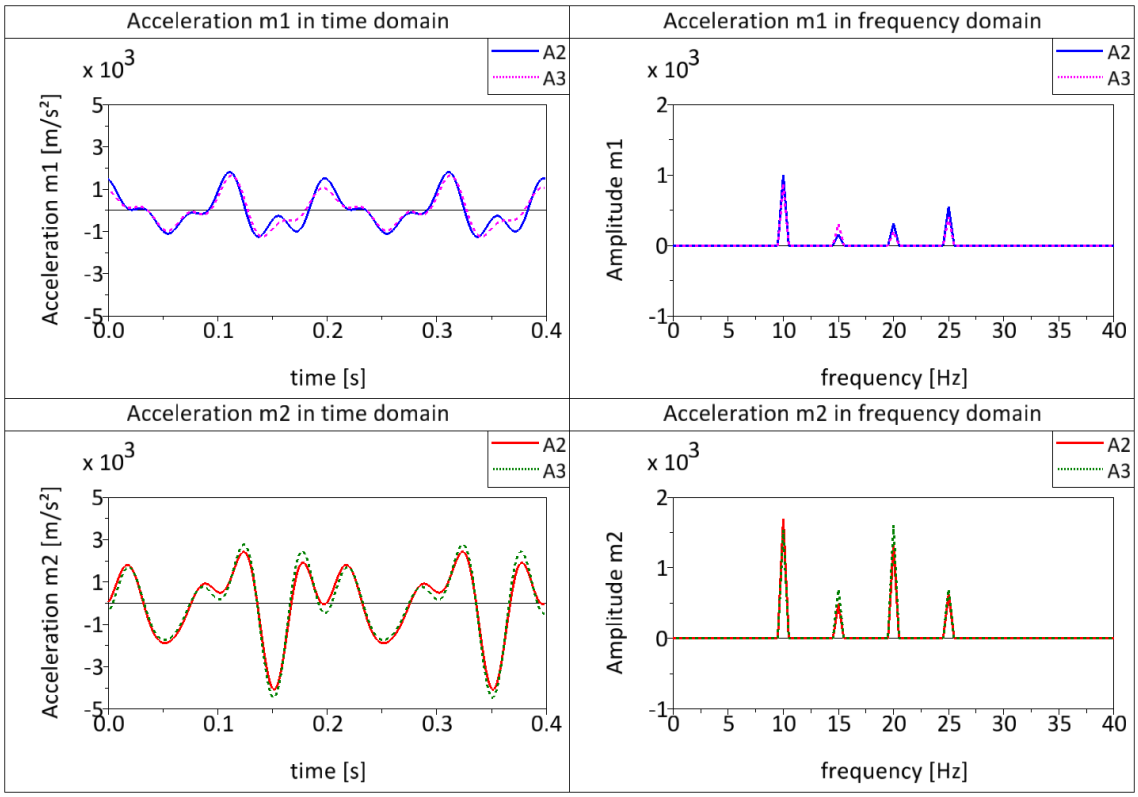

Figure 4.10: Comparison A2 and A3 in time and frequency domain

Another interesting aspect is to calculate the forces by neglecting the influence of the neighboring subsystems. So the force $\mathrm{f}_{x1}(t)$ only contains the structural dynamic behavior of the subsystem 1 and the force $\mathrm{f}_{x2}(t)$ contains the structural dynamic behavior of the subsystem 2. The Eq. (4.14) and Eq. (4.15) show the differential equations, whereupon the right side represents the forces $\mathrm{f}_{x1}(t)$ and $\mathrm{f}_{x2}(t)$.

$$m_1\ddot{x}_1 + d_1\dot{x}_1 + k_1x_1 = m_{U1} \cdot \Omega_1^2 \cdot l_1 \cdot sin(\Omega_1 t) - m_{U1}\ddot{x}_1 + \mathrm{f}_{ext,x}(t) \qquad (4.14)$$

$$m_2\ddot{x}_2 + d_2\dot{x}_2 + k_2x_2 = m_{U2} \cdot \Omega_2^2 \cdot l_2 \cdot sin(\Omega_2 t) - m_{U2}\ddot{x}_2 \qquad (4.15)$$

This approach can reduce modeling time and support the use of simultaneous engineering, because the engineers can model their systems independent of each other.

The comparison of the forces for this example system shows significantly different excitation amplitudes in Figure 4.11, because the point impedances are different to the original structural dynamic behavior.

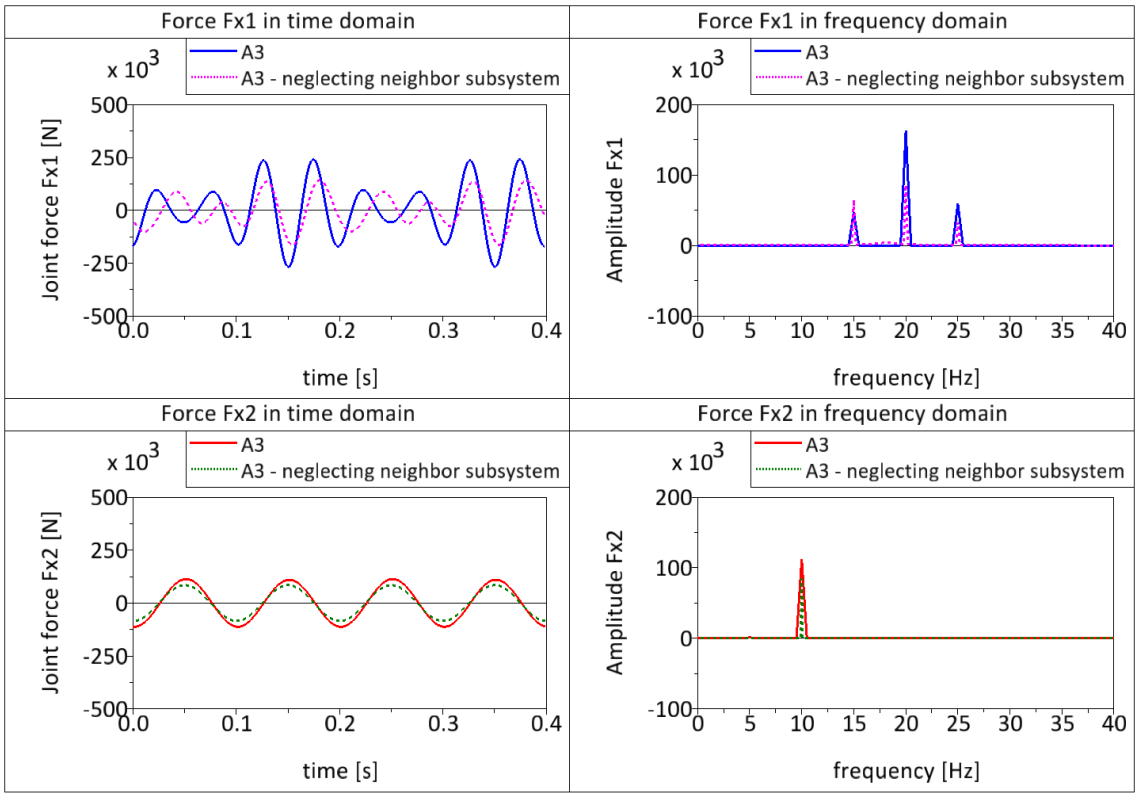

Figure 4.11: Comparison of forces A3 (considering neighbor subsystems and A3 neglecting neighbor subsystems) in time and frequency domain

By impressing the forces on the two-mass oscillator, as shown in Eq. (4.13), the comparison of the accelerations shows significant differences in Figure 4.12.

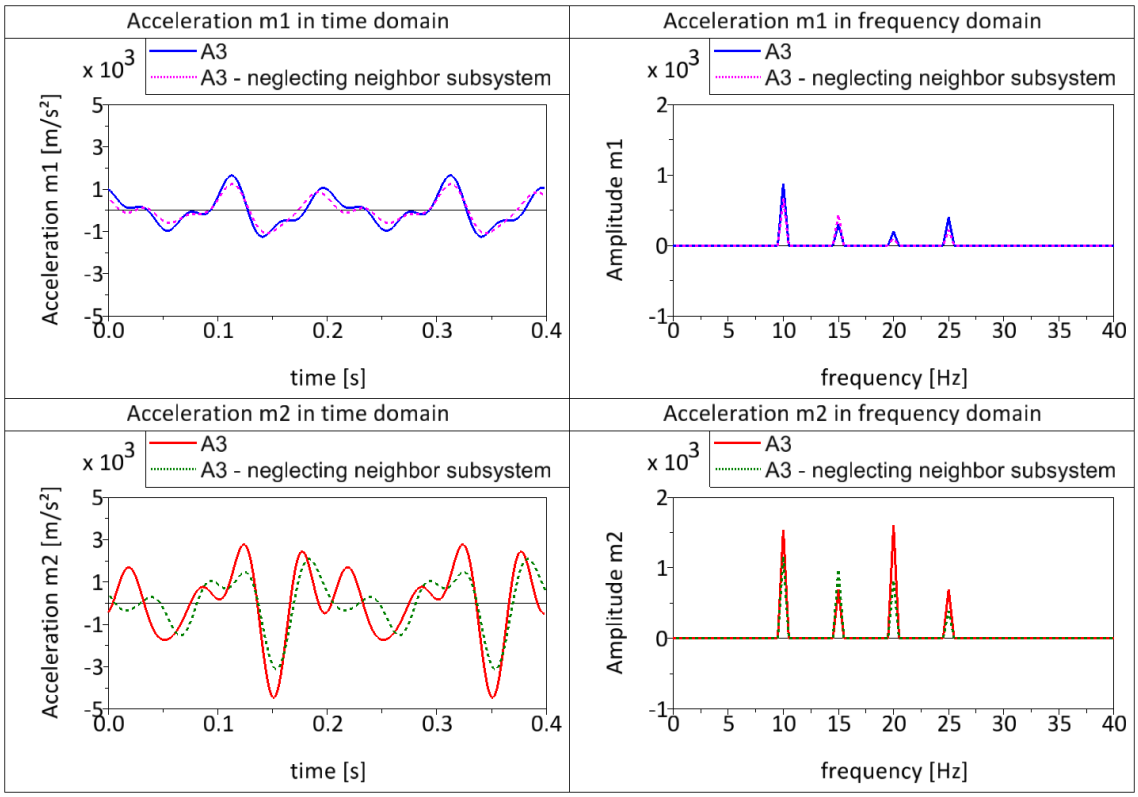

Figure 4.12: Comparison of accelerations A3 (considering neighbor subsystems and A3 neglecting neighbor subsystems) in time and frequency domain

So the engineer needs helpful criteria to decide, if it is necessary to model the neighboring subsystems and their coupling to subsystem of interest. Such a deciding method is explained in chapter 4.2.6.

4.2.5 Abstraction level A4

The abstraction level A4 considers the structural coupling and excitation interaction effects, because the system is modeled with all subsystems and excitations. So there is one model and one differential equation (4.16) that have to be solved by the computer.

$$\begin{bmatrix} m_1 & 0 \\ 0 & m_2 \end{bmatrix}\begin{bmatrix} \ddot{x}_1 \\ \ddot{x}_2 \end{bmatrix} + \begin{bmatrix} d_1 + d_2 & -d_2 \\ -d_2 & d_2 \end{bmatrix}\begin{bmatrix} \dot{x}_1 \\ \dot{x}_2 \end{bmatrix} + \begin{bmatrix} k_1 + k_2 & -k_2 \\ -k_2 & k_2 \end{bmatrix}\begin{bmatrix} x_1 \\ x_2 \end{bmatrix} = \begin{bmatrix} m_{U1} \cdot \Omega_1^2 \cdot l_1 \cdot sin(\Omega_1 t) - m_{U1}\ddot{x}_1 + \mathrm{f}_{ext,x}(t) \\ m_{U2} \cdot \Omega_2^2 \cdot l_2 \cdot sin(\Omega_2 t) - m_{U2}\ddot{x}_2 \end{bmatrix} \quad (4.16)$$

This seems to be the most accurate abstraction level, but here should be mentioned the explanations in chapter 3.4, 3.5, and (Most 2011). So the uncertainty of the model rises with the complexity and abstraction level of the model. It is also a very time-consuming abstraction level, because the modeling of the system cannot be paralleled. The solving time of the equation can also be very time-consuming compared to a decoupled abstraction level.

If we look at the calculated forces in Figure 4.13, we see the difference between the calculation with and without excitation interaction. So the force f_{x1} shows a significant difference in frequency domain. The amplitude at 10 Hz is only contained in the abstraction level A4, because the excitation interaction is regarded. Analogically, the frequencies 15 Hz, 20 Hz, 25 Hz in the joint force f_{x2} are only contained in the abstraction level A4. The reason is to find in the term $-m_{U2}\ddot{x}_2$ and $-m_{U1}\ddot{x}_1$. So if the amplification factor of acceleration $\ddot{x}_2$ or $\ddot{x}_1$ in the frequency of interest is high, the excitation interaction is high, too.

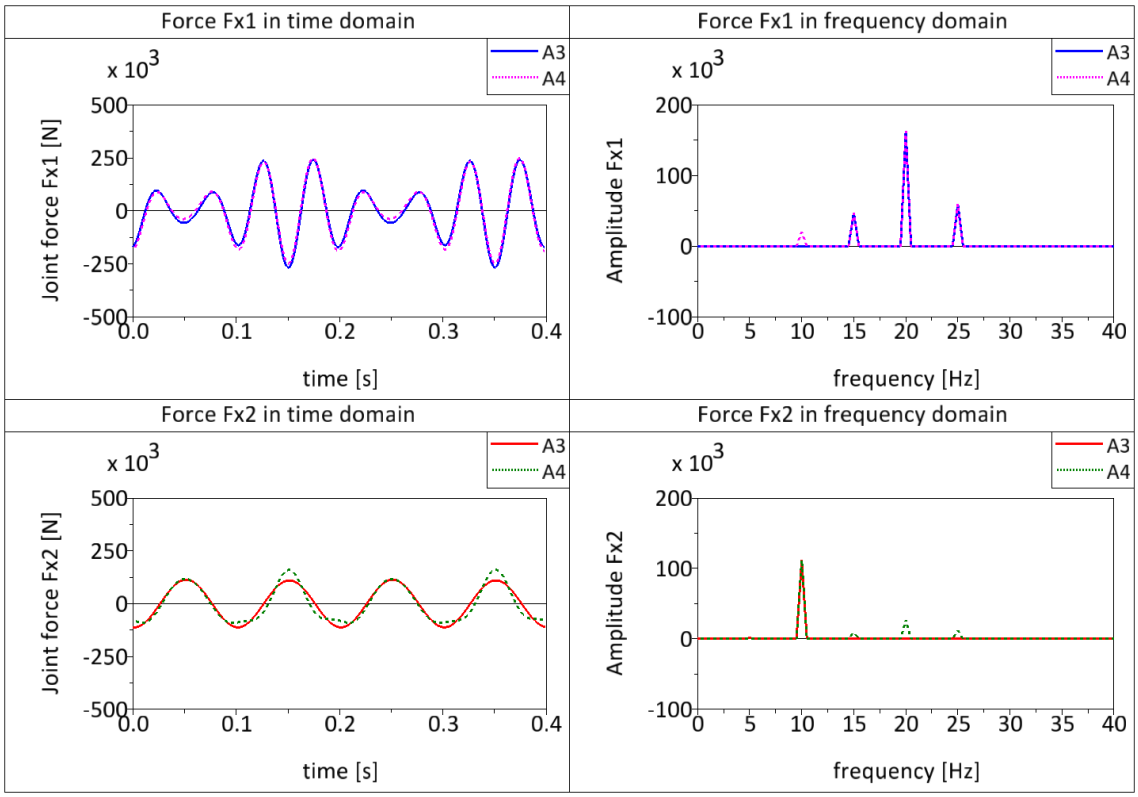

Figure 4.13: Comparison forces of A3 and A4 in time and frequency domain

Figure 4.14 shows the influence of the excitation interaction to the acceleration results of m_1 and m_2. The results of abstraction level A3 an A4 contain all excitation frequencies, but the amplitudes differ from each other, significantly.

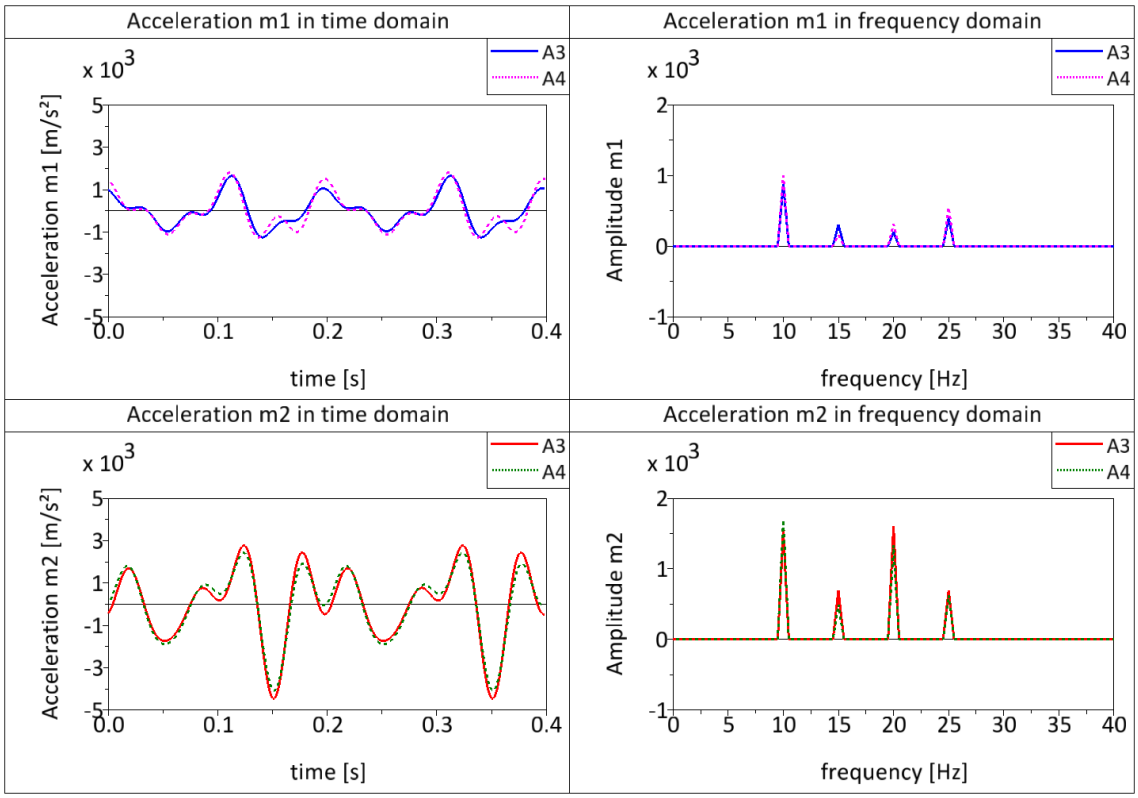

Figure 4.14: Comparison A3 and A4 in time and frequency domain

For the engineer it is important to know, if he or she has to consider the excitation interaction or not. So he or she can choose the right abstraction level for their calculation aim.

4.2.6 Decision method of considering structural coupling effects

In chapter 2.4.2, we make a distinction between two kinds of structural coupling, the “structural coupling of subsystems” and the “structural coupling of excitation components”.

4.2.6.1 Structural coupling of excitation components

Let's start with the explanation of the assessment method for "structural coupling of excitation components". By using the single-mass oscillator with a rotating mass (subsystem 2 in chapter 4.2), the differential equation (4.17) describes the system.

$$m_2\ddot{x}_2 + d_2\dot{x}_2 + k_2x_2 = m_{U2} \cdot \Omega_2^2 \cdot l_2 \cdot sin(\Omega_2 t) - m_{U2}\ddot{x}_2 \qquad (4.17)$$

The equation can be written in the impedance form to calculate in frequency domain, see Eq. (4.18).

$$Z_{22}x_2 = \mathrm{f}_2 \qquad (4.18)$$

Z_{22} is the point impedance of the system. Figure 4.15 shows a typical point impedance of a single-mass oscillator with different Lehr's damping measures.

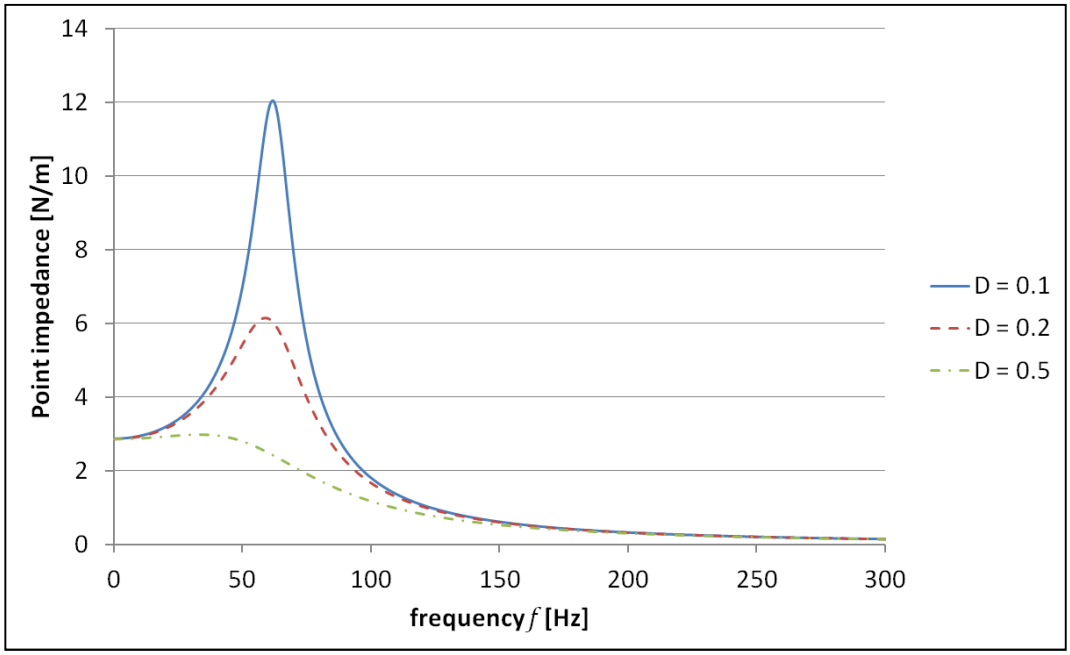

Figure 4.15: Typical point impedance of a single-mass oscillator with different Lehr's damping measures

With lower frequency the point impedance aspire to a constant value. If the frequency 0 Hz is reached, the calculation is a quasi-static calculation and the dynamic behavior of the structure can be neglected. To give the engineer a feeling for the deviation by

considering the structural coupling of excitation components, a criterion is developed in this section.

At first we look at the deviation between a calculation by considering the structural dynamic behavior and neglecting the structural dynamic behavior. To develop the criterion we use the amplification function of a simple single-mass oscillator. The Eq. (4.19) represents the amplification function of a single-mass oscillator with $\eta = \frac{\Omega}{\omega}$. In chapter 2.3.1, the equation is explained in detail.

$$\Gamma(\eta) = \frac{1}{\sqrt{(1-\eta^2)^2 + (2D\eta)^2}} \qquad (4.19)$$

If Ω moves to zero, the frequency ratio η moves to zero and represents a quasi-static excitation. So the deviation between $\Gamma_{quasi-static}$ and $\Gamma_{dynamic}(\Omega)$ is important for the criterion. If η moves to zero, $\Gamma_{quasi-static}$ moves to 1. Now it is possible to write an equation that shows the deviation to the quasi-static model

$$deviation = \frac{\Gamma_{dynamic}(\Omega) - 1}{1}. \qquad (4.20)$$

Assume that a maximal deviation of ±1 % is sufficiently accurate, so a frequency distance of $\Omega = \frac{1}{10}\omega$ can be allowed. In Eq. (4.21) the excitation frequency Ω is substituted by the necessary distance to the eigen angular frequency for calculating the amplification.

$$\Gamma_{dynamic}\left(\Omega = \frac{1}{10}\omega\right) = \frac{1}{\sqrt{\left(1 - \left(\frac{\omega}{\frac{1}{10}\omega}\right)^2\right)^2 + \left(2D\frac{\omega}{\frac{1}{10}\omega}\right)^2}} = \frac{1}{\sqrt{0.9801 + 0.04\,D}} \qquad (4.21)$$

Eq. (4.21) shows that the Lehr's damping measure has a small content to the amplification function and can be neglected, if the system is weak damped. In Figure 4.16 it is shown that the amplitude deviation is between -1 % and +1 % for a frequency distance of $\Omega = \frac{1}{10}\omega$ and a non-critical damped system by varying the Lehr's damping measure.

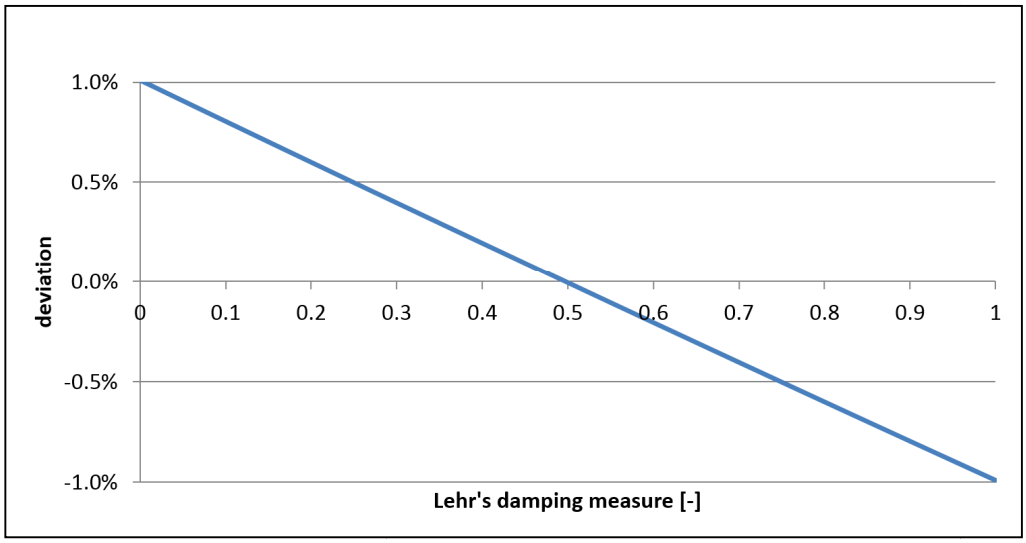

Figure 4.16: Amplitude deviation to the quasi-static calculation by variation of the Lehr's damping measure

Now we know that the first eigenfrequency of an excitation case has to be ten times higher than the maximal frequency of excitation, if the amplitude deviation of ±1 % is accurate enough.

4.2.6.2 Structural coupling of subsystems

The aim of the assessment method is to help the engineer to decide, if he or she has to model the neighboring subsystems. Because the neighboring subsystems can influence the structural dynamic behavior of the subsystem of interest or rather the calculated force.

The method is developed by using a model of a single-mass oscillator and a two-mass oscillator. These simple discrete models describe the general effect of structural coupling of subsystems and can be seen analogous to complex coupled systems like an engine or a building. (see Figure 4.17) In this research, the subsystem 1 is fixed to the ground which represents e. g. a building. The subsystem 2 is coupled to the subsystem 1 and represents e. g. a machine in a building.

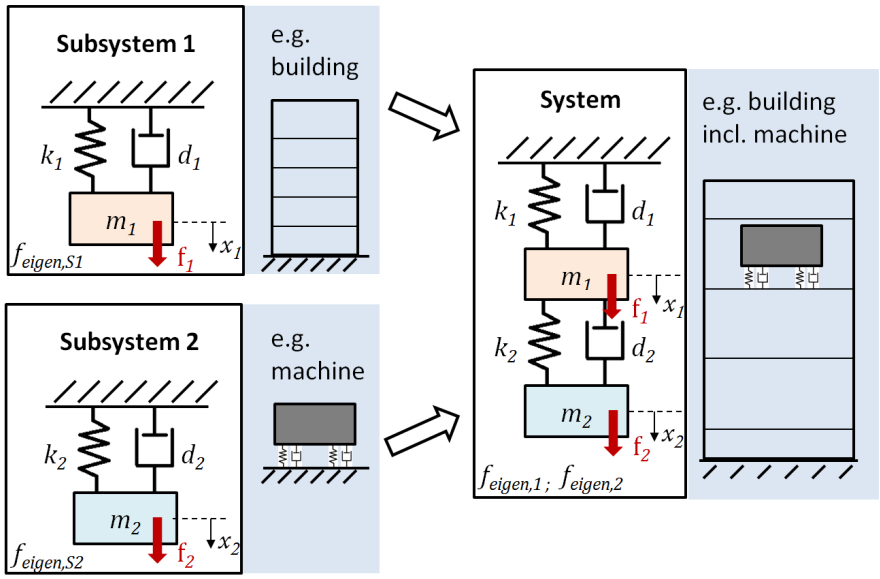

Figure 4.17: The two-mass oscillator and the comparison to a complex coupled system

In the following section, the methods are explained that are used for this research.

4.2.6.2.1 Methods to develop the assessment method

Solving of equations

Each system in Figure 4.17 can be mathematically described by the general equation of motion

$$\mathbf{M}\ddot{\mathbf{x}} + \mathbf{D}\dot{\mathbf{x}} + \mathbf{K}\mathbf{x} = \mathbf{f}(t)\,. \qquad (4.22)$$

In frequency domain the system (e. g. a two-mass oscillator) can be described by the impedance form. A detailed explanation about the impedance form can be found in chapter 3.5.3.

$$\begin{bmatrix} Z_{11} & Z_{12} \\ Z_{21} & Z_{22} \end{bmatrix} \begin{bmatrix} x_1 \\ x_2 \end{bmatrix} = \begin{bmatrix} f_1 \\ f_2 \end{bmatrix} \qquad (4.23)$$

So the approach is: If the point impedances Z_{11} or Z_{22} of the total system is similar to the Z_{11} or Z_{22} of the subsystem, than the neighboring subsystems can be neglected. To predict the degree of structural coupling, the masses, the eigenfrequencies, and the Lehr's damping measures of the subsystems are used to develop simple criteria.

In the following analysis, the QR algorithm is used for solving the eigenvalue problem

$$\mathbf{M}\ddot{\mathbf{x}} + \mathbf{D}\dot{\mathbf{x}} + \mathbf{K}\mathbf{x} = \mathbf{0}\,. \tag{4.24}$$

The QR algorithm is a numerical method to solve the general eigenvalue problem and calculates the eigenvalues and eigenvectors. In chapter 2.5.3.5, (Gourlay and Watson 1973), and (Börm and Mehl 2012) the QR algorithm and further algorithms are explained in detail.

In Eq. (4.25) and Eq. (4.26) the output matrices are shown with example values by using the QR algorithm.

$$eigenvalues = \begin{bmatrix} 10 & 0 \\ 0 & 20 \end{bmatrix} \tag{4.25}$$

$$eigenvectors = \begin{bmatrix} 0.4 & -0.2 \\ 0.6 & 0.8 \end{bmatrix} \tag{4.26}$$

Now the eigenvalue matrix has to be divided by 2π to get the eigenfrequencies of the two-mass oscillator. To describe the eigenmode of an oscillation, it is necessary to look at the eigenfrequency and the appending eigenvector. If the elements of an eigenvector have the same prefix, the motion of the masses is in-phase. If the elements of an eigenvector have different prefixes, the motion of the masses is out-of-phase. So the two possible mode shapes of the two-mass oscillator can be described.

To assess the influence of the damping, it is required to look at the amplification function of the systems. Let's start with the calculation of the amplification function of a single-mass oscillator. The calculated amplification function in Eq. (2.64) is based on the differential equation for a force excited single-mass system, as shown in Eq. (4.27).

$$m\ddot{x} + d\dot{x} + kx = \mathrm{f}(t) \tag{4.27}$$

A detailed derivation is shown in chapter 2.3.1.

$$\Gamma(\Omega) = \frac{1}{\sqrt{\left(1 - \left(\frac{\Omega}{\omega}\right)^2\right)^2 + \left(2D\frac{\Omega}{\omega}\right)^2}} \tag{4.28}$$

The diagram in Figure 4.18 shows an amplification function for a single-mass oscillator with different Lehr's damping measures. It can be seen that the maximum amplification decreases with increasing Lehr's damping measures.

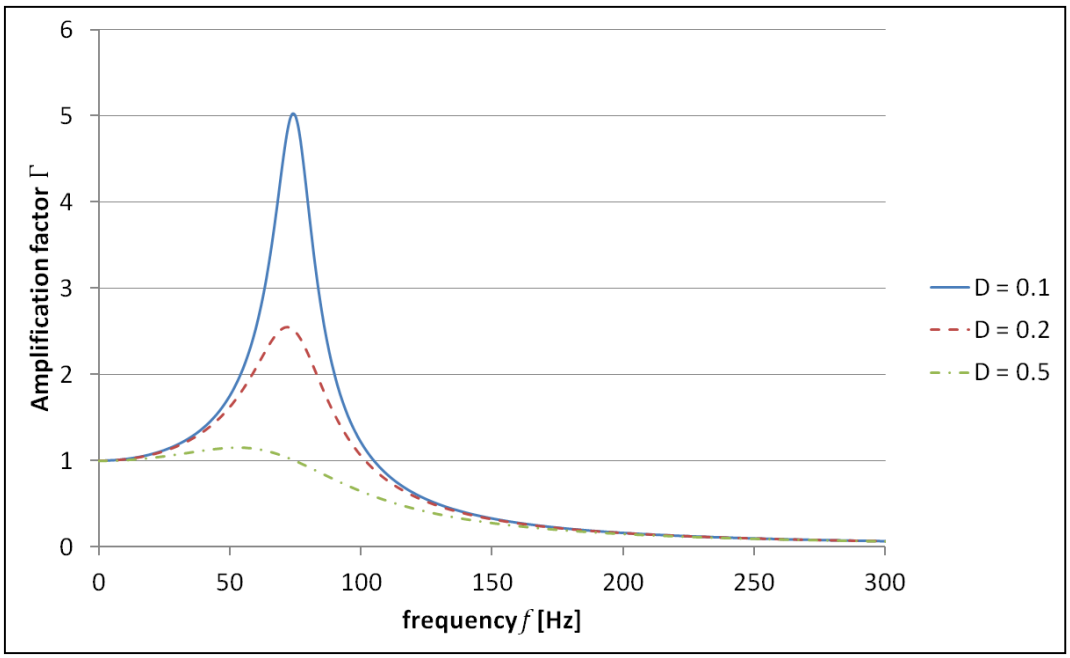

Figure 4.18: Amplification functions of single-mass oscillators with different Lehr's damping measures

For the analysis in this work, the maximum amplification factor in the resonance of the system is the most important output parameter. Due to the highest amplitude deviation to the total system can be found in the resonance of the system.

The calculation of the amplification function for a multi-mass oscillator is more complex. The differential equation of a force excited multi-mass oscillator can be calculated in the complex number plane, see Eq. (4.29).

$$[\mathbf{K} + i\Omega\mathbf{D} - \Omega^2\mathbf{M}]\hat{\mathbf{x}} = \hat{\mathbf{f}} \qquad (4.29)$$

Dissolved after $\hat{\mathbf{x}}$, the amplification function can be defined as

$$\Gamma(\Omega) = [\mathbf{K} + i\Omega\mathbf{D} - \Omega^2\mathbf{M}]^{-1}. \qquad (4.30)$$

So the equation can be solved step by step for each excitation frequency Ω.

Design of Experiments and Response Surface Modeling

The Design of Experiments analysis (DOE) and the following Response Surface Modeling (RSM) are important methods for the research. So both methods are explained in this chapter, based on the manual "Theoretical Background for Optimus" from Noesis Solutions (Noesis Solutions 2013). Most analyses use both methods. At first a DOE generates data points by using a systematic approach. Then the RSM uses the collected data points to determine a mathematical model. Another way is to decide for a hypothesis of a mathematical model at first and use the DOE to find out the model parameters.

Let's start with the explanation of the DOE analysis. The aim of a DOE is to get a lot of information with a small number of experiments. To reach this aim, the DOE offers a lot of methods that can be used for different kinds of applications. Generally, the DOE methods can be classified in two groups, the random designs and the orthogonal designs. The random design means that the selection procedure for the value of input parameters is a random process. One of the common used random designs is the Latin Hypercube Designs which is explained in (Siebertz et al. 2010).

In the research in this work, the adjustable full factorial method is used. This method belongs to the type of orthogonal designs. Orthogonal designs means that the input parameters of the model can be varied independently of each other. So there are not any correlations between the parameters. One of the common orthogonal methods is the factorial design. The full factorial design means that every setting of every parameter appears with every setting of every other parameter. So the number of experiments N can be calculated by Eq. (4.31).

$$N = \prod_{1}^{\mathrm{k}} n_i \qquad i = 1, \dots, \mathrm{k} \tag{4.31}$$

k is the number of parameters and n_i represents the number of levels[2] of a parameter. The disadvantage of this method is that the number of experiments increases exponentially. To reduce the number of experiments, the number of levels or the number of parameters can be reduced. So the two-level full factorial design uses two

[2] Number of levels means number of different values for one parameter.

levels for every parameter, the lowest and the highest value. The number of experiments N can be calculated quite simple, as shown in Eq. (4.32).

$$N = 2^{\mathrm{k}} \qquad i = 1, \dots, \mathrm{k} \tag{4.32}$$

There is also a three-level full factorial that is necessary when the mathematical response is of second order. So it is possible to solve a quadratic model. Each input parameter has three levels, the lowest, middle and highest value. The number of experiments can be calculated by the Eq. (4.33).

$$N = 3^{\mathrm{k}} \qquad i = 1, \dots, \mathrm{k} \tag{4.33}$$

The method which is used in this work is called adjustable full factorial design. The number of levels for each parameter can be chosen by the engineer. So it is possible to solve models with a higher order then three. Also nonlinear effects can be solved by using a very high number of levels. With Eq. (4.31), the number of experiments can be calculated. This method is not efficient, because the number of experiments is very large. To reduce the time and effort, it is possible to use the fractional design in many cases. To get more information about the fractional design, the explanations in (Montgomery 2012) can be recommended. For the analysis in this work, the calculation time is very short and the number of input parameter is three. So the time-consuming approach of the adjustable full factorial design can be tolerated.

After collecting all data from the DOE, the RSM uses the data to determine the characteristic diagrams. The characteristic diagrams can also be called response surface which describes the relationship between the input parameters and the output values. Two common types of response surface models are the Least Squares Fitting and the Interpolation.

The basic idea of Least Squares Fitting is to find a curve to a set of input and output values. The sum of the squares of error of the points from the curve should be minimal. To generate the curve, it is possible to calculate with a vertical error or a horizontal error.

For the analysis in this work, the interpolation method is used. For the use of this method, the function must exactly fit the values of the DOE. To do this, it is necessary to generate further data points based on the set of identified data points. To use the

interpolation method, there are a lot of mathematical approaches like linear interpolation, spline interpolation, polynomial interpolation, radial basis functions (RBF), and so on.

The RBF has to approximate a valued function. The notation of the approximated function is defined as $s(x)$ in Eq. (4.34). Further information about the RBF can be find in (Liu 2013).

$$s(x) = \sum_{i=1}^{N} \lambda_i \phi(|x - x_i|) \qquad (4.34)$$

λ_i is a real-valued weight and $|x - x_i|$ is a distance between two points. Popular functions for the basic function $\phi(\cdot)$ are linear, cubic, thin-plate spline, and multi-quadratic functions. The analysis with RBF can be very time-consuming and not suitable for noisy data, because the RBF is an exact approximation approach and the conditions of interpolation are too strict. For the analysis in this work the RBF can be used, because the data are calculated very exactly and thus the uncertainty is very low.

4.2.6.2.2 Classification and criteria

The structural dynamic behavior of a system can be described by the amplification function. The amplification function is defined by the mass, stiffness, and damping of the system. Now we want to use the comparison of the amplification function of the decoupled subsystems to predict a structural coupling effect between the subsystems. To compare the amplification functions, we use the ratios of easily accessible parameters, which describe the amplification function of the subsystems. So we use the mass, eigenfrequency, and the Lehr's damping measure. The parameters describe the amplification function of each system and are easy to assign by a modal analysis.

At first the structural coupling between two subsystems can be classified in two groups, the strong structural coupling and the weak structural coupling. The weak structural coupling is defined as

$$f_{eigen,S1} > f_{eigen,S2} \qquad (4.35)$$

and the strong structural coupling is defined as

$$f_{eigen,S1} < f_{eigen,S2} \,. \tag{4.36}$$

So the first criterion can be defined as frequency ratio of the two subsystems. For the weak structural coupling the Eq. (4.37) is applicable

$$frequency\ ratio = \frac{f_{eigen,S1} - f_{eigen,S2}}{f_{eigen,S1}} \tag{4.37}$$

and for the strong structural coupling the Eq. (4.38) is applicable

$$frequency\ ratio = \frac{f_{eigen,S2} - f_{eigen,S1}}{f_{eigen,S2}} \,. \tag{4.38}$$

The frequency ratio is always a value between 0 and 1. A high frequency ratio shows that the eigenfrequency of the subsystems are far apart. To assess the influence of structural coupling it is necessary to define a second criterion, the mass ratio

$$mass\ ratio = \frac{m_2}{m_1} \,. \tag{4.39}$$

The mass ratio allows the prediction of the mass inertia. If the mass ratio is low, the mass inertia of subsystem 2 is low against the subsystem 1. The third criterion to assess the amplitudes of the systems is called damping ratio. It is the ratio of the Lehr's damping measure of both subsystems and defined in Eq. (4.40).

$$damping\ ratio = \frac{D_2}{D_1} \tag{4.40}$$

The equation of the mass and damping ratio is the same for both classifications of structural coupling (weak structural coupling and strong structural coupling).

In most applications, the engineer is interested in the eigenfrequency and the amplification function of a system. So the eigenfrequency and amplification factors of the reduced decoupled subsystem should be very similar to the values of the coupled system.

A two-mass oscillator with a weak structural coupling can split up in two single-mass oscillators, shown in Figure 4.19. Generally, the two-mass oscillator has two eigenfrequencies and mode shapes. One eigenfrequency belongs to a mode shape whose motion of the two masses is in-phase. The other eigenfrequency belongs to a mode shape whose motion of the masses is out-of-phase. In this work, the

eigenfrequency $f_{eigen,1}$ belongs to the in-phase motion and the eigenfrequency $f_{eigen,2}$ belongs to the out-of-phase motion.

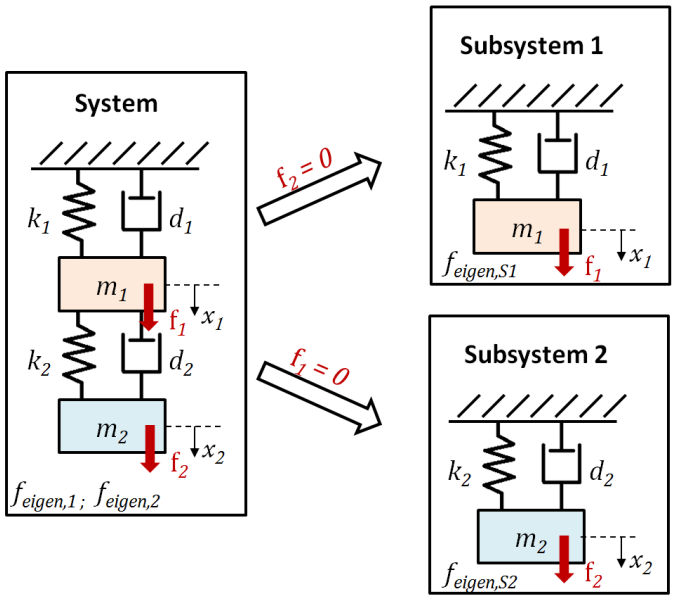

Figure 4.19: Model reduction for systems with weak structural coupling

If the structural coupling of the subsystems is low enough, then the eigenfrequency and the amplification factor of the reduced decoupled subsystem are very similar to the ones of the coupled system. Subsystem 1 is similar to the eigenfrequency $f_{eigen,2}$ and subsystem 2 is similar to the eigenfrequency $f_{eigen,1}$.

So further criteria can be defined as deviation of frequency in Eq. (4.41) and Eq. (4.42). The smaller the value of the deviation criterion, the closer is the eigenfrequency of the decoupled subsystem to the eigenfrequency of the coupled system. For very low structural couplings the deviation tends to zero.

$$deviation\ of\ frequency_{Subsystem\ 1} = \frac{f_{eigen,S1} - f_{eigen,2}}{f_{eigen,S1}} \qquad (4.41)$$

$$deviation\ of\ frequency_{Subsystem\ 2} = \frac{f_{eigen,S2} - f_{eigen,1}}{f_{eigen,S2}} \qquad (4.42)$$

The second deviation criterion deals with the amplification function. For some applications, it is not enough to predict the eigenfrequency and the amplitudes of the motions are interesting, too. The amplification function of the decoupled subsystems should be similar with the amplification function of the coupled system in the

frequency range of interest. To assess the deviation of amplitude in this work, the maximum amplification factor of the function is used. So for the assessment of subsystem 1, the Eq. (4.43) can be applied.

$$deviation\ of\ amplitude_{Subsystem\ 1} = \frac{\Gamma_{max,S1} - \Gamma_{max,2}}{\Gamma_{max,S1}} \qquad (4.43)$$

And for the assessment of subsystem 2, the Eq. (4.44) can be applied.

$$deviation\ of\ amplitude_{Subsystem\ 2} = \frac{\Gamma_{max,S2} - \Gamma_{max,1}}{\Gamma_{max,S2}} \qquad (4.44)$$

With all these criteria, it is possible to generate a characteristic diagram for the two-mass oscillator and its subsystems. This characteristic diagram should help an engineer to guess the influence of subsystems to the coupled system. But till now, the method can only be used for weak structural couplings.

For strong structural coupled systems, it is necessary to use different deviation criteria and subsystems. At first the two-mass oscillator can split up in two subsystems, as shown in Figure 4.20. Subsystem 1* considers the subsystem 1 with an additional mass m_2. This subsystem is similar to the in-phase eigenmode of the coupled system. And the subsystem 2 is similar to the out-of-phase eigemode of the coupled system.

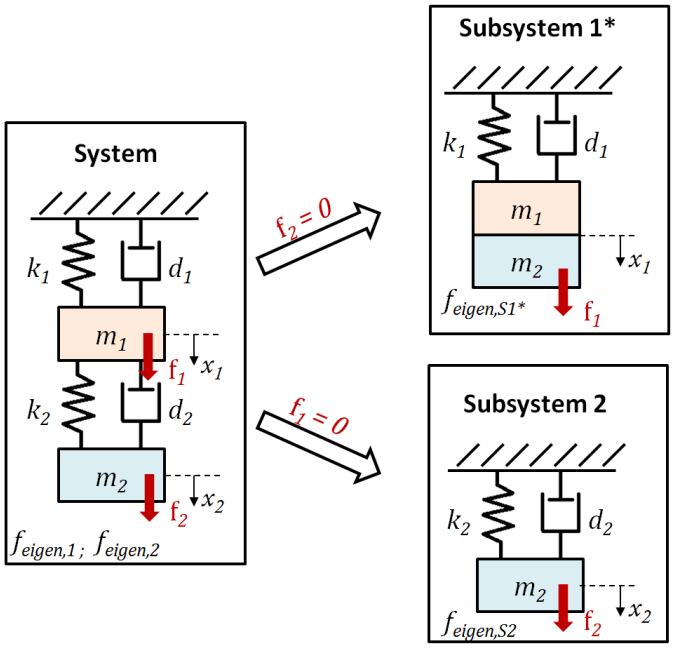

Figure 4.20: Model reduction for systems with strong structural coupling

Let's define the deviation criteria for both decoupled subsystems. In Eq. (4.45) and Eq. (4.46) the deviation of frequency is shown for subsystem 1* and subsystem 2.

$$deviation\ of\ frequency_{Subsystem\ 1^*} = \frac{f_{eigen,S1^*} - f_{eigen,1}}{f_{eigen,S1^*}} \quad (4.45)$$

$$deviation\ of\ frequency_{Subsystem\ 2} = \frac{f_{eigen,S2} - f_{eigen,2}}{f_{eigen,S2}} \quad (4.46)$$

Like in the definition of the weak structural coupling, it is necessary to have criteria for the amplification function of the systems. In Eq. (4.47) and Eq. (4.48) the deviation of amplitudes for both decoupled subsystems is defined.

$$deviation\ of\ amplitude_{Subsystem\ 1^*} = \frac{\Gamma_{max,S1^*} - \Gamma_{max,1}}{\Gamma_{max,S1^*}} \quad (4.47)$$

$$deviation\ of\ amplitude_{Subsystem\ 2} = \frac{\Gamma_{max,S2} - \Gamma_{max,2}}{\Gamma_{max,S2}} \quad (4.48)$$

Now all criteria and models are described and the DOE analysis can be started. For all DOE analysis the adjustable full factorial design is used. The input parameters are frequency ratio, mass ratio and damping ratio. For all input parameter ten levels are used. The total number of experiments for each DOE is 1000. The output parameters are the deviation of frequency and the deviation of amplitude. After performing the DOE, the RSM calculates the characteristic diagram. For the RSM in this work, the RBF with a cubic basic function is used.

4.2.6.2.3 Discussion and results

Weak structural coupling:

Let's start with the results of the research for weak structural couplings. The Figure 4.21 shows the characteristic diagram for subsystem 1. The engineer can use the diagram to guess the maximal deviation of frequency for his or her complex coupled system.

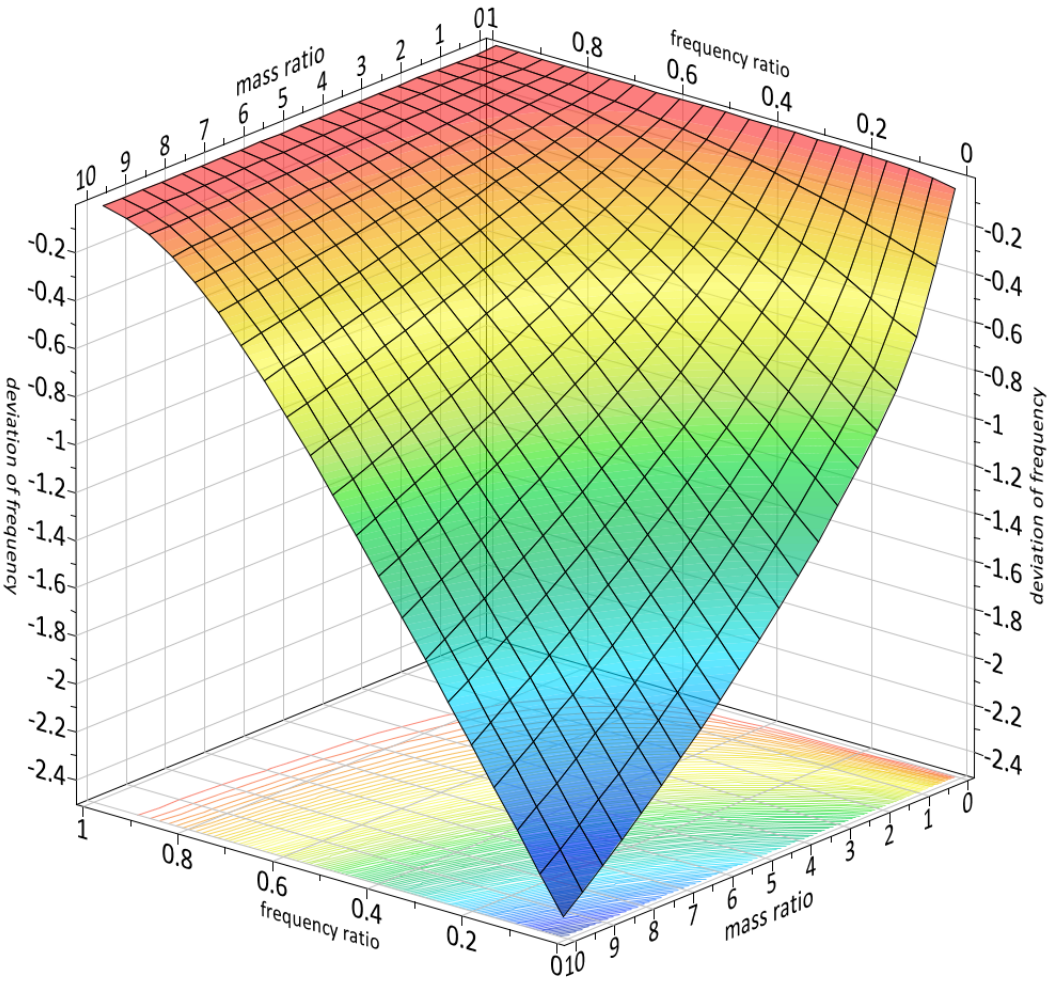

Figure 4.21: Characteristic diagram for frequency weighting of subsystem 1 with weak structural coupling

The diagram shows the deviation of frequency to the coupled two-mass oscillator. The deviation of frequency moves towards zero with an increasing frequency ratio and a decreasing mass ratio.

$$deviation\ of\ frequency\ _{frequency\ ratio \to 1} \to 0 \qquad (4.49)$$

$$deviation\ of\ frequency\ _{mass\ ratio \to 0} \to 0 \qquad (4.50)$$

By using the frequency ratio and the mass ratio, the engineer can look in the diagram and guess the maximal deviation of frequency. If the value of the deviation of frequency is high, the structural coupling is high. If the value of the deviation of

frequency is low, the structural coupling is low. So the engineer has to decide, if he or she can tolerate the maximal deviation of frequency for his or her simulation.

For the simulation aim of operational vibrations on an absolute scale, the amplification function of a system is an important parameter. So it is insufficient to have a look at the deviation of frequency. A second criterion has to be taken into account, the deviation of amplitude. In Figure 4.22 the diagram shows an opportunity to guess the influence of the damping ratio on the deviation of amplitude.

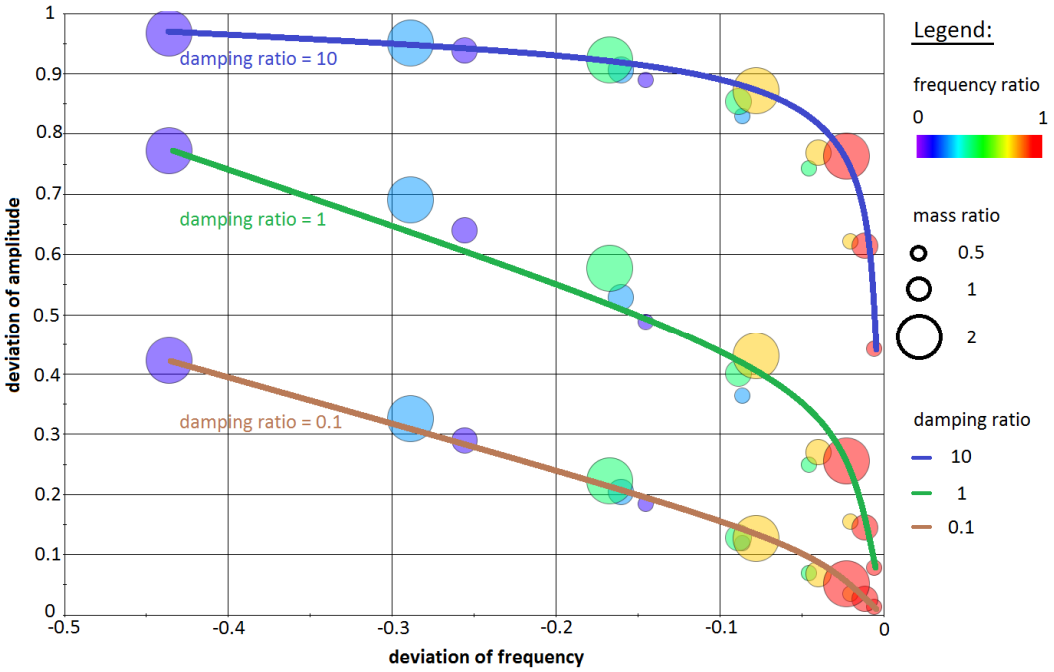

Figure 4.22: Diagram for frequency and amplitude weighting of subsystem 1 with weak structural coupling

With decreasing mass ratio and increasing frequency ratio, the deviation of frequency and the deviation of amplitude moves towards zero. For the damping ratio three values are shown. With decreasing damping ratio, the deviation of amplitude moves towards zero. The damping ratio provides a certain level of amplitude deviation for both other criteria. The deviation of frequency is not influenced significantly by the damping ratio. So the engineer can have a look at the diagram and guess the influence of the structural coupling. Now he or she is able to decide, if he or she can tolerate the maximum deviations for his or her simulation.

If the engineer is accountable for the design of the subsystem 2, he or she has to use the diagram in Figure 4.23 and Figure 4.24. The Figure 4.23 shows the characteristic diagram for the frequency weighting.

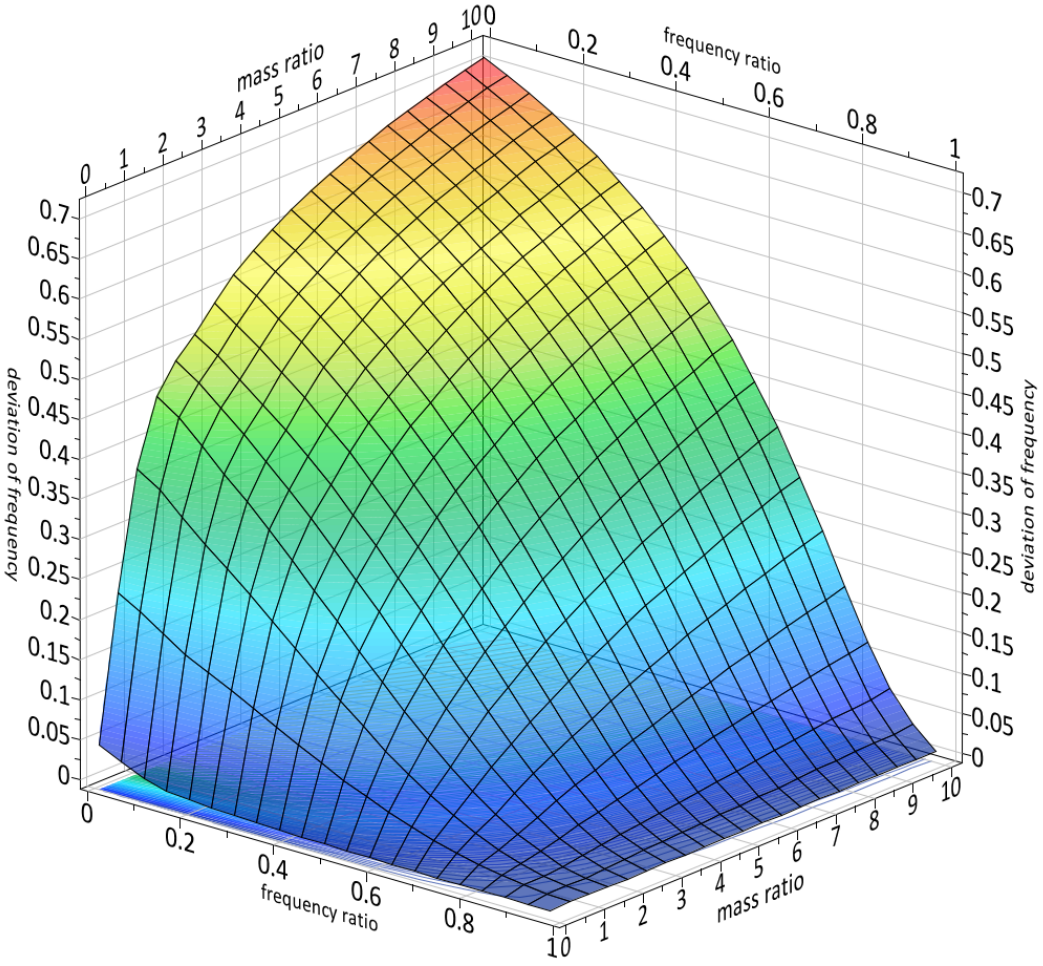

Figure 4.23: Characteristic diagram for frequency weighting of subsystem 2 with weak structural coupling

The diagram can be used to guess the maximum deviation of frequency to the coupled system by using the mass ratio and the frequency ratio. With decreasing mass ratio and increasing frequency ratio, the deviation of frequency moves towards zero.

$$deviation\ of\ frequency_{\ frequency\ ratio \to 1} = 0 \qquad (4.51)$$

$$deviation\ of\ frequency_{\ mass\ ratio \to 0} = 0 \qquad (4.52)$$

The comparison with the characteristic diagram for the frequency weighting of subsystem 1 in Figure 4.21 shows that the structural coupling has more influence on subsystem 1 than on subsystem 2. The maximum deviation of frequency in the same range of frequency ratio and mass ratio is significantly higher for subsystem 1.

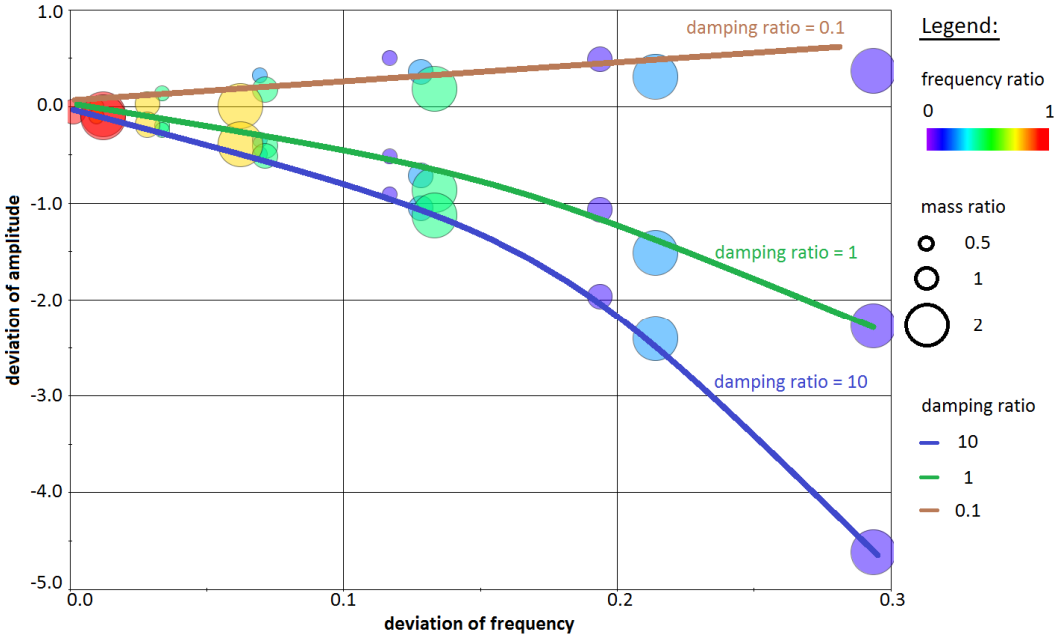

Figure 4.24: Diagram for frequency and amplitude weighting of subsystem 2 with weak structural coupling

Figure 4.24 shows the deviation of frequency and the deviation of amplitude by considering the frequency ratio, mass ratio, and damping ratio. In this case, it is important to have a high frequency ratio and a low mass ratio to reach a small deviation of amplitude. The damping ratio is important as well, but a very low damping ratio in combination with a middle frequency ratio or mass ratio can result in a big deviation of amplitude. So it is more important for the engineer to look at the frequency ratio and mass ratio to guess the deviation of frequency and amplitude.

Strong structural coupling:

In this section, the diagrams which are used to guess the influence of strong structural coupling are explained in detail. At first the deviations of subsystem 1* are analyzed. In chapter 4.2.6.2.2, the subsystem 1* is defined as subsystem 1 with the additional mass of subsystem 2. Figure 4.25 shows the characteristic diagram to guess the deviation of

frequency for subsystem 1* with strong structural coupling between subsystem 1 and subsystem 2.

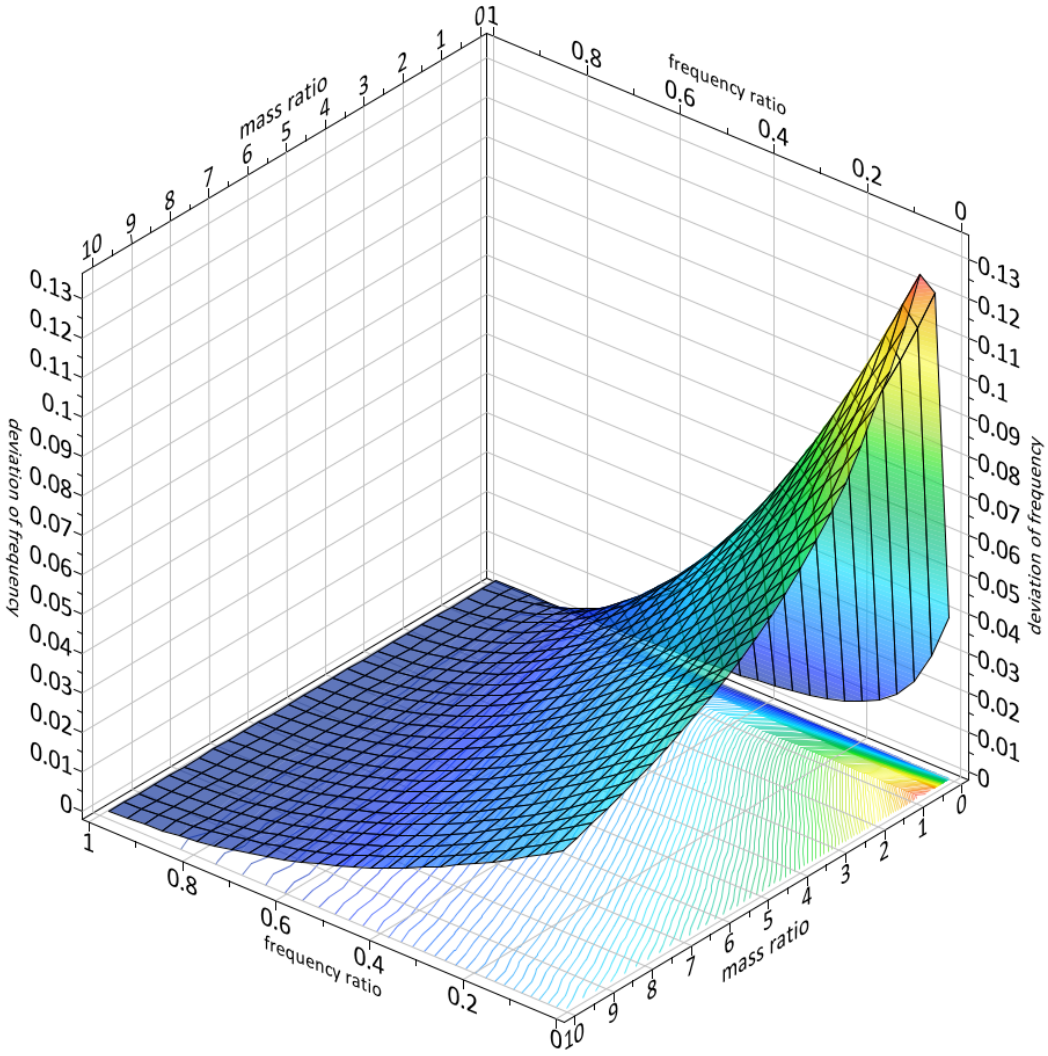

Figure 4.25: Characteristic diagram for frequency weighting of subsystem 1* with strong structural coupling

Generally, the deviation of frequency decreases with a high frequency ratio. With a very high mass ratio or a very low mass ratio, the deviation of frequency decreases, too. The turning point depends on the frequency ratio. With an increasing frequency ratio, the turning point of the mass ratio moves to 1. With a decreasing frequency ratio, the turning point of the mass ratio moves to 0.5. The dependency of the turning point is shown in Figure 4.26.

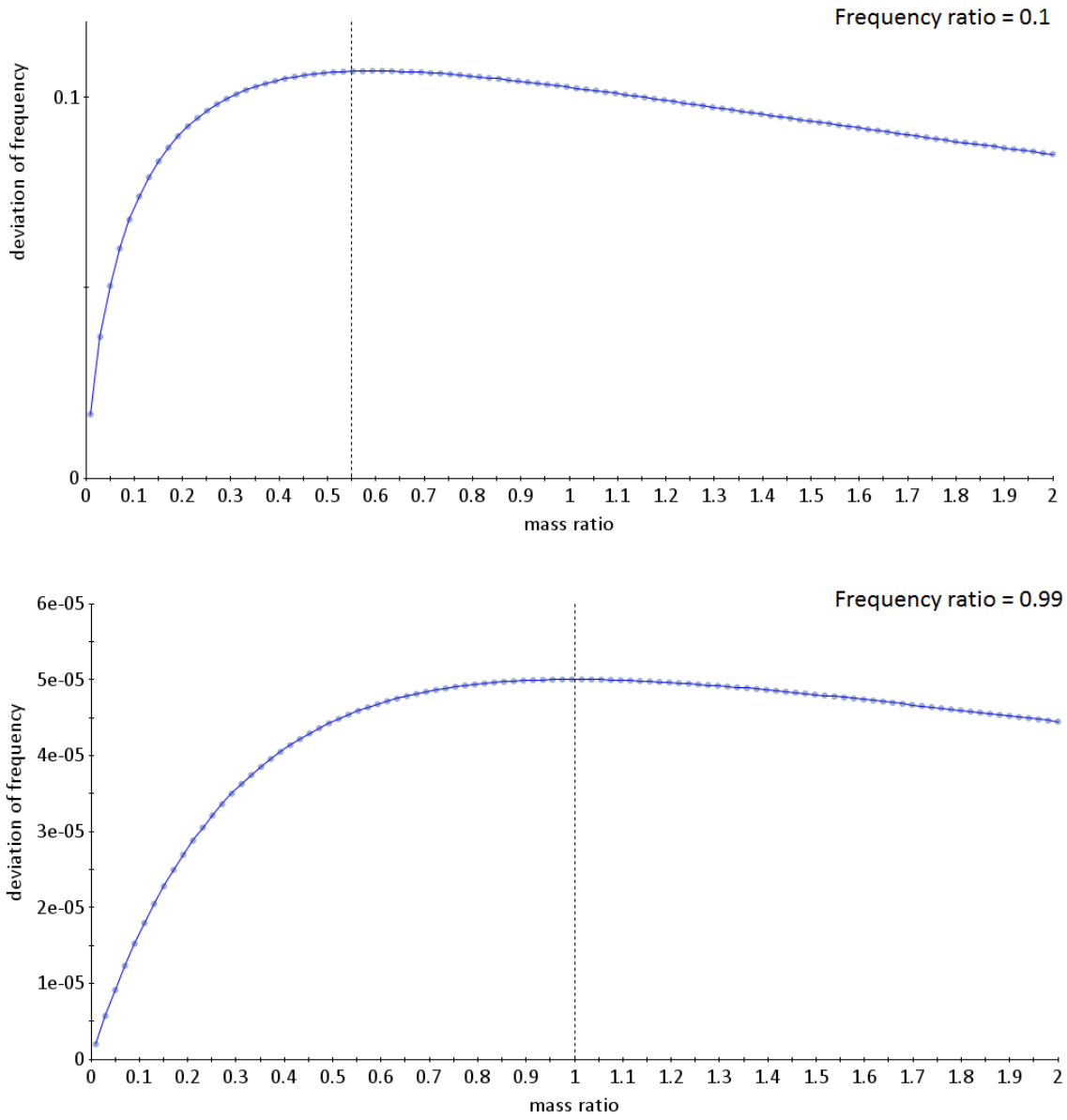

Figure 4.26: Turning point dependency on the frequency ratio

Figure 4.27 shows the diagram to guess the deviation of frequency and the deviation of amplitude. A high damping ratio tends to result in high deviation of amplitude. A very low damping ratio can result in a high deviation of amplitude, too. But the diagram shows that a low damping ratio is not as critical as a high damping ratio. Another way to shrink the deviation of amplitude is to increase the mass ratio. With a high mass ratio, the deviation of amplitude and the deviation of frequency decreases. The third way to shrink the deviation of frequency and the deviation of amplitude is to increase the frequency ratio.

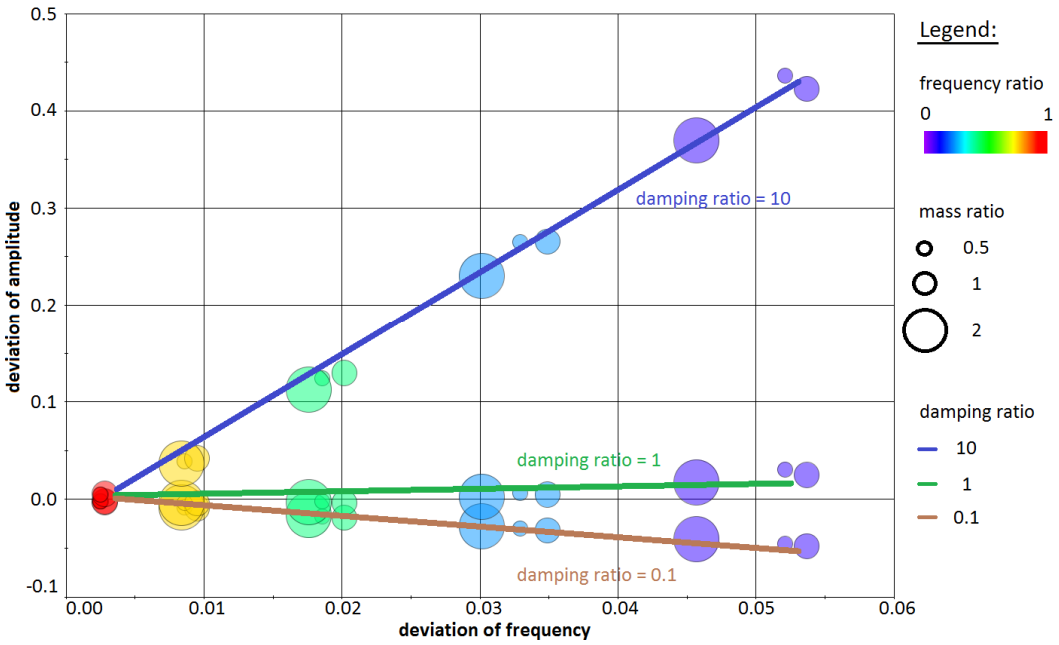

Figure 4.27: Diagram for frequency and amplitude weighting of subsystem 1* with strong structural coupling

If the engineer is interested in subsystem 2, he or she has to use the diagrams in Figure 4.28 and Figure 4.29. With the characteristic diagram in Figure 4.28, he or she is able to guess the maximum deviation of frequency. The interpretation of the diagram shows that the frequency ratio has a very small influence on the deviation of frequency. But the mass ratio has a very big influence on the deviation of frequency. So the engineer has to look at the frequency ratio, if the mass ratio is very low.

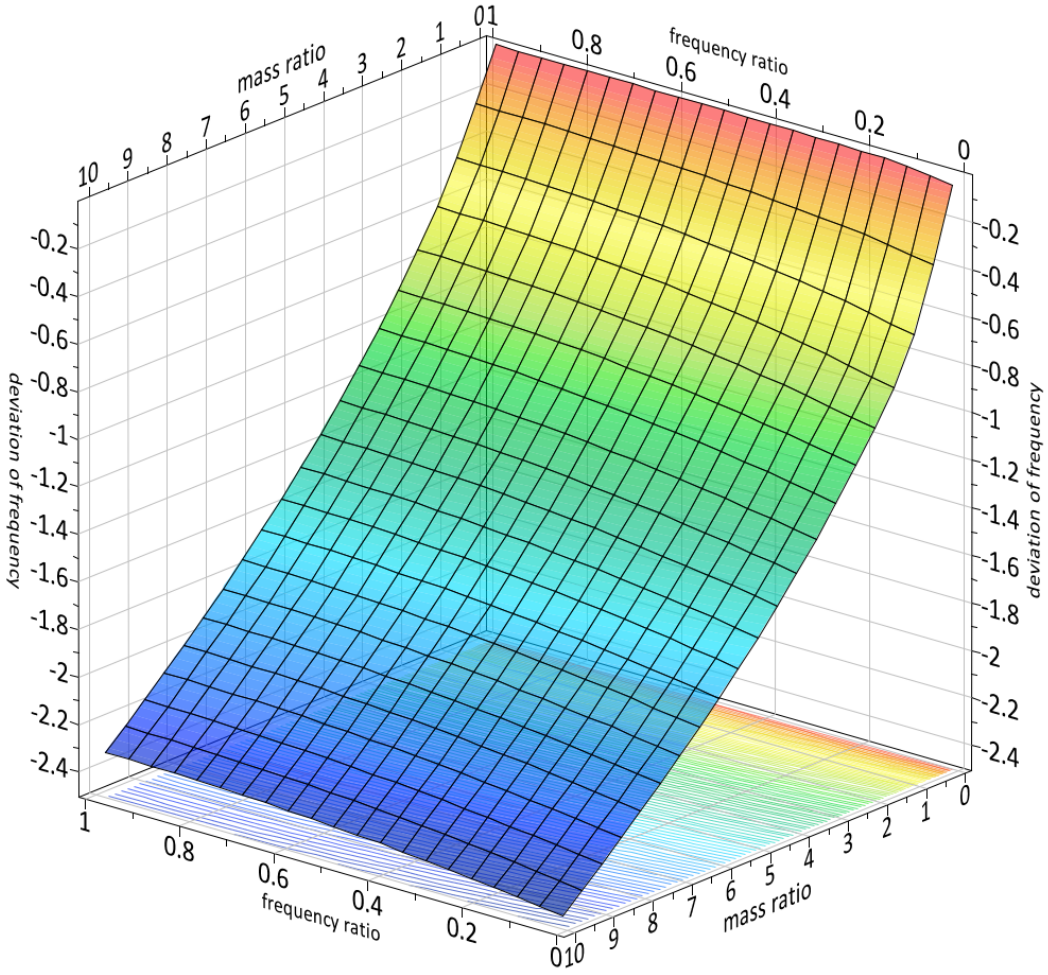

Figure 4.28: Characteristic diagram for frequency weighting of subsystem 2 with strong structural coupling

Figure 4.29 shows the diagram to guess the deviation of amplitude for subsystem 2. The interpretation of the diagram shows that a calculation of operational vibrations cannot be successful on an absolute scale. So the deviation of amplitude and the deviation of frequency are influenced by the mass ratio in opposite direction. With an increasing mass ratio, the deviation of amplitude decreases and the deviation of frequency increases. Thus, the amplitude moves to the value of the coupled system, but the frequency goes away from the value of the coupled system. Another argument is the high level of the deviation of amplitude and frequency. Figure 4.29 shows that the minimum deviation of amplitude for the considered parameter space is roundabout 74 %. So the engineer should not use subsystem 2 for analysis on an absolute scale.

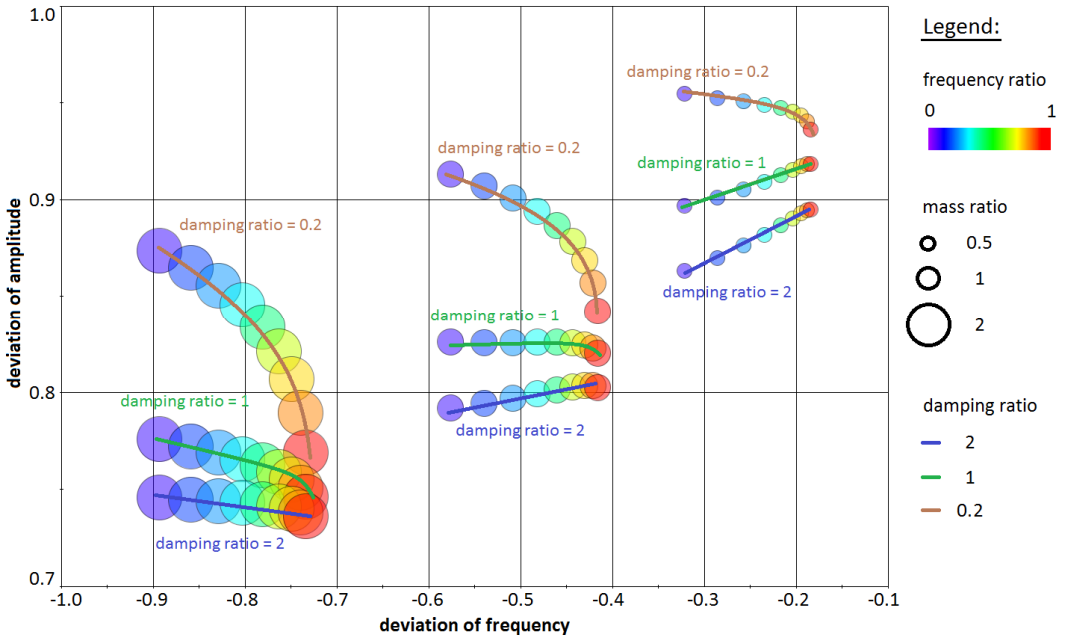

Figure 4.29: Diagram for frequency and amplitude weighting of subsystem 2 with strong structural coupling

4.2.7 Application of the developed assessment method

Let's explain the general process to apply the developed assessment method in the previous chapter. Starting from the thought that the coupled system is described in Eq. (4.53) and can be separated into the subsystem A (Eq. (4.54)) and subsystem B (Eq. (4.55)).

$$\mathbf{M}\ddot{\mathbf{x}} + \mathbf{D}\dot{\mathbf{x}} + \mathbf{K}\mathbf{x} = \mathbf{f} \qquad (4.53)$$

$$\mathbf{M_A}\ddot{\mathbf{x}} + \mathbf{D_A}\dot{\mathbf{x}} + \mathbf{K_A}\mathbf{x} = \mathbf{f_A} \qquad (4.54)$$

$$\mathbf{M_B}\ddot{\mathbf{x}} + \mathbf{D_B}\dot{\mathbf{x}} + \mathbf{K_B}\mathbf{x} = \mathbf{f_B} \qquad (4.55)$$

Here we assume that subsystem B is coupled to subsystem A and subsystem A is fixed to the ground. In the first step, the eigenfrequencies of the subsystems have to be calculated. So we get the eigenfrequency vector $\boldsymbol{f_A}$ and $\boldsymbol{f_B}$.

$$\boldsymbol{f}_\mathbf{A} = [f_{A1}, f_{A2}, \dots, f_{An}]^T \qquad (4.56)$$

$$\boldsymbol{f}_{\mathbf{B}} = [f_{B1}, f_{B2}, \dots, f_{Bn}]^T \qquad (4.57)$$

The eigenfrequency vectors start with the lowest eigenfrequency and end with the highest eigenfrequency. Now the kind of coupling can be determined by comparing each eigenfrequency of subsystem A with each eigenfrequency of subsystem B, as shown in Figure 4.30.

	f_{A1}	f_{A2}	…	f_{An}
f_{B1}	$f_{A1} > f_{B1}$	$f_{A2} > f_{B1}$	… > f_{B1}	$f_{An} > f_{B1}$
f_{B2}	$f_{A1} > f_{B2}$	$f_{A2} > f_{B2}$	… > f_{B2}	$f_{An} > f_{B2}$
…	$f_{A1} >$ …	$f_{A2} >$ …	… > …	$f_{An} >$ …
f_{Bn}	$f_{A1} > f_{Bn}$	$f_{A2} > f_{Bn}$	… > f_{Bn}	$f_{An} > f_{Bn}$

Figure 4.30: Comparison matrix of eigenfrequencies

If the term in the cell is complied, then the coupling is a weak structural coupling; otherwise it is a strong coupling. Accordingly to the matrix it can be determined, if it is possible to use a decoupled consideration. So if all terms are complied, the coupling from subsystem A to subsystem B is a weak structural coupling. If there are no satisfied terms in the matrix, the coupling from subsystem A to subsystem B is a strong structural coupling. And if some terms are complied and some terms are not complied, there is a mix of the kind of couplings. So a decoupled consideration is impossible for the whole frequency range, except the mass ratio is very low and tends to zero.

At first we assume that all terms are complied and the frequency ratio for weak structural couplings can be calculated by the Eq. (4.37). Otherwise the Eq. (4.38) for strong structural couplings has to be used. Afterwards the deviation of frequency can be guessed by using the lowest frequency ratio in the matrix, the mass ratio of the oscillating masses and the characteristic diagram. Now the structural coupling effect of subsystems can be assessed for using the modal analysis. If the operational vibrations

should be calculated, the criterion of the damping ratio has to be used additionally. Here the Lehr's damping measures for each eigenmode of the subsystems has to be calculated to get the Lehr's damping measure vectors in Eq. (4.58) and Eq. (4.59).

$$\boldsymbol{D}_{\mathbf{A}} = [D_{A1}, D_{A2}, \dots, D_{An}]^T \quad (4.58)$$

$$\boldsymbol{D}_{\mathbf{B}} = [D_{B1}, D_{B2}, \dots, D_{Bn}]^T \quad (4.59)$$

Now it is possible to generate a comparison matrix of Lehr's damping measures, as shown in Figure 4.31.

	D_{A1}	D_{A2}	…	D_{An}
D_{B1}	D_{B1}/D_{A1}	D_{B1}/D_{A2}	$D_{B1}/\dots$	D_{B1}/D_{An}
D_{B2}	D_{B2}/D_{A1}	D_{B2}/D_{A2}	$D_{B2}/\dots$	D_{B2}/D_{An}
…	…/ D_{A1}	…/ D_{A2}	…/ …	…/ D_{An}
D_{Bn}	D_{Bn}/D_{A1}	D_{Bn}/D_{A2}	D_{Bn}/D_{A1}	D_{Bn}/D_{An}

Figure 4.31: Comparison matrix of Lehr's damping measures

To assess the influence of the coupling to the amplitudes of the operational vibrations, the damping ratios have to be used in the characteristic diagram.

At the end a flowchart of the schematic assessment process is shown in Figure 4.32 and Figure 4.33. Furthermore, the method is applied in the next chapter to see the application at a more complex example.

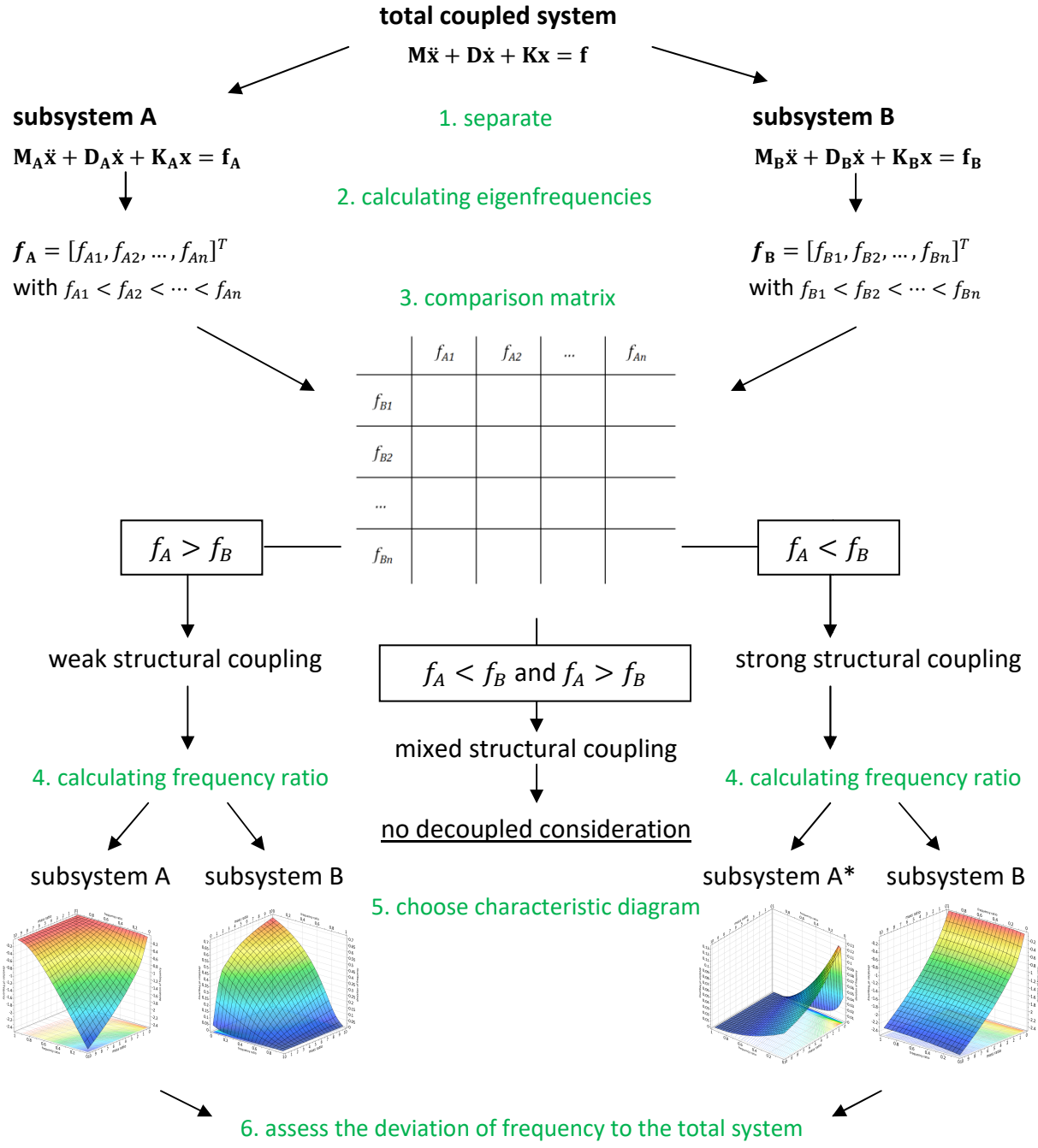

Figure 4.32: Flowchart of the schematic assessment process for the assessment of the frequency influence

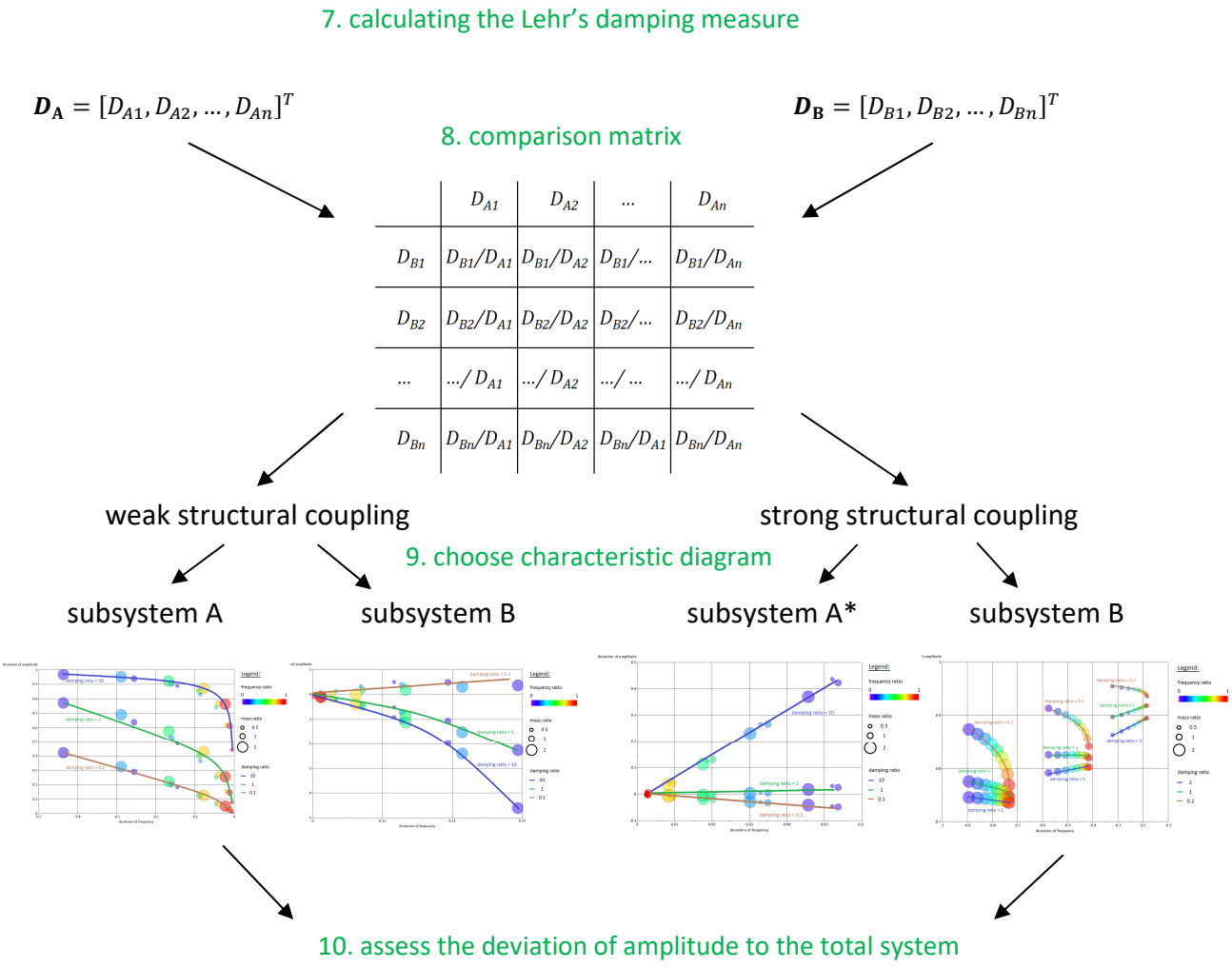

Figure 4.33: Adjusted flowchart of the schematic assessment process for the assessment of the amplitude influence

4.3 Explanation of the abstraction levels for a flexible-body system

In this chapter, we will use the knowledge of the previous chapter and explain some new effects that can be observed by using three-dimensional flexible-body systems.

4.3.1 Description of the total system

Figure 4.34 shows the total flexible-body system with the total mass and the considered eigenfrequencies with modal damping factors.

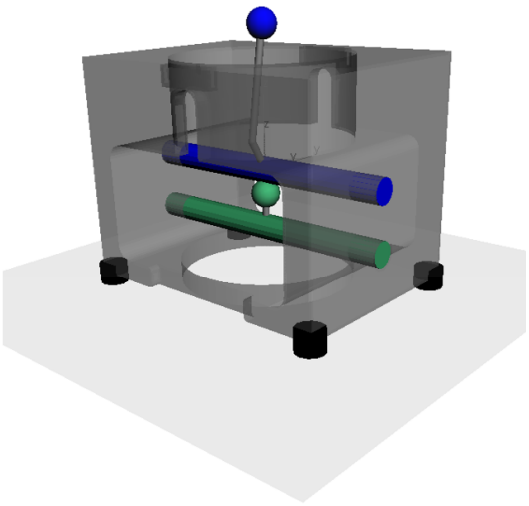

Total mass: 154.2 kg

Mode	Eigenfrequency [Hz]	Modal damping factor [-]
1	12.1	0.038
2	13.2	0.042
3	13.2	0.042
4	21.7	0.068
5	21.7	0.068
6	75.1	0.085
7	86.3	0.151
8	86.5	0.097
9	120.6	0.111
10	132.9	0.337
11	140.9	0.169
12	155.7	0.105
13	166.2	0.712
14	170.3	0.656
15	218.2	0.064
16	232.3	0.345
17	233.5	0.726
18	234.1	0.696
19	296.0	0.087
20	408.2	0.798

Figure 4.34: Total flexible-body system

The total system can be distributed in three subsystems:

- Grey system housing
- Blue rotating shaft (3000 rpm) with oscillating mass (crank drive)
- Green rotating shaft (9000 rpm) with eccentric mass (unbalanced shaft)

The system housing (subsystem 1) consists of a modal-reduced substructure (grey) and four mountings (black) with a linear stiffness and damping factor. Figure 4.35 shows the subsystem 1 with the total mass and the considered eigenfrequencies with modal damping factors.

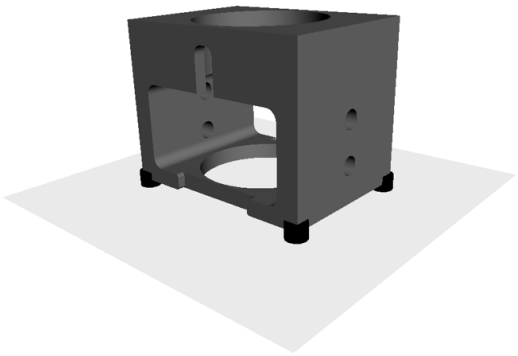

Total mass: 92.5 kg

Mode	Eigenfrequency [Hz]	Modal damping factor [-]
1	133.2	0.084
2	140.1	0.075
3	229.3	0.124
4	271.8	0.173
5	346.1	0.211
6	392.1	0.255

Figure 4.35: Subsystem 1 - system housing

Subsystem 2 represents a crank drive with an oscillating mass point m_{osc} (blue sphere), two rigid connection rods (grey), a modal-reduced shaft (blue), and two mountings at the ends of the shaft with linear stiffness and damping factors. Figure 4.36 shows subsystem 2, the total mass, and the eigenfrequencies with modal damping factors.

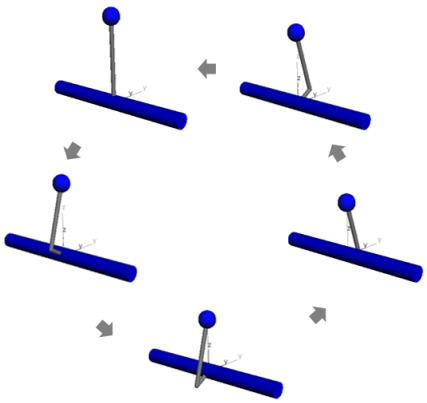

Total mass: 3.5 kg

Mode	Eigenfrequency [Hz]	Modal damping factor [-]
1	140.2	0.040
2	141.0	0.040
3	148.0	0.047
4	149.0	0.178
5	241.7	0.075
6	241.7	0.075

Figure 4.36: Subsystem 2 - crank drive

Subsystem 3 is an unbalanced shaft, which consists of a rotating mass point (green sphere), a rigid connection rod (grey), and a modal-reduced shaft (green). Figure 4.37 shows subsystem 3, the total mass, and the eigenfrequencies with modal damping factors.

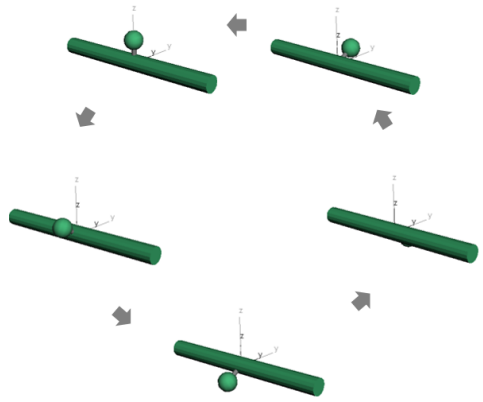

Total mass: 58.2 kg

Mode	Eigenfrequency [Hz]	Modal damping factor [-]
1	34.2	0.460
2	34.5	0.449
3	34.5	0.446
4	39.3	0.823
5	40.9	0.785
6	206.4	0.269

Figure 4.37: Subsystem 3 - unbalanced shaft

4.3.2 Abstraction level A1

In the abstraction level A1, the excitation forces of the system are calculated by using rigid bodies. So the excitation components are modeled as mass and their inertia. The process neglects the structural dynamic behavior during the excitation force calculation. For the calculation of the operational vibrations, the calculated forces are impressed on the total system with structural dynamic behavior.

4.3.2.1 Force calculation of subsystem 2

Subsystem 2 represents a crank drive so that the total force $f_{crank\ drive}$ can be calculated by using numerical methods or Eq. (4.60). Figure 4.38 shows the relevant parameter.

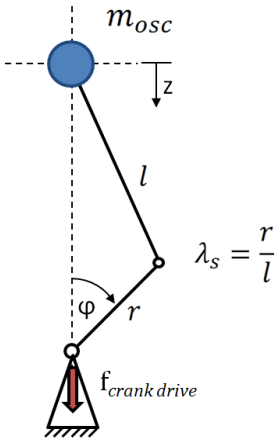

Figure 4.38: Crank drive

$$f_{crank\,drive} = m_{osc} \cdot r \cdot (2\pi\Omega)^2 \cdot \left[cos\,\varphi + \lambda_S \frac{cos\,(2\varphi) + \lambda_S^2\ sin^4\,\varphi}{\sqrt{(1 - \lambda_S^2\ sin^2\varphi)^3}} \right] \qquad (4.60)$$

The derivation of Eq. (4.60) can be found in (Dubbel et al. 2001). The shaft is modeled as a rigid body with two rigid mountings and the crank drive is fixed in the middle of the shaft, so the calculated force has to be divided by two. Eq. (4.61) shows the mount forces f_1^{S2} and f_2^{S2}, which has to be impressed on the total system in the second calculation step.

$$f_1^{S2} = f_2^{S2} = \frac{f_{crank\,drive}}{2} \qquad (4.61)$$

Figure 4.39 shows the calculated forces in time and frequency domain.

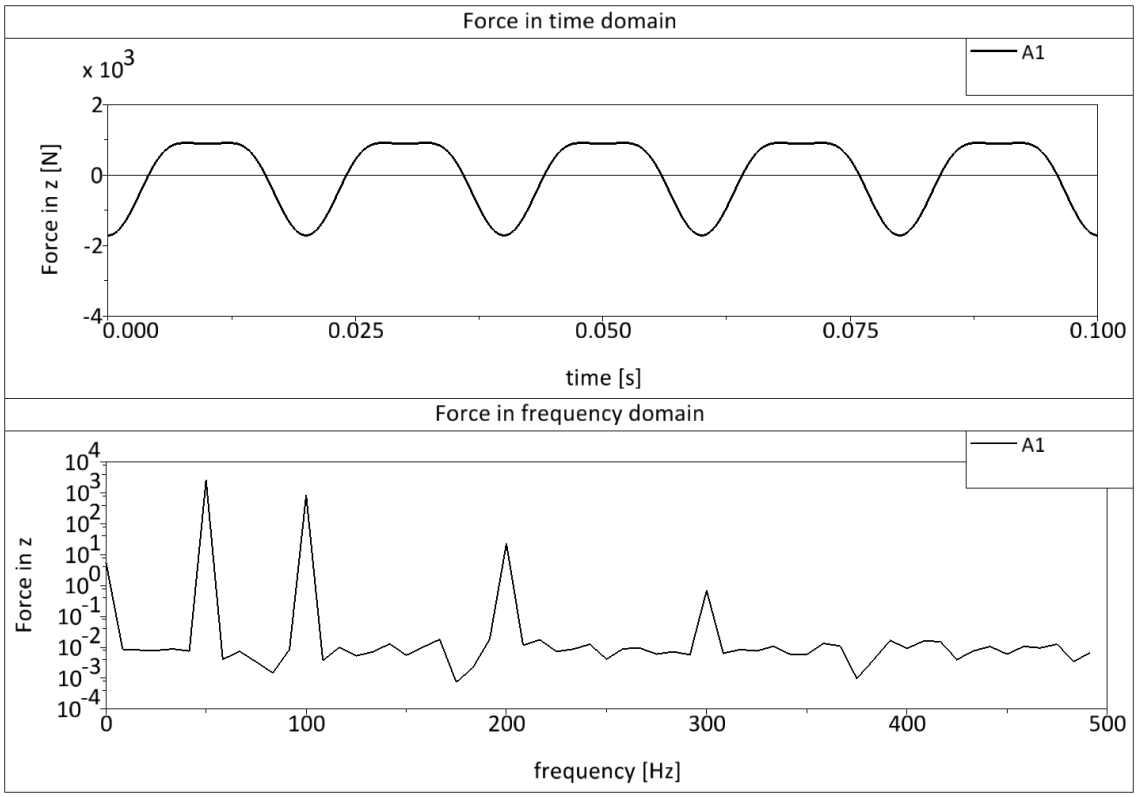

Figure 4.39: Analytical calculated force of subsystem 2

In frequency domain it can be seen that the oscillating mass results in a periodic force. The periodic force consists of many frequencies also called orders. An order is defined as a multiple of the rotational frequency.

$$Order_n = n \cdot \Omega \qquad (4.62)$$

So the first peak (50 Hz) is called first order, the second peak (100 Hz) is called second order, and so on. Referring to the explained amplitude modulation in chapter 4.2.1, the uneven orders excluding the first order are zero.

4.3.2.2 Force calculation of subsystem 3

Subsystem 3 shows an unbalanced shaft, whose mounting forces can be calculated by numerical methods or the Eq. (4.63).

$$\mathrm{f}_1^{S3} = \mathrm{f}_2^{S3} = \frac{1}{2} \cdot m_{rot} \cdot r \cdot (2\pi\Omega)^2 \qquad (4.63)$$

Figure 4.40 shows the mounting forces in time and frequency domain.

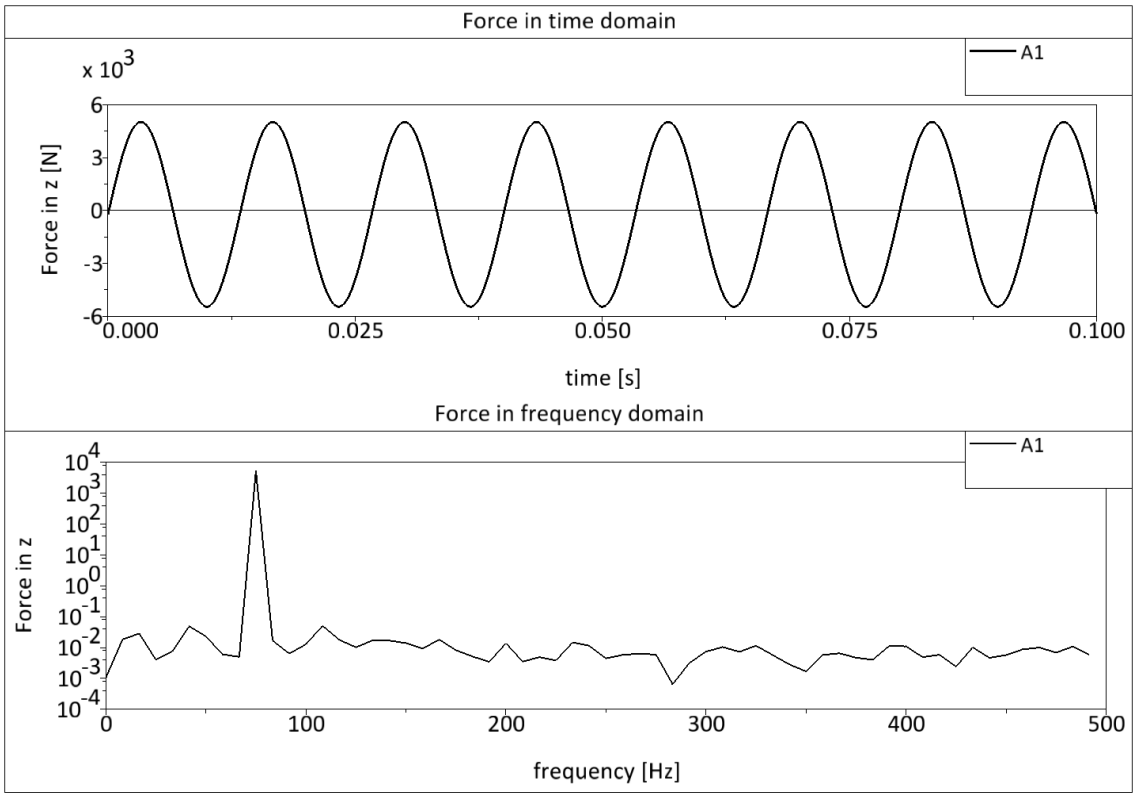

Figure 4.40: Analytical calculated force of subsystem 3

The forces are called harmonic force, because it only consists of one frequency.

4.3.2.3 Calculation of the operational vibration

Now the calculated forces have to be impressed on the flexible structure. In chapter 4.2.2, it is defined that the excitation components have to be coupled to the system housing, because of the explained Block Force Method. But at first we want to use the explained assessment method in chapter 4.2.6. If the excitation subsystem does not influence the structural dynamic behavior of the total system significantly, the subsystem does not have to be modeled and can be neglected.

Application of the assessment method for structural coupling effects:

Subsystem 2 and subsystem 3 are coupled to subsystem 1, so the influence of subsystem 2 and subsystem 3 to subsystem 1 has to be checked. Let's start with the coupling of subsystem 2 to subsystem 1. At first all eigenfrequencies have to be compared to each other to decide, if it is a strong or a weak structural coupling. Figure 4.41 shows a matrix that compares the eigenfrequencies of subsystem 1 and subsystem 2, referring to Eq. (4.35) and Eq. (4.36) in chapter 4.2.6.2.2. The green color is used for a weak structural coupling and red color for a strong structural coupling. Because of a balanced ratio between a weak and strong structural coupling, it can be concluded that a mixed structural coupling exists. Generally, it is necessary to consider the structural coupling at a mixed structural coupling matrix if the mass ratio is not very low. But we want to have a look at the whole assessment method, so we go on with the next step of the procedure.

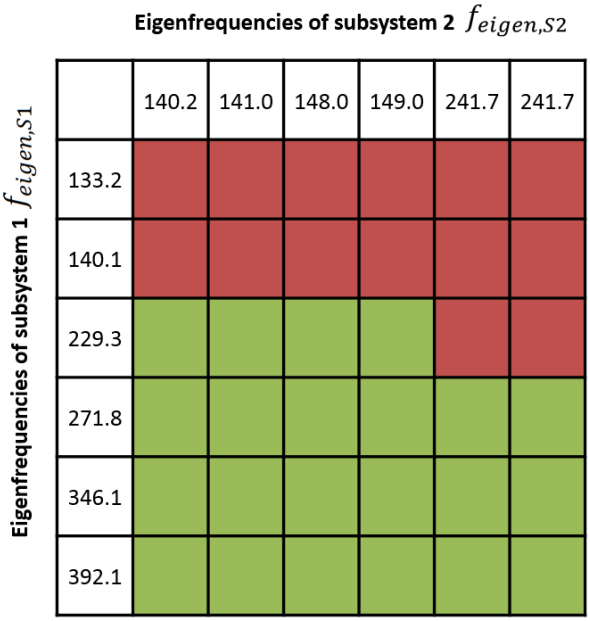

Figure 4.41: Identification matrix for strong or weak structural coupling

Now the frequency ratios can be calculated based on the Eq. (4.37) and Eq. (4.38) in chapter 4.2.6.2.2. Figure 4.42 shows the values for the frequency ratio. The green color indicates a high frequency ratio and red color shows a low frequency ratio. It can be seen a mix of low and high frequency ratios. Because of many low frequency ratios and

the mixed kinds of structural coupling, a decoupled observation cannot be recommended.

Eigenfrequencies of subsystem 1 $f_{eigen,S1}$ \ Eigenfrequencies of subsystem 2 $f_{eigen,S2}$	140.2	141.0	148.0	149.0	241.7	241.7
133.2	0.050	0.055	0.100	0.106	0.449	0.449
140.1	0.001	0.006	0.053	0.060	0.420	0.420
229.3	0.388	0.385	0.355	0.350	0.051	0.051
271.8	0.484	0.481	0.455	0.452	0.111	0.111
346.1	0.595	0.593	0.572	0.569	0.302	0.302
392.1	0.642	0.640	0.623	0.620	0.384	0.384

Figure 4.42: Frequency ratio matrix

Furthermore, the criteria “mass ratio” in Eq. (4.64) should be used, but the value has to be very small to compensate the low frequency ratios. In the first approximation, the masses of the subsystems can be used to guess the structural coupling effect.

$$mass\ ratio = \frac{m_2}{m_1} = \frac{58.2\ kg}{92.5\ kg} = 0.629 \qquad (4.64)$$

The analysis of the damping ratio can be omitted, because of the predicted high structural coupling. As a result, it is necessary to model subsystem 2 and their coupling to subsystem 1 in order to consider the structural dynamic behavior of the total system.

Now the structural coupling of subsystem 3 to the coupled system (subsystem 1 and subsystem 2) can be analyzed. Let’s start with the identification matrix for strong and weak structural coupling in Figure 4.43.

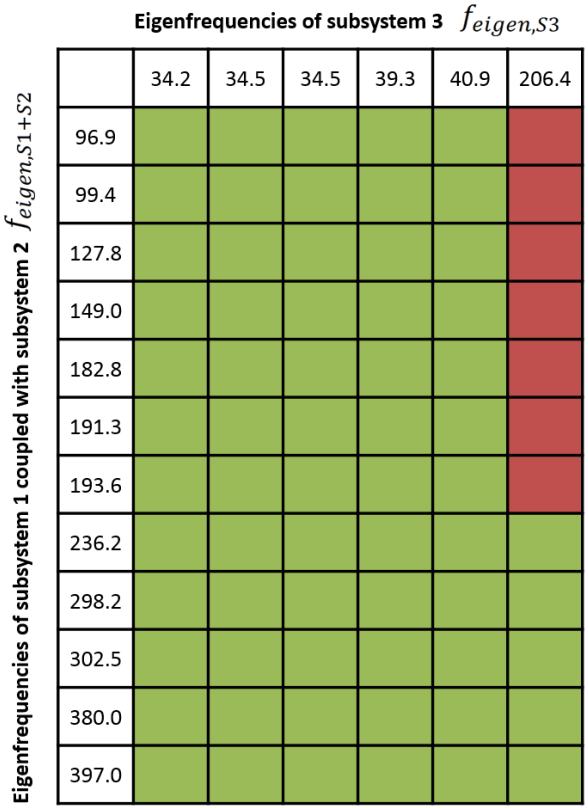

Figure 4.43: Identification matrix for strong and weak structural coupling

So it can be seen that a weak structural coupling dominated the identification matrix and the frequency ratio matrix in Figure 4.44 shows very high values excluding the last column.

Eigenfrequencies of subsystem 1 coupled with subsystem 2 $f_{eigen,S1+S2}$	Eigenfrequencies of subsystem 3 $f_{eigen,S3}$					
	34.2	34.5	34.5	39.3	40.9	206.4
96.9	0.647	0.644	0.644	0.595	0.578	0.530
99.4	0.656	0.653	0.653	0.605	0.588	0.518
127.8	0.732	0.730	0.730	0.693	0.680	0.381
149.0	0.770	0.769	0.768	0.736	0.725	0.278
182.8	0.813	0.811	0.811	0.785	0.776	0.115
191.3	0.821	0.820	0.820	0.795	0.786	0.073
193.6	0.823	0.822	0.822	0.797	0.789	0.062
236.2	0.855	0.854	0.854	0.834	0.827	0.126
298.2	0.885	0.884	0.884	0.868	0.863	0.308
302.5	0.887	0.886	0.886	0.870	0.865	0.318
380.0	0.910	0.909	0.909	0.897	0.892	0.457
397.0	0.914	0.913	0.913	0.901	0.897	0.480

Figure 4.44: Frequency ratio matrix

So the mode shape of the eigenfrequency 206.4 Hz should be analyzed. The mode shape is a torsion of the shaft, which does not influence the eigenfrequencies of the total system significantly. Due to the nodal point of the system torsion mode is in the rotation axis of the shaft, so the last column can be neglected. In regard to the frequency ratio matrix the subsystem 1 does not influence the structural dynamic behavior of the total system significantly. Now the second criteria should be calculated in Eq. (4.65).

$$mass\ ratio = \frac{m_3}{m_1 + m_2} = \frac{3.5\ kg}{150.7\ kg} = 0.0232 \qquad (4.65)$$

By using the mass ratio (0.0232) and the minimum frequency ratio (0.647) in the characteristic diagram (Figure 4.21, Chapter 4.2.6.2.3), it can be seen that the deviation of frequency should be low. So probably the subsystem 3 does not have a significant influence to the eigenmodes of the total system. To assess the influence to the amplitudes of the operational vibrations, the damping ratio should be analyzed.

Figure 4.45 shows the damping ratio matrix, but the influence to the results is not significant, because the mass ratio is very low. To conclude, it can be recommended that the structural dynamic behavior of subsystem 3 can be neglected to calculate the operational vibrations of subsystem 1.

Damping of subsystem 1 coupled with subsystem 2 D_{S1+S2} \ Damping of subsystem 3 D_{S3}	0.460	0.449	0.446	0.823	0.785	0.269
0.051	9.007	8.795	8.744	16.125	15.376	5.274
0.046	10.034	9.798	9.741	17.962	17.128	5.875
0.046	10.086	9.849	9.791	18.056	17.218	5.906
0.178	2.576	2.515	2.501	4.611	4.397	1.508
0.085	5.405	5.278	5.247	9.676	9.227	3.165
0.076	6.020	5.878	5.844	10.776	10.276	3.525
0.080	5.746	5.611	5.578	10.287	9.810	3.365
0.082	5.623	5.490	5.458	10.066	9.598	3.292
0.168	2.742	2.677	2.661	4.908	4.680	1.605
0.117	3.934	3.842	3.819	7.043	6.716	2.304
0.207	2.221	2.169	2.156	3.976	3.792	1.301
0.254	1.813	1.770	1.760	3.245	3.094	1.061

Figure 4.45: Damping ratio matrix

Now the calculated forces can be impressed on the system to calculate the operational vibrations. Figure 4.46 shows the operational vibrations by using the abstraction level A1. Figure 4.46 shows three different calculations for the operational vibration of one point of subsystem 1 to approve the recommendation of the preliminary assessment. The red curve represents the recommendation of the preliminary assessment. So the forces are impressed on subsystem 1 coupled with subsystem 2. The comparison with the blue curve - which represents the force-impressing on the total system - shows that subsystem 3 has not a significant influence on the structural dynamic behavior of the total system. The black curve represents the force-impressing on subsystem 1 and

verifies that subsystem 2 has a significant influence on the structural dynamic behavior of the total system, because of a significant different operational vibration.

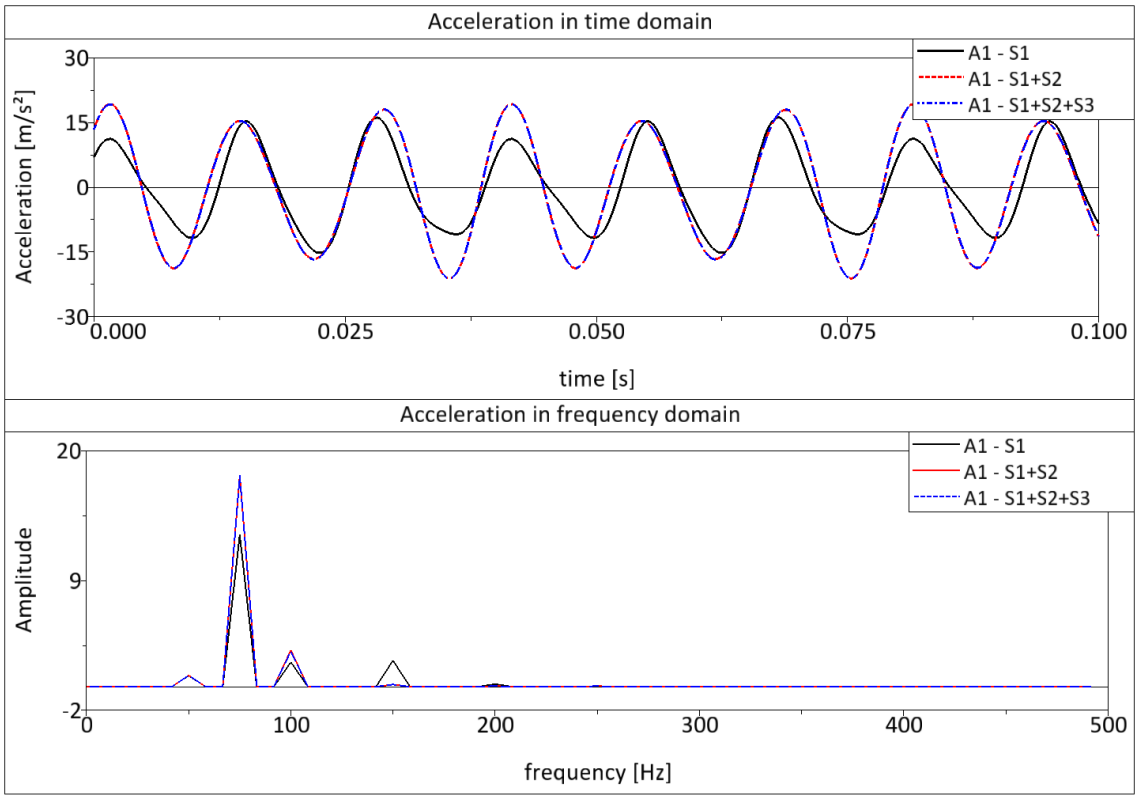

Figure 4.46: Operational vibration by using the abstraction level A1 with different coupled subsystems

4.3.3 Abstraction level A2

In the abstraction level A2, the Blocked Force Method (chapter 3.5.3) is used to calculate the operational vibration of subsystem 1. The difference to abstraction level A1 is the calculation of the excitation forces. The abstraction level A2 considers the structural dynamic behavior of the total system and a part of the excitation interaction. Why the abstraction level only considers a part of the excitation interaction is explained in chapter 4.3.5.

4.3.3.1 Force Calculation

The force calculation is based on a model, with respect to the structural dynamic behavior of the excitation subsystems. The structural coupling to other subsystems is not modeled, so the calculated forces do not contain the structural dynamic behavior of the total system.

Figure 4.47 and Figure 4.48 compare the calculated forces by using the rigid body method and the flexible body method with modeling of the structural dynamic behavior. Figure 4.47 shows the calculated forces of subsystem 2 in time and frequency domain. In time domain can be seen that the structural dynamic behavior has a significant influence on the force. The most significant difference can be found at 150 Hz. So the calculation with flexible components shows amplitudes in the uneven orders compared to the calculation with rigid components. In the next chapter, the reason of the effect is explained by a detailed analysis of rotating shafts.

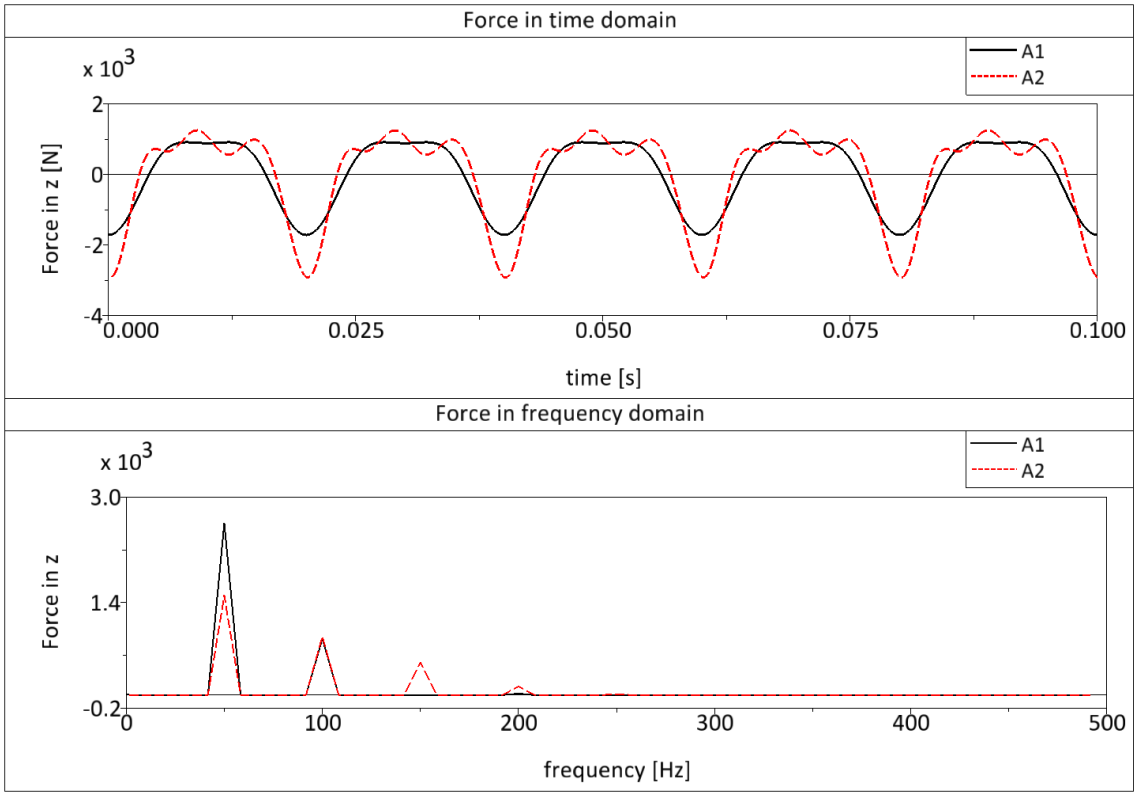

Figure 4.47: Comparison of the calculated excitation force of subsystem 2

Figure 4.48 shows the calculated force of subsystem 3 in time and frequency domain. It can be seen that the frequency content is the same by using both abstraction levels. But the amplitude of the force is significantly different. So we have to add-on the criterion of chapter 4.2.6.1, which helps the engineer to decide, if the rotating components can be modeled as rigid or flexible components.

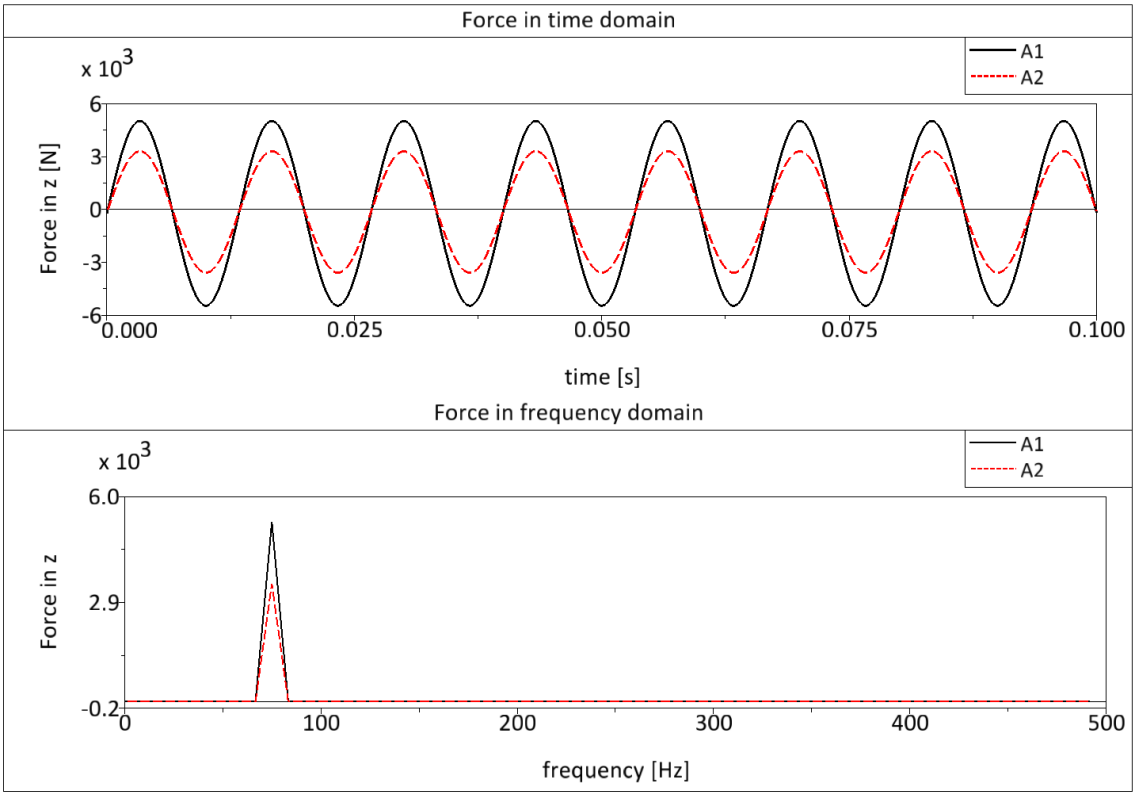

Figure 4.48: Comparison of the calculated excitation force of subsystem 3

4.3.3.1.1 Add-on of assessment criterion to model rotating shafts

To help the engineer by choosing the most efficient modeling method for his or her problem, this chapter will show a developed method for subsystems with rotating shafts. At first we have to understand the described effect of the third order in Figure 4.47. Therefore, it is necessary to use a simple model like a slider-crank. Eq. (4.66) shows the analytical calculation with rigid bodies of the oscillating force

$$\mathrm{f}_{osc} = m_{osc} \cdot r \cdot (2\pi\Omega)^2 \cdot \left[cos\,\varphi + \lambda_S \frac{\cos(2\varphi) + \lambda_S^2\ sin^4\,\varphi}{\sqrt{(1 - \lambda_S^2\ sin^2\varphi)^3}} \right]. \qquad (4.66)$$

Figure 4.49 shows a general slider-crank with all forces. Furthermore, the analytical calculated oscillating force f_{osc} in time and frequency domain is displayed. But there are not displayed uneven orders excluding the first order.

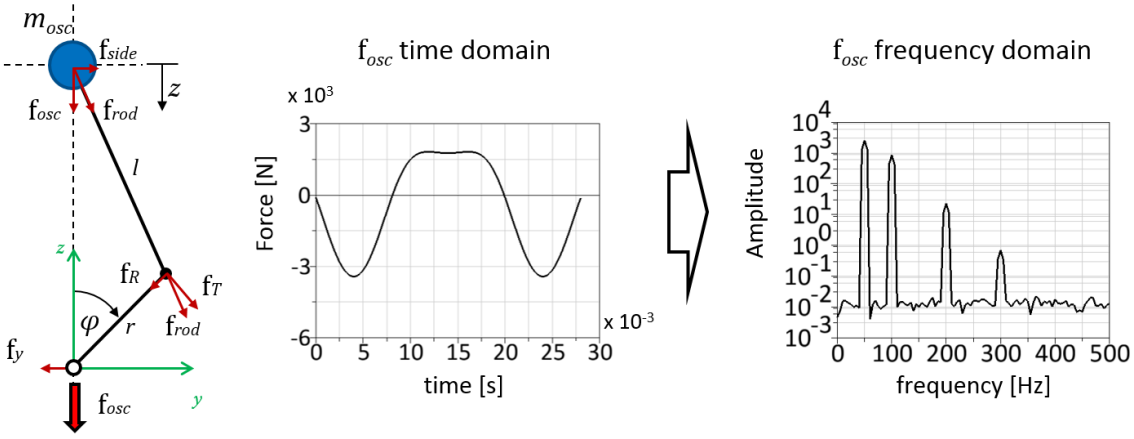

Figure 4.49: Illustration of a general slider-crank and their oscillating force in time and frequency domain

By following the force path from the oscillating mass to the bearing, the rod force f_{rod} is split up in the radial force f_R and tangential force f_T. Figure 4.50 shows the radial and tangential force in frequency domain. It can be seen that all orders are contained in contrast to the oscillation force in Figure 4.49.

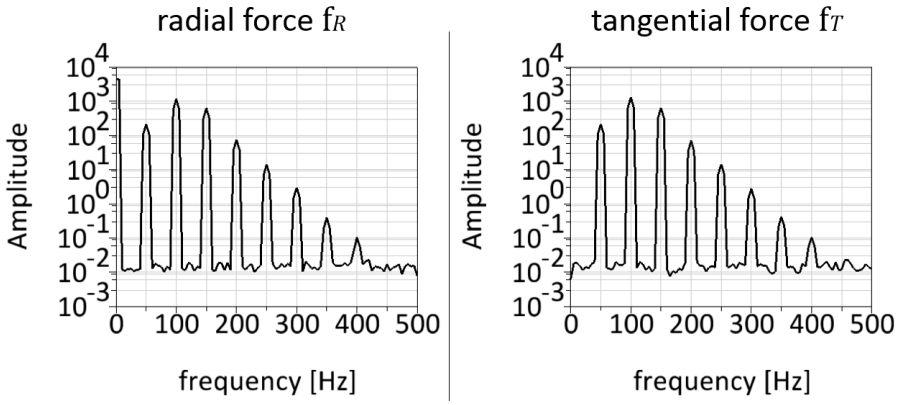

Figure 4.50: Radial and tangential force in frequency domain

These forces rotate with the rotational frequency Ω around the fixed bearing. So it is necessary to transform the forces from the rotating coordinate system to the global coordinate system, this is called amplitude modulation. By considering the phase of the radial and tangential forces, the explained amplitude modulation in chapter 4.2.1 leads to the equal result as the Eq. (4.66) for the oscillating force. So the amplitude of the uneven orders goes to zero, due to the amplitude modulation. But this calculation is only applicable for ideal rigid shafts, so we have to look at the results by implementing a rod-stiffness. Figure 4.51 shows a comparison between a rigid model and a flexible model. The flexible model is modified by a radial stiffness of the rod. The diagrams show the oscillating force in time and frequency domain and it can be seen that the flexible model leads to amplitudes at the uneven orders. The reason of this effect is that the radial force f_R in the rotating coordinate system excited the rod in all orders. So the motion of the oscillating mass is influenced by the flexible rod, as shown on the right side of Figure 4.51. The mass oscillate in all orders and the acceleration multiplied with the mass is equal to the oscillating force $f_{osc,flexible}$ in the bearing. The same effect can be shown by using a tangential stiffness or a torsion stiffness.

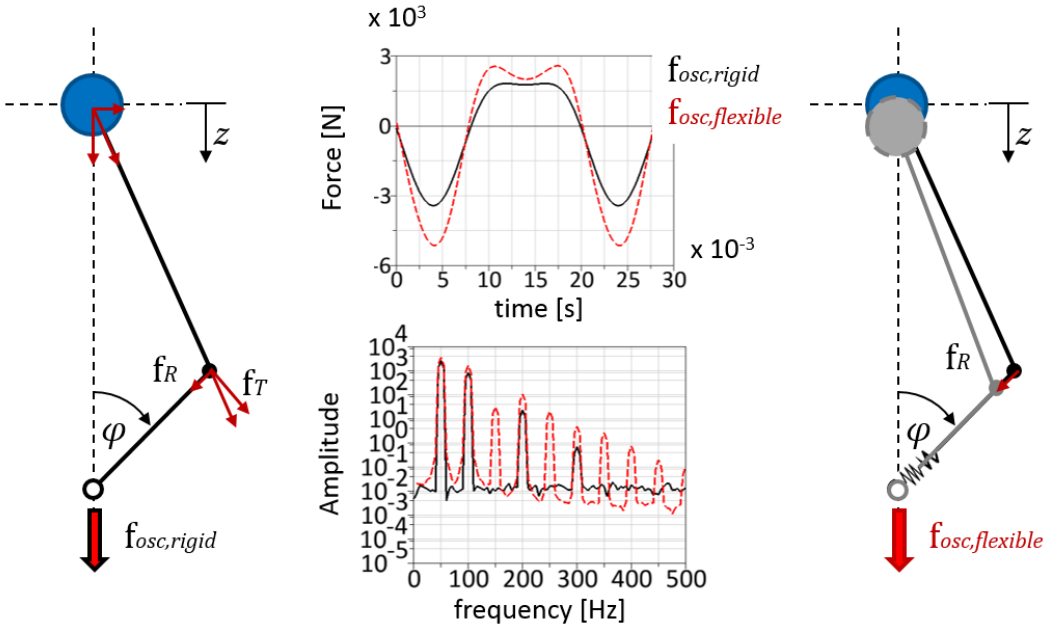

Figure 4.51: Comparison of the oscillating force by using a rigid model and a flexible model

Now the reason for the difference between the calculated forces by using the rigid body and flexible body method is identified. It is based on the structural dynamic

behavior of the rotating shaft. So it is necessary to analyze the structural dynamic behavior of a rotating shaft in detail, to generate a criterion which helps the engineer to decide, if a shaft can be modeled as a rigid body.

The research model is shown in Figure 4.52.

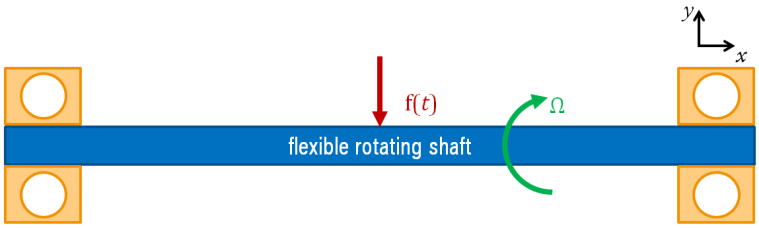

Figure 4.52: Research model for the analysis of the structural dynamic behavior

The shaft rotates with the rotational frequency Ω and is excited by the force $\mathrm{f}(t)$. The force $\mathrm{f}(t)$ represents a sine-wave whose frequency rises with time but the amplitude stays constant, so it can be also called force sweep. Now the observation of the bearing force shows the structural dynamic behavior of the flexible rotating shaft. For this analysis we combine the excitation force and measured bearing force by using the global and rotating coordinate system.

Let's start with the excitation in the global coordinate system and the measurement of the bearing force in the global coordinate system, too. If the shaft is ideal rigid, the force $\mathrm{f}(t)$ will split up to the two bearings. So each bearing is charged by the half amplitude of the force $\mathrm{f}(t)$ independent from the excitation frequency. A flexible shaft has an eigenfrequency. If the excitation force oscillates with the same frequency as the eigenfrequency of the shaft, the bearing force has the maximum amplitude. So Figure 4.53 shows the resulting bearing force in time and frequency domain. It can be seen that the exciting frequency is equal to the resulting frequency of the bearing force and the eigenfrequency can be identified by the highest amplitude in frequency domain.

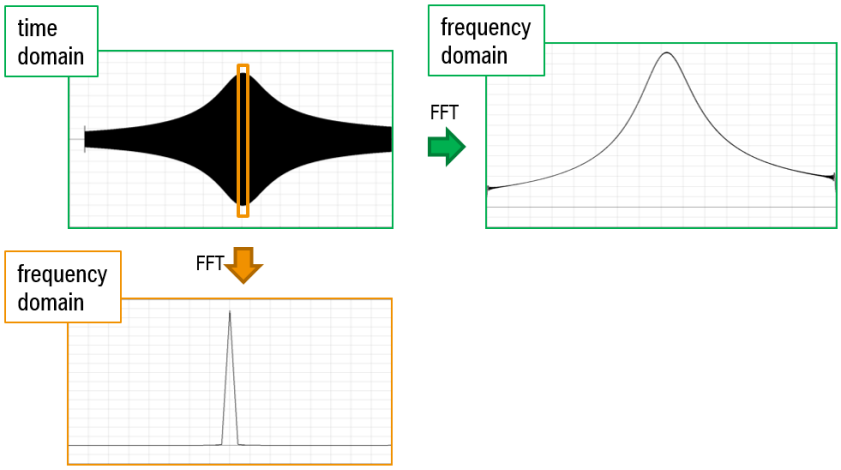

Figure 4.53: Dynamic behavior analysis of a shaft - excitation force and measured bearing force in the global coordinate system

Now the excitation force is impressed in the global coordinate system, but the bearing force is measured in the rotating coordinate system. So there is an amplitude modulation from the global coordinate system to the rotating coordinate system. Figure 4.54 shows the measured bearing force in time and frequency domain. It can be seen that the excitation force frequency is not equal to the measured bearing force, because of the amplitude modulation. So we always see two measured frequencies for one excitation frequency. In time domain, the highest amplitude of the bearing force can be measured at the excitation frequency of the global eigenfrequency. The Fourier Transform does not show the excitation frequency but the modulated frequencies, which can be calculated by Eq. (4.67).

$$f_{modulated} = \left| f_{excitation} \pm f_{rotating\ speed} \right| \qquad (4.67)$$

As result the highest amplitude in the rotating coordinate system is reached, if the excitation frequency is equal to the global eigenfrequency, but the oscillation in the rotating coordinate system is defined by the modulated frequencies.

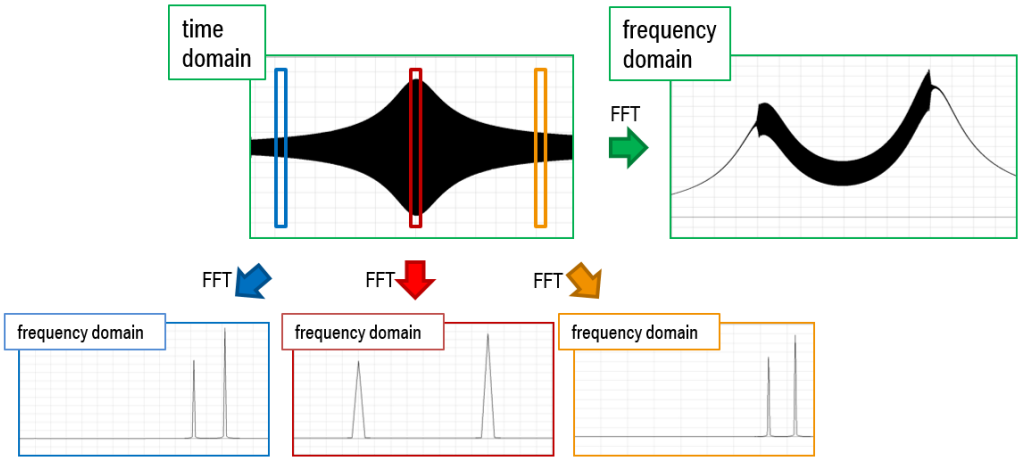

Figure 4.54: Dynamic behavior analysis of a shaft - excitation force in the global coordinate system and measured bearing force in the rotating coordinate system

Now the excitation force is impressed on the shaft in the rotating coordinate system and the bearing force is measured in the global coordinate system. Figure 4.55 shows the measured bearing force in time and frequency domain. Due to the amplitude modulation, the measured force frequency can be calculated by the Eq. (4.67). As result the highest force amplitudes in the bearing can be reached by exciting the shaft with the modulated eigenfrequencies in the rotating coordinate system. The reason is the shaft oscillating in the global eigenfrequency, during the excitation in the modulated eigenfrequencies. This can be seen in Figure 4.55 by the frequency domain of the blue and orange cutout.

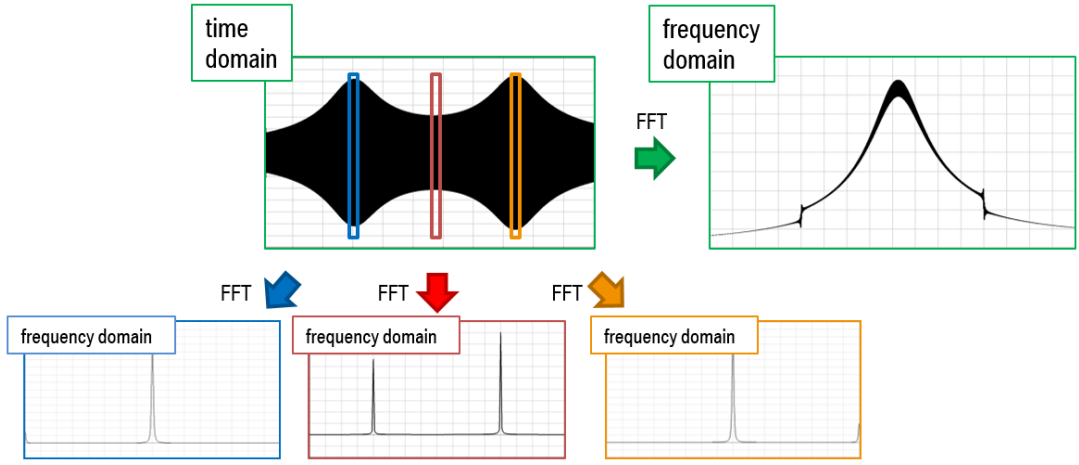

Figure 4.55: Dynamic behavior analysis of a shaft - excitation force in the rotating coordinate system and measured bearing force in the global coordinate system

In the last scenario, the shaft is excited in the rotating coordinate system and the bearing force is measured in the rotating coordinate system. Figure 4.56 shows that there is not an amplitude modulation and the excited frequency is equal to the measured frequency. But the eigenfrequencies of the shaft can be identified by the modulated eigenfrequencies. So the shaft has the highest amplitudes, if it is excited by the modulated eigenfrequencies.

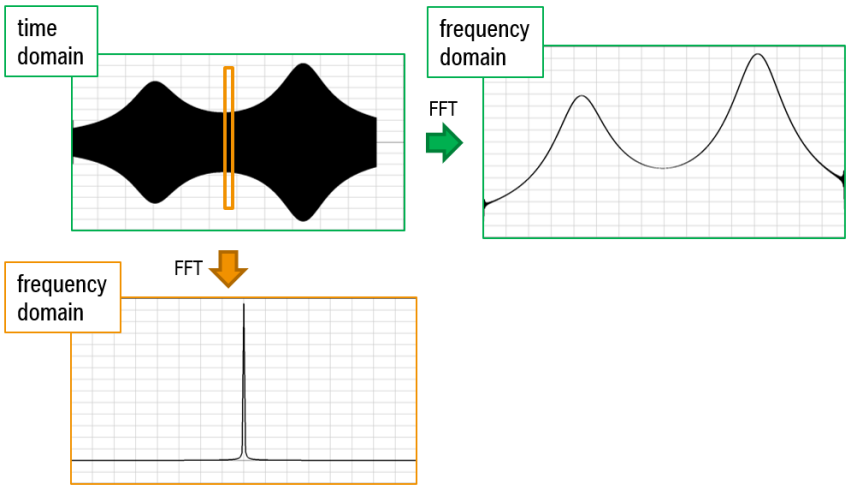

Figure 4.56: Dynamic behavior analysis of a shaft - excitation force and measured bearing force in the rotating coordinate system

Figure 4.51 shows that the radial and tangential forces of the general slider-crank excite the rotating shaft in their rotating coordinate system and influence the motion of the oscillating mass. So it is important to use the modulated eigenfrequencies to decide, if the shaft can be modeled as a rigid body or a flexible body. To give the engineer a feeling for the deviation by using a rigid body model, a criterion is necessary.

The developed criterion in chapter 4.2.6.1 can be also used in this decision case. Referring to the developed criterion, we know that the first eigenfrequency of a system has to be ten times higher than the maximal frequency of interest to use a rigid modeled system, if the deviation of ±1 % is enough accurate. For rotating shafts, it is additionally necessary to regard the rotational frequency. So we have to take the lowest modulated frequency to apply this criterion.

Let's summarize the procedure to decide how the shaft should be modeled. At first the modulated eigenfrequencies of the shaft have to calculate. The second step is to compare the frequency of interest and the lower modulated eigenfrequency of the shaft. If the lower modulated eigenfrequency is ten times higher than the frequency of interest, the shaft can be modeled as a rigid body with respect to the ±1 % deviation of the resulting amplitude.

4.3.3.2 Calculation of the operational vibration

After impressing the forces on subsystem 1 coupled with subsystem 2, the operational vibration in Figure 4.57 can be calculated. It may be expected the operational vibrations are significantly different, because of the influence of the structural dynamic behavior in the force calculation.

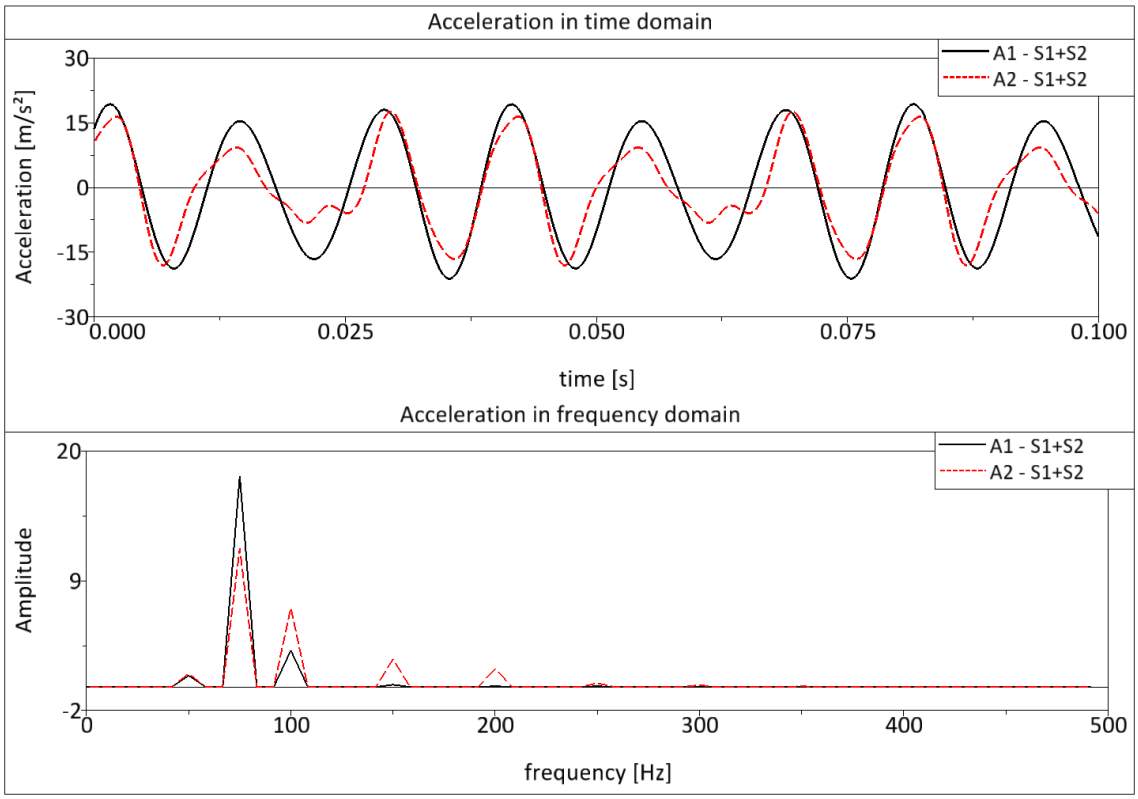

Figure 4.57: Operational vibration by using the abstraction level A1 and A2

It can be seen that the frequency content and the amplitudes are different. So the third order of subsystem 2 can be seen in the operational vibration of abstraction level A2 instead of abstraction level A1.

4.3.4 Abstraction level A3

The abstraction level A3 uses the principle of cutting forces, which is explained in chapter 3.5.4. It differs from the abstraction level A2 by modeling of the excitation force calculation and the modeling of the force-impressing model. It considers the structural dynamic behavior of the total system, but neglects the excitation interaction completely.

4.3.4.1 Force calculation

Let's start with the calculation of the excitation forces of subsystem 2. In the abstraction level A2, the calculated forces only contain the structural dynamic behavior of the subsystem. In the abstraction level A3, the forces contain the structural dynamic behavior of the total system. Dependent on the necessary memory space of the coupled subsystem, the calculation time can rise immediately. Figure 4.58 and Figure 4.59 compare the calculated forces by using the abstraction level A2 and abstraction level A3. Due to the significant structural coupling between subsystem 1 and subsystem 2, which was shown in chapter 4.3.2, Figure 4.58 shows differences in their amplitudes of oscillation. The frequency content is the same, because the structural coupling does not influence the motion sequence of the excitation components. So the operational vibration of the excitation components can only be assessed by regarding subsystem 1, as in the abstraction level 3. The reason is that the abstraction level 2 does not regard the structural coupling to subsystem 1 and calculates wrong amplitudes.

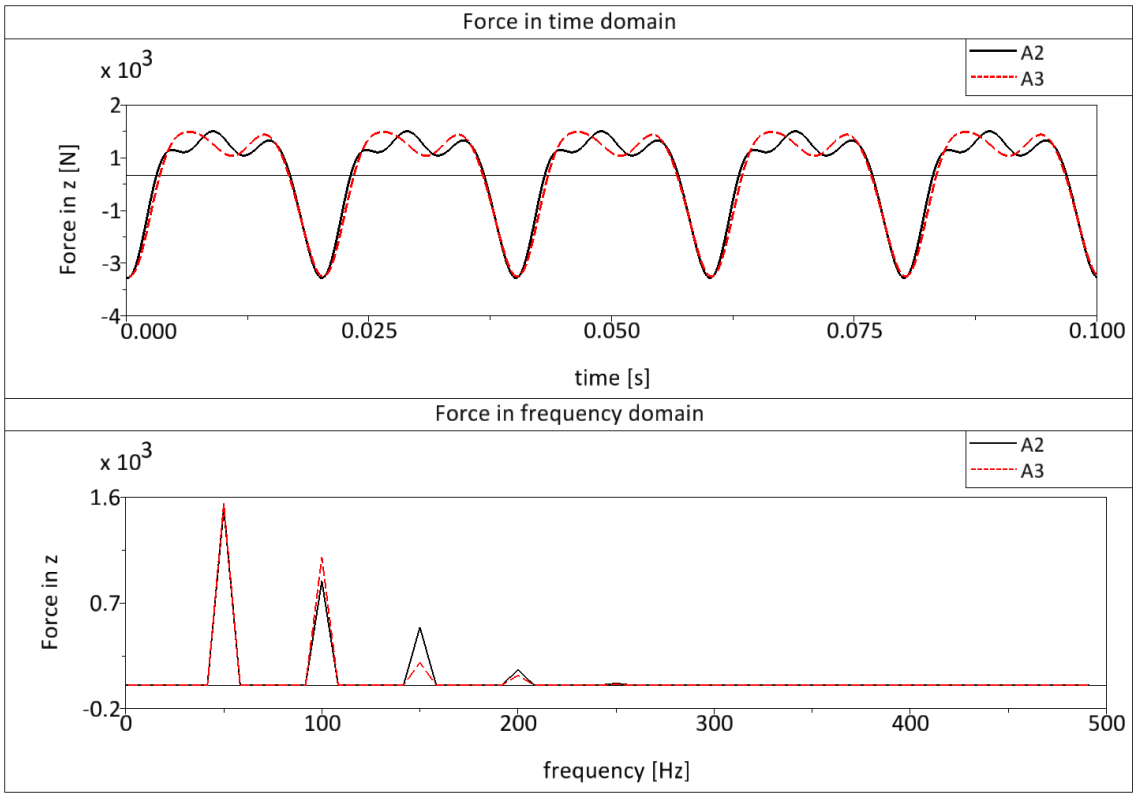

Figure 4.58: Comparison of the calculated excitation force for subsystem 2

Figure 4.59 does not show a significant difference between the abstraction levels, neither the amplitudes nor the frequency content. The reason is the decoupling effect between the subsystems (1 & 2) and subsystem 3, so the subsystem (1 & 2) does not have a significant influence on subsystem 3. As a result the operational vibrations of the excitation components can be assessed without considering the neighboring subsystems of subsystem 3. But it is necessary to know that the excitation interaction from subsystem 2 to subsystem 3 is neglected.

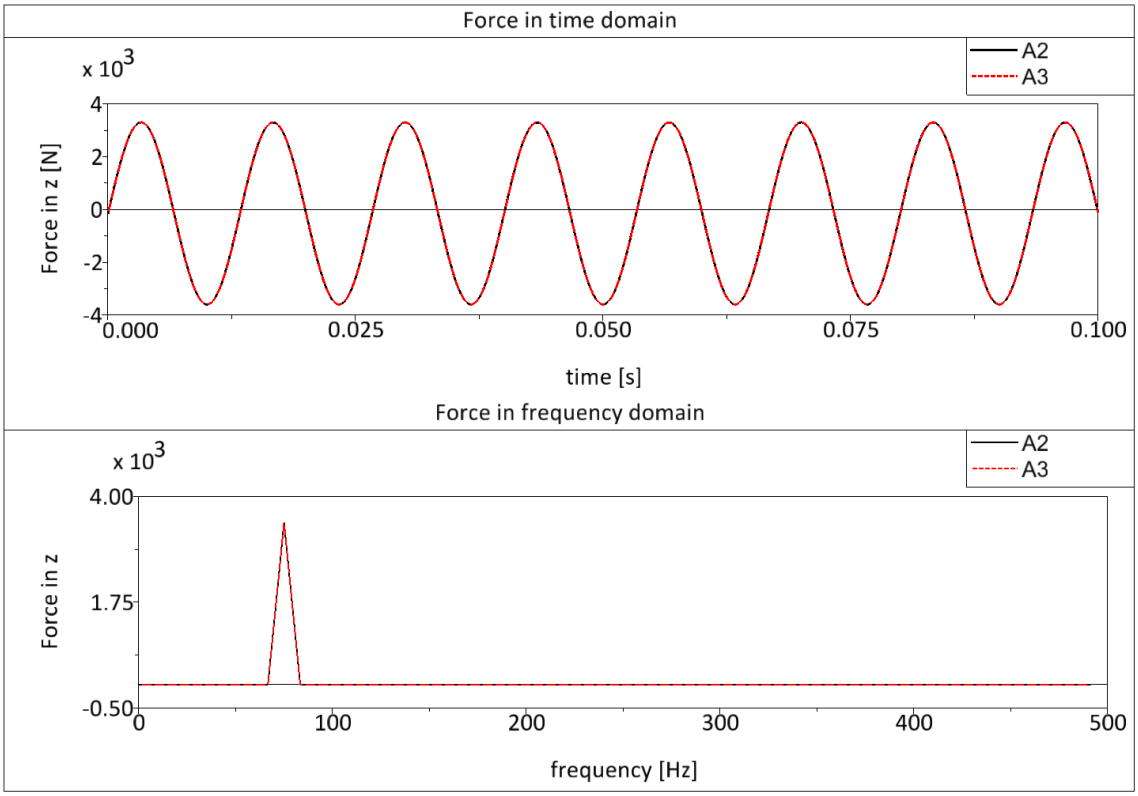

Figure 4.59: Comparison of the calculated excitation force for subsystem 3

4.3.4.2 Calculation of the operational vibration

Now the calculated forces have to be impressed on subsystem 1. Due to the principle of cutting forces, the calculated forces contain the structural dynamic behavior of the total system and the force can be impressed on the system of interest to calculate their operational vibrations. But neither the calculated forces nor the calculated operational vibrations contain the excitation interaction. Figure 4.60 shows the comparison of the operational vibration by using the abstraction level A2 and A3. The difference between the curves results from the neglected excitation interaction in the abstraction level A3. The abstraction level A2 contains one part of the excitation interaction, which is based on the structural coupling of the subsystems. In the next chapter, the excitation interaction is explained in detail.

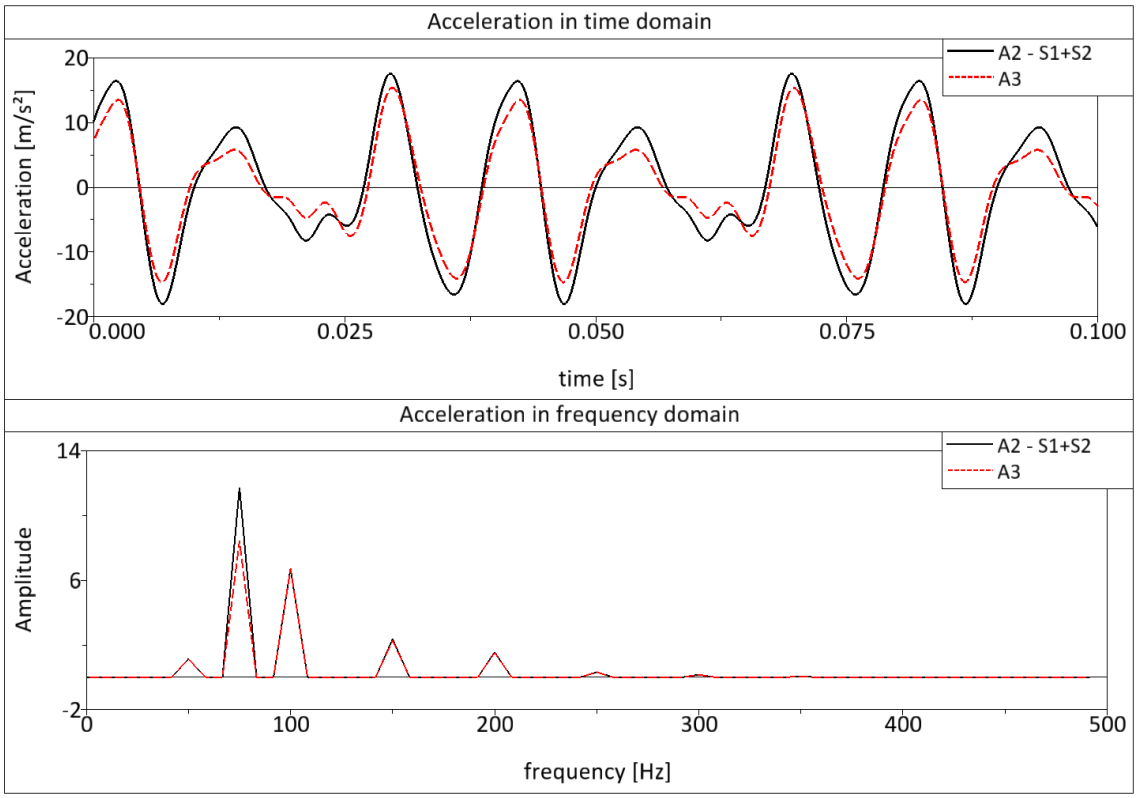

Figure 4.60: Operational vibration by using the abstraction level A2 and A3

4.3.5 Abstraction level A4

The abstraction level A4 is the mathematically most difficult abstraction level and considers the structural dynamic behavior of the total system and the excitation interaction. But it is also the most time-consuming abstraction level, because of the modeling time, calculation time, and the non-usability of the simultaneous engineering approach. So the abstraction level A4 needs one model which contains all subsystems and their couplings. So it is not possible that one engineer works on one subsystem and another engineer works on another subsystem. Here one engineer has to build up one complex coupled model.

4.3.5.1 Force calculation

The force calculation is attended by the calculation of the operational vibrations. For special assessments it can be useful to use the principle of cutting forces. So it is possible to calculate the forces by using a MBS-Software and impress them on a FEM-Model in time or frequency domain. Figure 4.61 and Figure 4.62 show a comparison of the calculated forces by using the abstraction level A3 and A4, because the abstraction level A3 only contains the structural dynamic behavior of the total system and no excitation interaction. In Figure 4.61 a significant excitation interaction from subsystem 3 to subsystem 2 at 75 Hz and 125 Hz can be seen. This excitation interaction represents the total excitation interaction from subsystem 3 to subsystem 2.

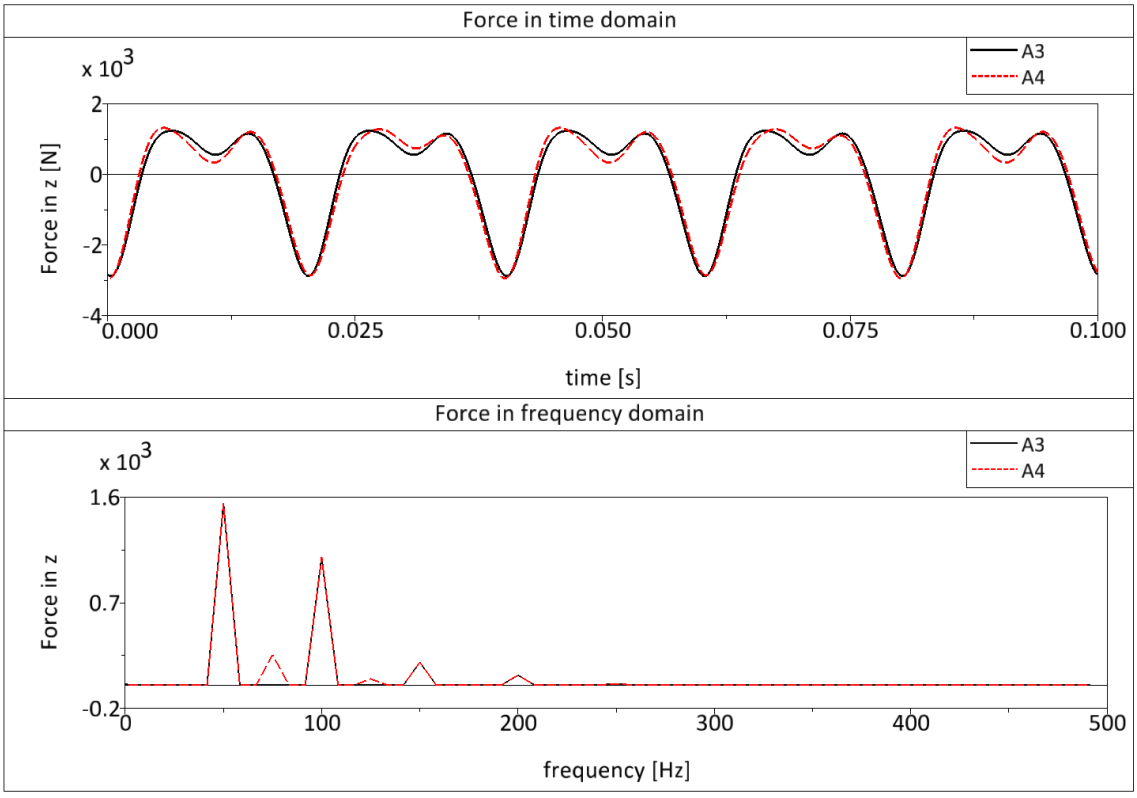

Figure 4.61: Comparison of the calculated excitation force of subsystem 2

Figure 4.62 shows the excitation interaction from subsystem 2 to subsystem 3, but the curves do not show any significant difference in their amplitude or frequency. This

suggests that subsystem 2 does not have a significant influence on subsystem 3 and subsystem 3 can be assessed by neglecting the excitation interaction with subsystem 2.

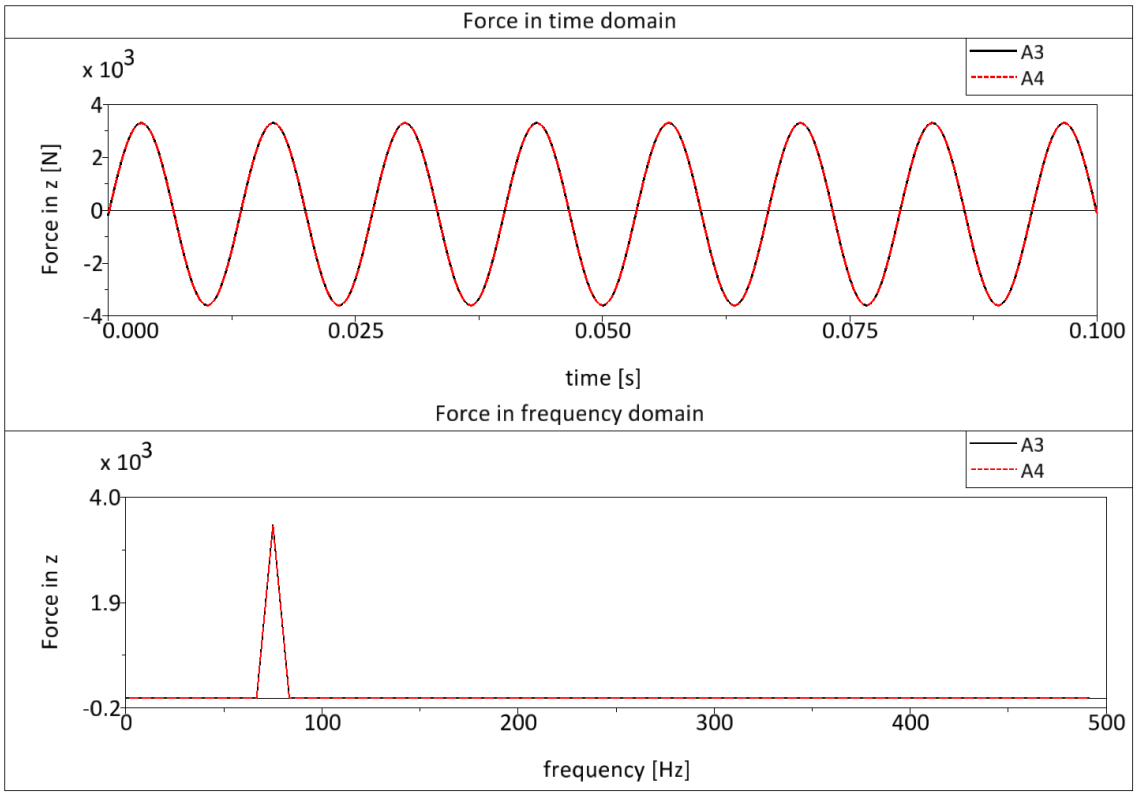

Figure 4.62: Comparison of the calculated excitation force of subsystem 3

4.3.5.2 Calculation of the operational vibration

Figure 4.63 shows the comparison of the operation vibrations by using the abstraction level A3 and A4. Here can be seen the total influence of the excitation interaction in time and frequency domain. So the amplitude at 75 Hz is significantly higher by considering the excitation interaction and a small peak can be seen at 125 Hz. The two differences can be separated by two kinds of excitation interaction, the structural excitation interaction and the motion manipulation of the excitation interaction.

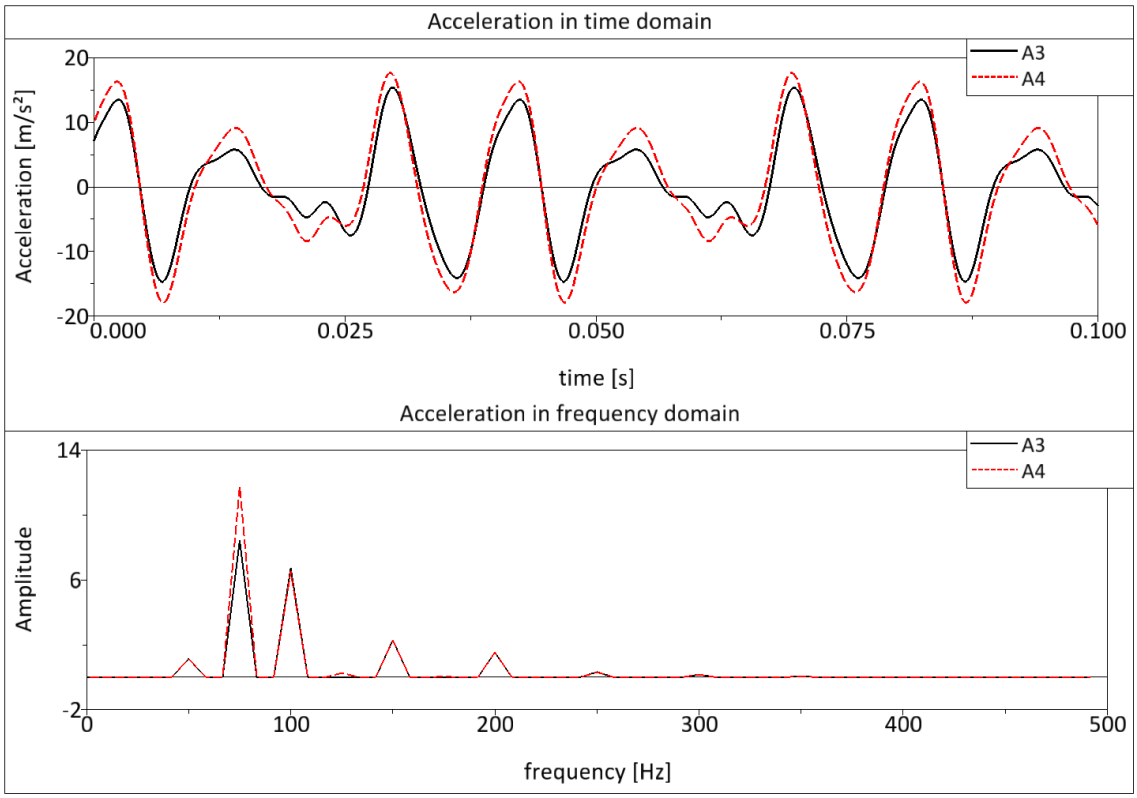

Figure 4.63: Operational vibration by using the abstraction level A3 and A4

As mentioned in the previous chapter, the abstraction level A2 considers the structural excitation interaction, but not the motion manipulation of excitation interaction. So it is possible to separate the two kinds of excitation interaction. Figure 4.64 shows the comparison of the operational vibrations by using the abstraction level A2 and A4. The differences between the curves represent the motion manipulation of the excitation interaction.

The amplitude difference at 75 Hz can only be seen in Figure 4.63, which represents the total excitation interaction. So it is not a motion manipulation, but a structural excitation interaction. And the peak at 125 Hz can be seen in both figures, so the peak results from the motion manipulation of the excitation interaction.

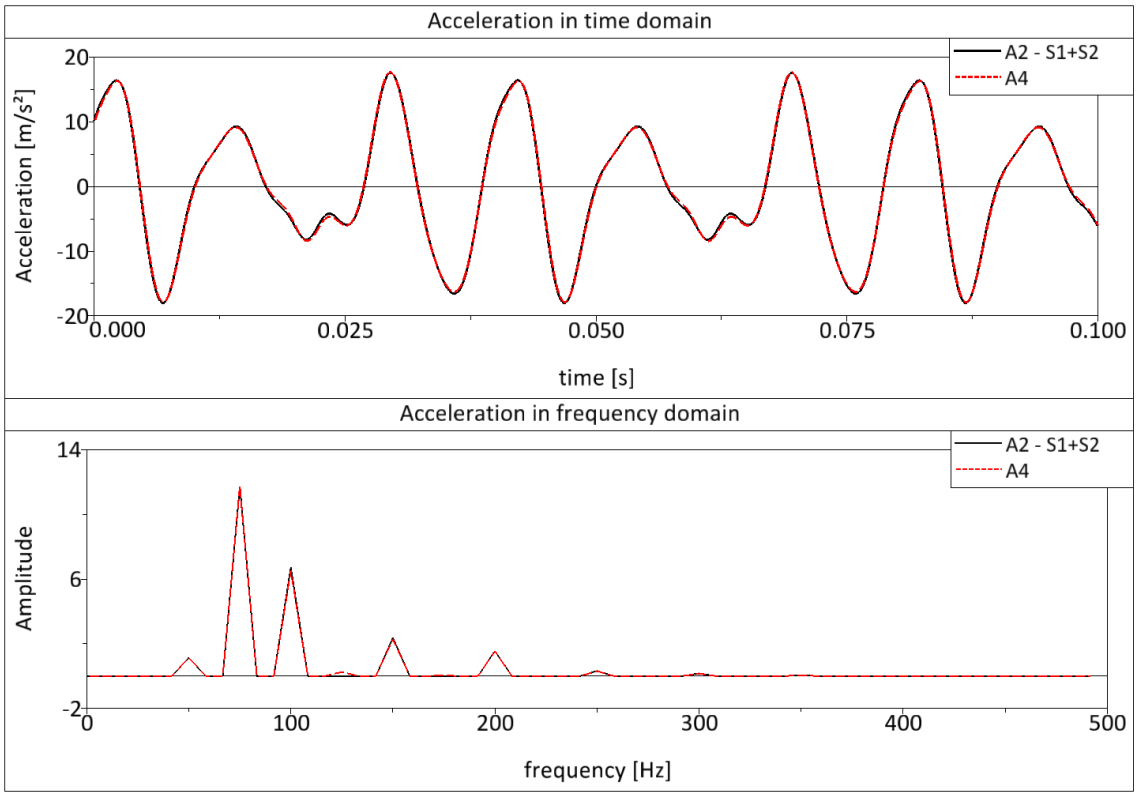

Figure 4.64: Operational vibration by using the abstraction level A2 and A4

4.4 Explanation of the abstraction levels for a complex reference system

This chapter applies the abstraction levels to a complex reference model. Here the complex reference model is an engine which is used in the automotive industry.

4.4.1 Description of the total system

The complex reference system can be distributed in three subsystems:

- System housing (Figure 4.65)
- Crank drive with a rotational frequency of 3000 rpm (Figure 4.66)
- Balance shafts with a rotational frequency of 6000 rpm (Figure 4.67)

Subsystem 1 consists of a modal-reduced substructure and four mountings with a linear stiffness and damping factor. Figure 4.65 shows the system housing with the total mass and the eigenfrequencies till 500 Hz.

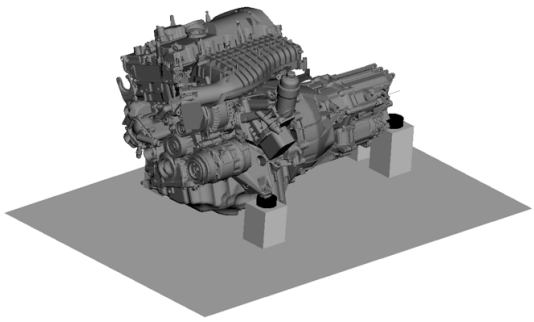

Mode	Eigenfrequency [Hz]	Modal damping factor [-]
1	6.2	0.051
2	11.6	0.055
3	15.5	0.080
4	20.0	0.132
5	27.6	0.111
6	28.0	0.076
7	68.2	0.037
8	90.6	0.035
9	132.8	0.035
10	151.2	0.035
11	182.2	0.035
12	208.1	0.038

Total mass: 141.0 kg

Mode	Eigenfrequency [Hz]	Modal damping factor [-]
13	219.5	0.035
14	233.3	0.036
15	247.8	0.039
16	292.8	0.037
17	299.0	0.041
18	310.6	0.036
19	318.9	0.036
20	335.2	0.038
21	348.5	0.036
22	361.0	0.037
23	392.9	0.035
24	411.6	0.035
25	417.8	0.035
26	422.8	0.035
27	427.6	0.035
28	431.8	0.035
29	439.5	0.037
30	456.1	0.036
31	483.3	0.035
32	486.5	0.035
33	487.0	0.035
34	494.7	0.035
35	499.6	0.035

Figure 4.65: Subsystem 1 - system housing

Subsystem 2 consists of a modal-reduced substructure (crankshaft) and the rigid bodies: piston and piston-rod. The crankshaft bearings are modeled by linear stiffness and damping factors. As a result of the rotation of the crank drive, excitation forces in the bearings can be calculated. The excitation forces can be split up in forces of the rotating masses and in forces of the oscillating masses. Figure 4.66 shows the total mass of the crank drive and the eigenfrequencies till 500 Hz.

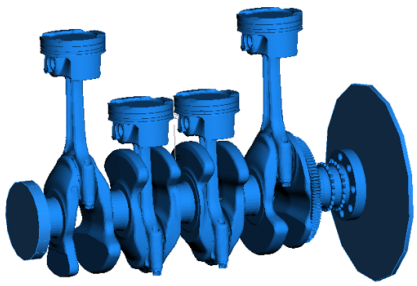

Total mass: 27.2 kg

Mode	Eigenfrequency [Hz]	Modal damping factor [-]
1	5.3	0.001
2	15.1	0.031
3	143.6	0.006
4	215.9	0.005
5	435.6	-0.003
6	446.3	0.009
7	475.3	-0.010

Figure 4.66: Subsystem 2 - rotating crank drive

Subsystem 3 consists of two balance shafts which are modeled as model-reduced substructures. During the rotation of the unbalanced mass of the shaft, the harmonic excitation force can be calculated in the linear bearings. The balance shafts rotate two times faster than the crank drive, so it is possible to compensate the second order of the crank drive. Figure 4.67 shows the total mass and the eigenfrequencies till 500 Hz of subsystem 3.

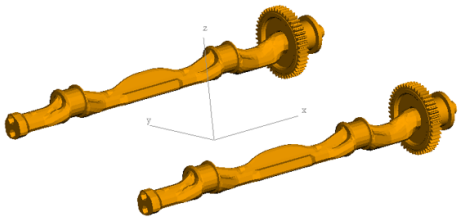

Total mass: 1.3 kg per shaft

Mode	Eigenfrequency [Hz]	Modal damping factor [-]
1	221.6	0.070
2	221.6	0.070
3	273.9	0.054
4	274.1	0.054
5	284.3	0.060
6	284.4	0.060
7	339.9	0.107
8	339.9	0.107

Figure 4.67: Subsystem 3 - rotating balance shafts

4.4.2 Abstraction level A1

As in the previous chapters and complexity levels, the forces are calculated by using rigid bodies in the abstraction level A1. Afterwards the calculated forces of subsystem 2 and subsystem 3 are impressed on the flexible total system which contains the structural dynamic behavior till 500 Hz. Figure 4.68 shows the operational vibration of one point on the surface of subsystem 1. The time domain and the frequency domain of the accelerations on the surface can be seen. Each peak in frequency domain represents a frequency order caused by the excitation forces. Generally, there are orders with a higher frequency than 300 Hz, too. But in this example the calculated force amplitudes of the excitation subsystems are too small, so they cannot be seen in the diagram.

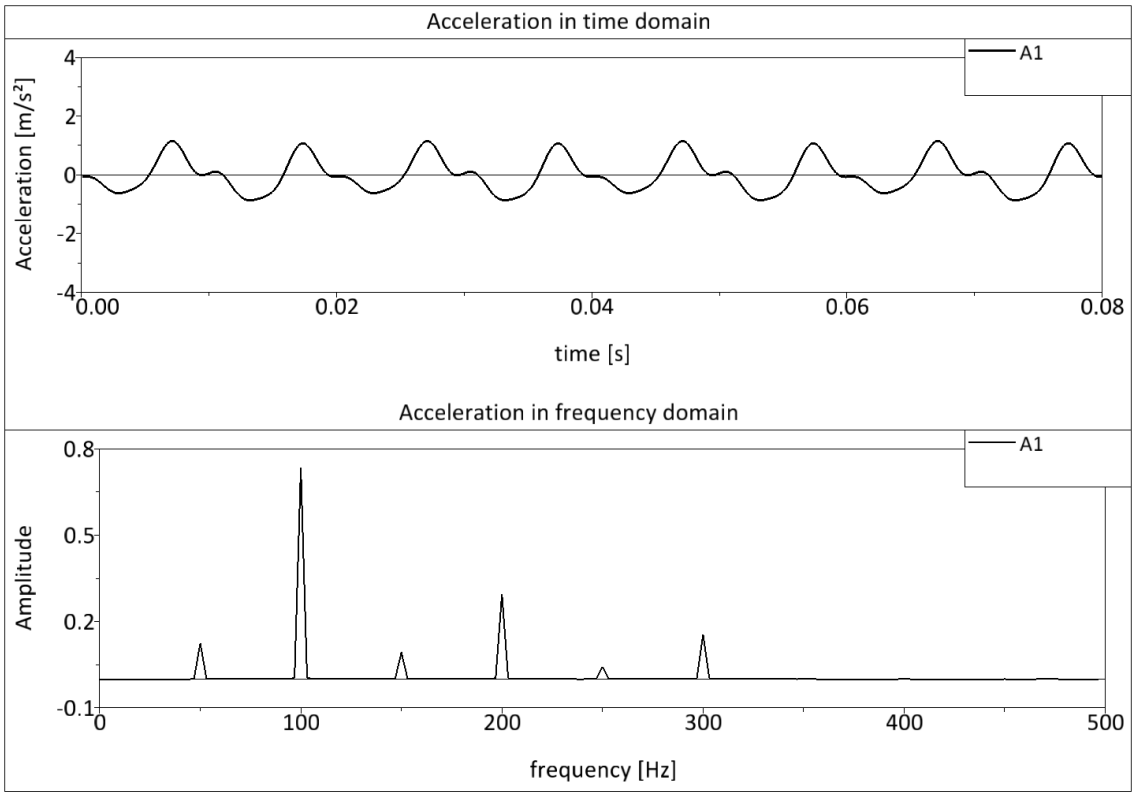

Figure 4.68: Operational vibration by using the abstraction level A1

4.4.3 Abstraction level A2

The abstraction level A2 is based on the Blocked Force Method. So the forces are calculated by using flexible excitation components. Figure 4.69 shows the comparison of the calculated operational vibration in time and frequency domain by using the abstraction level A1 and A2. In both domains a significant difference between the abstraction levels can be seen. The difference is a result of the consideration of the flexible excitation components with their structural dynamic behavior. The frequency domain shows that both abstraction levels contain the same frequency content, but the amplitudes are differing.

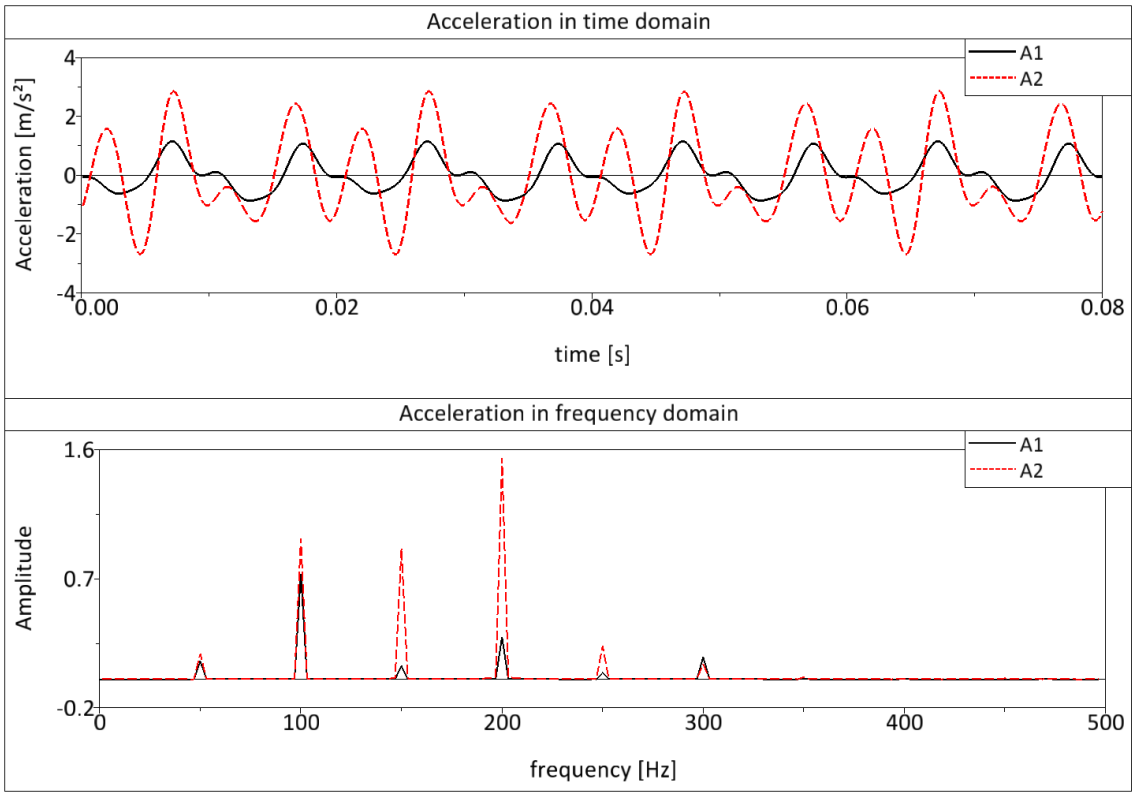

Figure 4.69: Operational vibration by using the abstraction level A1 and A2

4.4.4 Abstraction level A3

The abstraction level A3 is based on the principle of cutting forces. So the abstraction level considers the structural dynamic behavior of the total system and neglects the excitation interaction completely. The abstraction level A2 considers the structural dynamic behavior of the total system and a part of the excitation interaction which is described in chapter 4.3.5. Figure 4.70 shows the comparison of the operational vibrations by using the abstraction level A2 and A3. At the moment we think that the difference in time and frequency domain is only a result of neglecting the excitation interaction by using the abstraction level A3.

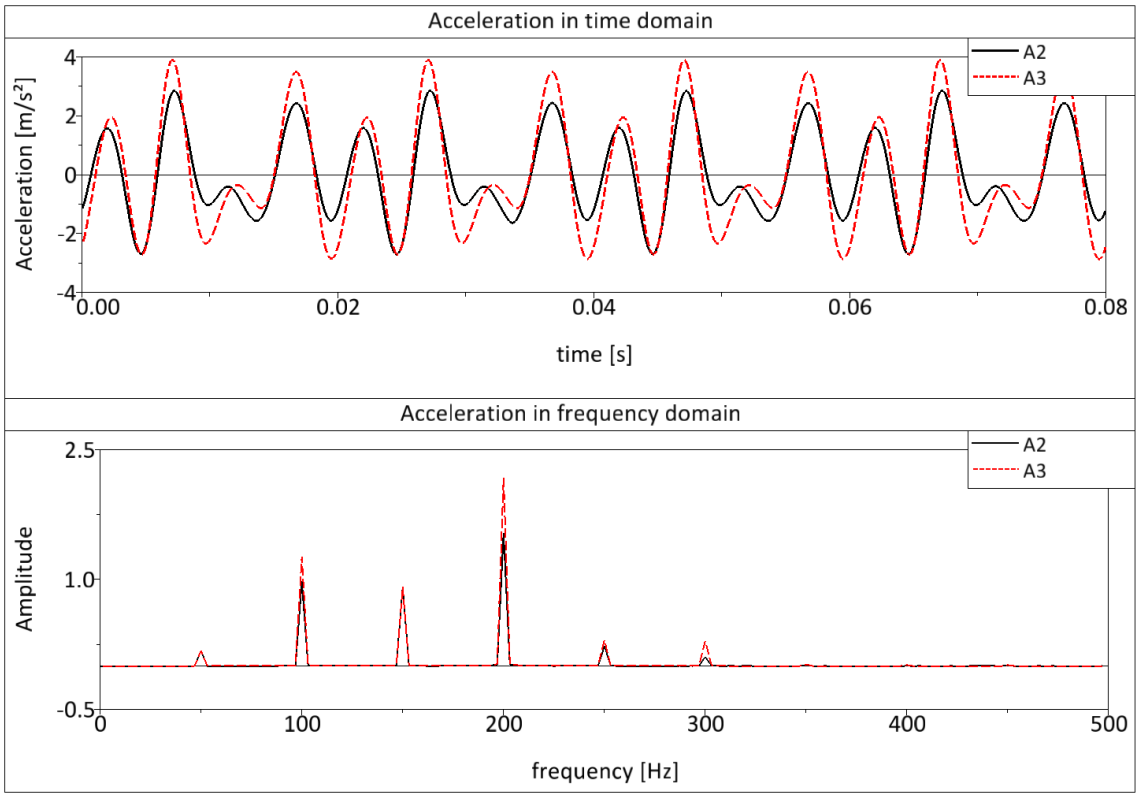

Figure 4.70: Operational vibration by using the abstraction level A2 and A3

But a further analysis shows that the excitation interaction is not the unique reason for the difference. Now we only look at the system housing (subsystem 1) with the crank drive (subsystem 2) and compare the operational vibrations by using the abstraction level A2 and A3. So we neglect the subsystem 3 completely. Theoretically, the accelerations in time and frequency domain have to be the same, because the system does not have a second excitation subsystem and does not contain excitation interaction. But Figure 4.71 shows a difference between both methods (Blocked Force Method and Cutting Force Principle). The difference is a result of the geometrically nonlinearity of the crank drive, which represents a limit of the Blocked Force Method. The Block Force Method only considers the correct structural dynamic behavior of the total system by using linear models. In this example, the crankshaft has different eigenfrequencies for the first and second bending mode shape (see Figure 4.72). So during the rotation, the system has another structural dynamic behavior at each time step which is not considered in the Blocked Force Method.

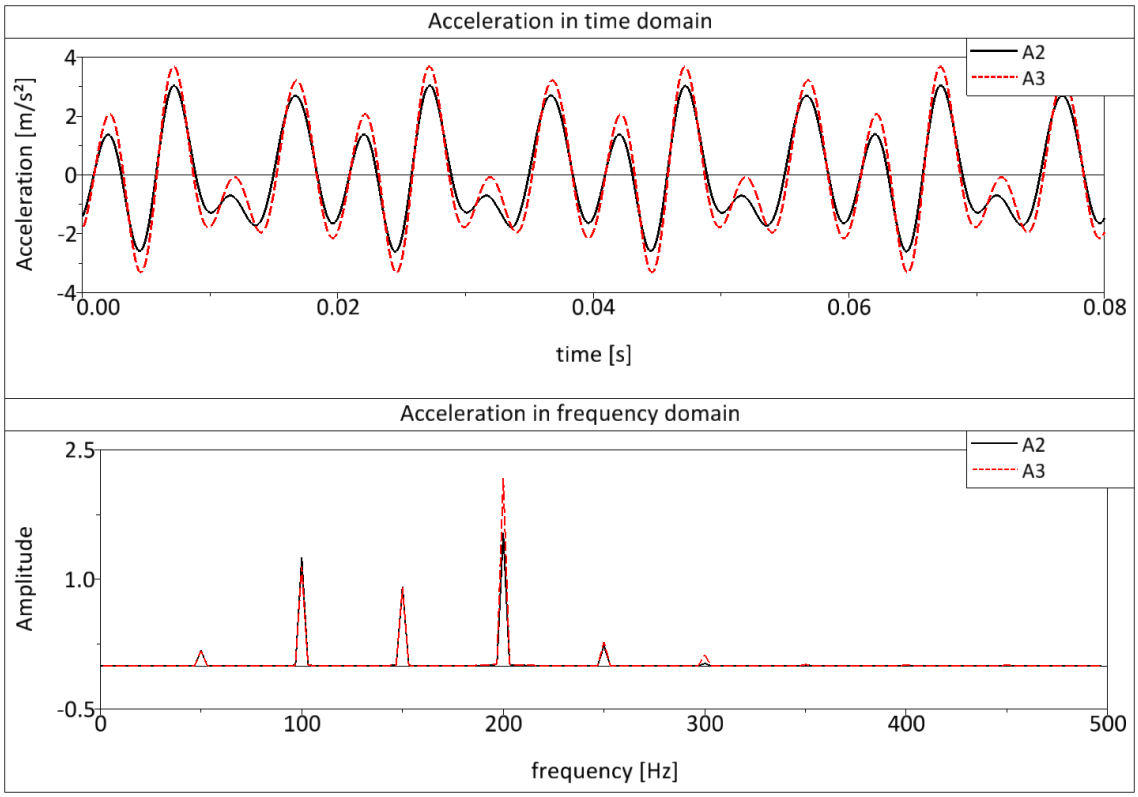

Figure 4.71: Operational vibration of the complex reference system without subsystem 3 by using the abstraction level A2 and A3

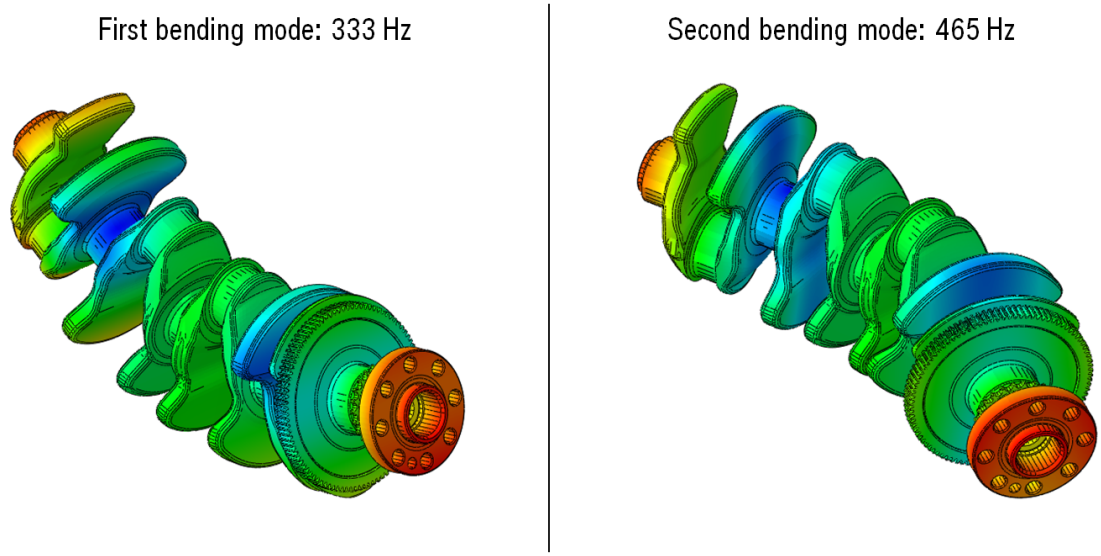

Figure 4.72: First and second bending mode of the crankshaft

Now the effect should be explained by taking the example of a simple flexible-body system. We look at a shaft with a circular cross section. So the shaft has the same eigenfrequency for the first (y-direction) and second (z-direction) bending mode. Now an eccentric mass is fixed to the shaft, so the eigenfrequency for the first and second bending mode is different. The following analysis looks at the amplification function of the system for different angularity. Therefore, the excitation and the measurement are always in z-direction. Figure 4.73 shows the amplification function in z-direction of the system, if the eccentric mass is in line with the z-axis. So there is the eigenfrequency $f_{eigen,1}$ observable, due to the eigenmode in y-direction is not excited.

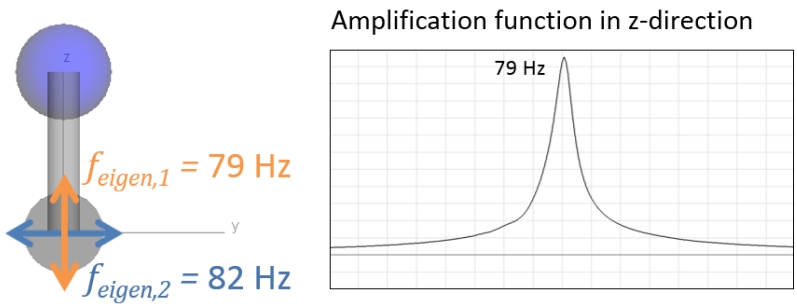

Figure 4.73: Amplification function in z-direction, if eccentric mass is in line with the z-axis

Figure 4.74 shows the amplification function in z-direction, if the system is rotated by 45°. So the eccentric mass is between the z- and y-axis. In the amplification function the first and second bending mode can be observed, because both mode shapes are excited by the force in z-direction.

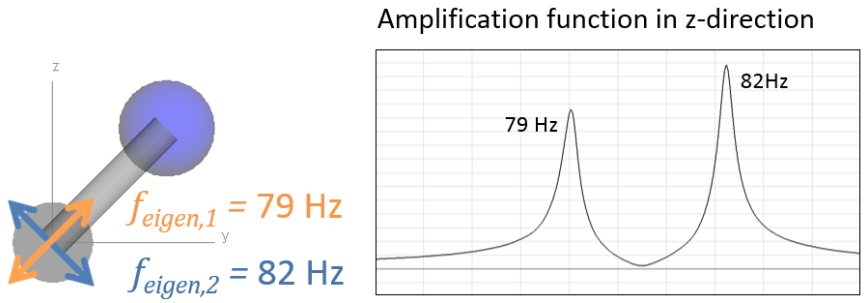

Figure 4.74: Amplification function in z-direction, if eccentric mass is between the z- and y-axis

The amplification function in Figure 4.75 only shows the eigenfrequency $f_{eigen,2}$, because the eccentric mass is in line with the y-axis and the mode shape of frequency

$f_{eigen,1}$ oscillate in y-direction. So the amplification function with excitation and measurement in z-direction does not observe the first bending mode.

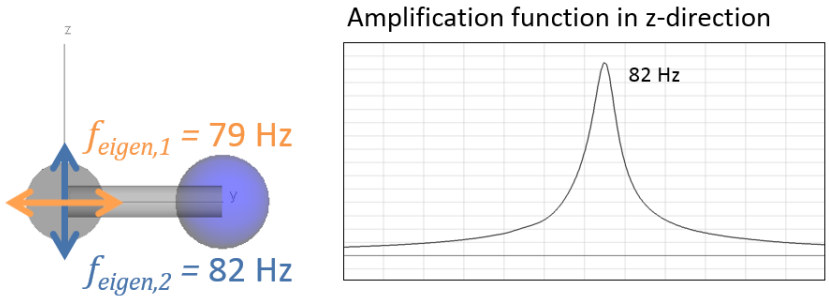

Figure 4.75: Amplification function in z-direction, if eccentric mass is in line with the y-axis

Let's imagine that the system is rotating with a defined rotational frequency. So the amplification function in z-direction is different at each time step. If the rotating system is coupled to a system housing, the rotating system will influence the structural dynamic behavior of the total system differently at each time step. That is the reason why the Blocked Force Method does not work, if a moved system influences the structural dynamic behavior of the total system differently in each time step. An analogous effect can be seen when comparing the Blocked Force Method and the principle of cutting forces in the results of the complex reference model.

4.4.5 Abstraction level A4

The abstraction level A4 considers the structural dynamic behavior of the total system at each time step and the excitation interaction. So it considers the most physical effects. Figure 4.76 shows the comparison of abstraction level A3 and A4 by using the accelerations on the surface of the system housing (subsystem 1) in time and frequency domain. The differences are a result of neglecting the excitation interaction in the abstraction level A3.

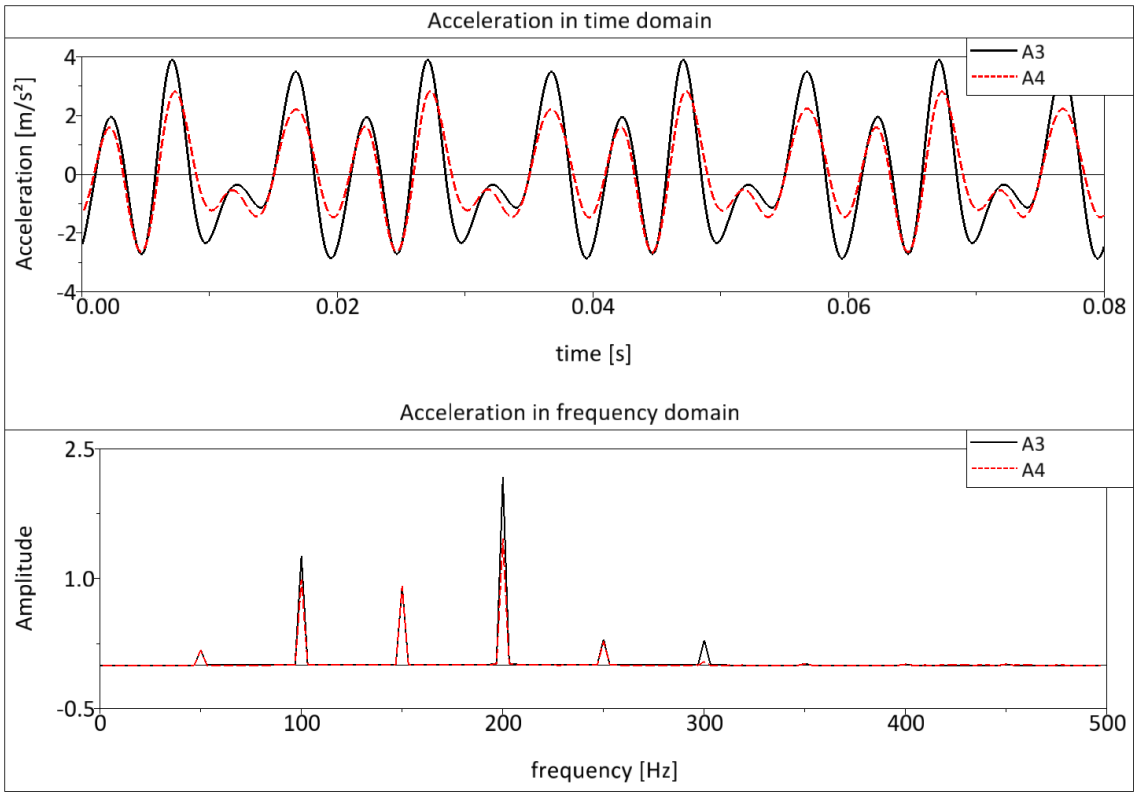

Figure 4.76: Operational vibration by using the abstraction level A3 and A4

Figure 4.77 shows the comparison of abstraction level A2 and A4. So it can be seen that the difference in time and frequency domain is smaller than the difference between the abstraction level A3 and A4.

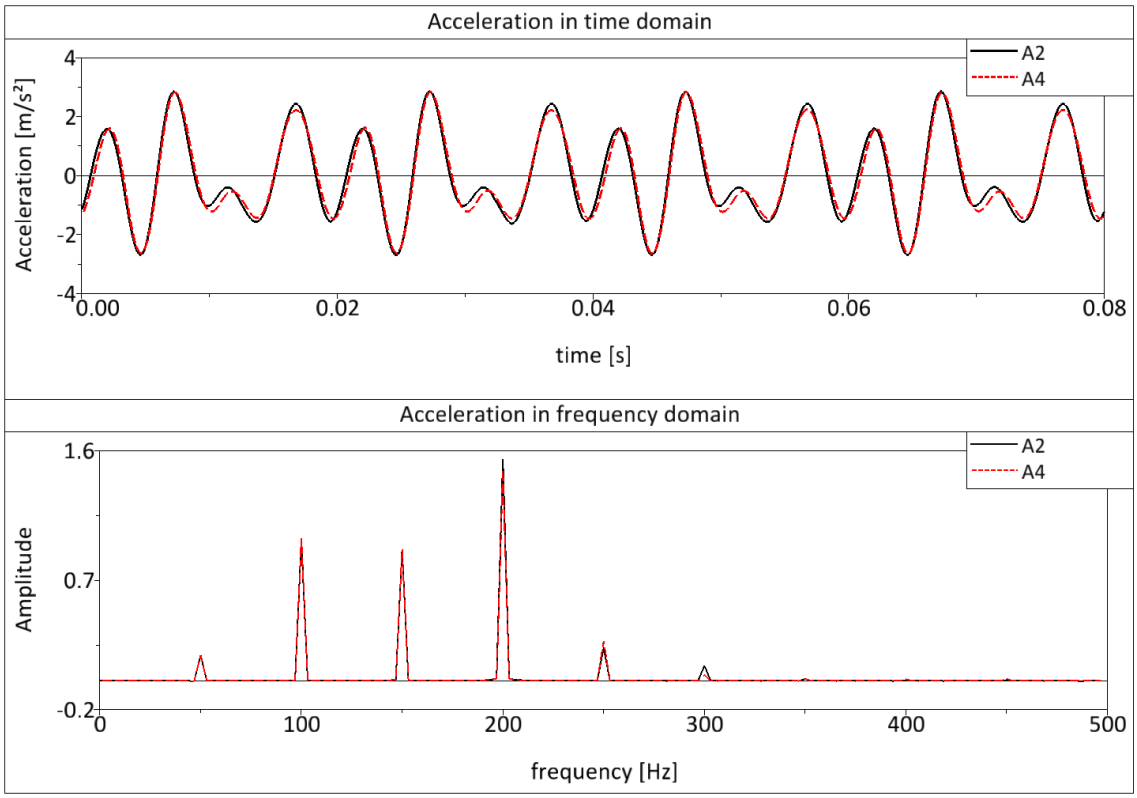

Figure 4.77: Operational vibration by using the abstraction level A2 and A4

In summary, the abstraction level A2 considers a part of the excitation interaction, but neglects the correct structural dynamic behavior at each time step. The abstraction level A3 considers the correct structural dynamic behavior at each time step, but neglects the excitation interaction completely. In this case, the excitation interaction has more influence on the operational vibration than the correct structural dynamic behavior at each time step.

5 Conclusion

The research in this work attempted to separate physical effects by using developed abstraction levels and to help the engineers for modeling complex coupled systems. It was intended that the developed methods and abstraction levels are generally applicable in many specialist fields and the identified effects are explained by using models with different complexity levels. For this purpose the work investigates the structural coupling of subsystems and the excitation interaction between subsystems.

In the context of the work, five kinds of physical effects can be identified, which can be separated by the developed abstraction levels and additional assessment methods. The first effect is called “structural coupling of excitation components”, which shows the influence of the structural dynamic behavior of the excitation component to the operational vibration of the total system. The second effect is called “structural coupling of subsystems”, which shows the influence of the structural dynamic behavior of subsystems to the structural dynamic behavior of neighboring subsystems and the total system. Another effect is the differentiation of considering the structural dynamic behavior of the total system for each point of time or only for one point of time. The fourth effect is a part of the excitation interaction between subsystems and is called “structural excitation interaction”. It represents the interaction of the structural dynamic behavior of the excitation components without manipulating the motion of the components. The “motion manipulation of excitation components” is the fifth effect and the second part of the excitation interaction effect.

For separating the mentioned effects, four abstraction levels are developed in this work. In Figure 5.1 an overview of all abstractions levels and the considered effects are shown. Overall the structural coupling of subsystems can be considered in each abstraction level. The dissertation shows an assessment method that uses defined criteria and characteristic diagrams to assess the deviation of results if a subsystem is neglected. This method helps to save time and capacity for modeling and calculating

the system. So it can be recommended that as many subsystems as possible should be neglected.

The abstraction level A1 considers the structural dynamic behavior of the total system for one point of time. The effects of structural coupling of excitation components and structural excitation interaction are considered by the abstraction level A2. The abstraction level A3 neglects the total excitation interaction, but considers the structural dynamic behavior of the total system for each point of time. Especially for rotating shafts, a method is shown to assess the influence of the dynamic behavior of the shaft by considering the rotational frequency. The abstraction level that considers the most physical effects is called A4. It considers the total structural dynamic behavior for each point of time as well as the total excitation interaction (structural excitation interaction and motion manipulation of excitation interaction).

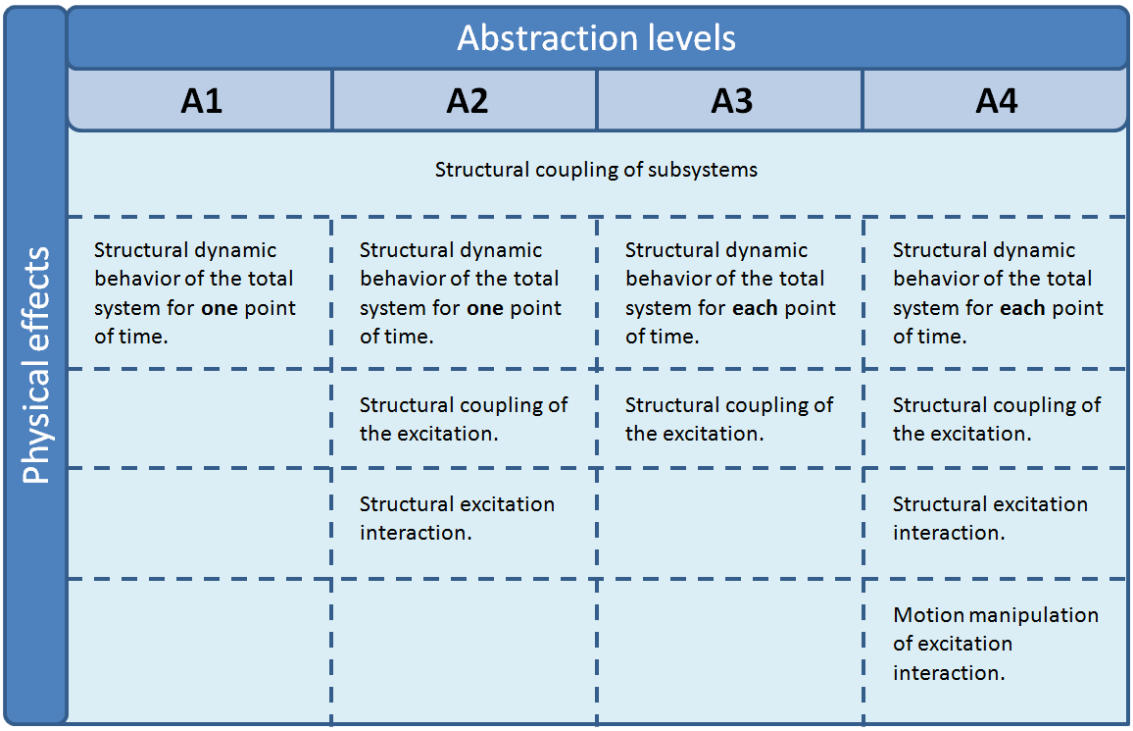

Figure 5.1: Overview of abstraction levels and the considered physical effects

The physical effects can be separated by subtracting the results which are generated using the mentioned abstraction levels. At first the limitation of the Blocked Force Method has to be checked. The method is applicable if the structural dynamic behavior of the total system is equal for each point of time. If the Blocked Force Method can be

used, the physical effects can be completely separated by subtracting the results. For example, the effect “structural excitation interaction” should be separated. So the calculated results by using the abstraction level A3 have to be subtracted from the results which are calculated by using abstraction level A2. Referring to this example, the different effects can be separated by subtracting the results of the abstraction levels.

Further theses and researches can base on this thesis for extending the developed methods. So the methods can be extended by nonlinear stiffness and damping factors.

References

Altenbach, H. (2012): Kontinuumsmechanik. Einführung in die materialunabhängigen und materialabhängigen Gleichungen. 2. Aufl. Berlin: Springer Verlag.

Aris, R. (1994): Mathematical modelling techniques. New York: Dover Publications.

Bathe, K.-J. (1996): Finite element procedures. Englewood Cliffs, N.J: Prentice Hall.

Bohn, P. (2006): Wechselwirkungen von Schwingungen zwischen Motor-Getriebe-Verbund und Kurbeltrieb als Grundlage für Körperschallanalysen. Dissertation. Technische Universität Berlin, Berlin. Verkehrs- und Maschinensysteme.

Börm, S.; Mehl, C. (2012): Numerical methods for eigenvalue problems. Berlin, Boston: De Gruyter (De Gruyter graduate lectures).

Brigham, E. (1995): FFT. Schnelle Fourier-Transformation. 6. Aufl. München, Wien: Oldenbourg (Einführung in die Nachrichtentechnik).

Buck, R. (2005): Prinzipien zur Auslegung von Tilgerelementen. 1. Symposium: Feder- und Dämpfungssysteme im Kraftfahrzeug. FH Joanneum. Graz, 11.05.2005.

Bungartz, H.-J.; Buchholz, M.; Pflüger, D.; Zimmer, S. (2009): Modellbildung und Simulation. Eine anwendungsorientierte Einführung. Berlin, Heidelberg: Springer Verlag.

Clough, R. W.; Penzien, J. (1975): Dynamics of structures. New York: McGraw-Hill.

Cooley, J. W.; Tukey, J. W. (1965): An Algorithm for the Machine Calculation of Complex Fourier Series. In: *Mathematics of Computation* 19 (90), S. 297.

Craig, R. R.; Bampton, M. C. (1968): Coupling of Substructures for Dynamic Analyses. AIAA Journal 6.

Cremer, L.; Heckl, M.; Petersson, B. (2005): Structure-borne sound. Structural vibrations and sound radiation at audio frequencies. 3. Aufl. Berlin, New York: Springer Verlag.

Dassault Systèmes (Hg.) (2013): Abaqus 6.13 Documentation.

de Klerk, D. (2004): Effektive hybride Analyse von gekoppelter mechanischer Subsysteme. Eine Untersuchung der Víerpoltheorie und der Frequency Based Substructuring Methode nach Jetmundsen. Master thesis. TU Delft, Delft.

Dresig, H. (2001): Schwingungen mechanischer Antriebssysteme. Modellbildung, Berechnung, Analyse, Synthese. Berlin [u.a.]: Springer Verlag.

Dubbel, H.; Beitz, W.; Grote, K.-H. (2001): Taschenbuch für den Maschinenbau. 20. Aufl. Berlin [u.a.]: Springer Verlag.

Duddeck, H. (1993): Entwicklung der Berechnungsmodelle des Bauingenieurs. In: *Bautechnik* 70 (11), S. 640–649.

Eibner, S. (2010): Bestimmung des Elastizitätsmoduls mittels Ultraschall an Aluminiumlegierungen, Stahl und Grauguss. Diplomarbeit. Universität der Bundeswehr München, München. Institut für Werkstoffkunde.

Engler, G.; Katzula, U. (1983): Richtlinie zur verminderten Anregung körperschallerregter Motorgeräusche. In: *Kraftfahrzeugtechnik* 1983 (10), S. 298–323.

Fröbel, T.; Stein, P. (2011): Die Kopplung von Partialmodellen aus Sicht der Informatik. In: *Bautechnik Sonderdruck* 88 (6), S. 65–69.

Gaul, L.; Fiedler, C. (2013): Methode der Randelemente in Statik und Dynamik. Berlin: Springer Vieweg.

Gelbert, G. (2007): Modalanalyse am Zweimassenschwinger. Technische Universität Berlin, Berlin. Institut für Prozess- und Anlagentechnik.

Gourlay, A. R.; Watson, G. A. (1973): Computational methods for matrix Eigenproblems. London, New York: Wiley.

Guyan, R. J. (1965): Reduction of Stiffness and Mass Matrices. AIAA Journal 3 (2).

Helmholtz, H. (1853): Ueber einige Gesetze der Vertheilung elektrischer Ströme in körperlichen Leitern, mit Anwendung auf die thierisch-elektrischen Versuche (Schluss.) In: *Annalen der Physik und Chemie* 1853 (89), S. 153–377.

Hempel, J. (Hg.) (2002): Schwingungstechnik für Automobile. Weinheim: Vibracoustic.

Hixson, E. L. (2010): Mechanical Impedance/Mobility. In: A. Piersol, T. Paez und C. Harris (Hg.): Harris' shock and vibration handbook. 6. Aufl. New York: McGraw-Hill.

Hughes, T. (2000): The finite element method. Linear static and dynamic finite element analysis. Mineola, NY: Dover Publications.

Iesulauro, E. (2002): Decohesion of grain boundaries in statistical representations of aluminium polycristal. Diploma thesis. Cornell University, Cornell.

Informationsverarbeitung in der Produktentwicklung (2003). Ausg. dt./engl. Berlin: Beuth (VDI-Richtlinien, 2211).

Jog, C. (2002): Foundations and Applications of Mechanics. Boca Raton, Fla, New Delhi: CRS Press; Narosa Pub. House.

Jordan, S.; Nimtz, C. (2009): Lexikon Philosophie. Hundert Grundbegriffe. Stuttgart: Reclam, Philipp, jun. GmbH, Verlag.

Karplus, W. J. (1977): The spectrum of mathematical modeling and systems simulation. In: *Mathematics and Computers in Simulation* 1977 (19), S. 3–10.

Keßler, K.; Träbing, C. (2001): Kurbelgehäusedynamik. Strukturdynamisch-elastodynamische Kopplung des Systems Kurbelgehäuse-Kurbelwelle-Kolben-Zylinder zur Ermittlung körperschallrelevanter Anregungsmechanismen durch rechnergestützte Simulation. Abschlussbericht. Unter Mitarbeit von Univ. Prof. Dr.-Ing. G. Knoll, Dipl.-Ing K. Keßler und Dipl.-Ing. C. Träbing. Forschungsverein Verbrennungskraftmaschinen e.V.; Institut für Maschinenelemente und Konstruktionstechnik, Universität Gh Kassel. Frankfurt am Main (692).

Keuth, H. (Hg.) (2004): Karl Popper: Logik der Forschung. Berlin: Oldenbourg Akademieverlag.

Klein, B. (2010): FEM. Grundlagen und Anwendungen der Finite-Element-Methode im Maschinen- und Fahrzeugbau. 8. Aufl. Wiesbaden: Vieweg + Teubner.

Knetsch, T. (2003): Unsicherheiten in Ingenieurberechnungen. Dissertation. Otto-von-Guericke-Universität Magdeburg, Magdeburg. Fakultät für Verfahrens- und Systemtechnik.

Knoll, G.; Lang, J.; Schönen, R. (1993): Strukturdynamik von Kurbelwelle und Motorblock mit elastohydrodynamischer Grundlagerkopplung. In: *VDI Fortschritt-Berichte, Reihe 11 Schwingungstechnik* (201). Düsseldorf.

Krätzig, W.; Harte, R.; Könke, C.; Petryna, Y. (2014): Tragwerke 2. Theorie und Berechnungsmethoden statisch unbestimmter Stabtragwerke. Unter Mitarbeit von Wilfried B. Krätzig, Reinhard Harte, Carsten Könke und Yuri S. Petryna. 5. Aufl. Berlin: Springer Vieweg.

Krätzig, W.; Harte, R.; Meskouris, K.; Wittek, U. (2010): Tragwerke 1. Theorie und Berechnungsmethoden statisch bestimmter Stabtragwerke. 5. Aufl. Berlin: Springer Vieweg.

Lahmer, T.; Stein, P.; Bock, B. (2011): Synthese und Analyse von gekoppelten Modellen im konstruktiven Ingenieurbau. In: *Bautechnik Sonderdruck* 88 (6), S. 8–11.

Lanczos, C. (1950): An iteration method for the solution of eigenvalue problem of linear differential and integral operators. In: *Journal of research of the National Bureau of Standards* 45, S. 255-282.

Leibbrandt, M. (2002): Numerische Integrationsverfahren in der Schwingungssimulation. Dissertation. RWTH-Aachen, Aachen.

Liu, J. (2013): Radial basis function (RBF) neural network control for mechanical systems. Design, analysis and Matlab simulation. Berlin, New York, Beijing: Springer Verlag; Tsinghua Univ. Press.

Magnus, K.; Popp, K.; Sextro, W. (2013): Schwingungen: Physikalische Grundlagen und mathematische Behandlung von Schwingungen. 9. Aufl. Wiesbaden: Springer Vieweg

Maurer Söhne (2011): Schwingungstilger und Viskodämpfer. Technische Informationen und Produkte, 02/2011.

Mayr, M. (2002): Technische Mechanik. 3. Aufl. München, Wien: Hanser.

Montgomery, P. (1995): A block Lanczos algorithm for finding dependencies over GF(2), Eurocrypt 95, Lecture notes in computer science (921) Berlin: Springer Verlag, S. 106-120

Montgomery, D. (2012): Design and analysis of experiments. 8. Aufl. Hoboken, NJ: John Wiley & Sons.

Most, T. (2005): Stochastic crack growth simulation in reinforced concrete structures by means of coupled finite element and meshless methods. Dissertation. Bauhaus-Universität Weimar, Weimar. Fakultät Bauingenieurwesen.

Most, T. (2011): Assessment of structural simulation models by estimating uncertainties due to model selection and model simplification. In: *Computers and Structures* 2011 (89), S. 1664–1672.

Neubauer, A. (2012): DFT - Diskrete Fourier-Transformation. Elementare Einführung. Bonn: Springer Verlag.

Newton, I. (1687): Philosophiæ Naturalis Principia Mathematica.

Noesis Solutions (2013): Optimus - Theoretical Background. Hg. v. Noesis Solutions. Belgium.

Norton, E. L. (1926): Design of finite networks for uniform frequency characteristic. Technical Report TM26-0-1860. Bell Laboratories.

Ottosen, N.; Ristinmaa, M. (2005): The mechanics of constitutive modeling. Amsterdam, London: Elsevier.

Payer, E. (2001): Neue Methoden zur Festigkeits- und Akustikberechnung von Verbrennungsmotoren. Symposium "Computersimulation in der Fahrzeugtechnik". Graz, 25.04.2001.

Petersen, C. (1993): Stahlbau. Grundlagen der Berechnung und baulichen Ausbildung von Stahlbauten. 3. Aufl. Braunschweig, Wiesbaden: Vieweg Verlagsgesellschaft.

Petersson, B.; Gibbs, B. (2000): Towards a structure-borne sound source characterization. In: *Applied Acoustics* 61 (3), S. 325–343.

Randall, R. (1987): Frequency analysis. 3. Aufl., Bremen: Brüel & Kjaer.

Reuter, M. (2012): Multikriterielle Bewertungsmethode für die Prognosequalität von komplexen Ingenieurmodellen. Dissertation. Bauhaus-Universität Weimar, Weimar.

Rill, G.; Schaeffer, T. (2014): Grundlagen und Methodik der Mehrkörpersimulation. Wiesbaden: Springer Vieweg

Rixen, D. J.; Boogaard, A.; van der Seijs, M. V.; van Schothorst, G.; van der Poel, T. (2013): Source description in vibration transmission between substructures: blocked forces and free velocities. In: *Journal of Sound an Vibration*. (submitted)

Rombach, G. (2008): Die Prüfung der Standsicherheit am ganzheitlichen Gebäudemodell. In: *Der Prüfingenieur* 2008 (33), S. 42–52.

Russ, H. (2004): Wissenschaftstheorie, Erkenntnistheorie und die Suche nach Wahrheit. Eine Einführung. Stuttgart: Kohlhammer

Schiehlen, W. (1990): Multibody System Handbook. Berlin: Springer Verlag.

Schilling, S. (2003): Beitrag zur Lösung ingenieurtechnischer Entwurfsaufgaben unter Verwendung Evolutionärer Algorithmen. Dissertation. Bauhaus-Universität Weimar, Weimar.

Schwertassek, R.; Wallrapp, O. (1999): Dynamik flexibler Mehrkörpersysteme. Braunschweig/Wiesbaden: Friedr. Vieweg & Sohn.

Siebertz, K.; van Bebber, D.; Hochkirchen, T. (2010): Statistische Versuchsplanung. Design of Experiments (DOE). Heidelberg, Dordrecht, [u.a.]: Springer Verlag.

Smith, G. D. (1985): Numerical solution of partial differential equations. Finite difference methods. 3. Aufl. Oxford [Oxfordshire], New York: Clarendon Press; Oxford University Press (Oxford applied mathematics and computing science series).

Stein, B. (2001): Model Construction in Analysis and Synthesis Tasks. Habilitation. Universität Paderborn, Paderborn.

Stein, P.; Most, T.; Nikulla, S.; Wudtke, I. (2010): Collected definitions for models and related terms. GRK 1462. Weimar.

Stelzmann, U.; Groth, C.; Müller, G. (2008): FEM für Praktiker - Band 2: Strukturdynamik. 5. Aufl. Renningen: Expert-Verlag.

Theiler, M.; Könke, C. (2013): Damping in bolted joints. In: *Proceedings of International Conference on Structural Engineering Dynamics (ICEDyn)* 2013. Sesimbra, Portugal.

Thévenin, L. (1883): Sur un nouveau théorème d'électricité dynamique (On a new theorem of dynamic electricity). In: *Comptes rendus hebdomadaires des séances de l'Académie des Sciences* (97), S. 159–161.

van der Valk, P. L. C.; Rixen, D. J. (2013): Substituting Internal Forces for Blocked Forces or Free Interface Displacements in Substructured Simulations. In: *Topics in Experimental Dynamic Substructuring, Volume 2: Proceedings of the 31st IMAC, A Conference on Structural Dynamics*, 2013.

Velten, K. (2009): Mathematical modeling and simulation. Introduction for scientists and engineers. Weinheim: Wiley-VCH.

Versteeg, H. K.; Malalasekera, W. (2007): An introduction to computational fluid dynamics: The finite volume method. 2. Aufl. Harlow, England, New York: Prentice Hall.

Vollmer, G. (1985): Was können wir wissen? Stuttgart: Hirzel.

Vöth, S. (2006): Dynamik schwingungsfähiger Systeme. Von der Modellbildung bis zur Betriebsfestigkeitsrechnung mit MATLAB/SIMULINK. 1. Aufl. Wiesbaden: Friedr. Vieweg & Sohn Verlag.

Waller, H.; Schmidt, R. (1989): Schwingungslehre für Ingenieure. Theorie, Simulation, Anwendungen. Mannheim, Wien, Zürich: BI-Wiss.-Verl.

Wauer, J. (2008): Kontinuumsschwingungen. Vom einfachen Strukturmodell zum komplexen Mehrfeldsystem. 1. Aufl. Wiesbaden: Vieweg + Teubner.

Werner, F. (2010): Realität - Modell - Norm. In: *Stahlbau* 79 (10), S. 711–719.

Woernle, C. (2011): Mehrkörpersysteme. Eine Einführung in die Kinematik und Dynamik von Systemen starrer Körper. Berlin, New York: Springer Verlag.

Zienkiewicz, O.; Taylor, R.; Zhu, J. (2005): The finite element method. Its basis and fundamentals. 6. Aufl. Oxford [u. a.]: Butterworth-Heinemann.